Applied Nonlinear Control of Unmanned Vehicles with Uncertain Dynamics

by

Yannick Morel

Dissertation submitted to the Faculty of the
Virginia Polytechnic Institute and State University
in partial fulfillment of the requirements for the degree of
Doctor of Philosophy
in
Mechanical Engineering

Advisory Committee
Dr. Alexander Leonessa, Chairman
Dr. Andrew Kurdila,
Dr. Steve Southward,
Dr. Daniel J. Stilwell,
Dr. Craig Woolsey

April 17$^{\text{th}}$, 2009
Blacksburg, Virginia

Keywords: autonomous vehicles, nonlinear control, adaptive control, nonlinear observers, control input saturation, output feedback, collaborative control.

Applied Nonlinear Control of Unmanned Vehicles with Uncertain Dynamics

Yannick Morel

Abstract

The presented research concerns the control of unmanned vehicles. The results introduced in this dissertation provide a solid control framework for a wide class of nonlinear uncertain systems, with a special emphasis on issues related to implementation, such as control input amplitude and rate saturation, or partial state measurements availability. More specifically, an adaptive control framework, allowing to enforce amplitude and rate saturation of the command, is developed. The motion control component of this framework, which works in conjunction with a saturation algorithm, is then specialized to different types of vehicles. Vertical take-off and landing aerial vehicles and a general class of autonomous marine vehicles are considered. A nonlinear control algorithm addressing the tracking problem for a class of underactuated, non-minimum phase marine vehicles is then introduced. This motion controller is extended, using direct and indirect adaptive techniques, to handle parametric uncertainties in the system model. Numerical simulations are used to illustrate the efficacy of the algorithms. Next, the output feedback control problem is treated, for a large class of nonlinear and uncertain systems. The proposed solution relies on a novel nonlinear observer which uses output measurements and partial knowledge of the system's dynamics to reconstruct the entire state for a wide class of nonlinear systems. The observer is then extended to operate in conjunction with a full state feedback control law and solve both the output feedback control problem and the state observation problem simultaneously. The resulting output feedback control algorithm is then adjusted to provide a high level of robustness to both parametric and structural model uncertainties. Finally, in a natural extension of these results from motion control of a single system to collaborative control of a group of vehicles, a cooperative control framework addressing limited communication issues is introduced.

Contents

List of Figures

Chapter 1

Introduction

1.1. Motivation and Current Methodologies for Control of Autonomous Vehicles

Autonomous vehicles have proven proficient in handling a considerable variety of tasks. For instance, Autonomous Marine Vehicles (AMVs) are utilized to perform oceanographic surveys, coastal patrols, and pipeline maintenance. In addition, use of unmanned vehicles in military operations is steadily increasing. The Office of Naval Research is considering mobile robotic solution to minimize human involvement in hazardous areas such as minefields. Similarly, Unmanned Aerial Vehicles (UAVs) have been employed in recent conflicts for scouting and surveillance missions, and Unmanned Ground Vehicles (UGVs) are expected, in the near future, to provide improved combat effectiveness and personnel safety to ground forces. Missions assigned to autonomous vehicles typically require or greatly benefit from a high degree of agility and maneuverability, which can only be provided by a high performance motion control system.

Uncertain Systems

Design of motion control algorithms for uncertain systems is a challenging endeavor. In particular, numerous models exist which characterize the dynamical behavior of the considered systems, many of which include parametric and/or structural uncertainties. Numerous techniques addressing issues stemming from uncertainties on the system's model can be found in the literature. One of such techniques is known as adaptive control and is divided in two distinct categories. Direct adaptive methods ([10–16]) consist in replacing uncertain constant parameters in a control law by time varying estimates. The procedure relies on a certainty equivalence principle ([10,12]), the essence of which is that, given a few assumptions on the form of the control command (such as that the uncertain parameters appear linearly, for instance), it is possible to derive estimate update laws providing stability guarantees in spite of the uncertainty. Indirect adaptive techniques ([13–16]) distinguish themselves from the direct ones in that the uncertain parameters are estimated as part of the system model, as opposed to being estimated as part of the control command. While both approaches provide the same functionality, direct adaptive results are prevalent in the literature. Structural uncertainties, which imply that the uncertainty on the system model is not limited to constant parameters, are classically handled using Neural Network (NN) based techniques ([15,17]), which rely on the capacity of a Single Hidden Layer NN (SHL-NN) to approximate continuous functions with arbitrary accuracy ([15]). Robust control techniques ([18–22]) constitute a powerful alternative to adaptive algorithms in addressing model uncertainties. The approach typically relies on the existence and knowledge of an upper bound of the norm of the uncertainty. The control algorithm is then designed with consideration for this upper bound, in order to achieve stability even in a worst case situation. While robust control

techniques originate from linear control theory ([18]), they have been extended to various classes of nonlinear systems ([23, 24]), such as, for instance, systems in the so-called robust strict-feedback form ([10]).

Control Input Saturation

Additional difficulties arise from the fact that actuation systems for autonomous vehicles only provide a limited amount of control authority, resulting in rate and amplitude saturation of the control command. Most control algorithms for autonomous vehicles in the literature do not account for this saturation, which can result in poor performance when implemented. The importance of addressing saturation constraints in the control design is even greater for adaptive algorithms. As the adaptation mechanism is left free to operate while the feedback loop is severed by actuator saturation, unstable controller modes are allowed to drift, potentially leading to severe windup effects and instability. The research literature on adaptive control with actuator saturation effects is rather limited. Notable exceptions include [25–33]. However, the results reported in [25–32] are confined to linear plants with amplitude saturation. Of particular interest is the positive μ-modification framework introduced in [32], which was applied to a specific class of nonlinear systems in [33]. The result presented in [33], however, does not consider rate saturation. Many practical applications involve nonlinear dynamical systems with simultaneous control amplitude *and* rate saturation, which may further exacerbate the control problem. For example, in advanced tactical fighter aircraft with high maneuverability requirements, pilot induced oscillations ([34, 35]) can cause actuator amplitude and rate saturation in the control surfaces, leading to catastrophic failures.

Separation Principle

Another difficulty stems from the fact that, while motion controllers are more conveniently derived assuming full state measurements, full state information is not necessarily available for feedback. The literature features a wide variety of results solving the output feedback control problem; that is, solving the control problem when full state measurements are unavailable ([10,36]). Reliance on a separation principle is a popular and effective scheme to address the problem. The procedure consists in dividing the output feedback problem into two relatively simpler problems. More specifically, the approach commonly involves derivation of a full state feedback control law as a first step. Then, since the full state is not available for feedback, the unavailable states are estimated and these estimates are used in place of the actual states in the control law. Hence, following this separation principle, one can effectively solve the output feedback problem by designing a full state feedback controller and a state observer.

Observers for Nonlinear Systems

The observation problem for linear systems has received considerable attention from the research community over the years, and a wide range of results can be found in the literature, with outstanding contributions from Kalman ([37, 38]) and Luenberger ([39, 40]), to name but a few. However, models for unmanned vehicles are typically nonlinear in nature, and the observation problem for nonlinear systems constitutes a challenging problem which is still largely open.

The strength of the observation techniques developed for linear systems naturally led to attempts at extending them to nonlinear systems. Extended Kalman filtering ([41, 42]), for

instance, is the result of one such tangent, and has shown its utility in a number of cases ([43]). Alternately, when only the output appears nonlinearly in the system's dynamics, it is possible to construct an observer for which the observation error dynamics are linear ([10, 44]). Linear techniques can thus be used to solve the observation problem for this particular type of systems, which are sometimes referred to as being in output feedback form ([10]).

The observation problem becomes more difficult if the considered nonlinear system is not in output feedback form, that is, if unmeasured states appear nonlinearly in the system's dynamics. High gain observers ([44,45]) can be used to address the problem for such systems. Such techniques essentially consist in selecting observer gains sufficiently large such that the negative influence of nonlinearities on the observation errors is overcome. The approach can however lead to large transient observation errors, due to an issue referred to as peaking phenomenon ([44]). In [46], the authors present an alternate design methodology for nonlinear observers applicable to systems which are not in output feedback form, with an approach taking advantage of the notions of immersion and invariance ([47]). Although the technique is of great interest, it requires solving a set of partial differential equations, which, quoting the authors, can be "extremely difficult." Nevertheless, observers for a number of nonlinear systems can be constructed using the approach, a pair of them being presented in [46].

Output Feedback Control

The practice of relying on a separation principle to solve the output feedback problem originates from linear control theory. Indeed, for linear systems, existence of such a separation principle is well established ([48]). Its implications are that one can solve the optimal

linear quadratic gaussian problem by separately solving the optimal estimation and control problems. However, this separation principle does not *in general* hold for nonlinear systems ([10]), and substituting observed states for their actual counterparts in a full state feedback control law can in some instances lead to finite escape time, even in the case of exponentially decaying observation errors, as shown in [10]. Issues stemming from observation errors can in some cases be addressed by adjusting the state feedback control law, using nonlinear damping to offset observation errors. However, this particular technique requires exponentially convergent nonlinear observers, which are generally limited to systems linear in the unmeasured states, thus limiting the scope of the procedure to some extent ([10]).

Alternately, the existence of a separation principle for a wide class of nonlinear systems was investigated and established for specific types of observers. In [49, 50], the authors demonstrated that estimates of unmeasured states obtained from high-gain observers ([44]) can be used in state feedback laws. The resulting closed-loop trajectory is shown to approach the state feedback trajectory (i.e. the hypothetical trajectory obtained if full state information was available and used in the control law) as the observation gains increase. The philosophy of the approach is to generate a time-scale separation between observation and control algorithms. In other words, the observation errors are made to decay rapidly enough that their impact on the controller's performance is limited. The approach is powerful and has been successfully applied to a large number of problems (see [45, 51, 52] for a few examples). However, high-gain observers suffer from a well documented issue, known as peaking phenomenon ([53]). The issue originates from the observer's high gains, which can lead to large peaks during the observer's transient. These can in turn find themselves propagated to the actual system through the control command. The issue is significant and can lead to

instability, but can oftentimes be accounted for by saturating the control input ([50]).

Approaches similar to the above high-gain observer based output feedback can be found in [54, 55]. A subtle but significant difference is that the systems considered are in canonical form, such that the states are successive derivatives of the system output. Hence, the problem of reconstructing the entire state using only output measurements is reduced to estimating the successive derivatives of the available output. Several techniques allowing to estimate derivatives with arbitrary accuracy can be found in the literature ([54, 56, 57]). The results in [54, 55] rely on the High-Order Sliding Mode Differentiator (HOSMD) introduced in [54]. While the resulting control algorithms were shown to perform well when applied to particular experimental setups ([55]), the algorithms rely on the assumption that the HOSMD can provide an exact estimate of the derivatives with finite convergence time. Although this property of HOSMDs is theoretically demonstrated in [54], whether it holds for practical applications appears to be arguable. Practical restrictions can indeed significantly complicate the problem, to an extent that, in the opinion of the authors of [55], "exact derivative reconstruction is not achievable" in practice.

Output Feedback Control of Uncertain Systems

Design of output feedback controllers for uncertain nonlinear systems is a challenging task which still constitutes an active topic of research to this day ([58–60]). Difficulties essentially stem from two different issues, which are the lack of full state measurements, and the uncertainty on the system's dynamics. While either one of this problems has been treated extensively in the literature, fewer algorithms address both simultaneously.

A number of results addressing the output feedback control problem for uncertain systems

can be found. The problem can, in some instances, be solved by extending previously discussed output feedback techniques using either adaptive or robust techniques to handle system uncertainty. For example, in [58], the authors present a robust state feedback control algorithm, which is used with a high gain observer. This robust separation-based approach guarantees uniform ultimate boundedness of the tracking errors, in spite of uncertainty on the system model. Alternately, in [60], the authors develop an adaptive separation-based algorithm, in which a full state feedback controller, developed using dynamic surface control ([61]), operates in conjunction with a neural-based adaptive observer. While separation-based techniques still appear to be prevalent, alternate approaches can be found. For instance, in [62], the authors avoid design of a state observer by reconstructing the system's output dynamics using a single-hidden-layer neural network.

In [10], the authors introduce the concept of observer backstepping, in which an observer providing exponentially decreasing observation errors is constructed. Then, a backstepping based control algorithm is designed. However, whereas in classical separation-based schemes the control law is designed to control the actual system, in the observer backstepping approach, it is constructed for a new system, composed of a combination of the actual system and of the observer. More specifically, the system which is controlled corresponds to the real system, but the equations for the unmeasured states are replaced by their counterparts from the observer. While the approach is powerful, it requires systems which are linear in the unmeasured states. In [59], the authors extend the above idea by constructing an adaptive output predictor and explicitly designing their control algorithm to control this predictor.

1.2. Contribution of the Dissertation

The objective of the presented work is to produce a control framework for unmanned vehicles, with special emphasis on issues related to implementation. Reaching this objective is only possible through the combination and synergy of a significant number of results, a number of which have a contribution to the current state of the art extending beyond control of autonomous vehicles.

Control Input Saturation

Chapter 2 introduces a model reference direct adaptive control framework, accounting for amplitude and rate saturation of the control command ([1]). The algorithm is presented in two successive steps. First, a Model Reference Adaptive Controller (MRAC, [11]) is introduced. Then, the trajectories of the reference system are reshaped to allow operation of the control algorithm within the actuation system's limitations, while maintaining established stability guarantees. The obtained control algorithm applies to a wide variety of nonlinear dynamical systems with parametric uncertainties. Few control algorithms account for actuator saturation. The only alternate algorithm relevant to nonlinear systems is itself limited to amplitude saturation ([32]). The algorithm presented in Chapter 2 improves upon the state of the art by allowing to account for both amplitude and rate saturation of the control input.

Control of Unmanned Quadrotor Aerial Vehicles

Chapter 3 presents a more specialized direct adaptive controller ([2]), designed to solve the tracking control problem for a quadrotor, which is a particular type of vertical take-off

and landing autonomous vehicle. The presented control algorithm provides an improvement over other adaptive control algorithms designed for this specific type of vehicle ([63, 64]), in particular by explicitly addressing actuator dynamics. In addition, the algorithm in Chapter 3 can readily be augmented to include the saturation algorithm introduced in Chapter 2, further strengthening its contribution.

Control of Autonomous Marine Vehicles

Chapters 4 to 6 are concerned with the control of marine vehicles. Chapter 4 introduces a neural-based adaptive controller, addressing the tracking problem for a wide variety of autonomous marine vehicles ([3]). While the algorithm itself constitutes an application of classical nonlinear and adaptive control techniques, it provides a useful control framework which is robust to uncertainties. In Chapter 5, this framework is specialized to a particular class of marine vehicles, which exhibit unstable internal dynamics (non-minimum phase marine vehicles, see [5, 6, 65] and Figure 1.1). The non-minimum phase nature of the class of vehicles considered is rarely addressed in the literature on marine vehicles, with [66] being a notable exception. The presented approach improves upon the result in [66], as the latter is limited to way-point maneuvering, while the proposed controller solves the trajectory tracking problem. The control algorithm in Chapter 5 is then modified in Chapter 6, using both direct ([4, 5]) and indirect ([6]) adaptive control techniques, to address parametric uncertainties in the vehicle's

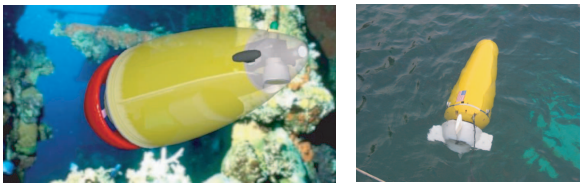

Figure 1.1: Examples of non-minimum phase AMVs, Squid1 AUV (left), Squid2 AUV (right).

model. Two distinct direct adaptive control algorithms are derived, and both perform remarkably well in simulation ([4,5]). However, derivation of these algorithms relies on specific approximations. The indirect adaptive algorithm introduced in Chapter 6 constitutes an interesting alternative to the presented direct adaptive controllers. Indeed, while performing comparably in simulations, it removes the aforementioned approximations and offers rigorously derived stability guarantees. The indirect adaptive control algorithm in Chapter 6 is based on the control strategy presented in the early part of Chapter 5, but relies on a partial state predictor to solve the tracking problem in spite of parametric uncertainties ([6]).

Nonlinear Observer

While Chapters 2 through 6 address full state feedback control problems, Chapter 7 to 9 are concerned with the output feedback problem. The approach pursued is similar to that in separation-based algorithms. More specifically, the problem is solved by designing a state observer (or output predictor), to work in conjunction with a state feedback control law (such as those presented in Chapters 2 to 6). One of the difficulties in pursuing the approach lies in the design of an observer for nonlinear systems. The most commonly found nonlinear observers in the literature are high gain observers ([44, 45]), which suffer from the peaking phenomenon. Alternative schemes relevant to large classes of systems are few and far between. The algorithm in [46] provides one such alternative, but it requires solving a set of partial differential equations, which can in general prove difficult, and thus limits the practicality of the approach. The novel nonlinear observer introduced in Chapter 7 provides an attractive solution to the considered problem, as it relaxes high-gain requirements and proposes a solution which, while still fairly general, is also eminently practical.

Observer Based Output Feedback

The output feedback control algorithm introduced in Chapter 8 builds upon the result in Chapter 7, and introduces a state observer whose output is guaranteed to predict the actual system's output with arbitrary accuracy, for any admissible control signal. Then, a state feedback controller is designed to control the *observer*'s output. In that extent, the control algorithm fundamentally differentiates itself from classical separation-based controllers, which directly control the *actual system*'s output. This intrinsic difference allows to effectively and elegantly circumvent issues inherent to separation-based algorithms, such as the peaking phenomenon. The algorithm in Chapter 8 is then modified in Chapter 9 to handle model uncertainties, which further strengthens the contribution of the scheme.

Collaborative Control of Underwater Vehicles

As previously mentioned, a single autonomous vehicle is able to perform a considerable variety of missions. However, depending on the task to be performed, several simple cooperating autonomous robotic systems can provide an easier, cheaper, more flexible and more fault tolerant solution than a single, more powerful robot ([67]). A wide range of problems have been identified as being solvable through a robotic-team approach ([68]). Some of these, such as exploration, foraging ([69]), and material handling tasks ([70]), have been shown to benefit from multiple-robot swarm solutions. Others require more involved collaboration between two or more robots working as a team.

Design of cooperative control algorithms is an involved process. Particular care has to be given to communication related issues. Indeed, communication requirements and bandwidth limitations have proven to be the Achilles' heel of many cooperative control approaches avail-

able in the literature. Chapter 10 ([9]) presents a general framework for cooperative control of autonomous vehicles, satisfying limited-bandwidth, short range and asynchronous communication requirements ([9]). The presented algorithm proposes the use of additional computing power to allow for significantly reduced bandwidth utilization. Cooperation between vehicles is obtained through coupling of their respective reference systems. This technique of introducing coupling through a reference system is referred to as indirect cooperation. It has been successfully applied to the control of dynamically interconnected systems ([71–73]), but has yet to be applied to cooperative control of autonomous vehicles.

Future Research

While the results presented in this dissertation form a solid framework for control of unmanned vehicles, the proposed solutions could be extended and improved in a number of ways. Suggestions for future research are offered in Chapter 11.

Chapter 2

Adaptive Control for Nonlinear Uncertain Systems with Actuator Amplitude and Rate Saturation Constraints [1]

The result presented in this chapter was the object of an article published in the International Journal of Adaptive Control and Signal Processing in January 2009 ([1]). This work was also presented at the 2007 ASME International Mechanical Engineering Conference and Exposition ([74]).

2.1. Introduction

In light of the increasingly complex and highly uncertain nature of dynamical systems requiring controls, it is not surprising that reliable system models for many high performance engineering applications are unavailable. While model based control techniques have shown their efficacy in solving a considerable number of problems, uncertainty of the considered system's model complicates the control problem. Robust controllers can be used to address

issues stemming from such uncertainties. However, they may unnecessarily sacrifice system performance. Adaptive controllers offer similar benefits, but can tolerate greater system uncertainty levels and provide improved closed-loop performance. However, an implicit assumption inherent to most adaptive control frameworks is that the adaptive control law is implemented without any regard to actuator amplitude and rate saturation constraints. In practice, electromechanical control actuation devices are subject to amplitude and/or rate constraints, leading to saturation nonlinearities reflecting the corresponding limitations on control amplitudes and control rates. As a consequence, actuator nonlinearities arise frequently in practice and can severely degrade closed-loop system performance, in some cases driving the system to instability.

In this chapter, a direct adaptive control framework for adaptive tracking of multivariable nonlinear uncertain systems with amplitude and rate saturation constraints is presented. In particular, the Lyapunov-based direct adaptive control framework developed in [75, 76] is extended to guarantee asymptotic stability of the closed-loop tracking system; that is, asymptotic stability with respect to the closed-loop system states associated with the tracking error dynamics in spite of actuator amplitude and rate saturation constraints. More specifically, a reference (governor or supervisor) dynamical system is constructed to address tracking and regulation by deriving adaptive update laws that guarantee that the error system dynamics are asymptotically stable, and the adaptive controller gains are Lyapunov stable. In the case where the actuator amplitude and rate are limited, the adaptive control signal to the reference system is modified to effectively robustify the error dynamics to the saturation constraints, thus guaranteeing asymptotic stability of the error states.

This chapter is organized as follows. Section 2.2 introduces a nonlinear control law rel-

evant to a wide variety of systems. Using a direct adaptive control technique, the control algorithm is then extended to account for parametric uncertainties in the system model. The controller is further modified in Section 2.3, in which a dynamic compensator is used to generate the control command. Section 2.4 describes the algorithm allowing the controller derived in Section 2.3 to account for amplitude and rate saturation of the command. Numerical simulation results are presented in Section 2.5. Section 2.6 concludes this chapter.

2.2. Adaptive Tracking for Nonlinear Uncertain Systems

In this section, the problem of characterizing adaptive feedback tracking control laws for a general class of nonlinear uncertain systems is considered. Specifically, the controlled nonlinear uncertain system $\mathcal{G}$, given by

$$\dot{x}(t) = f(x(t)) + Bu(t), \qquad x(0) = x_0, \qquad t \geq 0, \tag{2.1}$$

will be considered, where $x(t) \in \mathbb{R}^n$, $t \geq 0$, is the state vector, $u(t) \in \mathbb{R}^m$, $t \geq 0$, is the control input, $f : \mathbb{R}^n \to \mathbb{R}^n$, the matrix $B \in \mathbb{R}^{n \times m}$ is of the form $B = \left[\begin{array}{cc} 0_{m \times (n-m)} & B_{\mathrm{s}}^{\mathrm{T}} \end{array} \right]^{\mathrm{T}}$, with $B_{\mathrm{s}} \in \mathbb{R}^{m \times m}$ full rank and such that there exists $\Lambda \in \mathbb{R}^{m \times m}$ for which $B_{\mathrm{s}}\Lambda$ is positive definite. The control input $u(\cdot)$ in (2.1) is restricted to the class of admissible controls such that (2.1) has a unique solution forward in time. Here, it is assumed that a desired trajectory $x_{\mathrm{d}}(t)$, $t \geq 0$, is given and the aim is to determine the control input $u(t)$, $t \geq 0$, so that $\lim_{t \to \infty} \| x(t) - x_{\mathrm{d}}(t) \| = 0$.

In order to achieve this, a reference system $\mathcal{G}_{\mathrm{r}}$ is constructed. It is given by

$$\dot{x}_{\mathrm{r}1}(t) = A_{\mathrm{r}} x_{\mathrm{r}1}(t) + B_{\mathrm{r}} r(t), \qquad x_{\mathrm{r}1}(0) = x_{\mathrm{r}1_0}, \qquad t \geq 0, \tag{2.2}$$

where $x_{\mathrm{r}1}(t) \in \mathbb{R}^n$, $t \geq 0$, is the reference state vector, $r(t) \in \mathbb{R}^m$, $t \geq 0$, is the reference input, and $A_{\mathrm{r}} \in \mathbb{R}^{n \times n}$ and $B_{\mathrm{r}} \in \mathbb{R}^{n \times m}$ are such that the pair $(A_{\mathrm{r}}, B_{\mathrm{r}})$ is stabilizable. In the following, a command $u(t)$, $t \geq 0$, and a bounded piecewise continuous reference function $r(t)$, $t \geq 0$, will be designed such that $\lim_{t \to \infty} \|x(t) - x_{\mathrm{r}1}(t)\| = 0$ and $\lim_{t \to \infty} \|x_{\mathrm{r}1}(t) - x_{\mathrm{d}}(t)\| = 0$, respectively, so that $\lim_{t \to \infty} \|x(t) - x_{\mathrm{d}}(t)\| = 0$. Theorem 2.2.1 provides a control architecture that achieves tracking error convergence in the case where the dynamics in (2.1) are known. The case where $\mathcal{G}$ is uncertain is addressed in Theorem 2.2.2. The statement of this result requires definition of the tracking error $e(t) \triangleq x(t) - x_{\mathrm{r}1}(t)$, $t \geq 0$, whose dynamics are described by

$$\dot{e}(t) = (f(x(t)) + Bu(t)) - (A_{\mathrm{r}} x_{\mathrm{r}1}(t) + B_{\mathrm{r}} r(t)), \qquad e(0) = x_0 - x_{\mathrm{r}_0} \triangleq e_0, \qquad t \geq 0. \quad (2.3)$$

Theorem 2.2.1. Consider the nonlinear system $\mathcal{G}$ given by (2.1) and the reference system $\mathcal{G}_{\mathrm{r}}$ given by (2.2). Assume there exist gain matrices $\Theta^* \in \mathbb{R}^{m \times s}$ and $\Theta_{\mathrm{r}}^* \in \mathbb{R}^{m \times m}$, and a continuously differentiable function $F : \mathbb{R}^n \to \mathbb{R}^s$ such that

$$0 = f(x) + B\Lambda\Theta^* F(x) - A_{\mathrm{r}} x, \qquad x \in \mathbb{R}^n, \quad (2.4)$$

$$0 = B\Lambda\Theta_{\mathrm{r}}^* - B_{\mathrm{r}}. \quad (2.5)$$

Furthermore, let $K \in \mathbb{R}^{m \times n}$ be given by

$$K = -R_2^{-1} B_{\mathrm{r}}^{\mathrm{T}} P, \quad (2.6)$$

where the $n \times n$ positive definite matrix P satisfies

$$0 = A_{\mathrm{r}}^{\mathrm{T}} P + P A_{\mathrm{r}} - P B_{\mathrm{r}} R_2^{-1} B_{\mathrm{r}}^{\mathrm{T}} P + R_1 \quad (2.7)$$

and $R_1 \in \mathbb{R}^{n \times n}$ and $R_2 \in \mathbb{R}^{m \times m}$ are arbitrary positive definite matrices. Then the feedback control law

$$u(t) = \Lambda \left(\Theta_1^* \varphi_1(t) + \Theta_{\mathrm{r}}^* r(t) \right), \qquad t \geq 0, \quad (2.8)$$

where

$$\Theta_1^* \triangleq \left[\begin{array}{ccc} \Theta^*, & \Theta_{\mathrm{r}}^*, & \Lambda^{\mathrm{T}} B^{\mathrm{T}} \end{array} \right] \in \mathbb{R}^{m \times (m+n+s)}, \tag{2.9}$$

$$\varphi_1(t) \triangleq \left[\begin{array}{ccc} F^{\mathrm{T}}(x(t)), & e^{\mathrm{T}}(t) K^{\mathrm{T}}, & -\frac{1}{2} k_\lambda e^{\mathrm{T}}(t) P \end{array} \right]^{\mathrm{T}} \in \mathbb{R}^{m+n+s}, \ t \geq 0, \tag{2.10}$$

with $k_\lambda > 0$, guarantees that the zero solution $e(t) \equiv 0$, $t \geq 0$, of the error dynamics given by (2.3) is globally asymptotically stable.

Proof. Substituting the feedback control law given by (2.8) into (2.3), we obtain

$$\dot{e}(t) = f(x(t)) + B\Lambda\Theta_1^*\varphi_1(t) + B\Lambda\Theta_{\mathrm{r}}^* r(t) - A_{\mathrm{r}} x_{\mathrm{r}1}(t) - B_{\mathrm{r}} r(t), \quad e(0) = e_0, \quad t \geq 0, \tag{2.11}$$

which, using (2.9) and (2.10), can be rewritten as

$$\begin{aligned} \dot{e}(t) = {} & \Big(A_{\mathrm{r}} + B\Lambda\Theta_{\mathrm{r}}^* K - \frac{1}{2} k_\lambda B\Lambda\Lambda^{\mathrm{T}} B^{\mathrm{T}} P \Big) e(t) + (f(x(t)) + B\Lambda\Theta^* F(x(t)) - A_{\mathrm{r}} x(t)) \\ & + (B\Lambda\Theta_{\mathrm{r}}^* - B_{\mathrm{r}})\, r(t), \quad e(0) = e_0, \quad t \geq 0. \end{aligned} \tag{2.12}$$

Now, using (2.4) and (2.5), it follows from (2.12) that

$$\dot{e}(t) = (A_{\mathrm{r}} + B_{\mathrm{r}} K - \frac{1}{2} k_\lambda B\Lambda\Lambda^{\mathrm{T}} B^{\mathrm{T}} P) e(t), \qquad e(0) = e_0, \qquad t \geq 0. \tag{2.13}$$

Next, consider the Lyapunov function candidate

$$V(e) = e^{\mathrm{T}} P e, \tag{2.14}$$

where $P > 0$ satisfies (2.7). Note that $V(0) = 0$ and, since P is positive definite, $V(e) > 0$ for all $e \neq 0$. Now, letting $e(t)$, $t \geq 0$, denote the solution to (2.13) and using (2.7), it follows from (2.13) that the Lyapunov derivative along the closed-loop system trajectories of (2.13) is given by

$$\dot{V}(e(t)) = -e^{\mathrm{T}}(t)(R_1 + K^{\mathrm{T}} R_2 K + K_e) e(t) < 0, \qquad t \geq 0, \tag{2.15}$$

where $K_e \triangleq k_\lambda PB\Lambda\Lambda^{\mathrm{T}}B^{\mathrm{T}}P \geq 0$. Hence, the zero solution $e(t) \equiv 0$ of the error dynamics given by (2.13) is globally asymptotically stable. □

Theorem 2.2.1 provides sufficient conditions for characterizing tracking controllers for a given nominal nonlinear dynamical system $\mathcal{G}$. The next result shows how to construct adaptive gains $\Theta_1(t) \in \mathbb{R}^{m\times(m+n+s)}$ and $\Theta_{\mathrm{r}}(t) \in \mathbb{R}^{m\times m}$, $t \geq 0$, which allow to achieve tracking control in spite of system uncertainty. This result does not require explicit knowledge of the gain matrices Θ^* and Θ_{r}^*; all that is required is the existence of Θ^* and Θ_{r}^* such that the matching conditions (2.4) and (2.5) hold.

Theorem 2.2.2. Consider the nonlinear system $\mathcal{G}$ given by (2.1) and the reference system $\mathcal{G}_{\mathrm{r}}$ given by (2.2). Assume there exist unknown gain matrices $\Theta^* \in \mathbb{R}^{m\times s}$ and $\Theta_{\mathrm{r}}^* \in \mathbb{R}^{m\times m}$, and a continuously differentiable function $F : \mathbb{R}^n \to \mathbb{R}^s$ such that (2.4) and (2.5) hold. Furthermore, let $K \in \mathbb{R}^{m\times n}$ be given by (2.6), where $P = \left[\begin{array}{cc} P_1 & P_2 \end{array}\right] > 0$ satisfies (2.7) with $P_1 \in \mathbb{R}^{n\times(n-m)}$ and $P_2 \in \mathbb{R}^{n\times m}$. In addition, let $\Gamma_1 \in \mathbb{R}^{(m+n+s)\times(m+n+s)}$ and $\Gamma_{\mathrm{r}} \in \mathbb{R}^{m\times m}$ be positive definite. Then the adaptive feedback control law

$$u(t) = \Lambda\left(\Theta_1(t)\varphi_1(t) + \Theta_{\mathrm{r}}(t)r(t)\right), \qquad t \geq 0, \tag{2.16}$$

where $\Theta_1(t) \in \mathbb{R}^{m\times(m+n+s)}$, $t \geq 0$, and $\Theta_{\mathrm{r}}(t) \in \mathbb{R}^{m\times m}$, $t \geq 0$, are estimates of Θ_1^* and Θ_{r}^*, respectively, with update laws

$$\dot{\Theta}_1(t) = -P_2^{\mathrm{T}}e(t)\varphi_1^{\mathrm{T}}(t)\Gamma_1, \qquad \Theta_1(0) = \Theta_{10}, \qquad t \geq 0, \tag{2.17}$$

$$\dot{\Theta}_{\mathrm{r}}(t) = -P_2^{\mathrm{T}}e(t)r^{\mathrm{T}}(t)\Gamma_{\mathrm{r}}, \qquad \Theta_{\mathrm{r}}(0) = \Theta_{\mathrm{r}0}, \tag{2.18}$$

guarantees that the closed-loop system given by (2.3), (2.17), and (2.18), with control input (2.16), is Lyapunov stable, and $e(t) \to 0$ as $t \to \infty$.

Proof. With $u(t)$, $t \geq 0$, given by (2.16) it follows from (2.4) and (2.5) that the error dynamics $e(t)$, $t \geq 0$, are given by

$$\dot{e}(t) = (A_{\mathrm{r}} + B_{\mathrm{r}}K - \frac{1}{2}k_\lambda B\Lambda\Lambda^{\mathrm{T}}B^{\mathrm{T}}P)e(t) + B\Lambda\left(\Theta_1(t) - \Theta_1^*\right)\varphi_1(t) + B\Lambda\left(\Theta_{\mathrm{r}}(t) - \Theta_{\mathrm{r}}^*\right)r(t), \quad e(0) = e_0, \quad t \geq 0. \tag{2.19}$$

Now, consider the Lyapunov function candidate

$$V(e, \Theta_1, \Theta_{\mathrm{r}}) = e^{\mathrm{T}}Pe + \mathrm{tr}\left[B_{\mathrm{s}}\Lambda(\Theta_1 - \Theta_1^*)\Gamma_1^{-1}(\Theta_1^{\mathrm{T}} - \Theta_1^{*\mathrm{T}})\right] + \mathrm{tr}\left[B_{\mathrm{s}}\Lambda(\Theta_{\mathrm{r}} - \Theta_{\mathrm{r}}^*)\Gamma_{\mathrm{r}}^{-1}(\Theta_{\mathrm{r}}^{\mathrm{T}} - \Theta_{\mathrm{r}}^{*\mathrm{T}})\right], \tag{2.20}$$

where $P > 0$ satisfies (2.7), and Γ_1 and Γ_{r} are positive definite. Note that $V(0, \Theta_1^*, \Theta_{\mathrm{r}}^*) = 0$ and, since P, Γ_1, Γ_{r}, and $B_{\mathrm{s}}\Lambda$ are positive definite, $V(e, \Theta_1, \Theta_{\mathrm{r}}) > 0$ for all $(e, \Theta_1, \Theta_{\mathrm{r}}) \neq (0, \Theta_1^*, \Theta_{\mathrm{r}}^*)$. Now, letting $e(t)$, $t \geq 0$, denote the solution to (2.19) and using (2.7), it follows that the Lyapunov derivative along the closed-loop system trajectories is given by

$$\begin{aligned}
\dot{V}(e(t), \Theta_1(t), \Theta_{\mathrm{r}}(t)) &= e^{\mathrm{T}}(t)P\dot{e}(t) + \dot{e}^{\mathrm{T}}(t)Pe(t) + 2\mathrm{tr}[B_{\mathrm{s}}\Lambda(\Theta_1(t) - \Theta_1^*)\Gamma_1^{-1}\dot{\Theta}_1^{\mathrm{T}}(t)] \\
&\quad + 2\mathrm{tr}[B_{\mathrm{s}}\Lambda(\Theta_{\mathrm{r}}(t) - \Theta_{\mathrm{r}}^*)\Gamma_{\mathrm{r}}^{-1}\dot{\Theta}_{\mathrm{r}}^{\mathrm{T}}(t)] \\
&= 2e^{\mathrm{T}}(t)PB\Lambda(\Theta_1(t) - \Theta_1^*)\varphi_1(t) + 2\mathrm{tr}[B_{\mathrm{s}}\Lambda(\Theta_1(t) - \Theta_1^*)\Gamma_1^{-1}\dot{\Theta}_1^{\mathrm{T}}(t)] \\
&\quad + 2e^{\mathrm{T}}(t)PB\Lambda(\Theta_{\mathrm{r}}(t) - \Theta_{\mathrm{r}}^*)r(t) + 2\mathrm{tr}[B_{\mathrm{s}}\Lambda(\Theta_{\mathrm{r}}(t) - \Theta_{\mathrm{r}}^*)\Gamma_{\mathrm{r}}^{-1}\dot{\Theta}_{\mathrm{r}}^{\mathrm{T}}(t)] \\
&\quad + e^{\mathrm{T}}(t)P(A_{\mathrm{r}} + B_{\mathrm{r}}K)e(t) + e^{\mathrm{T}}(t)(A_{\mathrm{r}} + B_{\mathrm{r}}K)^{\mathrm{T}}Pe(t) - e^{\mathrm{T}}(t)K_e e(t).
\end{aligned} \tag{2.21}$$

Next, using (2.17) and (2.18) and the fact that $PB = P_2B_{\mathrm{s}}$, we obtain

$$\begin{aligned}
\dot{V}(e(t), \Theta_1(t), \Theta_{\mathrm{r}}(t)) &= -e^{\mathrm{T}}(t)(R_1 + K^{\mathrm{T}}R_2K + K_e)e(t) + 2\mathrm{tr}[B_{\mathrm{s}}\Lambda(\Theta_1(t) - \Theta_1^*)(\varphi_1(t)e^{\mathrm{T}}(t)P_2 \\
&\quad + \Gamma_1^{-1}\dot{\Theta}_1^{\mathrm{T}}(t))] + 2\mathrm{tr}[B_{\mathrm{s}}\Lambda(\Theta_{\mathrm{r}}(t) - \Theta_{\mathrm{r}}^*)(r(t)e^{\mathrm{T}}(t)P_2 + \Gamma_{\mathrm{r}}^{-1}\dot{\Theta}_{\mathrm{r}}^{\mathrm{T}}(t))] \\
&= -e^{\mathrm{T}}(t)(R_1 + K^{\mathrm{T}}R_2K + K_e)e(t) \leq 0, \quad t \geq 0.
\end{aligned} \tag{2.22}$$

Hence, the closed-loop system given by (2.3) and (2.16)–(2.18) is Lyapunov stable, and, by the LaSalle-Yoshizawa theorem ([10], see also Appendix A), $\lim_{t\to\infty} e^{\mathrm{T}}(t)(R_1 + K^{\mathrm{T}}R_2K + K_e)e(t) = 0$, and hence, $\lim_{t\to\infty} e(t) = 0$. □

Remark 2.2.1. Note that the conditions in Theorem 2.2.2 imply that $e(t) \to 0$ as $t \to \infty$, and hence, it follows from (2.17) and (2.18) that $\dot{\Theta}_1(t) \to 0$ and $\dot{\Theta}_{\mathrm{r}}(t) \to 0$ as $t \to \infty$.

It is important to note that the adaptive law (2.16)–(2.18) does *not* require explicit knowledge of the gain matrices Θ^* and Θ_{r}^*. Furthermore, no specific knowledge of the structure of the nonlinear dynamics $f(x)$ or the input matrix B are required to apply Theorem 2.2.2; all that is required is the existence of $F(x)$ and Λ such that the matching conditions (2.4) and (2.5) hold for a given reference system $\mathcal{G}_{\mathrm{r}}$. If (2.1) is in normal form with asymptotically stable internal dynamics [77], then a function $F : \mathbb{R}^n \to \mathbb{R}^s$, matrix $\Lambda \in \mathbb{R}^{m\times m}$, and stabilizable pair $(A_{\mathrm{r}}, B_{\mathrm{r}})$ such that (2.4) and (2.5) hold *without* requiring knowledge of the system dynamics can always be constructed. In order to see this, assume that the nonlinear uncertain system $\mathcal{G}$ is generated by

$$q_i^{(r_i)}(t) = f_{\mathrm{u}i}(q(t)) + b_i u(t), \qquad q(0) = q_0, \qquad t \geq 0, \qquad i = 1, \ldots, m, \tag{2.23}$$

where $q_i^{(r_i)}$ denotes the r_i^{th} time derivative of q_i, r_i denotes the relative degree with respect to the output q_i, $f_{\mathrm{u}i}(q) = f_{\mathrm{u}i}(q_1, \ldots, q_1^{(r_1-1)}, \ldots, q_m, \ldots, q_m^{(r_m-1)})$, the row vector $b_i \in \mathbb{R}^m$, and $q \in \mathbb{R}^{\hat{r}}$, where $\hat{r} = r_1 + \ldots + r_m$ is the (vector) relative degree of (2.23). Furthermore, since (2.23) is in a form where it does not possess internal dynamics, it follows that $\hat{r} = n$. The case where (2.23) possesses input-to-state stable internal dynamics can be handled as shown in [75].

Next, define $x_i \triangleq \Big[\, q_i, \ldots, q_i^{(r_i-2)} \Big]^{\mathrm{T}}$, $x_{m+1} \triangleq \Big[\, q_1^{(r_1-1)}, \ldots, q_m^{(r_m-1)} \Big]^{\mathrm{T}}$, and $x \triangleq \big[\, x_1^{\mathrm{T}}, \ldots, x_{m+1}^{\mathrm{T}} \big]^{\mathrm{T}}$, $i = 1, \ldots, m$, so that (2.23) can be described as (2.1) with

$$f(x) = \tilde{A}x + \tilde{f}_{\mathrm{u}}(x), \qquad B_{\mathrm{s}} = \left[\begin{array}{ccc} b_1^{\mathrm{T}} & \ldots & b_m^{\mathrm{T}} \end{array}\right]^{\mathrm{T}}, \tag{2.24}$$

where

$$\tilde{A} = \left[\begin{array}{c} A_0 \\ 0_{m\times n} \end{array}\right], \qquad \tilde{f}_{\mathrm{u}}(x) = \left[\begin{array}{c} 0_{(n-m)\times 1} \\ f_{\mathrm{u}}(x) \end{array}\right],$$

$A_0 \in \mathbb{R}^{(n-m)\times n}$ is a known matrix of zeros and ones capturing the multivariable controllable canonical form representation [78], and $f_{\mathrm{u}} : \mathbb{R}^n \to \mathbb{R}^m$ and $B \in \mathbb{R}^{m\times m}$ are unknown. In addition, $f_{\mathrm{u}}(x)$ can be parameterized as follows, $f_{\mathrm{u}}(x) = \Theta_{\ell} x + \Theta_{n\ell} f_{n\ell}(x)$, where $f_{n\ell} : \mathbb{R}^n \to \mathbb{R}^q$, $x \in \mathbb{R}^n$, and $\Theta_{\ell} \in \mathbb{R}^{m\times n}$ and $\Theta_{n\ell} \in \mathbb{R}^{m\times q}$ are uncertain constant matrices.

Next, to apply Theorem 2.2.2 to the uncertain system (2.1) with $f(x)$ and B_{s} given by (2.24), let $B_{\mathrm{r}} = \big[0_{m\times(n-m)}\, B_{\mathrm{rs}}^{\mathrm{T}}\big]^{\mathrm{T}}$, where $B_{\mathrm{rs}} \in \mathbb{R}^{m\times m}$, let $A_{\mathrm{r}} = \big[A_0^{\mathrm{T}},\, \Theta_{\mathrm{n}}^{\mathrm{T}}\big]^{\mathrm{T}}$, where $\Theta_{\mathrm{n}} \in \mathbb{R}^{m\times n}$ is a known matrix, let $\Theta^* \in \mathbb{R}^{m\times(n+q)}$ be given by

$$\Theta^* = (B_{\mathrm{s}}\Lambda)^{-1}[\, \Theta_{\mathrm{n}} - \Theta_{\ell},\, -\Theta_{n\ell}\,], \tag{2.25}$$

and let

$$F(x) = \left[\begin{array}{c} x \\ f_{n\ell}(x) \end{array}\right]. \tag{2.26}$$

In this case, it follows that, with $\Theta_{\mathrm{r}}^* = (B_{\mathrm{s}}\Lambda)^{-1} B_{\mathrm{rs}}$,

$$B\Lambda\Theta_{\mathrm{r}}^* = B_{\mathrm{r}} \tag{2.27}$$

and

$$\begin{aligned} f(x) + B\Lambda\Theta^* F(x) &= \tilde{A}x + \tilde{f}_{\mathrm{u}}(x) + \left[\begin{array}{c} 0_{(n-m)\times m} \\ B_{\mathrm{s}} \end{array}\right] \Lambda (B_{\mathrm{s}}\Lambda)^{-1} \left[\begin{array}{c} \Theta_{\mathrm{n}}x - \Theta_{\ell}x - \Theta_{n\ell} f_{n\ell}(x) \end{array}\right] \\ &= \tilde{A}x + \left[\begin{array}{c} 0_{(n-m)\times 1} \\ \Theta_{\mathrm{n}} x \end{array}\right] = A_{\mathrm{r}} x, \end{aligned} \tag{2.28}$$

where A_{r} is in multivariable controllable canonical form. Hence, choosing A_{r} and B_{r} such that $(A_{\mathrm{r}}, B_{\mathrm{r}})$ is stabilizable and choosing $R_1 > 0$ and $R_2 > 0$, it follows that there exists a positive definite matrix P satisfying the Riccati equation (2.7).

2.3. Dynamic Adaptive Tracking for Nonlinear Uncertain Systems

In this section, the results of Section 2.2 are extended by constructing an adaptive, dynamic controller for (2.1), with stability properties identical to those given by Theorem 2.2.2. The ultimate objective is to be able to account for both amplitude and rate saturation constraints in the control input. In order to be able to account for rate saturation, it is necessary to consider the time derivative of the command $u(t)$, $t \geq 0$. Amplitude saturation will be accounted for by setting this time derivative to zero. To that end, the command $u(t)$, $t \geq 0$, will be generated by a dynamic compensator of the form

$$\dot{x}_{\mathrm{c}}(t) = f_{\mathrm{c}}(x(t), x_{\mathrm{r}}(t), x_{\mathrm{c}}(t)), \qquad x_{\mathrm{c}}(0) = x_{\mathrm{c}0}, \qquad t \geq 0, \tag{2.29}$$

$$u(t) = x_{\mathrm{c}}(t), \tag{2.30}$$

where $x_{\mathrm{c}}(t) \in \mathbb{R}^m$, $t \geq 0$, is the compensator state, $x(t) \in \mathbb{R}^n$, $t \geq 0$, is the system state, $x_{\mathrm{r}}(t) \in \mathbb{R}^{m+n}$, $t \geq 0$, is a reference state, and $f_{\mathrm{c}} : \mathbb{R}^n \times \mathbb{R}^{m+n} \times \mathbb{R}^m \to \mathbb{R}^m$. In order to account for the compensator state, the reference system (2.2) is modified as

$$\dot{x}_{\mathrm{r}}(t) = \left[\begin{array}{cc} A_{\mathrm{r}} & B_{\mathrm{r}} \\ 0_{m\times n} & -T_{\mathrm{r}}^{-1} \end{array} \right] x_{\mathrm{r}}(t) + \left[\begin{array}{c} 0_{n\times m} \\ T_{\mathrm{r}}^{-1} \end{array} \right] r(t), \qquad x_{\mathrm{r}}(0) = \left[\begin{array}{c} x_{\mathrm{r}1_0} \\ x_{\mathrm{r}2_0} \end{array} \right], \qquad t \geq 0, \tag{2.31}$$

where $x_{\mathrm{r}}(t) = \left[\begin{array}{cc} x_{\mathrm{r}1}^{\mathrm{T}}(t) & x_{\mathrm{r}2}^{\mathrm{T}}(t) \end{array} \right]^{\mathrm{T}}$, $t \geq 0$, with $x_{\mathrm{r}1}(t) \in \mathbb{R}^n$, $x_{\mathrm{r}2}(t) \in \mathbb{R}^m$, $t \geq 0$, and $T_{\mathrm{r}} \in \mathbb{R}^{m\times m}$ is positive definite.

Next, consider the following desired control input, which is identical to the expression of

$u(t)$, $t \geq 0$, obtained in the previous section, given by

$$u_{\mathrm{d}}^*(t) \triangleq \Lambda \left(\Theta_1^* \varphi_1(t) + \Theta_{\mathrm{r}}^* x_{\mathrm{r}2}(t) \right), \qquad t \geq 0, \tag{2.32}$$

where $u_{\mathrm{d}}^*(t)$, $t \geq 0$, is such that for $u(t) = u_{\mathrm{d}}^*(t)$, $t \geq 0$, Theorem 2.2.1 guarantees that $e(t)$, $t \geq 0$, converges to zero. In the classical backstepping literature (see for example [10]), this desired control input is referred to as a "virtual command." Note that $r(t)$, $t \geq 0$, in (2.8) is replaced by $x_{\mathrm{r}2}(t)$, $t \geq 0$, in (2.32) to account for the modification to the reference system. With this definition for $u_{\mathrm{d}}^*(t)$, $t \geq 0$, the error dynamics (2.3) become

$$\dot{e}(t) = (A_{\mathrm{r}} + B_{\mathrm{r}} K + K_e) e(t) + B \left(u(t) - u_{\mathrm{d}}^*(t) \right), \qquad e(0) = e_0, \qquad t \geq 0. \tag{2.33}$$

Defining the error $e_u^*(t) \triangleq u(t) - u_{\mathrm{d}}^*(t)$, $t \geq 0$, the remaining problem is to find the appropriate expression for $f_{\mathrm{c}}(\cdot)$ such that $e_u^*(t)$, $t \geq 0$, converges to zero.

Note that a number of constant parameters in (2.32) are uncertain and need to be estimated, with appropriate update laws similar to those in Theorem 2.2.2. Ultimately, the expression $u(t)$, $t \geq 0$, should converge to is given by

$$u_{\mathrm{d}}(t) = \Lambda \left(\Theta_1(t) \varphi_1(t) + \Theta_{\mathrm{r}}(t) x_{\mathrm{r}2}(t) \right), \qquad t \geq 0, \tag{2.34}$$

where $\Theta_1(t) \in \mathbb{R}^{m \times (m+n+s)}$ and $\Theta_{\mathrm{r}}(t) \in \mathbb{R}^{m \times m}$, $t \geq 0$, are estimates of Θ_1^* and Θ_{r}^*, respectively. To this end, define the tracking error $e_u(t) \triangleq u(t) - u_{\mathrm{d}}(t)$, $t \geq 0$.

Statement of the next result requires a closed form expression of $\dot{u}_{\mathrm{d}}(t)$, $t \geq 0$. Using the update laws given by Theorem 2.2.2, and $\Theta_1(t) = \left[\begin{array}{cc} \Theta_{11}(t) & \Theta_{12}(t) \end{array} \right]$, $t \geq 0$, with $\Theta_{11}(t) \in \mathbb{R}^{m \times s}$ and $\Theta_{12}(t) \in \mathbb{R}^{m \times (m+n)}$, $t \geq 0$, yields

$$\begin{aligned} \dot{u}_{\mathrm{d}}(t) = \Lambda \Big(& - P_2^{\mathrm{T}} e(t) \left(\varphi_1^{\mathrm{T}}(t) \Gamma_1 \varphi_1(t) + x_{\mathrm{r}2}^{\mathrm{T}}(t) \Gamma_{\mathrm{r}} x_{\mathrm{r}2}(t) \right) + \Theta_{11}(t) F'(x(t)) (f(x(t)) + B u(t)) \\ & + \Theta_{12}(t) \left[\begin{array}{c} K \\ -\frac{1}{2} k_\lambda P \end{array} \right] \dot{e}(t) + \Theta_{\mathrm{r}}(t) T_{\mathrm{r}}^{-1} \left(r(t) - x_{\mathrm{r}2}(t) \right) \Big), \qquad t \geq 0, \end{aligned} \tag{2.35}$$

where $F'(x(t))$ denotes the Fréchet derivative of $F(\cdot)$ at $x(t)$, $t \geq 0$, $\Gamma_1 \in \mathbb{R}^{(m+n+s)\times(m+n+s)}$, $\Gamma_{\mathrm{r}} \in \mathbb{R}^{m\times m}$, $\Gamma_1 > 0$, and $\Gamma_{\mathrm{r}} > 0$. Note that the above expression can be rewritten as

$$\dot{u}_{\mathrm{d}}(t) \,=\, g(t) + h(t)\Theta_2^*\varphi_2(t), \qquad u_{\mathrm{d}}(0) = \Lambda\left(\Theta_{10}\varphi_1(0) + \Theta_{\mathrm{r}0}x_{\mathrm{r}2_0}\right), \qquad t \geq 0, \quad (2.36)$$

where

$$h(t) \triangleq \Lambda\Theta_1(t)\left[\begin{array}{c} F'(x(t)) \\ K \\ -\frac{1}{2}k_\lambda P \end{array}\right], \quad \Theta_2^* \triangleq B\left[\begin{array}{cc} -\Lambda\Theta^*, & I_m \end{array}\right], \quad \varphi_2(t) \triangleq \left[\begin{array}{c} F(x(t)) \\ u(t) \end{array}\right], \quad (2.37)$$

and

$$\begin{aligned} g(t) \triangleq \Lambda\Big(&- P_2^{\mathrm{T}}e(t)\left(\varphi_1^{\mathrm{T}}(t)\Gamma_1\varphi_1(t) + x_{\mathrm{r}2}^{\mathrm{T}}(t)\Gamma_{\mathrm{r}}x_{\mathrm{r}2}(t)\right) - \Theta_{12}(t)\left[\begin{array}{cc} K^{\mathrm{T}}, & -\frac{1}{2}k_\lambda P \end{array}\right]^{\mathrm{T}}\dot{x}_{\mathrm{r}1}(t) \\ &+\Theta_{\mathrm{r}}(t)T_{\mathrm{r}}^{-1}\left(r(t) - x_{\mathrm{r}2}(t)\right)\Big) + h(t)A_{\mathrm{r}}x(t). \end{aligned} \quad (2.38)$$

Note that (2.36) allows to isolate the unknown term Θ_2^* in $\dot{u}_{\mathrm{d}}(t)$, $t \geq 0$. In addition, (2.29), (2.30) and (2.36) yield the following expression for the time derivative of the new tracking error $e_u(t)$, $t \geq 0$,

$$\dot{e}_u(t) = f_{\mathrm{c}}(t) - g(t) - h(t)\Theta_2^*\varphi_2(t), \qquad e_u(0) = e_{u0}, \qquad t \geq 0. \quad (2.39)$$

By choosing $f_{\mathrm{c}}(t)$, $t \geq 0$, the error dynamics (2.39) can be reshaped as desired. In particular, if $\dot{e}_u(t)$, $t \geq 0$, is assigned, it follows from (2.39) that the corresponding dynamic compensator (2.29) is given by

$$f_{\mathrm{c}}(t) \,=\, g(t) + h(t)\Theta_2^*\varphi_2(t) + \dot{e}_u(t), \qquad t \geq 0. \quad (2.40)$$

The following result presents an expression for $f_{\mathrm{c}}(t)$, $t \geq 0$, which is similar to (2.40), with $\dot{e}_u(t)$, $t \geq 0$, replaced by an appropriate function which guarantees convergence of $e_u(t)$, $t \geq 0$, to zero.

Theorem 2.3.1. Consider the controlled nonlinear system $\mathcal{G}$ given by (2.1) and reference system (2.31). Assume there exist unknown gain matrices $\Theta^* \in \mathbb{R}^{m\times s}$ and $\Theta_{\mathrm{r}}^* \in \mathbb{R}^{m\times m}$, and a continuously differentiable function $F : \mathbb{R}^n \to \mathbb{R}^s$ such that (2.4) and (2.5) hold. Furthermore, let $K \in \mathbb{R}^{m\times n}$ be given by (2.6), where $P = \left[\begin{array}{cc} P_1 & P_2 \end{array}\right] > 0$ with $P_1 \in \mathbb{R}^{n\times(n-m)}$ and $P_2 \in \mathbb{R}^{n\times m}$, satisfies (2.7). Consider the control input $u(t)$, $t \geq 0$, generated by (2.29) and (2.30), where

$$f_{\mathrm{c}}(t) = g(t) + h(t)\Theta_2(t)\varphi_2(t) - 2\Theta_3(t)Pe(t) - K_u e_u(t), \qquad t \geq 0, \tag{2.41}$$

where $\varphi_2(t)$ and $h(t) \in \mathbb{R}^{m\times n}$, $t \geq 0$, are given by (2.37), $g(t) \in \mathbb{R}^m$, $t \geq 0$, is given by (2.38), $K_u \in \mathbb{R}^{m\times m}$ is positive definite, and $\Theta_2(t)$ and $\Theta_3(t)$, $t \geq 0$, are estimates of Θ_2^* and $\Theta_3^* \triangleq B^{\mathrm{T}} \in \mathbb{R}^{m\times n}$, respectively. The estimates $\Theta_1(t) \in \mathbb{R}^{m\times(m+n+s)}, \Theta_{\mathrm{r}}(t) \in \mathbb{R}^{m\times m}$, $\Theta_2(t) \in \mathbb{R}^{n\times(m+s)}$, and $\Theta_3(t) \in \mathbb{R}^{m\times n}$, $t \geq 0$, are given by

$$\dot{\Theta}_1(t) = -P_2^{\mathrm{T}} e(t)\varphi_1^{\mathrm{T}}(t)\Gamma_1, \qquad \Theta_1(0) = \Theta_{10}, \qquad t \geq 0, \tag{2.42}$$

$$\dot{\Theta}_{\mathrm{r}}(t) = -P_2^{\mathrm{T}} e(t)x_{\mathrm{r}2}^{\mathrm{T}}(t)\Gamma_{\mathrm{r}}, \qquad \Theta_{\mathrm{r}}(0) = \Theta_{\mathrm{r}0}, \tag{2.43}$$

$$\dot{\Theta}_2(t) = -h(t)^{\mathrm{T}} e_u(t)\varphi_2^{\mathrm{T}}(t)\Gamma_2, \quad \Theta_2(0) = \Theta_{20}, \tag{2.44}$$

$$\dot{\Theta}_3(t) = e_u(t)e^{\mathrm{T}}(t)P\Gamma_3, \qquad \Theta_3(0) = \Theta_{30}, \tag{2.45}$$

where $\Gamma_1 \in \mathbb{R}^{(m+n+s)\times(m+n+s)}$, $\Gamma_{\mathrm{r}} \in \mathbb{R}^{m\times m}$, $\Gamma_2 \in \mathbb{R}^{(m+s)\times(m+s)}$, and $\Gamma_3 \in \mathbb{R}^{n\times n}$ are positive definite matrices. In this case, the control input $u(t)$, $t \geq 0$, generated by (2.29) and (2.30) with (2.41), guarantees that the closed-loop system given by (2.3), (2.42)–(2.45), is Lyapunov stable and $(e(t), e_u(t)) \to (0, 0)$ as $t \to \infty$.

Proof. From (2.34) and the definition of $e_u(t)$, $t \geq 0$, it follows that

$$u(t) = \Lambda\left(\Theta_1(t)\varphi_1(t) + \Theta_{\mathrm{r}}(t)x_{\mathrm{r}2}(t)\right) + e_u(t), \qquad t \geq 0, \tag{2.46}$$

or, equivalently, using (2.10),

$$u(t) = \Lambda\left(\Theta^*F(x(t)) + \Theta_{\mathrm{r}}^*(x_{\mathrm{r}2}(t) + Ke(t))\right) - \frac{1}{2}k_\lambda\Lambda\Lambda^{\mathrm{T}}B^{\mathrm{T}}Pe(t) + \Lambda(\Theta_1(t) - \Theta_1^*)\varphi_1(t)$$
$$+\Lambda(\Theta_{\mathrm{r}}(t) - \Theta_{\mathrm{r}}^*)x_{\mathrm{r}2}(t) + e_u(t). \tag{2.47}$$

Substituting (2.4), (2.5), and (2.47) into (2.3), we obtain

$$\dot{e}(t) = (A_{\mathrm{r}} + B_{\mathrm{r}}K - \frac{1}{2}k_\lambda B\Lambda\Lambda^{\mathrm{T}}B^{\mathrm{T}}P)e(t) + B\Lambda(\Theta_1(t) - \Theta_1^*)\varphi_1(t) + B\Lambda(\Theta_{\mathrm{r}}(t) - \Theta_{\mathrm{r}}^*)x_{\mathrm{r}2}(t)$$
$$+Be_u(t), \quad e(0) = e_0, \quad t \geq 0. \tag{2.48}$$

Similarly, from (2.39), (2.41) and $\Theta_3^* = B^{\mathrm{T}}$, we obtain

$$\dot{e}_u(t) = -2B^{\mathrm{T}}Pe(t) - K_ue_u(t) + h(t)(\Theta_2(t) - \Theta_2^*)\varphi_2(t) + 2(\Theta_3^* - \Theta_3(t))Pe(t),$$
$$e_u(0) = e_{u0}, \quad t \geq 0. \tag{2.49}$$

Next, consider the Lyapunov function candidate

$$V(e, e_u, \Theta_1, \Theta_2, \Theta_3, \Theta_{\mathrm{r}}) = e^{\mathrm{T}}Pe + \frac{1}{2}e_u^{\mathrm{T}}e_u + \mathrm{tr}\left[B_{\mathrm{s}}\Lambda(\Theta_1 - \Theta_1^*)\Gamma_1^{-1}(\Theta_1^{\mathrm{T}} - \Theta_1^{*\mathrm{T}})\right]$$
$$+\mathrm{tr}\left[(\Theta_2 - \Theta_2^*)\Gamma_2^{-1}(\Theta_2^{\mathrm{T}} - \Theta_2^{*\mathrm{T}})\right] + \mathrm{tr}\left[(\Theta_3 - \Theta_3^*)\Gamma_3^{-1}(\Theta_3^{\mathrm{T}} - \Theta_3^{*\mathrm{T}})\right]$$
$$+\mathrm{tr}\left[B_{\mathrm{s}}\Lambda(\Theta_{\mathrm{r}} - \Theta_{\mathrm{r}}^*)\Gamma_{\mathrm{r}}^{-1}(\Theta_{\mathrm{r}}^{\mathrm{T}} - \Theta_{\mathrm{r}}^{*\mathrm{T}})\right], \tag{2.50}$$

where $P > 0$ satisfies (2.7). Note that $V(0, 0, \Theta_1^*, \Theta_2^*, \Theta_3^*, \Theta_{\mathrm{r}}^*) = 0$ and, since P, Γ_1, Γ_2, Γ_3, Γ_{r}, and $B_{\mathrm{s}}\Lambda$ are positive definite, $V(e, e_u, \Theta_1, \Theta_2, \Theta_3, \Theta_{\mathrm{r}}) > 0$ for all $(e, e_u, \Theta_1, \Theta_2, \Theta_3, \Theta_{\mathrm{r}}) \neq (0, 0, \Theta_1^*, \Theta_2^*, \Theta_3^*, \Theta_{\mathrm{r}}^*)$. Then, using (2.7) and (2.42)–(2.45), it follows that the Lyapunov derivative along the closed-loop system trajectories is given by

$$\dot{V}(e(t), e_u(t), \Theta_1(t), \Theta_2(t), \Theta_3(t), \Theta_{\mathrm{r}}(t)) = e^{\mathrm{T}}(t)P\dot{e}(t) + \dot{e}^{\mathrm{T}}(t)Pe(t) + e_u(t)^{\mathrm{T}}\dot{e}_u(t)$$
$$+2\mathrm{tr}[B_{\mathrm{s}}\Lambda(\Theta_1(t) - \Theta_1^*)\Gamma_1^{-1}\dot{\Theta}_1^{\mathrm{T}}(t)]$$

$$
\begin{aligned}
&+2\mathrm{tr}[(\Theta_3(t)-\Theta_3^*)\Gamma_3^{-1}\dot{\Theta}_3^{\mathrm{T}}(t)]\\
&+2\mathrm{tr}[B_{\mathrm{s}}\Lambda(\Theta_{\mathrm{r}}(t)-\Theta_{\mathrm{r}}^*)\Gamma_{\mathrm{r}}^{-1}\dot{\Theta}_{\mathrm{r}}^{\mathrm{T}}(t)]\\
&+2\mathrm{tr}[(\Theta_2(t)-\Theta_2^*)\Gamma_2^{-1}\dot{\Theta}_2^{\mathrm{T}}(t)]\\
=\;& e^{\mathrm{T}}(t)P(A_{\mathrm{r}}+B_{\mathrm{r}}K)e(t)+e^{\mathrm{T}}(t)(A_{\mathrm{r}}+B_{\mathrm{r}}K)^{\mathrm{T}}Pe(t)\\
&-e^{\mathrm{T}}(t)K_e e(t)-e_u^{\mathrm{T}}(t)K_u e_u(t)\\
&+2\mathrm{tr}[(\Theta_3(t)-\Theta_3^*)(\Gamma_3^{-1}\dot{\Theta}_3^{\mathrm{T}}(t)-Pe(t)e_u^{\mathrm{T}}(t))]\\
&+2\mathrm{tr}[B_{\mathrm{s}}\Lambda(\Theta_1(t)-\Theta_1^*)(\Gamma_1^{-1}\dot{\Theta}_1^{\mathrm{T}}(t)+\varphi_1(t)e^{\mathrm{T}}(t)P_2)]\\
&+2\mathrm{tr}[B_{\mathrm{s}}\Lambda(\Theta_{\mathrm{r}}(t)-\Theta_{\mathrm{r}}^*)(\Gamma_{\mathrm{r}}^{-1}\dot{\Theta}_{\mathrm{r}}^{\mathrm{T}}(t)+x_{\mathrm{r}2}(t)e^{\mathrm{T}}(t)P_2)]\\
&+2\mathrm{tr}[(\Theta_2(t)-\Theta_2^*)(\Gamma_2^{-1}\dot{\Theta}_2^{\mathrm{T}}(t)+\varphi_2(t)e_u^{\mathrm{T}}(t)h(t))]\\
=\;& -e^{\mathrm{T}}(t)(R_1+K^{\mathrm{T}}R_2K+K_e)e(t)-e_u^{\mathrm{T}}(t)K_u e_u(t)\\
\leq\;& 0, \qquad t\geq 0. \qquad (2.51)
\end{aligned}
$$

Hence, the closed-loop system given by (2.3), (2.39), (2.42)–(2.45) is Lyapunov stable. Furthermore, it follows from the LaSalle-Yoshizawa theorem [10] that $\lim_{t\to\infty} e^{\mathrm{T}}(t)(R_1 + K^{\mathrm{T}}R_2K + K_e)e(t) + e_u^{\mathrm{T}}(t)K_u e_u(t) = 0$, and hence $\lim_{t\to\infty} e(t) = 0$ and $\lim_{t\to\infty} e_u(t) = 0$. □

Remark 2.3.1. Note that a parallel can be drawn between (2.29) and the actuator dynamics of a physical system. In particular, the form of (2.29) was chosen to be an integrator for simplicity; however, (2.29) can be modified to represent the actuator dynamics of a particular system. Hence, the presented approach can account for actuator dynamics in the control framework.

The expression for $f_{\mathrm{c}}(\cdot)$ given by (2.41) implicitly depends upon the form of $\dot{u}_{\mathrm{d}}(t)$, $t \geq 0$. The control algorithm can be significantly simplified by using an estimate of $\dot{u}_{\mathrm{d}}(t)$, $t \geq 0$, as

detailed in the following corollary. The resulting control algorithm then guarantees ultimate boundedness of $e(t)$ and $e_u(t)$, $t \geq 0$; that is, convergence of $e(t)$ and $e_u(t)$, $t \geq 0$, to a neighborhood of the origin.

Corollary 2.3.1. Consider the controlled nonlinear system $\mathcal{G}$ given by (2.1) and reference system (2.31), and assume that the hypothesis of Theorem 2.3.1 hold with $k_\lambda > \lambda_{\min}(\Lambda\Lambda^{\mathrm{T}})$. In addition, define $u_{\mathrm{d}1}(t) \triangleq \Lambda\Theta_1(t)\varphi_1(t)$, $t \geq 0$, and assume that $\dot{u}_{\mathrm{d}1}(t)$, $t \geq 0$, can be approximated by $\dot{\nu}(t)$, $t \geq 0$, such that $\|u_{\mathrm{d}1}(t) - \nu(t)\| \leq \varepsilon \in \mathbb{R}$, $t \geq 0$. Finally, define $\hat{u}_{\mathrm{d}}(t) \triangleq \nu(t) + \Lambda\Theta_{\mathrm{r}}(t)x_{r2}(t)$ and $\hat{e}_u(t) \triangleq u(t) - \hat{u}_{\mathrm{d}}(t)$. Then, the control input generated by (2.29) and (2.30) with

$$f_{\mathrm{c}}(t) \;=\; f_{\hat{u}_{\mathrm{d}}}(t) - 2\Theta_3(t)Pe(t) - K_u\hat{e}_u(t), \tag{2.52}$$

where

$$f_{\hat{u}_{\mathrm{d}}}(t) \;\triangleq\; \dot{\nu}(t) + \Lambda\left(-P_2^{\mathrm{T}}e(t)x_{\mathrm{r}2}^{\mathrm{T}}(t)\Gamma_{\mathrm{r}}x_{\mathrm{r}2}(t) + \Theta_{\mathrm{r}}(t)T_{\mathrm{r}}^{-1}\left(r(t) - x_{\mathrm{r}2}(t)\right)\right), \qquad t \geq 0, \tag{2.53}$$

along with update laws (2.42), (2.43), and

$$\dot{\Theta}_3(t) \;=\; \hat{e}_u(t)e^{\mathrm{T}}(t)P\Gamma_3, \qquad \Theta_3(0) = \Theta_{30}, \qquad t \geq 0, \tag{2.54}$$

guarantees ultimate boundedness of the tracking errors $e(t)$ and $\hat{e}_u(t)$, $t \geq 0$, with an ultimate bound given by $\mathcal{D}_e \triangleq \{e, \hat{e}_u : e^{\mathrm{T}}(R_1 + K^{\mathrm{T}}R_2K)e + \hat{e}_u^{\mathrm{T}}K_u\hat{e}_u \leq \varepsilon^2\}$.

Proof. From the definitions of $u_{\mathrm{d}1}(t)$, $\hat{u}_{\mathrm{d}}(t)$, and $\hat{e}_u(t)$, $t \geq 0$, it follows that

$$u(t) = \Lambda\left(\Theta_1(t)\varphi_1(t) + \Theta_{\mathrm{r}}(t)x_{\mathrm{r}2}(t)\right) + \nu(t) - u_{\mathrm{d}1}(t) + \hat{e}_u(t), \qquad t \geq 0, \tag{2.55}$$

or, equivalently, using (2.10),

$$u(t) = \Lambda\left(\Theta^* F(x(t)) + \Theta_{\rm r}^*(x_{\rm r2}(t) + Ke(t))\right) - \frac{1}{2}k_\lambda \Lambda\Lambda^{\rm T} B^{\rm T} P e(t) + \Lambda(\Theta_1(t) - \Theta_1^*)\varphi_1(t) + \nu(t)$$
$$-u_{\rm d1}(t) + \Lambda(\Theta_{\rm r}(t) - \Theta_{\rm r}^*)x_{\rm r2}(t) + \hat{e}_u(t). \tag{2.56}$$

Substituting (2.4), (2.5), and (2.56) into (2.3), we obtain

$$\dot{e}(t) = (A_{\rm r} + B_{\rm r}K - \frac{1}{2}k_\lambda B\Lambda\Lambda^{\rm T}B^{\rm T}P)e(t) + B\Lambda(\Theta_1(t) - \Theta_1^*)\varphi_1(t) + B\Lambda(\Theta_{\rm r}(t) - \Theta_{\rm r}^*)x_{\rm r2}(t)$$
$$+B(\nu(t) - u_{\rm d1}(t)) + B\hat{e}_u(t), \qquad e(0) = e_0, \qquad t \geq 0. \tag{2.57}$$

Similarly, from (2.29), (2.30), (2.53), and the definition of $\hat{u}_{\rm d}(t)$ and $\hat{e}_u(t)$, $t \geq 0$, we obtain

$$\dot{\hat{e}}_u(t) = f_{\rm c}(t) - f_{\hat{u}_{\rm d}}(t), \qquad \hat{e}_u(0) = \hat{e}_{u0}, \qquad t \geq 0, \tag{2.58}$$

which, using (2.52) and $\Theta_3^* = B^{\rm T}$, can be rewritten as

$$\dot{\hat{e}}_u(t) = -2B^{\rm T}Pe(t) - K_u\hat{e}_u(t) + 2(\Theta_3^* - \Theta_3(t))Pe(t), \qquad \hat{e}_u(0) = \hat{e}_{u0}, \qquad t \geq 0. \tag{2.59}$$

Now, consider the Lyapunov function candidate

$$V_{\rm s}(e, \hat{e}_u, \Theta_1, \Theta_3, \Theta_{\rm r}) = e^{\rm T}Pe + \frac{1}{2}\hat{e}_u^{\rm T}\hat{e}_u + {\rm tr}\left[B_{\rm s}\Lambda(\Theta_1 - \Theta_1^*)\Gamma_1^{-1}(\Theta_1^{\rm T} - \Theta_1^{*\rm T})\right]$$
$$+{\rm tr}\left[(\Theta_3 - \Theta_3^*)\Gamma_3^{-1}(\Theta_3^{\rm T} - \Theta_3^{*\rm T})\right] + {\rm tr}\left[B_{\rm s}\Lambda(\Theta_{\rm r} - \Theta_{\rm r}^*)\Gamma_{\rm r}^{-1}(\Theta_{\rm r}^{\rm T} - \Theta_{\rm r}^{*\rm T})\right]. \tag{2.60}$$

Note that $V_{\rm s}(0, 0, \Theta_1^*, \Theta_3^*, \Theta_{\rm r}^*) = 0$ and, since P, Γ_1, Γ_3, $\Gamma_{\rm r}$, and $B_{\rm s}\Lambda$ are positive definite, we have $V_{\rm s}(e, \hat{e}_u, \Theta_1, \Theta_3, \Theta_{\rm r}) > 0$ for all $(e, \hat{e}_u, \Theta_1, \Theta_3, \Theta_{\rm r}) \neq (0, 0, \Theta_1^*, \Theta_3^*, \Theta_{\rm r}^*)$. Now, using (2.7), (2.42), (2.43), and (2.54), it follows that the Lyapunov derivative along the closed-loop system trajectories is given by

$$\dot{V}_{\rm s}(e(t), \hat{e}_u(t), \Theta_1(t), \Theta_3(t), \Theta_{\rm r}(t), t) = e^{\rm T}(t)P(A_{\rm r} + B_{\rm r}K)e(t) + e^{\rm T}(t)(A_{\rm r} + B_{\rm r}K)^{\rm T}Pe(t)$$

$$
\begin{aligned}
&-\hat{e}_u^{\mathrm{T}}(t)K_u\hat{e}_u(t) - k_\lambda e^{\mathrm{T}}(t)PB\Lambda\Lambda^{\mathrm{T}}B^{\mathrm{T}}Pe(t)\\
&+2\mathrm{tr}[B_{\mathrm{s}}\Lambda(\Theta_1(t)-\Theta_1^*)(\Gamma_1^{-1}\dot{\Theta}_1^{\mathrm{T}}(t)+\varphi_1(t)e^{\mathrm{T}}(t)P_2)]\\
&+2\mathrm{tr}[B_{\mathrm{s}}\Lambda(\Theta_{\mathrm{r}}(t)-\Theta_{\mathrm{r}}^*)(\Gamma_{\mathrm{r}}^{-1}\dot{\Theta}_{\mathrm{r}}^{\mathrm{T}}(t)+x_{\mathrm{r}2}(t)e^{\mathrm{T}}(t)P_2)]\\
&+2\mathrm{tr}[(\Theta_3(t)-\Theta_3^*)(\Gamma_3^{-1}\dot{\Theta}_3^{\mathrm{T}}(t)-Pe(t)\hat{e}_u^{\mathrm{T}}(t))]\\
&-2e^{\mathrm{T}}(t)PB(u_{\mathrm{d}1}(t)-\nu(t))\\
=\;& -e^{\mathrm{T}}(t)(R_1+K^{\mathrm{T}}R_2K)e(t)-2e^{\mathrm{T}}(t)PB(u_{\mathrm{d}1}(t)-\nu(t))\\
&-\hat{e}_u^{\mathrm{T}}(t)K_u\hat{e}_u(t)-k_\lambda e^{\mathrm{T}}(t)PB\Lambda\Lambda^{\mathrm{T}}B^{\mathrm{T}}Pe(t),\; t\geq 0, \quad (2.61)
\end{aligned}
$$

which, by completing the square, gives

$$
\begin{aligned}
\dot{V}_{\mathrm{s}}(e(t),\hat{e}_u(t),\Theta_1(t),\Theta_3(t),\Theta_{\mathrm{r}}(t),t) =\;& -e^{\mathrm{T}}(t)(R_1+K^{\mathrm{T}}R_2K)e(t)-\hat{e}_u^{\mathrm{T}}(t)K_u\hat{e}_u(t)\\
&-\|B^{\mathrm{T}}Pe(t)+(u_{\mathrm{d}1}(t)-\nu(t))\|^2+\|u_{\mathrm{d}1}(t)-\nu(t)\|^2\\
&-e^{\mathrm{T}}(t)PB\left(k_\lambda\Lambda\Lambda^{\mathrm{T}}-I_m\right)B^{\mathrm{T}}Pe(t), \qquad t\geq 0, \quad (2.62)
\end{aligned}
$$

where I_m is the $m\times m$ identity matrix. Since, by assumption, $\|u_{\mathrm{d}1}(t)-\nu(t)\|\leq\varepsilon$, $t\geq 0$, we obtain

$$
\begin{aligned}
\dot{V}_{\mathrm{s}}(e(t),\hat{e}_u(t),\Theta_1(t),\Theta_3(t),\Theta_{\mathrm{r}}(t),t) \leqslant\;& -e^{\mathrm{T}}(t)(R_1+K^{\mathrm{T}}R_2K)e(t)-\hat{e}_u^{\mathrm{T}}(t)K_u\hat{e}_u(t)+\varepsilon^2,\\
&t\geq 0. \quad (2.63)
\end{aligned}
$$

It follows from (2.63) that the Lyapunov derivative is strictly negative outside $\mathcal{D}_e$, which guarantees ultimate boundedness of $(e(t),\hat{e}_u(t))$, $t\geq 0$, with an ultimate bound given by $\mathcal{D}_e$ ([79, 80]). □

One technique which allows one to estimate the derivative of $u_{\mathrm{d}1}(t)$, $t\geq 0$, can be found in [56]. In particular, provided there exists $c>0$ such that $\dot{u}_{\mathrm{d}1}(t)\leq c$, $t\geq 0$, the technique

in [56] leads to an ε-estimate of $u_{\mathrm{d}1}(t)$, $t \geq 0$, and allows for the determination of an approximate value of c. More specifically, the algorithm in [56] can be used to approximate a signal $v(t)$ by $\nu(t)$, with bounded estimation error $s(t) \triangleq v(t) - \nu(t)$, $t \geq 0$, where $\nu(t)$, $t \geq 0$, is given by

$$\dot{\nu}(t) = k_0 \mathrm{sgn}(s(t)) + k_1(s(t) - \epsilon\,\mathrm{sat}(s(t)/\epsilon)) + k_2(t)\mathrm{sat}(s(t)/\epsilon)), \quad \nu(0) = \nu_0, \quad t \geq 0, \tag{2.64}$$

where the constants k_0, k_1 and ϵ are positive, $\mathrm{sgn}(s) \triangleq |s|/s$, for $s \neq 0$, and $\mathrm{sgn}(0) \triangleq 0$. In addition,

$$\mathrm{sat}(s) \triangleq \begin{cases} \mathrm{sgn}(s), & \text{for } \|s\| > 1, \\ s, & \text{for } \|s\| \leq 1, \end{cases} \tag{2.65}$$

and the gain $k_2(t)$, $t \geq 0$, is given by the update law

$$\dot{k}_2(t) = \begin{cases} \gamma\|s(t)\|, & \text{for } \|s\| > \epsilon, \\ 0, & \text{for } \|s\| \leq \epsilon, \end{cases} \qquad k_2(0) = k_{20}, \qquad t \geq 0, \tag{2.66}$$

with $\gamma > 0$. It is shown in [56] that, for sufficiently small $\eta > 0$, there exist $\epsilon < \eta$ and $t^* \geq 0$ such that $\|s(t)\| < \eta$, $t \geq t^*$.

2.4. Adaptive Tracking with Actuator Amplitude and Rate Saturation Constraints

In this section, the adaptive control framework presented in Section 2.3 is extended to account for actuator amplitude and rate saturation constraints, following the approach layed out in Figure 2.1. Recall that Theorem 2.2.2 guarantees asymptotic convergence of the tracking error $e(t)$, $t \geq 0$, to zero; that is, the state vector $x(t)$, $t \geq 0$, converges asymptotically to the reference state vector $x_{\mathrm{r}1}(t)$, $t \geq 0$. Furthermore, it is important to note that the compensator dynamics $f_{\mathrm{c}}(\cdot)$ given by (2.41) depend on the *reference input*

$r(t)$, $t \geq 0$, through $\dot{x}_{\mathrm{r}2}(t)$, $t \geq 0$. Since for a fixed set of initial conditions there exists a one-to-one mapping between the reference input $r(t)$, $t \geq 0$, and the reference state $x_{\mathrm{r}1}(t)$, $t \geq 0$, it follows that the control signal in (2.16) guarantees asymptotic convergence of the state $x(t)$, $t \geq 0$, to the reference state $x_{\mathrm{r}1}(t)$, $t \geq 0$, corresponding to the specified reference input $r(t)$, $t \geq 0$.

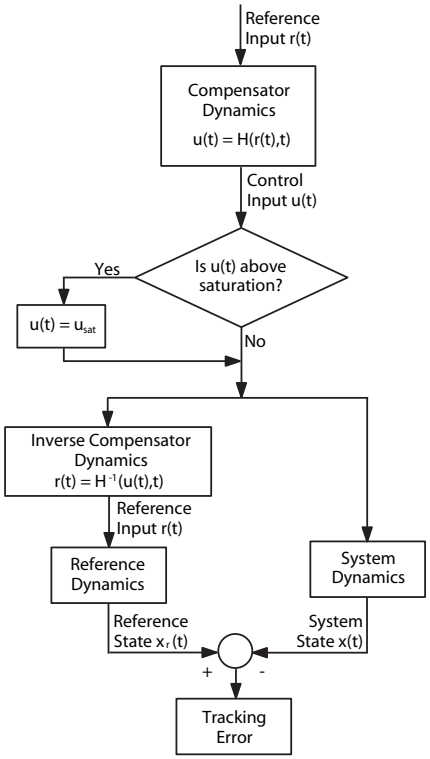

Figure 2.1: Saturation algorithm flowchart.

Of course, the reference input $r(t)$, $t \geq 0$, should be chosen so as to guarantee asymptotic convergence to a *desired* state vector $x_{\mathrm{d}}(t)$, $t \geq 0$. However, the choice of such a reference input $r(t)$, $t \geq 0$, is not unique since the reference state vector $x_{\mathrm{r}1}(t)$, $t \geq 0$, can converge to the desired state vector $x_{\mathrm{d}}(t)$, $t \geq 0$, without matching its transient behavior.

The following presents a framework wherein a family of reference inputs $r(t)$, $t \geq 0$, with associated reference state vectors $x_{\mathrm{r}1}(t)$, $t \geq 0$, are constructed and guarantee that a given reference state vector within this family converges to a desired state vector $x_{\mathrm{d}}(t)$, $t \geq 0$, in the face of actuator amplitude and rate saturation constraints.

From (2.29) and (2.30), it is clear that $\dot{u}(t)$, $t \geq 0$, is explicitly dependent on $f_{\mathrm{c}}(t)$, $t \geq 0$, which in turn depends upon the reference signal $r(t)$, $t \geq 0$. More specifically, from (2.29), (2.30), (2.38), and (2.41),

$$\dot{u}(t) = H(s(t), r(t))$$

$$= g_1(t) + h(t)\Theta_2(t)\varphi_2(t) - 2\Theta_3(t)Pe(t) - K_u e_u(t)$$
$$-\Lambda\Theta_{\rm r}(t)T_{\rm r}^{-1}r(t), \qquad t \geq 0, \tag{2.67}$$

where $s(t) \triangleq (x(t), x_{\rm r}(t), \Theta_{\rm r}(t), \Theta_2(t), \Theta_3(t), e(t), e_u(t))$ and

$$g_1(t) \triangleq \Lambda\Big(- P_2^{\rm T} e(t) \left(\varphi_1^{\rm T}(t)\Gamma_1\varphi_1(t) + x_{\rm r2}^{\rm T}(t)\Gamma_{\rm r}x_{\rm r2}(t)\right)$$
$$-\Theta_1(t) \left[\begin{array}{ccc} 0_{n\times s} & K^{\rm T} & -\frac{1}{2}k_\lambda P \end{array} \right]^{\rm T} \dot{x}_{\rm r1}(t) + \Theta_{\rm r}(t)T_{\rm r}^{-1}x_{\rm r2}(t)\Big)$$
$$+h(t)A_{\rm r}x(t). \tag{2.68}$$

Using (2.67), the reference input $r(t)$, $t \geq 0$, can be expressed as

$$r(t) = H^{-1}(s(t), \dot{u}(t))$$
$$= T_{\rm r}\Theta_{\rm r}^{-1}\Lambda^{-1}(g_1(t) + h(t)\Theta_2(t)\varphi_2(t) - 2\Theta_3(t)Pe(t)$$
$$-K_u e_u(t) - \dot{u}(t)). \tag{2.69}$$

The above expression relates the reference input to the time rate of change of the control input.

Next, it is assumed that the control signal is amplitude and rate limited so that $|u_i(t)| \leq u_{\max}$ and $|\dot{u}_i(t)| \leq \dot{u}_{\max}$, $t \geq 0$, $i = 1, \ldots, m$, where $u_i(t)$ and $\dot{u}_i(t)$ denote the ith component of $u(t)$ and $\dot{u}(t)$, respectively, and $u_{\max} > 0$ and $\dot{u}_{\max} > 0$ are given. Amplitude saturation of the command $u(t)$, $t \geq 0$, will be enforced by adjusting the rate of change of $u(t)$, $t \geq 0$, to zero. For the statement of the main result the following definitions are needed. For $i \in \{1, \ldots, m\}$ define

$$\sigma(u_i(t), \dot{u}_i(t)) \triangleq \left\{ \begin{array}{ll} 0 & \text{if } |u_i(t)| = u_{\max} \text{ and } u_i(t)\dot{u}_i(t) > 0, \qquad t \geq 0, \\ 1 & \text{otherwise,} \end{array} \right. \tag{2.70}$$

$$\sigma^*(u_i(t), \dot{u}_i(t)) \triangleq \min\left\{\sigma(u_i(t), \dot{u}_i(t)), \frac{\dot{u}_{\max}}{|\dot{u}_i(t)|}\right\}, \qquad t \geq 0. \tag{2.71}$$

Note that for $i \in \{1, \ldots, m\}$ and $t = t_1 > 0$, the function $\sigma^*(\cdot, \cdot)$ is such that the following properties hold:

i) If $|u_i(t_1)| = u_{\max}$ and $u_i(t_1)\dot{u}_i(t_1) > 0$, then $\dot{u}_i(t_1)\sigma^*(u_i(t_1), \dot{u}_i(t_1)) = 0$.

ii) If $|\dot{u}_i(t_1)| > \dot{u}_{\max}$ and $|u_i(t_1)| < u_{\max}$ or if $|\dot{u}_i(t_1)| > \dot{u}_{\max}$ and $|u_i(t_1)| = u_{\max}$ and $u_i(t_1)\dot{u}_i(t_1) \leq 0$, then $\dot{u}_i(t_1)\sigma^*(u_i(t_1), \dot{u}_i(t_1)) = \dot{u}_{\max}\mathrm{sgn}(\dot{u}_i(t_1))$,

iii) If no constraint is violated, then $\dot{u}_i(t_1)\sigma^*(u_i(t_1), \dot{u}_i(t_1)) = \dot{u}_i(t_1)$.

Finally, define the component decoupled diagonal nonlinearity $\Sigma(u, \dot{u})$ by

$$\Sigma(u(t), \dot{u}(t)) \triangleq \mathrm{diag}[\sigma^*(u_1(t), \dot{u}_1(t)), \sigma^*(u_2(t), \dot{u}_2(t)), \ldots, \sigma^*(u_m(t), \dot{u}_m(t))]. \quad (2.72)$$

Theorem 2.4.1. Consider the controlled nonlinear system $\mathcal{G}$ given by (2.1) and reference system (2.31). Assume there exist gain matrices $\Theta^* \in \mathbb{R}^{m \times s}$ and $\Theta_{\mathrm{r}}^* \in \mathbb{R}^{m \times m}$, and a continuously differentiable function $F : \mathbb{R}^n \to \mathbb{R}^s$ such that (2.4) and (2.5) hold. Furthermore, let $K \in \mathbb{R}^{m \times n}$ be given by (2.6), where $P > 0$ satisfies (2.7). In addition, for a given desired reference input $r_{\mathrm{d}}(t)$, $t \geq 0$, let the reference input $r(t)$, $t \geq 0$, be given by

$$r(t) = H^{-1}(s(t), \Sigma(u(t), \dot{u}^*(t))\dot{u}^*(t)), \qquad t \geq 0, \quad (2.73)$$

where $s(t) = (x(t), x_{\mathrm{r}}(t), \Theta_{\mathrm{r}}(t), \Theta_2(t), e(t), e_u(t))$ and $\dot{u}^*(t) \triangleq H(s(t), r_{\mathrm{d}}(t))$. Then the adaptive feedback control law (2.41), with update laws (2.42)–(2.45) and reference input $r(t)$, $t \geq 0$, given by (2.73), guarantees that the following statements hold:

i) The zero solution $(e(t), e_u(t)) \equiv (0, 0)$ to (2.3) and (2.39) is asymptotically stable.

ii) $|u_i(t)| \leq u_{\max}$ for all $t \geq 0$ and $i = 1, \ldots, m$.

iii) $|\dot{u}_i(t)| \leq \dot{u}_{\max}$ for all $t \geq 0$ and $i = 1, \ldots, m$.

Proof. Statement *i)* is a direct consequence of Theorem 2.3.1 with $r(t)$, $t \geq 0$, given by (2.73). To prove *ii)* and *iii)* note that it follows from (2.67), (2.69), and (2.73) that

$$\dot{u}(t) = H(s(t), r(t)) = H(s(t), H^{-1}(s(t), \Sigma(u(t), \dot{u}^*(t))\dot{u}^*(t))) = \Sigma(u(t), \dot{u}^*(t))\dot{u}^*(t), \ t \geq 0, \quad (2.74)$$

which implies $\dot{u}_i(t) = \sigma^*(u_i(t), \dot{u}_i^*(t))\dot{u}_i^*(t)$, $i = 1, \ldots, m$, $t \geq 0$. Hence, if the control input $u_i(t)$, $t \geq 0$, with a rate of change $\dot{u}_i^*(t)$, $i = 1, \ldots, m$, $t \geq 0$, does not violate the amplitude and rate saturation constraints, then it follows from (2.71) that $\sigma^*(u_i(t), \dot{u}_i^*(t)) = 1$ and $\dot{u}_i(t) = \dot{u}_i^*(t)$, $i = 1, \ldots, m$, $t \geq 0$. Alternatively, if the pair $(u_i(t), \dot{u}_i^*(t))$, $i = 1, \ldots, m$, $t \geq 0$, violates one or more of the input amplitude and/or rate constraints, then (2.70), (2.71), and (2.74) imply

i) $\dot{u}_i(t) = 0$ for all $t \geq 0$ if $|u_i(t)| = u_{\max}$ and $u_i(t)\dot{u}_i^*(t) > 0$; and

ii) $\dot{u}_i(t) = \dot{u}_{\max}\mathrm{sgn}(\dot{u}_i^*(t))$ for all $t \geq 0$ if $|\dot{u}_i^*(t)| > \dot{u}_{\max}$ and $|u_i(t)| < u_{\max}$ or if $|\dot{u}_i^*(t)| > \dot{u}_{\max}$ and $|u_i(t)| = u_{\max}$ and $u_i(t)\dot{u}_i(t) \leq 0$;

which, for $u_i(0) \leq u_{\max}$, guarantee that $|u_i(t)| \leq u_{\max}$ and $|\dot{u}_i(t)| \leq \dot{u}_{\max}$ for all $t \geq 0$ and $i = 1, \ldots, m$. □

Note that it follows from Theorem 2.4.1 that if the desired reference input $r_{\mathrm{d}}(t)$, $t \geq 0$, is such that the actuator amplitude and/or rate saturation constraints are not violated, then $r(t) = r_{\mathrm{d}}(t)$, $t \geq 0$, and hence, $x(t)$, $t \geq 0$, converges to $x_{\mathrm{d}}(t)$, $t \geq 0$. Alternatively, if there exists $t = t^* > 0$ such that the desired reference input drives one or more of the control inputs to the saturation boundary, then $r(t) \neq r_{\mathrm{d}}(t)$, $t > t^*$. However, as long

as the time interval over which the control input remains saturated is finite, the reference signal ultimately reverts to its desired value, and the tracking properties are preserved. Of course, if there exists a solution to the tracking problem wherein the input amplitude and rate saturation constraints are not violated when the tracking error is within certain bounds, then the approach is guaranteed to work.

2.5. Illustrative Numerical Examples

This section presents three numerical examples to demonstrate the utility of the proposed direct adaptive control framework for adaptive stabilization and tracking in the face of actuator amplitude and rate saturation constraints.

Example 2.5.1. Consider the uncertain controlled Liénard system given by

$$\ddot{z}(t)+\mu(z^4(t)-\alpha)\dot{z}(t)+\beta z(t)+\gamma\tanh(z(t))=bu(t), \quad z(0)=z_0, \quad \dot{z}(0)=\dot{z}_0, \quad t\geq 0, \tag{2.75}$$

where $\mu, \alpha, \beta, \gamma, b \in \mathbb{R}$ are unknown. Note that with $x_1 = z$ and $x_2 = \dot{z}$, (2.75) can be written in state space form (2.1) with $x = [x_1,\, x_2]^{\mathrm{T}}$, $f(x) = [x_2,\, -\beta x_1 - \gamma \tanh x_1 - \mu(x_1^4 - \alpha)x_2]^{\mathrm{T}}$, and $B = [0,\, b]^{\mathrm{T}}$. Here, it is assumed that $f(x)$ and B are unknown and can be parameterized as $f(x) = [x_2,\, \theta_\ell\, x + \theta_{n\ell 1} \tanh x_1 + \theta_{n\ell 2} x_1^4 x_2]^{\mathrm{T}}$ and $B = b\,[0,\, 1]^{\mathrm{T}}$, where $\theta_\ell \in \mathbb{R}^2$, $\theta_{n\ell 1} \in \mathbb{R}$, and $\theta_{n\ell 2} \in \mathbb{R}$ are unknown. Next, let $F(x) = [x^{\mathrm{T}},\, \tanh(x_1),\, x_1^4 x_2]^{\mathrm{T}}$, $A_{\mathrm{r}} = [A_0^{\mathrm{T}},\, \theta_{\mathrm{n}}^{\mathrm{T}}]^{\mathrm{T}}$, $B_{\mathrm{r}} = [0,\, b_{\mathrm{r}}]^{\mathrm{T}}$, $b_{\mathrm{r}} \in \mathbb{R}$, $\Lambda = 1$, $\Theta_{\mathrm{r}}^* = \frac{b_{\mathrm{r}}}{b}$, and $\Theta^* = [\theta_{\mathrm{n}} - \theta_\ell\,,\, -\theta_{n\ell 1},\, -\theta_{n\ell 2}]/b$, where $A_0 = [0,\, 1]$ and θ_{n} is an arbitrary vector, so that

$$B\Lambda\Theta_{\mathrm{r}}^* = \begin{bmatrix} 0 \\ b \end{bmatrix} \cdot 1 \cdot \frac{b_{\mathrm{r}}}{b} = \begin{bmatrix} 0 \\ b_{\mathrm{r}} \end{bmatrix} = B_{\mathrm{r}},$$

$$B\Lambda\Theta^* F(x) = \begin{bmatrix} 0 \\ b \end{bmatrix} \frac{1}{b}[\theta_{\mathrm{n}} - \theta_\ell\,,\, -\theta_{n\ell 1},\, -\theta_{n\ell 2}]F(x) = A_{\mathrm{r}}x - f(x),$$

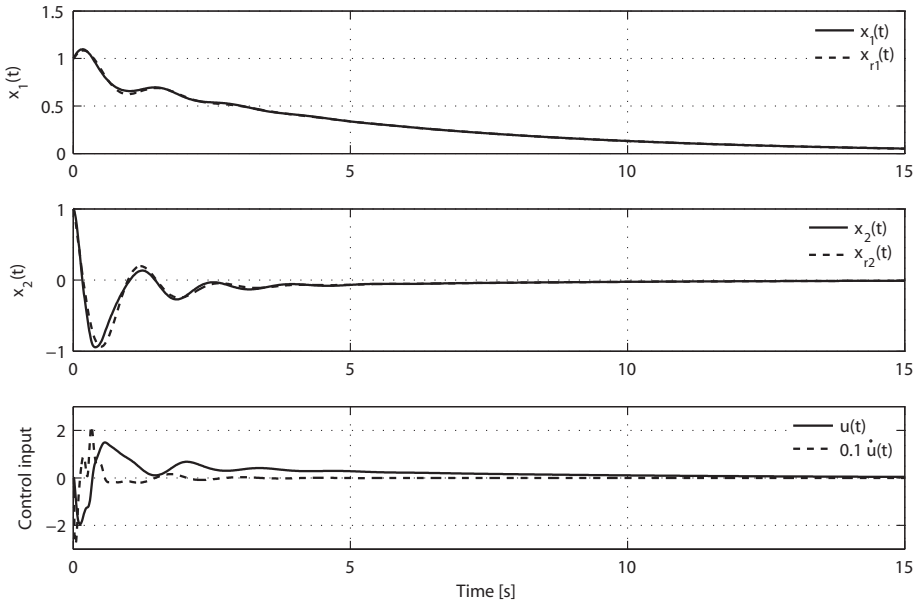

Figure 2.2: Stabilization of the Liénard system with no saturation constraints.

and hence, (2.4) and (2.5) hold. Now, it follows from Theorem 2.3.1 that the adaptive feedback controller (2.41) guarantees that $e(t) \to 0$ as $t \to \infty$ in the face of input amplitude and rate saturation constraints. In addition, $\theta_{\rm n} = [-4, -1.6]$, $R_1 = I_2$, and $R_2 = 1$, and a pair K and P satisfying (2.6) and (2.7) are given by

$$P = \begin{bmatrix} 1.2434 & 0.1036 \\ 0.1036 & 0.1891 \end{bmatrix}, \qquad K = \begin{bmatrix} -0.4142 & -0.7562 \end{bmatrix}. \tag{2.76}$$

In order to analyze this design it is assumed that $\mu = 2$, $\alpha = 1$, $\beta = 1$, $\gamma = 1$, $b = 3$, with initial condition $x(0) = [1,\, 1]^{\rm T}$, $u(0) = 0$, $x_{\rm r1}(0) = [0,\, 0]^{\rm T}$, $x_{\rm r2}(0) = 0$. First, a regulation problem is considered; that is, stabilization to the origin. The initial parameter estimates are chosen as $\Theta_{10} = [-1,\, -1,\, 0,\, 1,\, 1,\, 0,\, 4]$, $\Theta_{\rm r0} = 2$, $\Theta_{20} = \begin{bmatrix} 0 & 0 & 0 & 0 & 0 \\ 3 & 3 & -1 & -1 & 3 \end{bmatrix}$, and $\Theta_{30} = [0,\, 4]$. Figure 2.5.2.2 shows the case where no input saturation constraints are considered and Figure 2.5.2.3 shows the case where $u_{\max} = 1$ and $\dot{u}_{\max} = 2$.

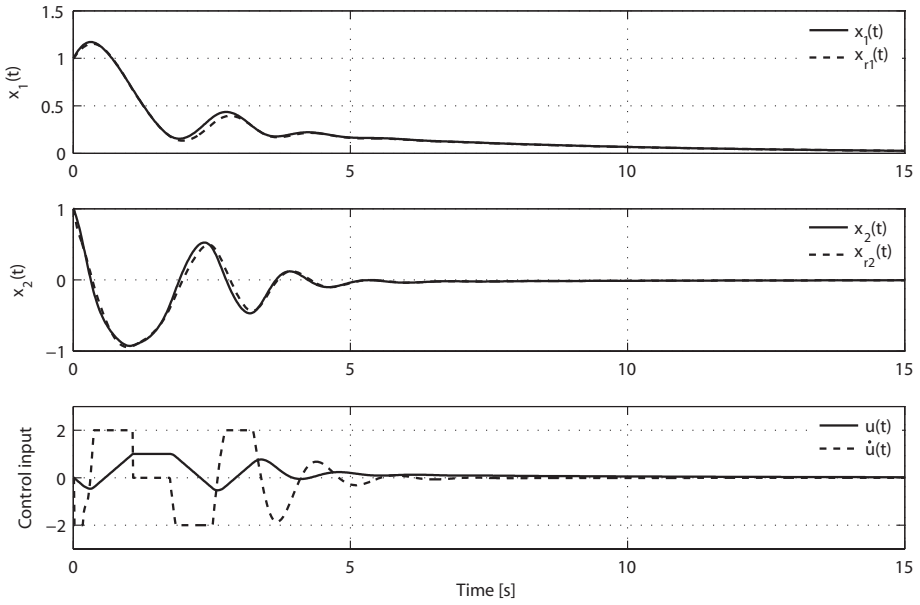

Figure 2.3: Stabilization of the Liénard system with amplitude and rate saturation constraints.

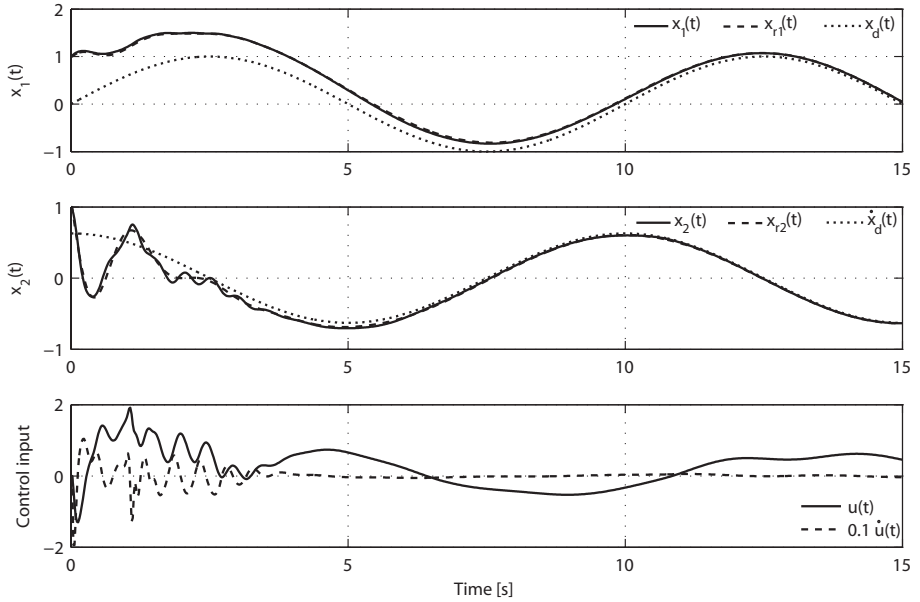

Figure 2.4: Tracking of the Liénard system with no saturation constraints.

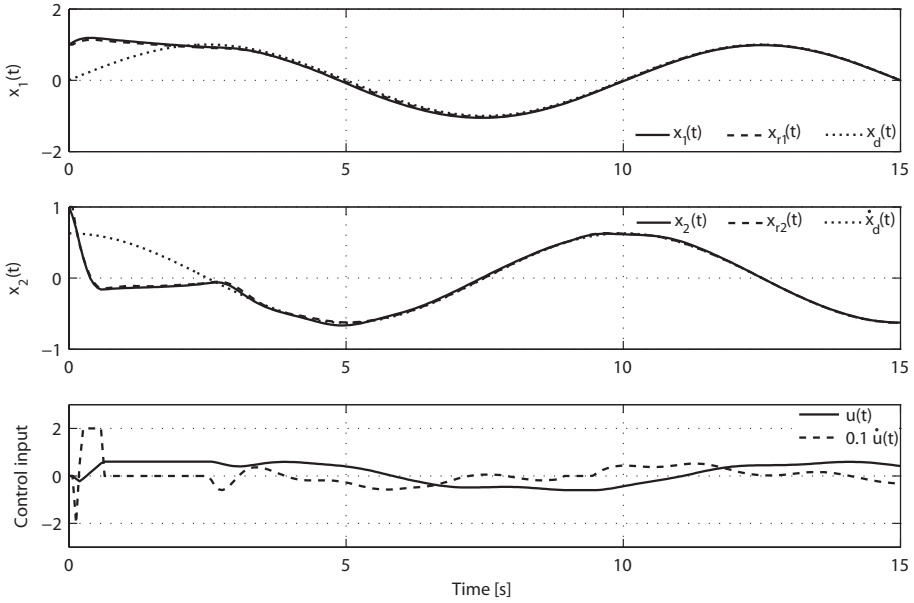

Figure 2.5: Tracking of the Liénard system with amplitude and rate saturation constraints.

Next, tracking of the signal $z_{\mathrm{d}}(t) = \sin(\pi/5\,t)$ is considered. Figure 2.5.2.4 shows the case where no input saturation constraints are considered, while Figure 2.5.2.5 shows the case where $u_{\max} = 0.6$ and $\dot{u}_{\max} = 2$. As seen in Figure 2.5, the control algorithm is able to achieve perfect tracking, in spite of the actuation constraint. Should the constraint prove too restrictive to physically allow the system to track the given desired trajectory, while the proposed formulation still guarantees that $x(t) \to x_{\mathrm{r}1}(t)$ as $t \to \infty$, it cannot be guaranteed that $x_{\mathrm{r}1}(t) \to x_{\mathrm{d}}(t)$ as $t \to \infty$. However, the approach provides a "close" agreement between the desired signal to be tracked and the achieved tracked signal for the given saturation levels, as illustrated by Figure 2.6. The amplitude saturation constraint is chosen as $u_{\max} = 0.53$, which, with $\dot{u}_{\max} = 2$, is too restrictive to allow perfect tracking of the given desired trajectory. At these amplitude and rate saturation levels, the control signal remains periodically saturated, and $x_{\mathrm{r}1}(t)$, $t \geq 0$, is unable to perfectly track the

desired trajectory. However, Figure 2.6 shows that the control algorithm still provides as close an agreement between the trajectory $x(t)$, $t \geq 0$, and $x_{\mathrm{d}}(t)$, $t \geq 0$, as made possible by the saturation constraint. Finally, consider a case where $\mu = -0.1$, $\alpha = 0$, $\beta = 1$, $\gamma = 1$, $b = 3$, with $u_{\max} = 4$ and $\dot{u}_{\max} = 1$. Figure 2.7 shows the results of a fifteen second numerical simulation (left), obtained with the adaptive controller of Theorem 2.3.1 and the reference input as described in Theorem 2.4.1. The resulting trajectory, represented by a solid line, converges smoothly towards the desired trajectory. However, if the reference input is not modified as described in Theorem 2.4.1, which implies that the adaptation mechanism in Theorem 2.3.1 is not aware of the saturation, then the closed-loop system's trajectory diverges. This is shown in Figure 2.7 by a dashed line, and is particularly clear when focusing on the first five seconds of the simulation (right).

Example 2.5.2. Consider the nonlinear dynamical system representing a controlled rigid spacecraft given by

$$\dot{x}(t) = -I_{\mathrm{b}}^{-1} X I_{\mathrm{b}} x(t) + I_{\mathrm{b}}^{-1} u(t), \qquad x(0) = x_0, \qquad t \geq 0, \tag{2.77}$$

where $x = [x_1,\, x_2,\, x_3]^{\mathrm{T}}$ represents the angular velocities of the spacecraft with respect to the body-fixed frame, $I_{\mathrm{b}} \in \mathbb{R}^{3\times 3}$ is an unknown positive definite inertia matrix of the spacecraft, $u(t) = [u_1,\, u_2,\, u_3]^{\mathrm{T}}$ is a control vector with control inputs providing body-fixed torques about three mutually perpendicular axes defining the body-fixed frame of the spacecraft, and X denotes the skew-symmetric matrix

$$X \triangleq \left[\begin{array}{ccc} 0 & -x_3 & x_2 \\ x_3 & 0 & -x_1 \\ -x_2 & x_1 & 0 \end{array} \right]. \tag{2.78}$$

Note that (2.77) can be written in state space form (2.1) with $f(x) = -I_{\mathrm{b}}^{-1} X I_{\mathrm{b}} x$ and

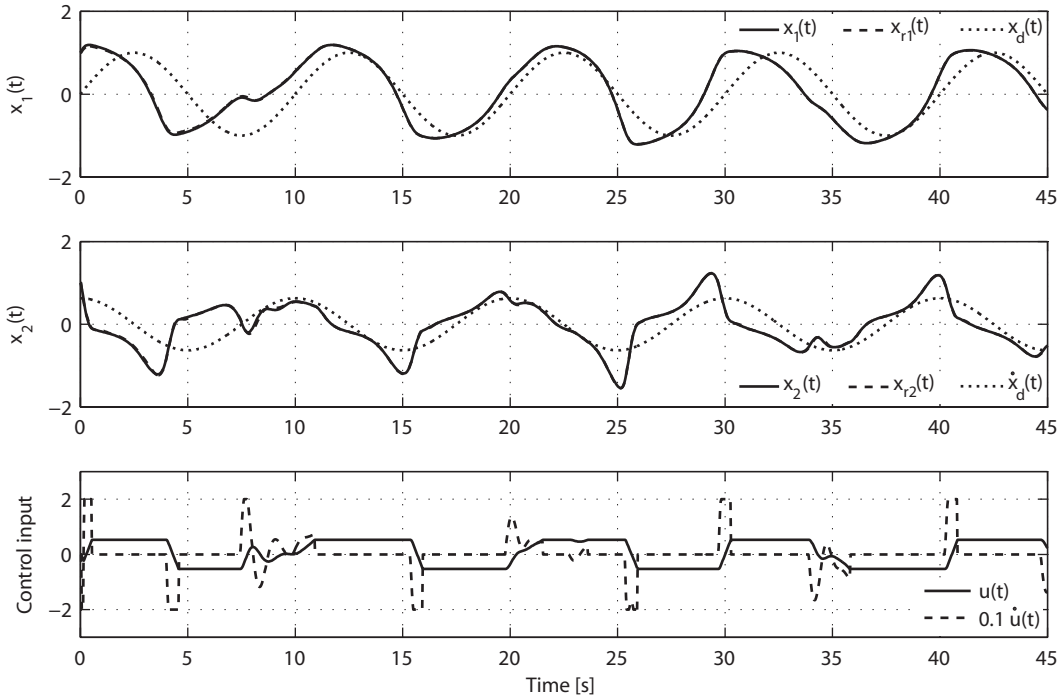

Figure 2.6: Tracking of the Liénard system with excessive amplitude and rate saturation constraints.

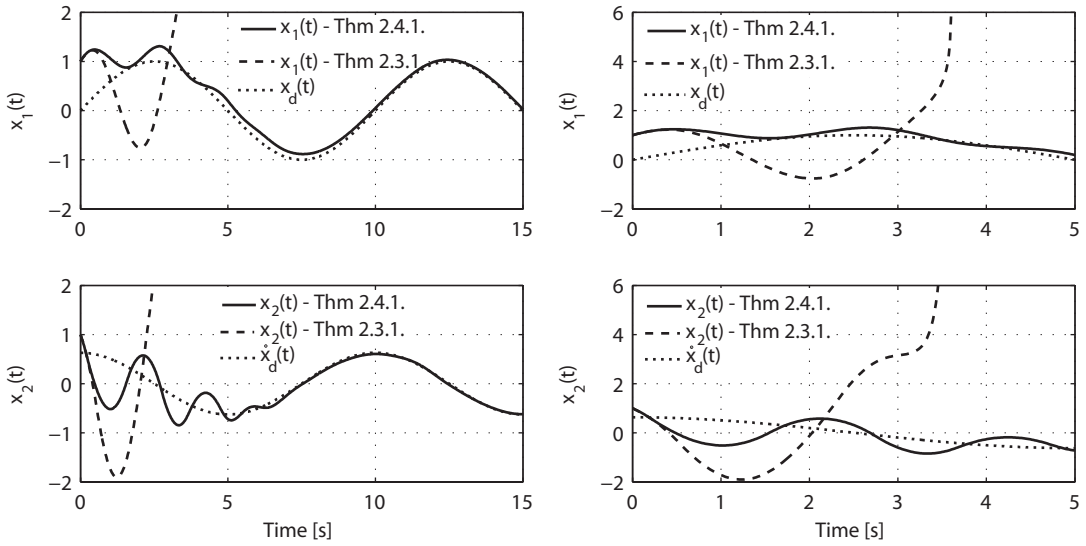

Figure 2.7: Tracking of the Liénard system with amplitude and rate saturation constraints.

$B = I_{\rm b}^{-1}$. Since $f(x)$ is a quadratic function, $f(x)$ can be parameterized as $f(x) = \Theta_{n\ell} f_{n\ell}(x)$, where $\Theta_{n\ell} \in \mathbb{R}^{3\times 6}$ is an unknown matrix and $f_{n\ell}(x) = [x_1^2,\, x_2^2,\, x_3^2,\, x_1x_2,\, x_2x_3,\, x_3x_1]^{\rm T}$.

Next, let $F(x) = [x^{\rm T},\, f_{n\ell}(x)^{\rm T}]^{\rm T}$, $B_{\rm r} = I_3$, $\Lambda = I_3$, $\Theta_{\rm r}^* = I_{\rm b}$, and $\Theta^* = I_{\rm b}[A_{\rm r},\, \Theta_{n\ell}]$, so that

$$
\begin{aligned}
B\Lambda\Theta_{\rm r}^* &= I_{\rm b}^{-1} I_3 I_{\rm b} = I_3 = B_{\rm r}, \\
f(x) - B\Lambda\Theta^* F(x) &= f(x) - I_{\rm b}^{-1} I_{\rm b}[A_{\rm r},\, \Theta_{n\ell}] F(x) = -A_{\rm r} x,
\end{aligned}
$$

and hence, (2.4) and (2.5) hold. Now, it follows from Theorem 2.4.1 that the dynamic adaptive controller (2.29)–(2.30), (2.41), guarantees that $e(t) \to 0$ as $t \to \infty$ when considering input amplitude and rate saturation constraints. Specifically,

$$
A_{\rm r} = \left[\begin{array}{ccc} 0 & 1 & 0 \\ 0 & 0 & 1 \\ -8 & -12 & -6 \end{array} \right],
$$

$R_1 = I_3$, and $R_2 = 0.1 I_3$, so that K and P satisfying (2.6) are given by

$$
P = \left[\begin{array}{ccc} 0.3738 & 0.1340 & -0.0369 \\ 0.1340 & 0.4401 & -0.0359 \\ -0.0369 & -0.0359 & 0.0709 \end{array} \right], \qquad K = -10P.
$$

In order to analyze this design it is assumed that

$$
I_{\rm b} = \left[\begin{array}{ccc} 20 & 0 & 0.9 \\ 0 & 17 & 0 \\ 0.9 & 0 & 15 \end{array} \right], \quad Q_1 = Q_2 = I_3,
$$

with initial condition $x(0) = [0.4,\, 0.2,\, -0.2]^{\rm T}$, $x_{\rm r1}(0) = x(0)$, $\Theta_{10} = \left[\begin{array}{cccc} I_3 & 0_{3\times 6} & I_3 & 0_{3\times 3} \end{array} \right]$, $\Theta_{20} = \left[\begin{array}{cc} -I_3 & 0_{3\times 9} \end{array} \right]$, and $\Theta_{30} = 0_{3\times 3}$, and $\Theta_{\rm r0} = I_3$. Figure 2.5.2.8 shows the angular velocities versus time for the case where no saturation constraints are enforced and the case where $u_{\max} = 1$ and $\dot{u}_{\max} = 0.5$. The corresponding control inputs and their time rate of change are shown in Figure 2.9 and Figure 2.10 . The control algorithm successfully regulates the system, in spite of the actuator saturation.

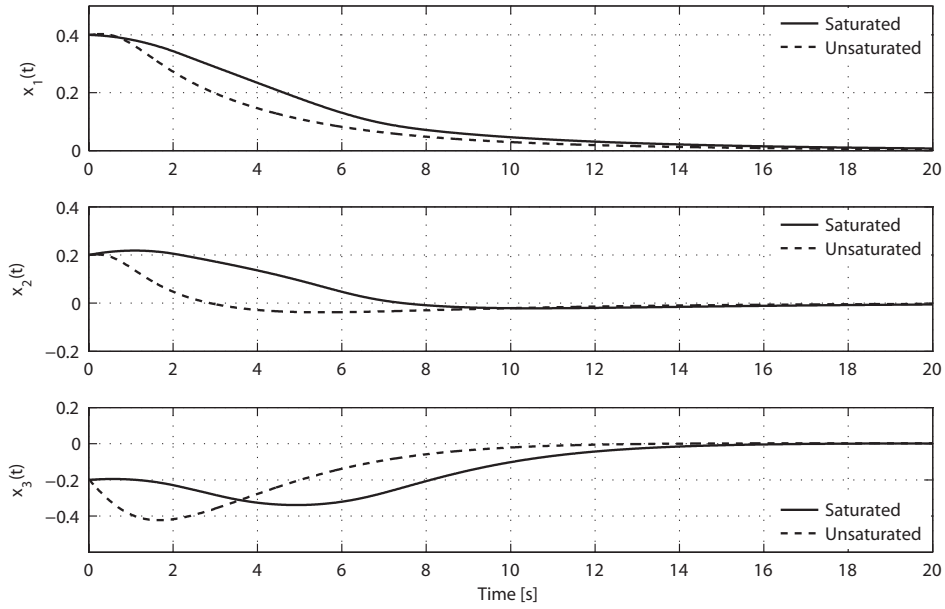

Figure 2.8: Spacecraft attitude regulation, angular velocities versus time.

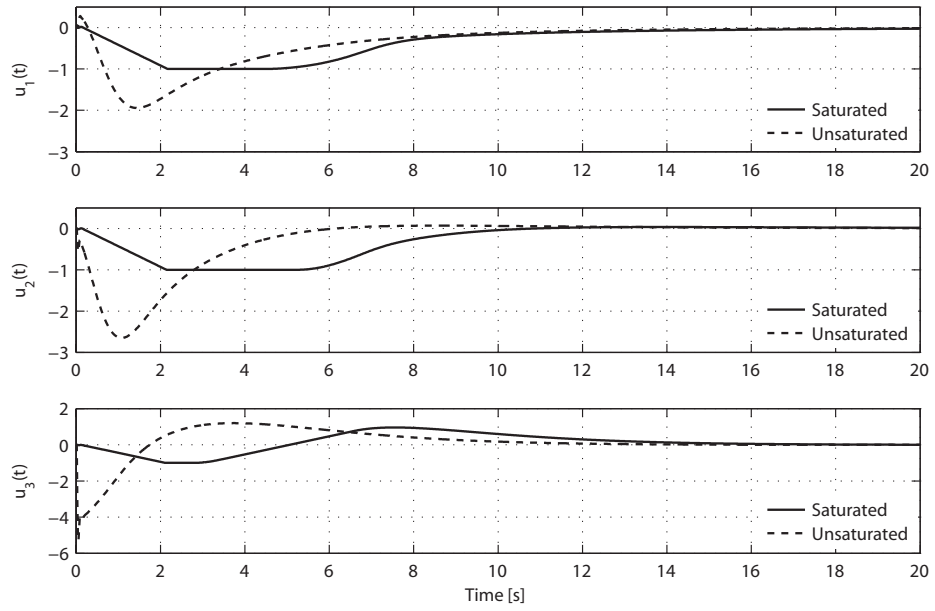

Figure 2.9: Spacecraft attitude regulation, control command, saturated and unsaturated.

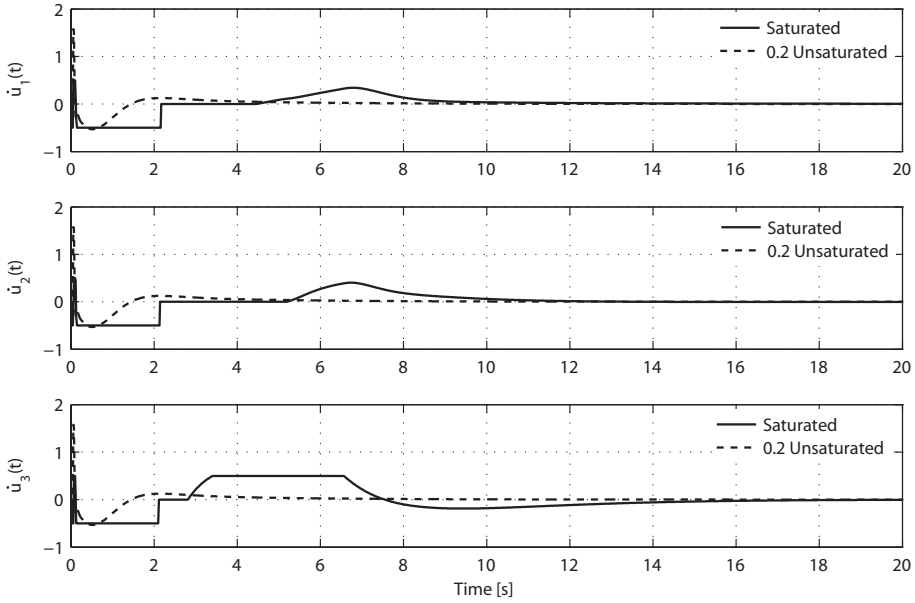

Figure 2.10: Spacecraft attitude regulation, control command rate, saturated and unsaturated.

Example 2.5.3. In this example, the proposed approach is compared with the $\mu-$modification technique developed in [33]. Consider the system

$$\dot{x}(t) = \theta_1 x(t) + \theta_2 x^3(t) - \theta_3 e^{-10(x(t)+1/2)^2} - \theta_4 e^{-10(x(t)-1/2)^2} + \theta_5 \sin(2x(t)) + \theta_6 u(t),$$
$$x(0) = x_0, \quad t \geq 0, \quad (2.79)$$

where θ_i, $i = 1, \ldots, 6$, are unknown parameters. For the simulation, it is assumed that $\Theta \triangleq [\, \theta_1 \;\; \theta_2 \;\; \theta_3 \;\; \theta_4 \;\; \theta_5 \;\; \theta_6] = \left[\, 1/5 \;\; 1/100 \;\; 1 \;\; 1 \;\; 1/2 \;\; 2 \,\right]$. The system given by (2.79) is considered in [33]. Defining $f(x) \triangleq \frac{1}{5}x + \frac{1}{100}x^3 - e^{-10(x+1/2)^2} - e^{-10(x-1/2)^2} + \frac{1}{2}\sin(2x)$, $B = 2$, and choosing $A_{\mathrm{r}} = -6$ and $B_{\mathrm{r}} = 6$, it follows that

$$f(x) - A_{\mathrm{r}} x = [\, 31/5,\, 1/100,\, 1,\, 1,\, 1\,][\, x,\, x^3,\, -e^{-10(x+1/2)^2},\, -e^{-10(x-1/2)^2},\, \sin(2x)\,]^{\mathrm{T}}. \quad (2.80)$$

Then, with

$$\Theta^* = \frac{1}{2}[\ 31/5,\ 1/100,\ 1,\ 1,\ 1/2\ ], \tag{2.81}$$

$$F(x) = [\ x,\ x^3,\ -e^{-10(x+1/2)^2},\ -e^{-10(x-1/2)^2},\ \sin(2x)\ ]^{\mathrm{T}}, \tag{2.82}$$

and $\Lambda = 1$, (2.4) holds. In addition, (2.5) holds with $\Theta_{\mathrm{r}}^* = 3$. Choosing $R_1 = 5$ and $R_2 = 0.1$ yields $P = 0.1024$ and $K = -6.1414$. In addition, the gains are chosen as follows, $K_u = 400$, $\Gamma_1 = 15.5I_7$, $\Gamma_2 = 15.5I_6$, and $\Gamma_3 = \Gamma_{\mathrm{r}} = 15.5$. The amplitude saturation constraint is chosen at $u_{\max} = 0.94$. The initial conditions are $x_0 = u_0 = 0$ and $\Theta_{\mathrm{r}}(0) = 5$, while all other parameter estimates are initially set to zero. The desired trajectory is defined as $x_{\mathrm{d}}(t) \triangleq 0.7(\sin(2t) + \sin(0.4t))$, $t \geq 0$.

When no rate saturation is enforced, the control law from Theorem 2.3.1 yields results very similar to those obtained by the $\mu-$modification algorithm presented in [33]; see Figure 2.11. The choice of design parameters for the $\mu-$algorithm are identical to those given in [33], and the obtained results replicate those shown in Figure 1.a of [33]. When enforcing amplitude saturation only, the two algorithms perform comparably. However, in addition to amplitude saturation, the proposed framework allows for rate saturation, whereas the $\mu-$modification framework of [33] does not account for rate saturation. Figure 2.12 shows the results for $u_{\max} = 0.94$ and $\dot{u}_{\max} = 3$. The trajectory and corresponding control effort are again compared to those obtained from the $\mu-$modification approach. As seen in Figure 2.12, the performance of the $\mu-$modification algorithm is significantly degraded by the presence of the rate saturation constraint, whereas the performance degradation using the proposed controller is marginal.

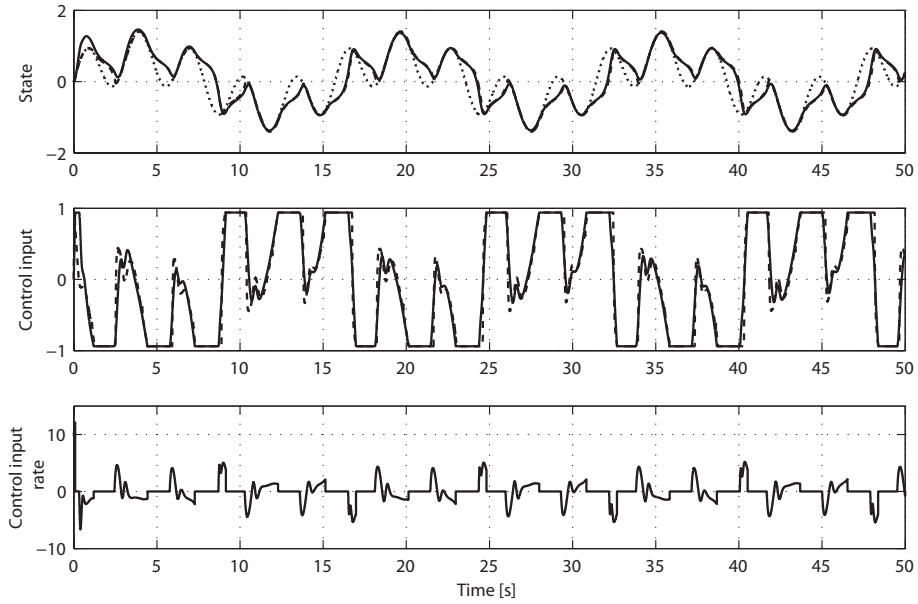

Figure 2.11: State and control input, with $u_{\max} = 0.94$ and no rate saturation ($\cdots$ desired trajectory, $--$ $\mu-$modification [33], —— Theorem 2.3.1).

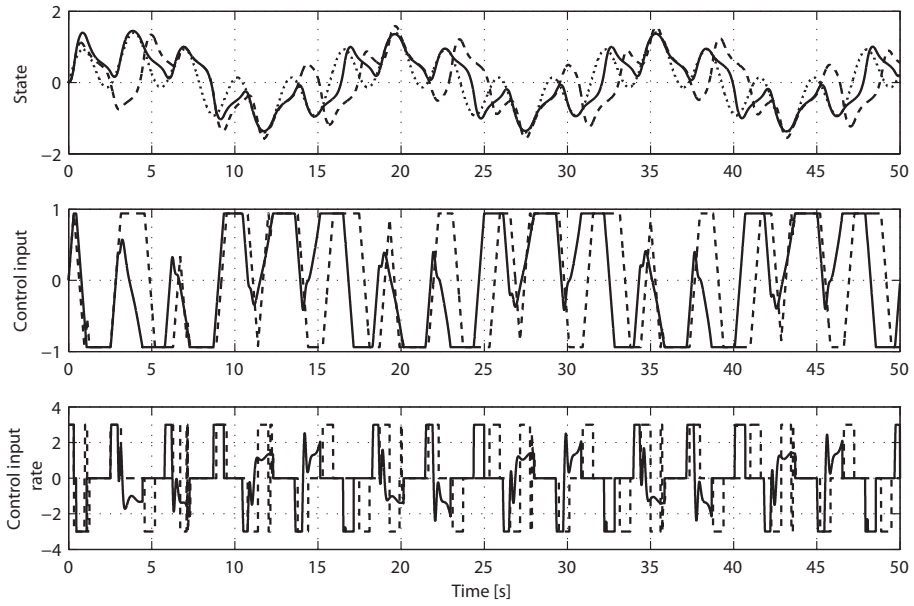

Figure 2.12: State and control input, with $u_{\max} = 0.94$ and $\dot{u}_{\max} = 3$ ($\cdots$ desired trajectory, $--$ $\mu-$modification [33], —— Theorem 2.3.1).

2.6. Conclusion

A direct adaptive nonlinear tracking control framework for multivariable nonlinear uncertain systems with actuator amplitude and rate saturation constraints was developed. By appropriately modifying the reference input to the reference system dynamics, the proposed approach guarantees asymptotic stability of the error system dynamics in the face of actuator amplitude and rate limitation constraints. Three numerical examples were presented to show the utility of the proposed adaptive tracking scheme. The proposed motion control algorithm is modular to some extent, in the sense that a general adaptive motion controller (described in Theorem 2.3.1) is augmented with a saturation algorithm (presented in Theorem 2.4.1). While the controller designed here is relevant to a wide variety of systems, following chapters will present more specialized control algorithms, dedicated to particular types of unmanned vehicles. Even if not explicitly shown (for brevity of exposition), these controllers will be augmented with the saturation algorithm presented in Theorem 2.4.1.

Chapter 3

Nonlinear Direct Adaptive Control Algorithm for Quadrotor Aerial Vehicles [2]

The work featured in this chapter was presented at the 2006 ASME International Mechanical Engineering Conference and Exposition ([2]).

3.1. Introduction

Numerous research groups have in recent years focused on control of Unmanned Aerial Vehicles (UAVs). This family of vehicles can be divided in two distinct classes. Airplanes can reach considerable speeds, allowing them to cover long distances in a relatively short amount of time. These vehicles naturally lend themselves well to missions pertaining to surveillance of extensive areas. They can be distinguished from Vertical Take-Off and Landing (VTOL) vehicles, as the latter are not able to reach comparable speeds, but are physically able to hover in the vicinity of an arbitrary entity. They are therefore particularly well suited for missions involving the monitoring of stationary or slow moving targets.

Focusing on the VTOL category of aircrafts, another distinction can be made between classical helicopters, which essentially use a single main rotor for lift, in conjunction with an auxiliary tail rotor used to adjust the vehicle's attitude, and quadrotors (see Figure 3.1), which use a combination of four rotors for both lift and attitude control. Although quadrotors feature more rotors than classical helicopters, they are of a simpler mechanical design, as the latter require a tilting mechanism to orient the main rotor to adjust pitch and roll, which is more easily accomplished, for quadrotors, using differential lift on pairs of rotors. This simplified mechanical design however puts the onus on the control system to provide levels of agility and maneuverability comparable to that of classical helicopters.

Controlling the motion of a quadrotor UAV is a challenging task. The interaction of the air flows generated by the four rotors contribute to complex aerodynamic forces affecting the vehicle's motion. The system's dynamics are not only nonlinear, but also difficult to satisfactorily characterize, due to the complexity of the system's aerodynamic properties. In addition, the vehicle's propulsion system (i.e. the rotors) can only provide a finite level of control authority.

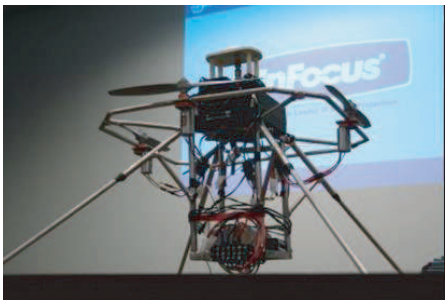

Figure 3.1: Quadrotor helicopter Banshee.

Due to the nonlinear nature of the system, linear control techniques are expected to perform relatively poorly ([81]), as they can not account nor compensate for nonlinear phenomenon affecting the vehicle's dynamics. In [82], a Proportional Integral Derivative (PID) controller and a Linear Quadratic (LQ) controller were implemented and proved capable of regulating the system. However, these designs rely on a linearized version of the vehicle's

model. The controllers perform adequately if the vehicle is in a configuration close to that the model was linearized about, but the performance dramatically deteriorates if the vehicle state significantly differs from this desired equilibrium. As a result, these controllers have difficulties in handling perturbations, and seem unlikely to allow for trajectory tracking.

A nonlinear controller should prove better suited to handle and account for nonlinearities in the vehicle's model. Indeed, a backstepping technique ([10]) yielded a control algorithm that, when implemented on the same system as that considered in [82], outperformed the PID and LQ controllers ([83]). Similarly, in [84, 85], feedback linearization ([77]) and a different backstepping approach were used and allowed to satisfactorily control the vehicle's altitude and yaw.

As previously mentioned, due to the presence of intricate aerodynamic forces, obtaining a mathematical model satisfactorily describing a quadrotor dynamical behavior is a difficult task. To handle uncertainties in the model, a robust feedback linearization approach was used in [63]. The obtained control law was shown to provide some level of robustness to parameter uncertainties through numerical simulation.

Alternatively, model uncertainties can be handled using adaptive techniques. In [62], a Single Hidden Layer Neural Network (SHL-NN) is used to compensate for unknown dynamics and allows implementation of the obtained controller with limited knowledge of the system's dynamics. The approach was extended in [64], allowing the control algorithm to satisfy control input saturation constraints, and successfully implemented on a physical system. The algorithm is however limited to control of the vehicle's pitch.

In the previous chapter, a model reference control framework relevant to a wide range of systems was developed (Section 2.2 and Section 2.3). The reference trajectory was modified

to ensure that the command remained within the capacities of the actuation system (Section 2.4). This chapter presents an alternative to the control algorithm in Theorem 2.3.1, which targets autonomous vehicles in general, and quadrotor UAVs in particular. This adaptive control algorithm solves the attitude and altitude tracking control problem for quadrotor aerial vehicles and accounts for the effects of actuator dynamics. A direct adaptive control law is derived, using an integrator backstepping technique ([10]). Section 3.2 details the considered mathematical model. The main result is presented in Section 3.3, along with a stability analysis. Results of numerical simulations are presented in Section 3.4 and illustrate the performance of the controller.

3.2. System Model

Kinematics

Considering motion in six degrees of freedom, the vehicle's position is described by

$$\eta_1 \triangleq \begin{bmatrix} x_{\mathrm{N}} & y_{\mathrm{E}} & z \end{bmatrix}^{\mathrm{T}}, \tag{3.1}$$

where $(x_{\mathrm{N}}, y_{\mathrm{E}})$ denotes the position of the vehicle in a two dimensional frame. The x_{N} axis is arbitrarily chosen to point North, the y_{E} axis East, while the z axis is pointing downward. The vector η_1 is expressed in an Earth Fixed Frame (EFF) of arbitrary origin. The vehicle's attitude is described by

$$\eta_2 \triangleq \begin{bmatrix} \phi & \theta & \psi \end{bmatrix}^{\mathrm{T}}, \tag{3.2}$$

where ϕ, θ and ψ denote the vehicle's roll, pitch, and yaw, respectively. Position and attitude are grouped in $\eta \triangleq \begin{bmatrix} \eta_1^{\mathrm{T}} & \eta_2^{\mathrm{T}} \end{bmatrix}^{\mathrm{T}}$. The body-fixed velocities are introduced with the following

notation,

$$\nu_1 \triangleq \begin{bmatrix} u & v & w \end{bmatrix}^{\mathrm{T}}, \qquad \nu_2 \triangleq \begin{bmatrix} p & q & r \end{bmatrix}^{\mathrm{T}}, \tag{3.3}$$

where u, v and w are the forward, lateral and downward velocities, expressed in the Body Fixed Frame (BFF, [86]), while p, q and r are the angular velocities in roll, pitch and yaw, respectively. Linear and angular velocities are grouped in the velocity vector $\nu \triangleq \begin{bmatrix} \nu_1^{\mathrm{T}} & \nu_2^{\mathrm{T}} \end{bmatrix}^{\mathrm{T}}$. The overall state of the vehicle is described by the state vector $x \triangleq \begin{bmatrix} \eta^{\mathrm{T}} & \nu^{\mathrm{T}} \end{bmatrix}^{\mathrm{T}}$.

The time derivatives of (3.1) and (3.2) are related to the velocities in (3.3) as follows ([86, 87]),

$$\dot{\eta}_1 = J_1(\eta_2)\nu_1, \tag{3.4}$$

$$\dot{\eta}_2 = J_2(\eta_2)\nu_2, \tag{3.5}$$

where

$$J_1(\eta_2) \triangleq \begin{bmatrix} c_\theta c_\psi & s_\phi s_\theta c_\psi - c_\phi s_\psi & c_\phi s_\theta c_\psi + s_\phi s_\psi \\ c_\theta s_\psi & s_\phi s_\theta s_\psi + c_\phi c_\psi & c_\phi s_\theta s_\psi - s_\phi c_\psi \\ -s_\theta & s_\phi c_\theta & c_\phi c_\theta \end{bmatrix}, \tag{3.6}$$

$$J_2(\eta_2) \triangleq \begin{bmatrix} 1 & s_\phi t_\theta & c_\phi t_\theta \\ 0 & c_\phi & -s_\phi \\ 0 & s_\phi/c_\theta & c_\phi/c_\theta \end{bmatrix}, \tag{3.7}$$

and s_ς, c_ς, and t_ς denote the sine, cosine and tangent of the angle ς, respectively. Equations (3.4) and (3.5) constitute the kinematic equations of the considered system.

Dynamics

The equations characterizing the dynamic behavior of the system are of the form ([87])

$$\dot{\nu}_1(t) = \frac{1}{m}C_1(\nu_2(t))\nu_1(t) + f_{\mathrm{g}}(\phi(t), \theta(t)) + \frac{1}{m}\begin{bmatrix} 0 & 0 & f_z(t) \end{bmatrix}^{\mathrm{T}}, \quad \nu_1(0) = \nu_{10}, \quad t \geqslant 0, \tag{3.8}$$

$$\dot{\nu}_2(t) = I^{-1}C_2(\nu_2(t))\nu_2(t) + I^{-1}\tau(t), \qquad \nu_2(0) = \nu_{20}, \tag{3.9}$$

where m is the mass of the vehicle,

$$I \triangleq \begin{bmatrix} i_x & 0 & 0 \\ 0 & i_y & 0 \\ 0 & 0 & i_z \end{bmatrix}, \tag{3.10}$$

is the rotational inertia matrix,

$$C_1(\eta_2) \triangleq \begin{bmatrix} 0 & r & -q \\ -r & 0 & p \\ q & -p & 0 \end{bmatrix}, \quad C_2(\eta_2) \triangleq \begin{bmatrix} 0 & -i_z r & i_y q \\ i_z r & 0 & -i_x p \\ -i_y q & i_x p & 0 \end{bmatrix}, \tag{3.11}$$

are Coriolis matrices, $f_{\mathrm{g}}(\phi, \theta) \triangleq g \begin{bmatrix} -s_\theta & c_\theta s_\phi & c_\theta c_\phi \end{bmatrix}^{\mathrm{T}}$ is the vector of restoring forces, g is gravity's acceleration, f_z is the thrust provided by the propulsion system, and τ regroups the torques and moments generated by the propellers.

The dynamical system (3.8)–(3.9) is augmented with the following equation, which represents the dynamical behavior of the actuation system, describing the effect of a Pulse Width Modulation (PWM) command on the produced thrust,

$$\dot{\tilde{\tau}}(t) = T^{-1} \left(-\tilde{\tau}(t) + g_{\mathrm{m}}^2 \tilde{B} \Lambda^{-1} p_2(t) \right), \qquad \tilde{\tau}(0) = \tilde{\tau}_0, \qquad t \geqslant 0, \tag{3.12}$$

where $T \in \mathbb{R}^{4\times4}$ is a diagonal matrix of time constants, $T > 0$, $\tilde{\tau} \triangleq \begin{bmatrix} f_z & \tau^{\mathrm{T}} \end{bmatrix}^{\mathrm{T}}$, $g_{\mathrm{m}} \in \mathbb{R}$,

$$\tilde{B} \triangleq \begin{bmatrix} k & 0 & 0 & 0 \\ 0 & lk & 0 & 0 \\ 0 & 0 & lk & 0 \\ 0 & 0 & 0 & d \end{bmatrix}, \qquad \Lambda \triangleq \frac{1}{4} \begin{bmatrix} 1 & 0 & 2 & 1 \\ 1 & -2 & 0 & -1 \\ 1 & 0 & -2 & 1 \\ 1 & 2 & 0 & -1 \end{bmatrix}, \tag{3.13}$$

where k, l and $d \in \mathbb{R}$, and, finally, $p_2 \in \mathbb{R}^4$ regroups the squares of the PWM command provided to the four motors.

Reference System

The control algorithm presented in this chapter follows a model reference framework. The following linear reference system is considered,

$$\dot{x}_{\mathrm{r}}(t) = A_{\mathrm{r}} x_{\mathrm{r}}(t) + B_{\mathrm{r}} r_{\mathrm{s}}(t), \qquad t \geq 0, \tag{3.14}$$

where $x_{\mathrm{r}}(t) \in \mathbb{R}^{2m}$ is the reference state, $A_{\mathrm{r}} \in \mathbb{R}^{2m \times 2m}$, $B_{\mathrm{r}} \in \mathbb{R}^{2m \times m}$ are constant matrixes, and $r_{\mathrm{s}}(t) \in \mathbb{R}^{m}$ is the reference input.

The reference system considered here is composed of three uncoupled second order oscillators. Each oscillator is characterized by a damping coefficient $\zeta_i > 0$, $i = 1, ..., m$, and a natural frequency $w_{0i} > 0$, $i = 1, ..., m$. This choice was mostly motivated by the simplicity of the corresponding reference dynamics. The dynamics of the i^{th} oscillator are given by

$$\ddot{x}_{\mathrm{r}i}(t) + 2\zeta_i \omega_{0i} \dot{x}_{\mathrm{r}i}(t) + \omega_{0i}^2 x_{\mathrm{r}i}(t) = \omega_{0i}^2 r_{\mathrm{s}i}(t), \qquad t \geq 0, \qquad i = 1, ..., m. \tag{3.15}$$

Thus, the reference system can be rewritten as

$$\begin{bmatrix} \dot{x}_{1\mathrm{r}}(t) \\ \dot{x}_{2\mathrm{r}}(t) \end{bmatrix} = \begin{bmatrix} 0_m & I_m \\ -\omega_0^2 & -A_{\mathrm{rm}} \end{bmatrix} \begin{bmatrix} x_{1\mathrm{r}}(t) \\ x_{2\mathrm{r}}(t) \end{bmatrix} + \begin{bmatrix} 0_m \\ \omega_0^2 \end{bmatrix} r_{\mathrm{s}}(t), \qquad t \geq 0, \tag{3.16}$$

where

$$x_{1\mathrm{r}}(t) \triangleq \begin{bmatrix} x_{\mathrm{r}1}(t) & ... & x_{\mathrm{r}m}(t) \end{bmatrix}^{\mathrm{T}}, \qquad t \geq 0, \tag{3.17}$$

$$x_{2\mathrm{r}}(t) \triangleq \begin{bmatrix} \dot{x}_{\mathrm{r}1}(t) & ... & \dot{x}_{\mathrm{r}m}(t) \end{bmatrix}^{\mathrm{T}}, \qquad t \geq 0, \tag{3.18}$$

and

$$A_{\mathrm{rm}} \triangleq \mathrm{diag}(2\zeta_1\omega_{01}, ..., 2\zeta_m\omega_{0m}), \qquad \omega_0 \triangleq \mathrm{diag}(\omega_{01}, ..., \omega_{0m}). \tag{3.19}$$

Finally, the desired trajectory for the vehicle may be written as

$$x_{\mathrm{d}}(t) = \left[\begin{array}{ccc} x_{\mathrm{d}1}(t) & \ldots & x_{\mathrm{d}m}(t) \end{array} \right]^{\mathrm{T}}, \qquad t \geq 0. \tag{3.20}$$

By choosing

$$r_{\mathrm{s}}(t) = \omega_0^{-2}(\ddot{x}_{\mathrm{d}}(t) + A_{\mathrm{rm}}\dot{x}_{\mathrm{d}}(t) + \omega_0^2 x_{\mathrm{d}}(t)), \qquad t \geq 0, \tag{3.21}$$

it follows that

$$\left[\begin{array}{c} \dot{x}_{1\mathrm{r}}(t) - \dot{x}_{\mathrm{d}}(t) \\ \dot{x}_{2\mathrm{r}}(t) - \ddot{x}_{\mathrm{d}}(t) \end{array} \right] = A_{\mathrm{r}} \left[\begin{array}{c} x_{1\mathrm{r}}(t) - x_{\mathrm{d}}(t) \\ x_{2\mathrm{r}}(t) - \dot{x}_{\mathrm{d}}(t) \end{array} \right], \qquad t \geq 0. \tag{3.22}$$

Since

$$A_{\mathrm{r}} \triangleq \left[\begin{array}{cc} 0_m & I_m \\ -\omega_0^2 & -A_{\mathrm{rm}} \end{array} \right], \tag{3.23}$$

is Hurwitz, it follows that $x_{1\mathrm{r}}(t) - x_{\mathrm{d}}(t) \to 0$ and $x_{2\mathrm{r}}(t) - \dot{x}_{\mathrm{d}}(t) \to 0$ as $t \to \infty$, i.e., the reference state converges to the desired trajectory. The remaining problem is to design a control command, $\tau(t) \in \mathbb{R}^m$, such that the tracking error converges to a fixed neighborhood around the origin. Considering that the mass, Coriolis/centrifugal and damping matrices of the real system contain unknown parameters and unknown terms, a control signal that accounts for these uncertainties needs to be considered.

3.3. Direct Adaptive Control Algorithm

This section introduces the considered tracking errors and presents the main result, which provides a control law solving the considered tracking problem, followed by a proof of stability.

Tracking Errors

Define $\eta_{\rm s} \triangleq \left[\begin{array}{cc} \eta_2^{\rm T} & k_{\rm sz} z \end{array}\right]^{\rm T}$, where $k_{\rm sz} \in \mathbb{R}$ is a scaling constant. The position of the reference system is given by $x_{\rm r1} \triangleq \left[\begin{array}{cc} x_{\rm ra}^{\rm T} & k_{\rm sz} x_{\rm rz} \end{array}\right]^{\rm T}$, where $x_{\rm ra} \in \mathbb{R}^3$ corresponds to three reference angles, and $x_{\rm rz} \in \mathbb{R}$ is a reference altitude. The considered position error is of the form

$$e_{\rm p}(x_{\rm r1}, \eta_{\rm s}) \triangleq x_{\rm r1} - \eta_{\rm s}. \tag{3.24}$$

A backstepping procedure ([10]) yields the following velocity error,

$$e_{\rm v}(x_{\rm r2}, x, \chi_1) \triangleq J_3^{-1}(\eta_2) x_{\rm r2} + \chi_1 - \nu_{\rm s}, \tag{3.25}$$

with $\nu_{\rm s} \triangleq \left[\begin{array}{cc} \nu_2^{\rm T} & k_{\rm sz} w \end{array}\right]^{\rm T}$,

$$J_3(\eta_2) \triangleq \left[\begin{array}{cc} J_2(\eta_2) & 0_{3\times 1} \\ 0_{1\times 3} & c_\phi\, c_\theta \end{array}\right], \tag{3.26}$$

where $0_{i\times j}$ denotes the $i \times j$ dimensional zero matrix, and χ_1 is obtained from the filter

$$\begin{aligned} T_1 \dot{\chi}_1(t) + \chi_1(t) \;=\; & J_3^{-1}(\eta_2(t)) \Big(k_{\rm sz} \left[\begin{array}{c} 0_{3\times 1} \\ u(t) s_\theta(t) - v(t) s_\phi(t) c_\theta(t) \end{array}\right] + G_1 e_{\rm p}(t) \Big) \\ & + \frac{1}{2} J_3^{\rm T}(\eta_2(t)) e_{\rm p}(t), \quad \chi_1(0) = \chi_{10}, \quad t \geqslant 0, \end{aligned} \tag{3.27}$$

where $T_1, G_1 \in \mathbb{R}^{4\times 4}$, $G_1 > 0$.

In addition, the acceleration error is of the form

$$e_\tau(x_{\rm r}, x, \chi_2, \tilde{\tau}, \Theta_1) \triangleq \hat{B}^{\rm T} \Theta_1 \varphi_1(x_{\rm r3}, \eta_2, \chi_2) - \tilde{\tau}, \tag{3.28}$$

where

$$\hat{B} \triangleq \left[\begin{array}{cccc} 0 & 1 & 0 & 0 \\ 0 & 0 & 1 & 0 \\ 0 & 0 & 0 & 1 \\ 1 & 0 & 0 & 0 \end{array}\right], \tag{3.29}$$

Θ_1 is an estimate of $\Theta_1^* \triangleq \left[\begin{array}{cc} \mathrm{diag}\left[\begin{array}{cccc} i_z - i_y, & i_x - i_z, & i_y - i_x, & 1 \end{array} \right] & M \end{array} \right]$, obtained from the update law

$$\dot{\Theta}_1(t) = e_{\mathrm{v}}(t)\varphi_1^{\mathrm{T}}(t)\Gamma_1 - \sigma_1\|e_{\mathrm{v}}(t)\|^2\Theta_1(t), \qquad \Theta_1(0) = \Theta_{10}, \qquad t \geqslant 0, \tag{3.30}$$

where $\Gamma_1 \in \mathbb{R}^{8\times 8}$, $\sigma_1 \in \mathbb{R}$, Γ_1, $\sigma_1 > 0$, and

$$\varphi_1(x_{\mathrm{r}3}, \eta_2, \chi_2) \triangleq \chi_2 + \left[\begin{array}{c} 0_{4\times 1} \\ J_3^{-1}(\eta_2)x_{\mathrm{r}3} \end{array} \right]. \tag{3.31}$$

Furthermore, $x_{\mathrm{r}3} \triangleq \dot{x}_{\mathrm{r}2}$, and χ_2 is obtained from the filter

$$T_2\dot{\chi}_2(t) + \chi_2(t) = f_{e_{\mathrm{v}}}(t) + \left[\begin{array}{c} 0_{4\times 1} \\ J_3^{\mathrm{T}}(\eta_2(t))e_{\mathrm{p}}(t) + G_2 e_{\mathrm{v}}(t) \end{array} \right], \quad \chi_2(0) = \chi_{20}, \quad t \geqslant 0, \tag{3.32}$$

where $T_2, G_2 \in \mathbb{R}^{4\times 4}$, $G_2 > 0$,

$$f_{e_{\mathrm{v}}}(x_{\mathrm{r}}, x, \alpha_1) \triangleq \left[\begin{array}{c} \left[\begin{array}{cccc} qr & pr & pq & pv - qu \end{array} \right]^{\mathrm{T}} \\ k_{\mathrm{sz}} g \left[\begin{array}{c} 0_{3\times 1} \\ -c_\phi c_\theta \end{array} \right] + \left(\frac{\mathrm{d}}{\mathrm{d}t} J_3^{-1}(\eta_2)\right) x_{\mathrm{r}2} + T_1^{-1}\alpha_1 \end{array} \right], \tag{3.33}$$

and α_1 is the filtering error associated with filter (3.27) given by

$$\alpha_1(x_{\mathrm{r}1}, x, \chi_1) \triangleq J_3^{-1}(\eta_2)\left(k_{\mathrm{sz}} \left[\begin{array}{c} 0_{3\times 1} \\ us_\theta - vs_\phi c_\theta \end{array} \right]^{\mathrm{T}} + G_1 e_{\mathrm{p}}(x_{\mathrm{r}1}, \eta_{\mathrm{s}}) \right) + \frac{1}{2} J_3^{\mathrm{T}}(\eta_2) e_{\mathrm{p}}(x_{\mathrm{r}1}, \eta_{\mathrm{s}}) - \chi_1. \tag{3.34}$$

In addition, define

$$\alpha_2(e_{\mathrm{p}}, e_{\mathrm{v}}, x_{\mathrm{r}}, x, \chi_2, \alpha_1) \triangleq f_{e_{\mathrm{v}}}(x_{\mathrm{r}}, x, \alpha_1) + \left[\begin{array}{c} 0_{4\times 1} \\ J_3^{-1}(\eta_2)e_{\mathrm{p}} + G_2 e_{\mathrm{v}} \end{array} \right] - \chi_2, \tag{3.35}$$

which is the filtering error corresponding to filter (3.32). Finally, define the error vector $e \triangleq \left[\begin{array}{ccc} e_{\mathrm{p}}^{\mathrm{T}} & e_{\mathrm{v}}^{\mathrm{T}} & e_\tau^{\mathrm{T}} \end{array} \right]^{\mathrm{T}}$, which regroups the three tracking errors.

Remark 3.3.1. The above velocity and acceleration errors were obtained following an integrator backstepping procedure similar to that presented in [10]. The procedure was

modified to simplify the expression of the final control command. In particular, using a technique derived from Dynamic Surface Control (DSC, [61]), specific parts of the virtual control commands ([10]) are replaced by their filtered equivalent (obtained from filters (3.27) and (3.32)). The resulting derivatives of the virtual control commands, which can be found in the control law, are significantly simplified.

Control Command

The main result of the chapter is stated in the following Theorem.

Theorem 3.3.1. Consider the dynamical system formed by (3.24), (3.25) and (3.28), and control law

$$p_2(t) \triangleq \Lambda\Theta_2(t)\varphi_2(t), \quad t \geqslant 0, \tag{3.36}$$

where $\Theta_2 \in \mathbb{R}^{4\times 12}$ is an estimate of $\Theta_2^* \triangleq \frac{1}{g_{\mathrm{m}}^2}\tilde{B}^{-1}T \begin{bmatrix} T^{-1} & \hat{B}^{\mathrm{T}}M^{-1} & I_4 \end{bmatrix}$, I_j is the j^{th} dimensional identity matrix, $M \triangleq \begin{bmatrix} I & 0_{3\times 1} \\ 0_{1\times 3} & \frac{m}{k_{\mathrm{s}z}} \end{bmatrix}$, and

$$\varphi_2(t) \triangleq \begin{bmatrix} \tilde{\tau}^{\mathrm{T}}(t) & e_{\mathrm{v}}^{\mathrm{T}}(t) & \tilde{\varphi}_2^{\mathrm{T}}(t) \end{bmatrix}^{\mathrm{T}}, \qquad t \geqslant 0, \tag{3.37}$$

$$\begin{aligned}\tilde{\varphi}_2(x_{\mathrm{r}}, x, \Theta_1, \chi_2, \alpha_2, r_{\mathrm{s}}, e_\tau) \triangleq\ & \hat{B}^{\mathrm{T}}\Big(\dot{\Theta}_1(x_{\mathrm{r}}, x, \Theta_1)\varphi_1(x_{\mathrm{r}3}, \eta_2, \chi_2) + \Theta_1 T_2^{-1}\alpha_2 \\ & + \Theta_{12}\left(\frac{d}{dt}J_3^{-1}(\eta_2)\right)x_{\mathrm{r}3} + \Theta_{12}J_3^{-1}(\eta_2)\dot{x}_{\mathrm{r}3}(x_{\mathrm{r}}, r_{\mathrm{s}})\Big) + G_3 e_\tau,\end{aligned} \tag{3.38}$$

where Θ_{12} is the $(1,4)\times(5,8)$ block of Θ_1, and $G_3 \in \mathbb{R}^{4\times 4}$, $G_3 > 0$. Finally, consider the update law

$$\dot{\Theta}_2(t) = e_\tau(t)\varphi_2^{\mathrm{T}}(t)\Gamma_2 - \sigma_2\|e_\tau(t)\|^2\Theta_2(t), \qquad \Theta_2(0) = \Theta_{20}, \qquad t \geqslant 0, \tag{3.39}$$

where $\Gamma_2 \in \mathbb{R}^{12\times 12}$, $\sigma_2 \in \mathbb{R}$, Γ_2, $\sigma_2 > 0$.

The control command (3.36) with update laws (3.30) and (3.39) guarantees convergence of $(e, \tilde{\Theta}_1, \tilde{\Theta}_2)$ to the compact set

$$\mathcal{M} \triangleq \Big\{(e, \tilde{\Theta}_1, \tilde{\Theta}_2) : e^{\mathrm{T}} G e \leqslant \frac{1}{2}\bar{\alpha}_1^2 + \|e_{\mathrm{v}} M^{-1}\Theta_1^*\|\bar{\alpha}_2,\ \mathrm{tr}[M^{-1}\tilde{\Theta}_1\Gamma_1^{-1}\tilde{\Theta}_1^{\mathrm{T}}] \leqslant \mathrm{tr}[M^{-1}\Theta_1^*\Gamma_1^{-1}\Theta_1^{*\mathrm{T}}],$$
$$\mathrm{tr}[\bar{B}\tilde{\Theta}_2\Gamma_2^{-1}\tilde{\Theta}_2^{\mathrm{T}}] \leqslant \mathrm{tr}[\bar{B}\Theta_2^*\Gamma_2^{-1}\Theta_2^{*\mathrm{T}}]\Big\}, \tag{3.40}$$

where $\tilde{\Theta}_1 \triangleq \Theta_1 - \Theta_1^*$, $\tilde{\Theta}_2 \triangleq \Theta_2 - \Theta_2^*$ are estimation errors, $G \triangleq \mathrm{diag}\begin{bmatrix} G_1 & G_2 & G_3 \end{bmatrix}$, $\bar{\alpha}_i$ is an upper bound to the filtering error α_i, $i = 1, 2$, and $\bar{B} \triangleq g_{\mathrm{m}}^2 T^{-1}\tilde{B}$.

Proof. Consider the Lyapunov function candidate

$$V(e, \tilde{\Theta}) \triangleq \frac{1}{2}e^{\mathrm{T}}e + \frac{1}{2}\mathrm{tr}\left(M^{-1}\tilde{\Theta}_1\Gamma_1^{-1}\tilde{\Theta}_1^{\mathrm{T}}\right) + \frac{1}{2}\mathrm{tr}\left(\bar{B}\tilde{\Theta}_2\Gamma_2^{-1}\tilde{\Theta}_2^{\mathrm{T}}\right), \tag{3.41}$$

where $\tilde{\Theta} \triangleq \begin{bmatrix} \tilde{\Theta}_1 & \tilde{\Theta}_2 \end{bmatrix}$. Note that $V(e, \tilde{\Theta})$ is $\mathcal{C}^1$ for all $e \in \mathbb{R}^{12}$ and $\tilde{\Theta} \in \mathbb{R}^{4\times 20}$, $V(e, \tilde{\Theta}) > 0$ for all $(e, \tilde{\Theta}) \in \mathbb{R}^{12} \cup R^{4\times 20} \setminus \{0\}$, and $V(0, 0) = 0$.

Note that the expression (3.25) of e_{v} allows to write the time derivative of e_{p} as

$$\dot{e}_{\mathrm{p}}(e, \eta_2, \alpha_1) = -G_1 e_{\mathrm{p}} + J_3(\eta_2)(\alpha_1 + e_{\mathrm{v}} - \frac{1}{2}J_3^{\mathrm{T}}(\eta_2)e_{\mathrm{p}}). \tag{3.42}$$

Similarly, (3.28) allows to express the time derivative of e_{v} as

$$\dot{e}_{\mathrm{v}}(e, x_{\mathrm{r}}, x, \chi_2, \alpha_2, \tilde{\Theta}_1) \;=\; -J_3^{\mathrm{T}}(\eta_2)e_{\mathrm{p}} - G_2 e_{\mathrm{v}} + M^{-1}(\Theta_1^*\alpha_2 - \tilde{\Theta}_1\varphi_1(x_{\mathrm{r}3}, \eta_2, \chi_2) + \hat{B}e_\tau). \tag{3.43}$$

Finally, the control command (3.36) allows to write the time derivative of e_τ as

$$\dot{e}_\tau(t) \;=\; -\hat{B}^{\mathrm{T}}M^{-1}e_{\mathrm{v}}(t) - G_3 e_\tau(t) - \bar{B}\tilde{\Theta}_2(t)\varphi_2(t),\ \ t \geqslant 0. \tag{3.44}$$

Using (3.42), (3.43) and (3.44), we obtain the following expression for the time derivative of the Lyapunov function candidate,

$$\dot{V}(t) = -e_{\mathrm{p}}^{\mathrm{T}}(t)G_1 e_{\mathrm{p}}(t) + e_{\mathrm{p}}^{\mathrm{T}}(t)J_3(\eta_2(t))(\alpha_1(t) - \frac{1}{2}J_3^{\mathrm{T}}(\eta_2(t))e_{\mathrm{p}}(t)) - e_\tau^{\mathrm{T}}(t)\bar{B}\tilde{\Theta}_2(t)\varphi_2(t)$$

$$+e_{\rm v}^{\rm T}(t)M^{-1}(\Theta_1^*\alpha_2(t)-\tilde{\Theta}_1(t)\varphi_1(t))+\mathrm{tr}[M^{-1}\tilde{\Theta}_1(t)\Gamma_1^{-1}\dot{\Theta}_1^{\rm T}(t)]$$
$$+\mathrm{tr}[\bar{B}\tilde{\Theta}_2(t)\Gamma_2^{-1}\dot{\Theta}_2^{\rm T}(t)]-e_{\rm v}^{\rm T}(t)G_2e_{\rm v}(t)-e_\tau^{\rm T}(t)G_3e_\tau(t),\quad t\geqslant 0, \tag{3.45}$$

which can be rewritten as

$$\dot{V}(t) = -e^{\rm T}(t)Ge(t)+\left[\begin{array}{cc} e_{\rm p}^{\rm T}(t) & e_{\rm v}^{\rm T}(t)\end{array}\right]P(\eta_2(t))\alpha(t)-\frac{1}{2}e_{\rm p}^{\rm T}(t)J_3(\eta_2(t))J_3^{\rm T}(\eta_2(t))e_{\rm p}(t)$$
$$+\mathrm{tr}[M^{-1}\tilde{\Theta}_1(t)(\Gamma_1^{-1}\dot{\Theta}_1^{\rm T}(t)-\varphi_1(t)e_{\rm v}^{\rm T}(t))]+\mathrm{tr}[\bar{B}\tilde{\Theta}_2(t)(\Gamma_2^{-1}\dot{\Theta}_2^{\rm T}(t)-\varphi_2(t)e_\tau^{\rm T}(t))],$$
$$t\geqslant 0, \tag{3.46}$$

where

$$P(\eta_2)\triangleq\left[\begin{array}{cc} J_3(\eta_2) & 0_{4\times 8}\\ 0_{4\times 4} & M^{-1}\Theta_1^*\end{array}\right],\quad \alpha\triangleq\left[\begin{array}{cc}\alpha_1^{\rm T} & \alpha_2^{\rm T}\end{array}\right]^{\rm T}. \tag{3.47}$$

Using update laws (3.30) and (3.39), (3.46) can be transformed into

$$\dot{V}(t) = -e^{\rm T}(t)Ge(t)+\left[\begin{array}{cc} e_{\rm p}^{\rm T}(t) & e_{\rm v}^{\rm T}(t)\end{array}\right]P(\eta_2(t))\alpha(t)-\frac{1}{2}e_{\rm p}^{\rm T}(t)J_3(\eta_2(t))J_3^{\rm T}(\eta_2(t))e_{\rm p}(t)$$
$$-\sigma_1\|e_{\rm v}(t)\|^2\mathrm{tr}[M^{-1}\tilde{\Theta}_1(t)\Gamma_1^{-1}\Theta_1^{\rm T}(t)]-\sigma_2\|e_\tau(t)\|^2\mathrm{tr}[\bar{B}\tilde{\Theta}_2(t)\Gamma_2^{-1}\Theta_2^{\rm T}(t)],\quad t\geqslant 0. \tag{3.48}$$

Note that, by completion of the square,

$$e_{\rm p}^{\rm T}J_3(\eta_2)\alpha_1 = -\frac{1}{2}(J_3^{\rm T}(\eta_2)e_{\rm p}-\alpha_1)^{\rm T}(J_3^{\rm T}(\eta_2)e_{\rm p}-\alpha_1)+\frac{1}{2}e_{\rm p}^{\rm T}J_3(\eta_2)J_3^{\rm T}(\eta_2)e_{\rm p}+\frac{1}{2}\|\alpha_1\|^2. \tag{3.49}$$

In addition, for $\|T_i\|$ sufficiently small, $\|\alpha_i(t)\|<\bar{\alpha}_i$, $t\geqslant 0$, $i=1,2$, and we obtain the following upper bound on $\dot{V}$,

$$\dot{V}(t)\leqslant\frac{\sigma_2}{2}\|e_\tau(t)\|^2(\mathrm{tr}[\bar{B}\Theta_2^*\Gamma_2^{-1}\Theta_2^{*\rm T}]-\mathrm{tr}[\bar{B}\tilde{\Theta}_2(t)\Gamma_2^{-1}\tilde{\Theta}_2(t)^{\rm T}])+\frac{1}{2}\bar{\alpha}_1^2+\|e_{\rm v}(t)M^{-1}\Theta_1^*\|\bar{\alpha}_2$$
$$-e(t)^{\rm T}Ge(t)+\frac{\sigma_1}{2}\|e_{\rm v}(t)\|^2(\mathrm{tr}[M^{-1}\Theta_1^*\Gamma_1^{-1}\Theta_1^{*\rm T}]-\mathrm{tr}[M^{-1}\tilde{\Theta}_1(t)\Gamma_1^{-1}\tilde{\Theta}_1^{\rm T}(t)]),\ t\geqslant 0. \tag{3.50}$$

Hence, $\dot{V}(t)$, $t\geq 0$, is strictly negative outside of $\mathcal{M}$, which guarantees convergence of $(e,\tilde{\Theta})$ to the compact set $\mathcal{M}$ ([88]). □

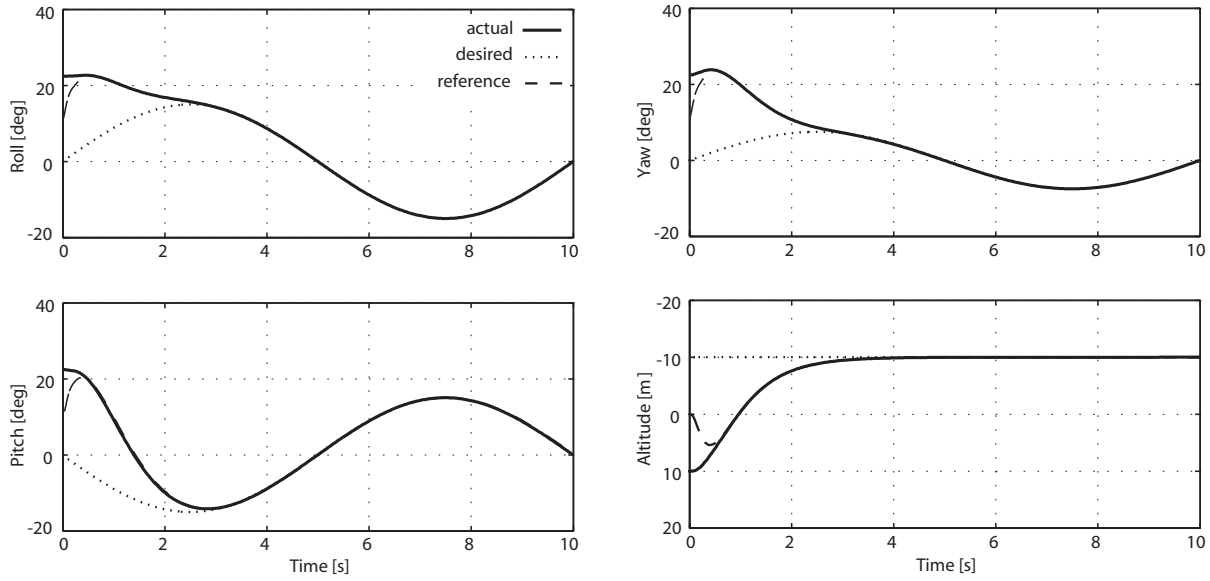

Figure 3.2: Orientation and altitude, actual, desired and reference trajectories.

3.4. Numerical Simulation

The control law (3.36) presented in Section 3.3 was tested through numerical simulations. The reference system used is of the form given by (3.16), with $\omega_0 = 10.2\, I_4$, and $A_{\mathrm{r}4} = 38.8\, I_4$. In addition, the following values were used in the vehicle's model, $m = 6$, $i_x = 5$, $i_y = 5$, $i_z = 1$, $g_{\mathrm{m}} = 10$, $l = 0.25$, $k = 2$, $d = 0.1$, $g = 9.81$, $T = 0.01\, I_4$. The control gains were chosen to be $G_1 = G_2 = G_3 = 10\, I_4$, and the learning coefficients $\Gamma_1 = I_8$, $\Gamma_2 = I_{12}$.

The chosen initial conditions are as follows, $\eta_{10} = \begin{bmatrix} 0 & 0 & 10 \end{bmatrix}^{\mathrm{T}}$, $\eta_{20} = \frac{\pi}{8}\begin{bmatrix} 1 & 1 & 1 \end{bmatrix}^{\mathrm{T}}$, $\nu = 0_{6\times 1}$, $x_{\mathrm{r}0} = \frac{\pi}{16}\begin{bmatrix} 1 & 1 & 1 & 0_{1\times 9} \end{bmatrix}^{\mathrm{T}}$, and the desired trajectory that $x_{\mathrm{r}1}$ is tracking is of the form $x_{\mathrm{d}}(t) = \begin{bmatrix} a\sin(bt) & -a\sin(bt) & \frac{a}{2}\sin(bt) & -10 \end{bmatrix}^{\mathrm{T}}, t \geqslant 0$, with $a = \frac{\pi}{12}$, $b = \frac{2\pi}{10}$. This reference trajectory has the vehicle elevating in altitude while its orientation is oscillating.

As seen on Figure 3.2, the actual roll (top left), pitch (bottom left) and yaw (top right)

converge rapidly and smoothly to their corresponding desired trajectory. Similarly, the altitude converges to its desired value (bottom right).

3.5. Conclusion

This chapter presented a novel direct adaptive controller solving the tracking control problem for quadrotor UAVs. A stability analysis proving convergence of the tracking errors to a neighborhood of the origin was provided, and the obtained control law was successfully tested through numerical simulations. This example illustrates the efficacy of backstepping and direct adaptive control techniques in solving the tracking problem for unmanned vehicles. In following chapters, similar techniques are used to solve the tracking problem for alternate types of autonomous vehicles.

Chapter 4

Neural-based Adaptive Control of Autonomous Marine Vehicles [3]

The result presented was the object of a chapter in the book "Current Trends in Nonlinear Systems and Control", published by Birkhäuser in 2004 ([3]).

4.1. Introduction

This chapter presents a neural-based MRAC algorithm for autonomous marine vehicles. The development of control algorithms for marine vehicles is the focus of a number of research groups across the world, and a variety of results can be found in the literature. Regulation problems have received significant attention. For instance, three different stabilization algorithms are introduced in [89] for a model of underactuated hovercraft. While providing interesting results, the control algorithms are designed for a specific model of hovercraft, whose model is significantly simpler than that of more common marine vehicles, as it does not contain many of the nonlinear, coupled drag terms that these generally feature.

Tracking controllers can also be found in the literature (see for example [90–96]). In [96],

the case of a surface ship equipped with a pair of propellers is considered. This controller showed interesting performance in simulation. However, the desired trajectory is limited to straight lines and circles. A similar problem is considered in [95], where the authors derive a controller that uses a state estimator to handle uncertainty on the state measurements. In [90], a global controller, which accounts for control amplitude saturation effects, is designed. Then, in [91], a velocity observer is added to the control framework, allowing the algorithm to operate without velocity measurements. A different type of propulsion system is considered in [93], which presents a controller for an underactuated AUV equipped with a propeller and a side thruster. The resulting controller handles constant and slowly varying external perturbations. Although these results are of interest, the majority of them rely on somewhat restrictive assumptions, such as that the system's model is fully known.

Such knowledge assumptions are natural and understandable, as the design of a motion controller very often relies on a mathematical model of the system to control. However, in the case of marine vehicles, it can prove rather challenging to obtain a model that will satisfactorily capture the dynamic behavior of the system. This is due in no small part to a number of hydrodynamic phenomenons such as skin friction about the vehicle's hull and propeller induced cavitation. Such occurrences contribute to a difficult modeling problem, to such an extent that current modeling techniques appear only partially capable of describing the dynamics of marine vehicles. Modeling of these can prove particularly challenging when the vehicle's velocity is varying, such as when it is following a search pattern or when its desired path is unsteady. To compensate for the corresponding uncertainties in the geometric and hydrodynamic parameters characterizing the system's model, adaptive control techniques can be used.

The design of adaptive controllers for marine vehicles has been widely studied. For example, in [97], a nonlinear model-based adaptive output feedback controller was developed for a surface vessel. Global asymptotic position tracking was achieved assuming the structure of the mathematical model was of a particular form, with constant inertia and damping matrices. This structure was also extended to include a bias term representing drift, currents and wave load. Simulations were presented, but fell short of demonstrating the controller's robustness to unmodeled dynamics.

In the following, we introduce a Neural Network Model Reference Adaptive Controller (NN-MRAC), whose learning capabilities allow adaptation to the particular system's model and operating conditions, thus improving tracking performance of the closed-loop when faced with limited system information. The controller is dynamic, in that it features time varying gains, whose update mechanism is derived using Lyapunov stability theory. The resulting control command, in conjunction with these update laws, guarantees ultimate boundedness of parameter estimates and tracking errors. The algorithm relies on the use of a Single Hidden Layer Neural Network (SHL-NN), which allows to solve the tracking problem in spite of structural uncertainties in the system model.

Section 4.2 presents a model for the class of dynamical systems considered in this chapter. The main results are introduced in Section 4.3, which presents the two derived control algorithms along with stability proofs. Concluding remarks are offered in Section 4.3.

4.2. Marine Vehicle Model

This section presents a generic mathematical model of a marine vehicle. In particular, the model assumes that pitch, roll and heave motions are negligible and feature only the three

degrees of freedom corresponding to surge, sway and yaw motions. Because of this choice, it will be assumed that the vehicle's state space $\mathcal{D}$ coincides with $\mathbb{R}^6$, although the control algorithm can be easily extended to higher dimensions. The notation used for the vehicle's generalized equations of motion follows [86], but is reduced to motion in the horizontal plane. The Earth Fixed Frame (EFF), denoted by x_{e}, y_{e} and z_{e}, is chosen so that the vehicle's center of gravity is at the origin at time $t = 0$. The x_{e} and y_{e} axes are directed toward the North and the East, respectively, while the z_{e} axis points downward in accordance with the right hand rule. This frame is assumed to be inertial, the acceleration due to the earth's rotation being considered negligible. The vehicle's configuration in the EFF is

$$\eta(t) \triangleq [x_{\mathrm{N}}(t), y_{\mathrm{E}}(t), \psi(t)]^{\mathrm{T}}, \qquad t \geq 0, \tag{4.1}$$

where $x_{\mathrm{N}}(t) \in \mathbb{R}$ and $y_{\mathrm{E}}(t) \in \mathbb{R}$ describe the distance traveled along the x_{e} and y_{e} directions respectively, and $\psi(t) \in \mathbb{R}$ describes the rotation about the z_{e} axis.

The Body Fixed Frame (BFF) has its origin fixed at the vehicle's center of gravity, the x_{b} axis points forward, the y_{b} axis starboard, and the z_{b} axis downward. The vehicle's velocity is defined in the BFF as

$$\nu(t) \triangleq [u(t), v(t), r(t)]^{\mathrm{T}}, \qquad t \geq 0, \tag{4.2}$$

where $u(t) \in \mathbb{R}$ and $v(t) \in \mathbb{R}$ are the components of the absolute velocity in the x_{b} and y_{b} directions respectively, and $r(t) \in \mathbb{R}$ describes the angular velocity about the z_{b} axis. The vectors $\eta(t)$ and $\nu(t)$ are related by the kinematic equation [86],

$$\dot{\eta}(t) = J(\eta(t))\nu(t), \qquad t \geq 0, \tag{4.3}$$

where

$$J(\eta) \triangleq \begin{bmatrix} \cos\psi & -\sin\psi & 0 \\ \sin\psi & \cos\psi & 0 \\ 0 & 0 & 1 \end{bmatrix}, \tag{4.4}$$

is the rotation matrix from BFF to EFF.

Using the form introduced in [86] and the previous notation, the marine vehicle's equation of motion is given by

$$M\dot{\nu}(t) + C(\nu(t))\nu(t) + D(\nu(t))\nu(t) + g(\eta(t)) = \hat{B}\tau(t), \qquad t \geq 0, \tag{4.5}$$

where $M \in \mathbb{R}^{3\times 3}$ is the mass matrix (including added mass, see [86]), $C(\nu(t)) \in \mathbb{R}^{3\times 3}$ contains Coriolis and centripetal terms, $D(\nu(t)) \in \mathbb{R}^{3\times 3}$ is the damping matrix, $g(\eta(t)) \in \mathbb{R}^3$ is the vector of restoring forces and moments, $\tau(t) \in \mathbb{R}^m$ is the input vector, and $\hat{B} \in \mathbb{R}^{3\times m}$ characterizes how the control inputs affect the vehicle's dynamics.

While the rigid body inertia, Coriolis, centripetal, and gravitational terms are described in [86], the hydrodynamic terms are much more challenging to model and depend on the particular geometry of the considered vehicle. In general, even very thorough hydrodynamic modeling efforts are only able to partially describe the dynamic behavior of a marine vehicle. In light of these considerations, the considered vehicle dynamics are of the form

$$\dot{\nu}(t) = f(x(t)) + B\tau(t), \qquad t \geq 0, \tag{4.6}$$

where $x \triangleq [\ \eta^{\mathrm{T}} \quad \nu^{\mathrm{T}}\ ]^{\mathrm{T}}$ is the state vector and

$$\begin{aligned} B &\triangleq M^{-1}\hat{B}, \\ f(x) &\triangleq -M^{-1}[C(\nu) + D(\nu)]\nu - M^{-1}g(\eta), \end{aligned}$$

are assumed to be unknown.

In addition, the results in Section 4.3 will make use of the following reference system,

$$\begin{bmatrix} \dot{x}_{1\mathrm{r}}(t) \\ \dot{x}_{2\mathrm{r}}(t) \end{bmatrix} = \begin{bmatrix} 0_m & I_m \\ -\omega_0^2 & -A_{\mathrm{rm}} \end{bmatrix} \begin{bmatrix} x_{1\mathrm{r}}(t) \\ x_{2\mathrm{r}}(t) \end{bmatrix} + \begin{bmatrix} 0_m \\ \omega_0^2 \end{bmatrix} r_{\mathrm{s}}(t), \qquad t \geq 0, \tag{4.7}$$

where $x_{1\mathrm{r}}(t)$, $x_{2\mathrm{r}}(t) \in \mathbb{R}^m$, $t \geq 0$, and

$$A_{\mathrm{rm}} \triangleq \mathrm{diag}(2\zeta_1\omega_{01}, ..., 2\zeta_m\omega_{0m}), \qquad \omega_0 \triangleq \mathrm{diag}(\omega_{01}, ..., \omega_{0m}). \tag{4.8}$$

4.3. Control Command

Theorem 2.2.1 and Theorem 2.2.2 provided control algorithms for a large class of nonlinear systems. In this section, we introduce a pair of control laws which provide comparable functionalities, but for a more specialized class of systems, whose general form is given by (4.3) and (4.6).

Theorem 4.3.1. Consider the vehicle dynamics (4.3), (4.6) and the reference dynamics (4.7). Introduce a tracking error $e_1(\eta, x_{1\mathrm{r}}) \in \mathbb{R}^m$, where $\eta \in \mathbb{R}^n$ and $x_{1\mathrm{r}} \in \mathbb{R}^m$ represent the vehicle and reference configuration, respectively, such that $e_1(\eta(t), x_{1\mathrm{r}}(t)) \equiv 0$, $t \geq 0$, if and only if perfect tracking is achieved. Assume that the error dynamics can be written in the form

$$\dot{e}_1(t) = Q_1(\eta(t), x_{1\mathrm{r}}(t))q_2(x(t), x_{\mathrm{r}}(t), \chi(t)), \qquad t \geq 0, \tag{4.9}$$

where $\chi(t) \in \mathbb{R}^m$ is an exogenous signal, $x(t) \in \mathcal{D}$ is the state of the system, $x_{\mathrm{r}}(t) \in \mathbb{R}^{2m}$ is the reference state, $Q_1 : \mathbb{R}^n \times \mathbb{R}^m \to \mathbb{R}^{m\times m}$, and $q_2 : \mathbb{R}^{2n} \times \mathbb{R}^{2m} \times \mathbb{R}^m \to \mathbb{R}^m$ is such that $\frac{\partial q_2(x,x_{\mathrm{r}},\chi)}{\partial \nu} B \in \mathbb{R}^{m\times m}$ is invertible. In addition, assume there exists a Lyapunov function candidate $V_s(e_1)$ such that $V_s'(e_1) = 0$ if and only if $e_1 = 0$. Next, consider the control command

$$\tau^*(x, x_{\mathrm{r}}, \chi, r_{\mathrm{s}}) = -\Lambda \left[H(x, x_{\mathrm{r}}, \chi)w(x, x_{\mathrm{r}}, \chi, r_{\mathrm{s}}) + \delta^*(x)\right], \tag{4.10}$$

where $\tau^*(x, x_{\mathrm{r}}, \chi, r_{\mathrm{s}}) \in \mathbb{R}^m$, $\Lambda \in \mathbb{R}^{m\times m}$ is invertible, and

$$H(x, x_{\mathrm{r}}, \chi) \triangleq \left(\frac{\partial q_2(x, x_{\mathrm{r}}, \chi)}{\partial \nu} B\Lambda\right)^{-1} \in \mathbb{R}^{m\times m}, \tag{4.11}$$

$$w(x, x_r, \chi, r_{\rm s}) \triangleq \frac{\partial q_2(x, x_{\rm r}, \chi)}{\partial \eta} J(\eta)\nu + \frac{\partial q_2(x, x_{\rm r}, \chi)}{\partial x_{\rm r}} \dot{x}_{\rm r} + \frac{\partial q_2(x, x_{\rm r}, \chi)}{\partial \chi} \dot{\chi} - \dot{q}_{\rm 2des}(x, x_{\rm r})$$
$$+ e_2(x, x_{\rm r}, \chi) + G_2^{-1} Q_1^{\rm T}(\eta, x_{\rm 1r}) V_s'^{\rm T}(e_1) \in \mathbb{R}^m, \tag{4.12}$$
$$\delta^*(x) \triangleq \left(\frac{\partial q_2(x, x_{\rm r}, \chi)}{\partial \nu} B\Lambda \right)^{-1} \frac{\partial q_2(x, x_{\rm r}, \chi)}{\partial \nu} f(x) \in \mathbb{R}^m, \tag{4.13}$$

with

$$q_{\rm 2des}(\eta, x_{\rm 1r}) \triangleq -\alpha(\eta, x_{\rm 1r}) G_1 Q_1^{\rm T}(\eta, x_{\rm 1r}) V_s'^{\rm T}(e_1) \in \mathbb{R}^m, \tag{4.14}$$
$$e_2(x, x_{\rm r}, \chi) \triangleq q_2(x, x_{\rm r}, \chi) - q_{\rm 2des}(\eta, x_{\rm 1r}) \in \mathbb{R}^m, \tag{4.15}$$

where $\alpha : \mathbb{R}^n \times \mathbb{R}^m \to \mathbb{R}^+$, $G_1 \in \mathbb{R}^{m \times m}$ is positive definite. Then the zero solution of the error dynamics associated with the closed loop given by (4.3), (4.6), (4.7), and (4.10) is asymptotically stable.

Proof. Using (4.9), the derivative of the Lyapunov function candidate $V_s(e_1)$ is given by

$$\dot{V}_s(t) = V_s'^{\rm T}(e_1(t)) Q_1(\eta(t), x_{\rm 1r}(t)) q_2(x(t), x_{\rm r}(t), \chi(t)), \qquad t \geq 0, \tag{4.16}$$

Using a backstepping approach derived from that presented in [10], we will use $q_2(x, x_{\rm r}, \chi)$ as a virtual control command. Ideally $q_2(x, x_{\rm r}, \chi)$ would be equal to $q_{\rm 2des}(\eta, x_{\rm 1r})$ defined by (4.14), such that

$$\dot{V}_s(t) \mid_{q_2 = q_{\rm 2des}} = -\alpha(\eta(t), x_{\rm 1r}(t)) V_s'(e_1(t)) Q_1(\eta(t), x_{\rm 1r}(t)) G_1 Q_1^{\rm T}(\eta(t), x_{\rm 1r}(t)) V_s'^{\rm T}(e_1(t)), \quad t \geq 0, \tag{4.17}$$

which is negative definite. Next, consider a new Lyapunov function candidate,

$$V^*(e_1, e_2) = V_s(e_1) + \frac{1}{2} e_2^{\rm T} G_2 e_2, \tag{4.18}$$

where $G_2 \in \mathbb{R}^{m\times m}$ is positive definite and e_2 is defined by (4.15). The time derivative of (4.18) is of the form

$$\dot{V}^*(t) = \dot{V}_s(e_1(t)) + e_2^{\mathrm{T}}(t)G_2\dot{e}_2(t), \qquad t \geq 0, \tag{4.19}$$

Next, taking the derivative of (4.15) and substituting the kinematic and dynamic equations, (4.3) and (4.6), we find the error dynamics to be of the form

$$\begin{aligned}\dot{e}_2(x, x_{\mathrm{r}}, \chi, r_{\mathrm{s}}, \tau^*) \;=\; & \frac{\partial q_2(x, x_{\mathrm{r}}, \chi)}{\partial \eta} J(\eta)\nu + \frac{\partial q_2(x, x_{\mathrm{r}}, \chi)}{\partial \nu}(f(x) + B\tau^*) + \frac{\partial q_2(x, x_{\mathrm{r}}, \chi)}{\partial x_{\mathrm{r}}}\dot{x}_{\mathrm{r}} \\ & + \frac{\partial q_2(x, x_{\mathrm{r}}, \chi)}{\partial \chi}\dot{\chi} - \dot{q}_{2\mathrm{des}}(x, x_{\mathrm{r}}),\end{aligned} \tag{4.20}$$

which, after substituting the control input (4.10), provides the following closed loop error dynamics

$$\dot{e}_1(x, x_{\mathrm{r}}, \chi) \;=\; Q_1(\eta, x_{1\mathrm{r}})q_2(x, x_{\mathrm{r}}, \chi), \tag{4.21}$$

$$\dot{e}_2(x, x_{\mathrm{r}}, \chi) \;=\; -e_2(x, x_{\mathrm{r}}, \chi) - G_2^{-1}Q_1^{\mathrm{T}}(\eta, x_{1\mathrm{r}}){V_s'}^{\mathrm{T}}(e_1). \tag{4.22}$$

Therefore, (4.19) becomes

$$\begin{aligned}\dot{V}^*(t) \;=\; & -\alpha(\eta(t), x_{1\mathrm{r}}(t))V_s'(e_1(t))Q_1(\eta(t), x_{1\mathrm{r}}(t))G_1Q_1^{\mathrm{T}}(\eta(t), x_{1\mathrm{r}}(t)){V_s'}^{\mathrm{T}}(e_1(t)) - e_2^{\mathrm{T}}(t)G_2e_2(t), \\ & t \geq 0,\end{aligned} \tag{4.23}$$

which is negative definite, proving asymptotic stability of the closed loop error dynamics. This concludes this proof. □

Remark 4.3.1. The matrix $H(\cdot)$ and function $\delta^*(x)$ in (4.10) are unknown, while the vector $w(x, x_{\mathrm{r}}, \chi, r_{\mathrm{s}})$ is a known function of the states and reference input.

The following result relies on the assumption that $\frac{\partial q_2(x,x_{\rm r},\chi)}{\partial \nu}$ is constant, and that Λ is constructed such that $H(x,x_{\rm r},\chi)=\Theta^*\in\mathbb{R}^{m\times m}$ is positive definite for all $(x,x_{\rm r},\chi)\in\mathbb{R}^{2n}\times\mathbb{R}^{2m}\times\mathbb{R}^m$. Since Θ^* and $\delta^*(x)$ from Theorem 4.3.1 are unknown, their estimates need to be introduced. In particular, Θ^* in (4.10) will be replaced by an estimate $\Theta(t)$, $t\geq 0$. Following the approach described in [98], the vector function $\delta^*(x)$ is approximated by the output of a linearly parameterized neural network $W(t)\sigma(x(t))$, $t\geq 0$, with maximum approximation error $\varepsilon^*>0$.

Theorem 4.3.2. Consider the system, tracking error and virtual command described in Theorem 4.3.1. Assume that $\frac{\partial q_2(x,x_{\rm r},\chi)}{\partial \nu}$ is constant, and that Λ is constructed such that $H(x,x_{\rm r},\chi)=\left(\frac{\partial q_2(x,x_{\rm r},\chi)}{\partial \nu}B\Lambda\right)^{-1}=\Theta^*\in\mathbb{R}^{m\times m}$ is positive definite for all $(x,x_{\rm r},\chi)\in\mathbb{R}^{2n}\times\mathbb{R}^{2m}\times\mathbb{R}^m$. Then, consider the following control law,

$$\tau(t)=-\Lambda\left[\Theta(t)w(x(t),x_{\rm r}(t),\chi(t),r_{\rm s}(t))+W(t)\sigma(x(t))\right],\qquad t\geq 0, \tag{4.24}$$

where $\Theta(t)\in\mathbb{R}^{m\times m}$ and $W(t)\in\mathbb{R}^{m\times q}$, $t\geq 0$, are parameter estimates, and $\sigma(x)\in\mathbb{R}^q$, $x\in\mathbb{R}^n$, is such that there exists $W^*\in\mathbb{R}^{m\times q}$ for which $W^*\sigma(x)=\delta^*(x)-\varepsilon(x)$, with $\|\varepsilon(x)\|<\varepsilon^*$ for all $x\in\mathbb{R}^{2n}$. Furthermore, let the parameter update laws be

$$\dot{\Theta}(t)=G_2e_2(t)w^{\rm T}(x(t),x_{\rm r}(t),\chi(t),r_{\rm s}(t))\Gamma_1-\sigma_1\Theta(t),\quad \Theta(0)=\Theta_0,\quad t\geq 0, \tag{4.25}$$

$$\dot{W}(t)=G_2e_2(t)\sigma^{\rm T}(x(t))\Gamma_2-\sigma_2W(t),\qquad W(0)=W_0, \tag{4.26}$$

where $\Gamma_1\in\mathbb{R}^{m\times m}$ and $\Gamma_2\in\mathbb{R}^{q\times q}$ are positive definite $\sigma_1>0$, and $\sigma_2>0$. Then the tracking error and the parameter estimates are ultimately bounded with a domain of convergence defined as

$$\mathcal{M}_{\rm c}\triangleq\{(e_1,e_2,\tilde{\Theta},\tilde{W}):V(e_1,e_2,\tilde{\Theta},\tilde{W})\leq\varsigma\}, \tag{4.27}$$

where $\tilde{\Theta}(t) \triangleq \Theta(t) - \Theta^*$, and $\tilde{W}(t) \triangleq W(t) - W^*$, $t \geq 0$. In addition,

$$V(e_1, e_2, \tilde{\Theta}, \tilde{W}) = V_s(e_1) + \frac{1}{2} e_2^{\mathrm{T}} G_2 e_2 + \frac{1}{2} \mathrm{tr}[\Theta^{*-1} B \Lambda \tilde{\Theta} \Gamma_1^{-1} \tilde{\Theta}^{\mathrm{T}}] + \frac{1}{2} \mathrm{tr}[\Theta^{*-1} B \Lambda \tilde{W} \Gamma_2^{-1} \tilde{W}^{\mathrm{T}}], \quad (4.28)$$

and

$$\varsigma \triangleq \max_{(e_1, e_2, \tilde{\Theta}, \tilde{W}) \in \mathcal{M}} V(e_1, e_2, \tilde{\Theta}, \tilde{W}), \quad (4.29)$$

$$\begin{aligned} \mathcal{M} \triangleq \{(e_1, e_2, \tilde{\Theta}, \tilde{W}) : \ & \mathrm{tr}[B \Lambda_1 \tilde{W} \Gamma_2^{-1} \tilde{W}^{\mathrm{T}}] \leq \mathrm{tr}[B \Lambda_1 W^* \Gamma_2^{-1} W^{*\mathrm{T}}], \\ & \mathrm{tr}[B \Lambda_1 \tilde{\Theta} \Gamma_1^{-1} \tilde{\Theta}^{\mathrm{T}}] \leq \mathrm{tr}[B \Lambda_1 \Theta^* \Gamma_1^{-1} \Theta^{*\mathrm{T}}], \\ & \left\| G_2^{\frac{1}{2}} e_2(x, x_{\mathrm{r}}, \chi) \right\| \leq \left\| G_2^{\frac{1}{2}} \frac{\partial q_2(x, x_{\mathrm{r}}, \chi)}{\partial \nu} B \Lambda_1 \right\| \varepsilon^* \}. \end{aligned} \quad (4.30)$$

Proof. The tracking error $e_1(t)$, $t \geq 0$, is obtained from (4.9). In addition, $e_2(t)$, $t \geq 0$, is obtained from

$$\begin{aligned} \dot{e}_2(x, x_{\mathrm{r}}, \chi, r_{\mathrm{s}}, \tau^*) = & \frac{\partial q_2(x, x_{\mathrm{r}}, \chi)}{\partial \eta} J(\eta) \nu + \frac{\partial q_2(x, x_{\mathrm{r}}, \chi)}{\partial \nu} (f(x) + B\tau) + \frac{\partial q_2(x, x_{\mathrm{r}}, \chi)}{\partial x_{\mathrm{r}}} \dot{x}_{\mathrm{r}} \\ & + \frac{\partial q_2(x, x_{\mathrm{r}}, \chi)}{\partial \chi} \dot{\chi} - \dot{q}_{2\mathrm{des}}(x, x_{\mathrm{r}}). \end{aligned} \quad (4.31)$$

Substituting (4.24) into (4.31) and using the fact that $H(x, x_{\mathrm{r}}, \chi) = \Theta^*$ allows to rewrite (4.31) as

$$\begin{aligned} \dot{e}_2(x, x_{\mathrm{r}}, \chi, r_{\mathrm{s}}, \Theta, W) = & \frac{\partial q_2(x, x_{\mathrm{r}}, \chi)}{\partial \eta} J(\eta) \nu + \frac{\partial q_2(x, x_{\mathrm{r}}, \chi)}{\partial \nu} f(x) + \frac{\partial q_2(x, x_{\mathrm{r}}, \chi)}{\partial x_{\mathrm{r}}} \dot{x}_{\mathrm{r}} - \dot{q}_{2\mathrm{des}}(x, x_{\mathrm{r}}) \\ & + \frac{\partial q_2(x, x_{\mathrm{r}}, \chi)}{\partial \chi} \dot{\chi} - \Theta^{*-1} \left[\Theta w(x, x_{\mathrm{r}}, \chi, r_{\mathrm{s}}) + W \sigma(x) \right]. \end{aligned} \quad (4.32)$$

Note that the assumption that $\frac{\partial q_2(x, x_{\mathrm{r}}, \chi)}{\partial \nu}$ is constant leads to a constant Θ^*, which is key in obtaining a control law that is linear in the unknown parameters, thus allowing application of the certainty equivalence principle. Substituting (4.12) and (4.13) into (4.32), we obtain

$$\dot{e}_2(x, x_{\mathrm{r}}, \chi, \tilde{\Theta}, \tilde{W}, r_{\mathrm{s}}) = -e_2(x, x_{\mathrm{r}}, \chi) - G_2^{-1} Q_1^{\mathrm{T}}(\eta, x_{1\mathrm{r}}) V_s'^{\mathrm{T}}(e_1) - \Theta^{*-1} \gamma(x, x_{\mathrm{r}}, \chi, \tilde{\Theta}, \tilde{W}, r_{\mathrm{s}}), \quad (4.33)$$

where

$$\gamma(x, x_{\mathrm{r}}, \chi, \tilde{\Theta}, \tilde{W}, r_{\mathrm{s}}) \triangleq \tilde{\Theta} w(x, x_{\mathrm{r}}, \chi, r_{\mathrm{s}}) + \tilde{W}\sigma(x) - \varepsilon(x). \tag{4.34}$$

To show ultimate boundedness of the closed loop error dynamics given by (4.9) and (4.33), the Lyapunov function candidate (4.28) is considered. The corresponding Lyapunov derivative is given by

$$\begin{aligned}\dot{V}(t) \;=\; & -\alpha(\eta(t), x_{1\mathrm{r}}(t)) V_s'(e_1(t)) Q_1(\eta(t), x_{1\mathrm{r}}(t)) G_1 Q_1^{\mathrm{T}}(\eta(t), x_{1\mathrm{r}}(t)) V_s'^{\mathrm{T}}(e_1(t)) - e_2^{\mathrm{T}}(t) G_2 e_2(t) \\ & + e_2^{\mathrm{T}}(t) G_2 \Theta^{*-1} \varepsilon(x(t)) + \mathrm{tr}[\Theta^{*-1} \tilde{\Theta}(t) (\Gamma_1^{-1} \dot{\Theta}^{\mathrm{T}}(t) - w(x(t), x_{\mathrm{r}}(t), \chi(t), r_{\mathrm{s}}(t)) e_2^{\mathrm{T}}(t) G_2)] \\ & + \mathrm{tr}[\Theta^{*-1} \tilde{W}(t) (\Gamma_2^{-1} \dot{W}^{\mathrm{T}}(t) - \sigma(x(t)) e_2^{\mathrm{T}}(t) G_2)], \qquad t \geq 0.\end{aligned}$$

Finally, the update laws (4.25) and (4.26) provide the following bound for the Lyapunov derivative,

$$\begin{aligned}\dot{V}(t) \leq & -\frac{\sigma_1}{2} \mathrm{tr}[\Theta^{*-1} \tilde{\Theta}(t) \Gamma_1^{-1} \tilde{\Theta}^{\mathrm{T}}(t)] + \frac{\sigma_1}{2} \mathrm{tr}[\Gamma_1^{-1} \Theta^{*\mathrm{T}}] - \frac{\sigma_2}{2} \mathrm{tr}[\Theta^{*-1} \tilde{W}(t) \Gamma_2^{-1} \tilde{W}^{\mathrm{T}}(t)] \\ & + \frac{\sigma_2}{2} \mathrm{tr}[\Theta^{*-1} W^* \Gamma_2^{-1} W^{*\mathrm{T}}] - \left\| G_2^{\frac{1}{2}} e_2(t) \right\| \left(\left\| G_2^{\frac{1}{2}} e_2(x, x_{\mathrm{r}}, \chi) \right\| - \left\| G_2^{\frac{1}{2}} \frac{\partial q_2(x, x_{\mathrm{r}}, \chi)}{\partial \nu} B \Lambda_1 \right\| \varepsilon^* \right).\end{aligned} \tag{4.35}$$

It follows that the solution of (4.25), (4.26), (4.9), and (4.33) is ultimately bounded and converges to the compact set $\mathcal{M}_{\mathrm{c}}$ ([88]). □

Remark 4.3.2. The assumptions taken ensure that one can always construct a design parameter Λ such that Θ^* is positive definite.

Remark 4.3.3. The condition that $\frac{\partial q_2(x, x_{\mathrm{r}}, \chi)}{\partial \nu}$ be constant is satisfied for a choice of $q_2(\cdot)$ that is linearly dependent on the system's velocity. In that sense, $q_2(\cdot)$ is itself a velocity,

which is consistent with the fact that the tracking error $e_2(t)$, $t \geq 0$, whose definition is the difference between $q_2(\cdot)$ and its desired value, is a velocity error. For instance, consider the case of a fully actuated vehicle, with the generic position error $e_1(t) = x_{\mathrm{r}1}(t) - \eta(t)$, $t \geq 0$. It follows from (4.3) and (4.7), that $\dot{e}_1(t) = x_{\mathrm{r}2}(t) - J(\psi(t))\nu(t)$, $t \geq 0$. Hence, by choosing

$$Q_1(t) = J(\psi(t)), \qquad q_2(t) = J^{\mathrm{T}}(\psi(t))x_{\mathrm{r}2}(t) - \nu(t), \qquad t \geq 0, \tag{4.36}$$

it directly follows that $\frac{\partial q_2(x,x_{\mathrm{r}},\chi)}{\partial \nu} = -I_3$.

Remark 4.3.4. Note that, if a particular choice of $\sigma(x)$ is known, for which there exists W^* such that $\delta^*(x) = W^*\sigma(x)$, then σ_1 and σ_2 can be chosen equal to zero and LaSalle-Yoshizawa theorem can be used to conclude Lyapunov stability of the tracking error dynamics' zero solution, asymptotic convergence of these errors to zero, and boundedness of the estimates $\Theta(t)$ and $W(t)$, $t \geq 0$.

Remark 4.3.5. Note that requiring that $\frac{\partial q_2(x,x_{\mathrm{r}},\chi)}{\partial \nu}$ be constant leads to a command that is linear in the uncertain parameters. This linearity facilitates proof of Theorem 4.3.2, which results from the application of the equivalence certainty principle. For some specific choices of tracking errors however, it becomes difficult to ensure that $\frac{\partial q_2(x,x_{\mathrm{r}},\chi)}{\partial \nu}$ is indeed constant. As will be shown in a later chapter, the flexibility provided by the inclusion of the exogenous signal $\chi(t)$, $t \geq 0$, can be used to judiciously alter the choice of tracking errors, resulting in a command linear in the uncertain parameters.

4.4. Conclusion

A neural network based MRAC algorithm was developed. Lyapunov stability theory was used to demonstrate that parameter estimates and tracking errors are ultimately bounded.

Use of a SHL-NN allowed derivation of a control algorithm in spite of structural uncertainties and thus severely limited knowledge of the system's dynamics. The presented control algorithm is relevant to a wide variety of marine vehicles, such as surface crafts and underwater vehicles. In addition, it was designed to accommodate both fully actuated and underactuated vehicles with stable internal dynamics. Application of the presented control framework to underactuated vehicles with unstable internal dynamics, although possible, is not necessarily straightforward, and will be addressed in the next chapter.

Chapter 5

Nonlinear Control of Non-Minimum Phase Autonomous Marine Vehicles [4, 5]

The following results were presented at the 4$^{\text{th}}$ Asian Control Conference in 2002 ([4]) and at the 2003 IEEE Conference on Decision and Control ([5]).

5.1. Introduction

As mentioned in the previous chapter, research on motion control of AMVs has received considerable attention from the community over the past decades ([92–96,99–103]). However, the tracking problem for one of the most commonly encountered class of marine vehicles (i.e. marine vehicles equipped with a fixed thruster and a rudder, [104]) is rarely considered. Notable exceptions include [100], which contains simplifying assumptions removing relevant dynamic behaviors.

The lack of a systematic study of this particular problem can be partially explained by the difficulty in solving the full motion control problem for an AMV equipped with

a fixed thruster and a rudder. Typically, the design of a motion controller relies on a mathematical model of the system to control. However, in the case of marine vehicles, obtaining a model that will satisfactorily capture the dynamic behavior of the system is fairly difficult. Another issue arises from the fact that the magnitude of the control effort generated by propulsion systems on AMVs is not only finite, but rather limited. Finally, considering motion in the horizontal plane exclusively, it is apparent that the considered class of AMVs feature three degrees of freedom (surge, sway and yaw), while the aforementioned propulsion system only provides two independent control inputs (surge force and either sway force or yawing moment). Hence, having one fewer independent control input than degree of freedom, the system is underactuated. Furthermore, the zero-dynamics ([105]) implied by this underactuation have proven to be intrinsically unstable ([5, 93]). This means that if the control approach is not carefully chosen, the behavior of the zero-dynamics might not be acceptable and the obtained controller will be of no practical use. A system featuring an unstable zero-dynamics is referred to as a non-minimum phase system ([106]).

Nevertheless, a number of control algorithms designed for underactuated marine vehicles can be found in the literature (for instance, [92–96]). In [92], a surface ship equipped with a pair of propellers is considered, and external disturbances such as ocean currents, are accounted for. In [93], a controller for an underactuated AMV equipped with a propeller and a side thruster is designed. The corresponding vehicle's model is fairly similar to that of a vehicle with a thruster and rudder, as it includes a coupling between sway force and yawing moment. The controller also handles constant and slow varying external perturbations.

In [103], the authors present a control framework relying on a particular error variable corresponding to the angle between the vehicle's longitudinal axis and the direction of the

vehicle's desired position, noted β. The resulting controller solves the regulation problem for an underactuated AMV. The introduction of this relative orientation is progressively spreading through the literature. It can be found in [66] and, more recently, in [107]. The control algorithm presented in this chapter builds upon the approach introduced in [103], using the same error variable β, but extending the problem to trajectory tracking, and dealing with unstable zero-dynamics. The control of underactuated marine vehicles with an unstable zero-dynamics (or underactuated non-minimum phase marine vehicles) is rarely treated. This control problem is considered in [66], however, the result in [66] is limited to way-point maneuvering and requires full knowledge of the system's model.

To solve the trajectory tracking problem for the considered class of systems, a back-stepping procedure is used ([10]). As mentioned previously, special care has to be taken in choosing the tracking errors since this choice affects the stability properties of the internal dynamics. More specifically, an inadequate choice of tracking errors can lead to an unstable behavior of the internal dynamics ([93, 104]). To address this issue, the presented approach builds upon that introduced in [103], following a control strategy similar to that presented in the previous chapter. In particular, the tracking errors are chosen as the distance between current and desired position, and relative direction of this desired position. The resulting behavior of the internal dynamics is investigated by assessing the stability of the zero-dynamics.

This chapter introduces a nonlinear control algorithm solving the tracking problem for the considered class of non-minimum phase marine vehicles. In Section 5.2, a control law guaranteeing good tracking performance for the considered error variables, assuming full knowledge of the system's model, is derived. The control algorithm is derived using a back-

stepping procedure ([10]). The stability of the resulting zero-dynamics is studied in Section 5.3. Section 5.4 concludes this chapter.

5.2. Nonlinear Control Algorithm

The control algorithm in Chapter 4 relied on a neural network to compensate for the system's dynamics. Accordingly, the specific form of M, $C(\nu)$, $D(\nu)$ and $g(\eta)$ in (4.5) does not directly affect the expression of the control laws in Theorem 4.3.1 and Theorem 4.3.2. In this chapter however, the aim is to develop a nonlinear control algorithm, the form of which depends upon that of the various terms in (4.5). In the following, it will be assumed that ([86])

$$M = \begin{bmatrix} m_1 & 0 & 0 \\ 0 & m_2 & m_{23} \\ 0 & m_{23} & m_3 \end{bmatrix}, \quad D(\nu) = \begin{bmatrix} d_{\mathrm{l}1} + d_{\mathrm{q}1}|u| & 0 & 0 \\ 0 & d_{\mathrm{l}2} + d_{\mathrm{q}2}|v| & d_{\mathrm{l}23} + d_{\mathrm{q}23}|r| \\ 0 & d_{\mathrm{l}23} + d_{\mathrm{q}23}|v| & d_{\mathrm{l}3} + d_{\mathrm{q}3}|r| \end{bmatrix}, \tag{5.1}$$

$$C(\nu) = \begin{bmatrix} 0 & 0 & -m_2 v - m_{23} r \\ 0 & 0 & m_1 u \\ m_2 v + m_{23} r & -m_1 u & 0 \end{bmatrix}, \tag{5.2}$$

where m_i, d_{li}, d_{qi}, $i = 1, 2, 3$, m_{23}, $d_{\mathrm{l}23}$ and $d_{\mathrm{q}23}$ are uncertain constant parameters. In addition, the vector of restoring forces and moments will be assumed to be the three-by-one zero matrix $0_{3\times 1}$, and the input matrix $\hat{B}$ is given by

$$\hat{B} \triangleq \begin{bmatrix} 1 & 0 \\ 0 & -1/l \\ 0 & 1 \end{bmatrix}, \tag{5.3}$$

where $l > 0$ represents the arm of the sway force generated by the rudder with respect to the center of gravity of the vehicle. Finally, the control input is $\tau(t) \triangleq \begin{bmatrix} \tau_1(t) & \tau_2(t) \end{bmatrix}^{\mathrm{T}} \in \mathbb{R}^2$, $t \geq 0$.

The dynamics (4.5) can be expressed in a more compact form by factorizing the uncertain

parameters,

$$\dot{\nu}(t) \,=\, \Theta_1^* \varphi_1(\nu(t)) + \Theta_2^* \tau(t), \qquad \nu(0) = \nu_0, \qquad t \geq 0, \tag{5.4}$$

with

$$\Theta_1^* \triangleq -M^{-1} \begin{bmatrix} d_{\mathrm{l}1} & 0 & 0 & d_{\mathrm{q}1} & 0 & 0 & 0 & 0 & -m_2 & -m_{23} \\ 0 & d_{\mathrm{l}2} & d_{\mathrm{l}23} & 0 & d_{\mathrm{q}2} & d_{\mathrm{q}23} & 0 & m_1 & 0 & 0 \\ 0 & d_{\mathrm{l}23} & d_{\mathrm{l}3} & 0 & d_{\mathrm{q}23} & d_{\mathrm{q}3} & m_2 - m_1 & m_{23} & 0 & 0 \end{bmatrix}, \tag{5.5}$$

$$\Theta_2^* \triangleq M^{-1}\hat{B} = \begin{bmatrix} \theta_{21}^* & 0 \\ 0 & \theta_{22}^* \\ 0 & \theta_{23}^* \end{bmatrix}, \quad \varphi_1(\nu) \triangleq \begin{bmatrix} \nu^{\mathrm{T}} & |u|u & |v|v & |r|r & uv & ur & vr & r^2 \end{bmatrix}^{\mathrm{T}}, \tag{5.6}$$

Consider the following tracking errors,

$$e_{\mathrm{d}}(\eta, x_{\mathrm{r}1}) \triangleq \| x_{\mathrm{r}1} - \begin{bmatrix} x & y \end{bmatrix}^{\mathrm{T}} \|, \tag{5.7}$$

$$\beta(\eta, x_{\mathrm{r}1}) \triangleq \mathrm{atan2}(x_{\mathrm{r}12} - y, x_{\mathrm{r}11} - x) - \psi, \tag{5.8}$$

where $x_{\mathrm{r}11}$ and $x_{\mathrm{r}12}$ are the components of $x_{\mathrm{r}1}$, so that $x_{\mathrm{r}1} \triangleq \begin{bmatrix} x_{\mathrm{r}11} & x_{\mathrm{r}12} \end{bmatrix}^{\mathrm{T}}$, $\mathrm{atan2}(\alpha_1, \alpha_2) \triangleq \arg(\alpha_1 + i\alpha_2)$, for all $(\alpha_1, \alpha_2) \in \mathbb{R}^2 \setminus (0,0)$, and $\arg(z)$ is the argument of $z \in \mathbb{C}$, such that $\arg(z) = \varphi$ whenever $z = |z|e^{i\varphi}$, with $\varphi \in (-\pi, \pi]$ and $i \triangleq \sqrt{-1}$.

The above errors are of particular geometric significance. More specifically, $e_{\mathrm{d}}(\cdot) \in \mathbb{R}^+$ represents the distance between system and reference position, while $\beta(\cdot) \in (-\pi, \pi]$ corresponds to the angle from the longitudinal, $u-$axis of the body fixed frame to the direction from system to the reference position. Note that, when $e_{\mathrm{d}}(\cdot) = 0$, $\beta(\cdot)$ is undefined ($\mathrm{atan2}(\alpha_1, \alpha_2)$ is undefined for $\alpha_1 = \alpha_2 = 0$).

The control objective is bounded-error tracking, or, more specifically, $(e_{\mathrm{d}}(t), \beta(t)) \to (a, 0)$ as $t \to \infty$, with $a > 0$. These errors are grouped in $e_1(\eta, x_{\mathrm{r}1}) \triangleq [\, e_{\mathrm{d}}(\eta, x_{\mathrm{r}1}),\ \beta(\eta, x_{\mathrm{r}1}) \,]^{\mathrm{T}}$, whose time derivative, following the notations used for Theorem 4.3.1, can be written as

$$\dot{e}_1(t) = Q_1(e_1(t)) q_2(\eta(t), \nu(t), x_{\mathrm{r}}(t)), \qquad e_1(0) = e_1(\eta_0, x_{\mathrm{r}10}), \qquad t \geq 0, \tag{5.9}$$

where

$$Q_1(e_1) \triangleq \begin{bmatrix} 1 & 0 \\ 0 & 1/e_{\rm d} \end{bmatrix} J_{\rm s}^{\rm T}(\beta), \qquad q_2(\eta, \nu, x_{\rm r}) \triangleq J_{\rm s}^{\rm T}(\psi) x_{\rm r2} + B_e(e_1(\eta, x_{\rm r1}))\nu, \tag{5.10}$$

with

$$J_{\rm s}(\cdot) \triangleq \begin{bmatrix} \cos(\cdot) & -\sin(\cdot) \\ \sin(\cdot) & \cos(\cdot) \end{bmatrix}, \qquad B_e(e_1) \triangleq \begin{bmatrix} -1 & 0 & e_{\rm d}\sin(\beta) \\ 0 & -1 & -e_{\rm d}\cos(\beta) \end{bmatrix}. \tag{5.11}$$

Now consider the following Lyapunov function candidate,

$$V_s(e_1) \triangleq e_{\rm d}\sin^2(\beta/2) + \frac{1}{2}(e_{\rm d} - a)^2. \tag{5.12}$$

Note that $V_s(e_1) = 0$ if and only if $e_d = a$ and $\beta = 0$. In addition, it follows from (4.14) and (5.12), choosing $\alpha(\eta, x_{\rm r1}) = e_{\rm d}(\eta, x_{\rm r1})$ and $G_1 = g_1 I_2$, with $g_1 > 0$, that

$$q_{\rm 2des}(e_1) = -e_{\rm d} J_{\rm s}(\beta) G_1 \gamma(e_1), \tag{5.13}$$

where $\gamma(e_1) \triangleq \begin{bmatrix} \sin^2(\beta/2) + e_{\rm d} - a & \sin(\beta)/2 \end{bmatrix}^{\rm T}$. The time derivative of $q_{\rm 2des}(t)$, $t \geq 0$, is of the form

$$\begin{aligned} \dot{q}_{\rm 2des}(t) \;=\; & J_{\rm s} G_1(\beta(t))\Big(\begin{bmatrix} e_{\rm d}(t) & \sin(\beta(t))/2 \\ 0 & \cos(\beta(t))/2 \end{bmatrix} + \begin{bmatrix} \gamma(e_1(t)) & \tilde{G}\gamma(e_1(t)) \end{bmatrix}\Big) J_{\rm s}^{\rm T}(\beta(t))(e_2(t) \\ & -e_{\rm d}(t) J_{\rm s}(\beta(t)) G_1 \gamma(e_1(t))), \qquad t \geq 0, \end{aligned} \tag{5.14}$$

with

$$S \triangleq \begin{bmatrix} 0 & 1 \\ -1 & 0 \end{bmatrix}, \quad \tilde{G} \triangleq G_1^{-1} S^{\rm T} G_1, \quad e_2(t) = q_2(\eta(t), \nu(t), x_{\rm r}(t)) - q_{\rm 2des}(e_1(t)), \quad t \geq 0. \tag{5.15}$$

The velocity error dynamics is of the form

$$\begin{aligned} \dot{e}_2(t) \;=\; & J_{\rm s}^{\rm T}(\psi(t))(-\omega_0^2 x_{\rm r1}(t) + (r(t)S - 2\zeta\omega_0)x_{\rm r2}(t) + \omega_0^2 r_{\rm s}(t)) + r(t)S q_2(t) - \dot{q}_{\rm 2des}(e_1(t), e_2(t)) \\ & + B_e(e_1(t))\Theta_1^* \varphi_1(\nu(t)) + B_e(e_1(t))\Theta_2^* \tau(t), \qquad e_2(0) = e_2(\eta_0, \nu_0, x_{\rm r0}), \qquad t \geq 0. \end{aligned} \tag{5.16}$$

Finally, choosing $\Lambda = I_2$ and $\chi(t) \equiv 0$, $t \geq 0$, it follows from Theorem 4.3.1 that the control command

$$\tau^*(t) = -(B_e(e_1(t))\Theta_2^*)^{-1}\Big(J_{\rm s}^{\rm T}(\psi(t))(-\omega_0^2 x_{\rm r1}(t) + (r(t)S - 2\zeta\omega_0)x_{\rm r2}(t) + \omega_0^2 r_{\rm s}(t)) + r(t)Sq_2(t) - \dot{q}_{\rm 2des}(e_1(t), e_2(t)) + e_2(t) + G_2^{-1}J_{\rm s}(\beta(t))\gamma(e_1(t)) + B_e(e_1(t))\Theta_1^*\varphi_1(\nu(t))\Big), \; t \geq 0, \quad (5.17)$$

guarantees that the solution $\left[\begin{array}{cc} e_{\rm d}(t) & \beta(t) \end{array}\right]^{\rm T} \equiv \left[\begin{array}{cc} a & 0 \end{array}\right]^{\rm T}$, $e_2(t) \equiv 0$, $t \geq 0$, to (5.9) and (5.16), is asymptotically stable.

5.3. Internal Dynamics Analysis

The control law presented in the previous section is such that the tracking error $e_1(\eta, x_{\rm r1})$ asymptotically converges to $\left[\begin{array}{cc} a & 0 \end{array}\right]^{\rm T}$. However, the stability analysis which led to the proof of Theorem 4.3.1 does not account for the behavior of the internal dynamics, which is essential in assessing the merit of the control approach.

Zero-dynamics

Consider the following change of coordinates,

$$\Phi(s) = \left[\begin{array}{c} \xi_1^1(s) \\ \xi_2^1(s) \\ \xi_1^2(s) \\ \xi_2^2(s) \\ \varsigma_1(s) \\ \varsigma_2(s) \end{array}\right] \triangleq \left[\begin{array}{c} e_{\rm d}(s) \\ L_f e_{\rm d}(s) \\ \beta(s) \\ L_f\beta(s) \\ \psi \\ m_4 v + m_5 r \end{array}\right], \quad (5.18)$$

where $s \triangleq (\eta, \nu, x_{\rm r})$, $f(s) \triangleq \left[\begin{array}{cccc} \nu^{\rm T}J^{\rm T}(\eta) & \varphi_1^{\rm T}(\nu)\Theta_1^{*\rm T} & x_{\rm r}^{\rm T}A_{\rm r}^{\rm T} \end{array}\right]^{\rm T}$, $m_4 \triangleq lm_2 + m_{23}$, $m_5 \triangleq m_3 + lm_{23}$, and $L_f h(s) \triangleq h'(s)f(s)$ denotes the Lie derivative of $h(s)$ with respect to $f(s)$. Note that $\Phi(\cdot)$ maps the six states (x, y, ψ, u, v, r) into six new states $(\xi_1^1, \xi_2^1, \xi_1^2, \xi_2^2, \varsigma_1, \varsigma_2)$,

while $x_{\rm r} \in \mathbb{R}^4$, for the purpose of this analysis, represents an exogenous signal. Computing $\Phi^{-1}(\cdot)$, it follows that

$$\eta(\xi,\varsigma,x_{\rm r}) \,=\, \left[\begin{array}{ccc} x_{\rm r11}-\xi_1^1\cos(\xi_1^2-\varsigma_1) & x_{\rm r12}-\xi_1^1\sin(\xi_1^2-\varsigma_1) & \varsigma_1 \end{array}\right]^{\rm T}, \tag{5.19}$$

$$\begin{aligned}\nu(\xi,\varsigma,x_{\rm r}) \,=\, & \frac{1}{m_6(\xi)}\left[\begin{array}{ccc} -m_6(\xi) & m_4\xi_1^1\sin(\xi_1^2) & \xi_1^1\sin(\xi_1^2) \\ 0 & -m_5 & -\xi_1^1\cos(\xi_1^2) \\ 0 & m_4 & 1 \end{array}\right] \\ & \left[\begin{array}{c} \xi_2^1\cos(\xi_1^2)-\xi_1^1\xi_2^2\sin(\xi_1^2)-x_{\rm r21}\cos(\varsigma_1)-x_{\rm r22}\sin(\varsigma_1) \\ \xi_2^1\sin(\xi_1^2)+\xi_1^1\xi_2^2\cos(\xi_1^2)+x_{\rm r21}\sin(\varsigma_1)-x_{\rm r22}\cos(\varsigma_1) \\ \varsigma_2 \end{array}\right], \end{aligned} \tag{5.20}$$

where $\xi \triangleq \left[\begin{array}{cccc} \xi_1^1 & \xi_2^1 & \xi_1^2 & \xi_2^2 \end{array}\right]^{\rm T}$, $\varsigma \triangleq \left[\begin{array}{cc} \varsigma_1 & \varsigma_2 \end{array}\right]^{\rm T}$, and $m_6(\xi) \triangleq m_5 - m_4\xi_1^1\cos(\xi_1^2)$.

Next, let $\mathcal{X}_0 \triangleq \{(\eta,\nu) : \xi = \xi_0\} \subset \mathbb{R}^6$, where $\xi_0 \triangleq \left[\begin{array}{cccc} a & 0 & 0 & 0 \end{array}\right]^{\rm T}$. Note that when $(\eta,\nu) \in \mathcal{X}_0$, $\Phi^{-1} : (\xi,\varsigma,x_{\rm r}) \to (\eta,\nu,x_{\rm r})$ is well defined if $\xi_1^1 \neq 0$ and $a \neq m_5/m_4$. The zero-dynamics is defined as the dynamics of the uncontrolled states $\varsigma_i(t)$, $t \geq 0$, $i = 1,2$, when $\xi(t) \equiv \xi_0$, $t \geq 0$, and it is given by

$$\dot{\varsigma}_1(t) = \frac{1}{m_5 - am_4}\left(\varsigma_2(t) + m_4\left[\begin{array}{cc} \sin(\varsigma_1(t)) & -\cos(\varsigma_1(t)) \end{array}\right] x_{2{\rm r}}(t)\right),\ \varsigma_1(0) = \psi_0,\ t \geq 0, \tag{5.21}$$

$$\dot{\varsigma}_2(t) = \left[\begin{array}{cc} l & 1 \end{array}\right]\left(D_0(\xi_0,\varsigma(t)) + C_0(\xi_0,\varsigma(t))\right)\left[\begin{array}{cc} v(\xi_0,\varsigma(t)) & r(\xi_0,\varsigma(t)) \end{array}\right]^{\rm T},\quad \varsigma_2(0) = m_4v_0 + m_5r_0, \tag{5.22}$$

where

$$D_0(\xi_0,\varsigma) \triangleq \left[\begin{array}{cc} d_{\rm l2} + d_{\rm q2}|v(\xi_0,\varsigma)| & d_{\rm l23} + d_{\rm q23}|r(\xi_0,\varsigma)| \\ d_{\rm l23} + d_{\rm q23}|v(\xi_0,\varsigma)| & d_{\rm l3} + d_{\rm q3}|r(\xi_0,\varsigma)| \end{array}\right],\ C_0(\xi_0,\varsigma) \triangleq u(\xi_0,\varsigma)\left[\begin{array}{cc} 0 & m_1 \\ m_2 - m_1 & m_{23} \end{array}\right]. \tag{5.23}$$

To illustrate the effect of the maximum allowable error $a > 0$ on the zero-dynamics, consider a simple reference trajectory with a constant $x_{\rm r2}$. The motion of a marine vehicle along a straight line is a control problem of importance, especially in the context of way-point maneuvering ([66]). The equilibrium configuration of interest for the zero-dynamics is the following,

$$\varsigma_{1,{\rm eq}} \,=\, {\rm atan2}\left(x_{\rm r22}, x_{\rm r21}\right), \tag{5.24}$$

$$\varsigma_{2,\mathrm{eq}} = 0, \tag{5.25}$$

as it corresponds to the vehicle traveling along the straight desired trajectory with a positive velocity $u(t)$, $t \geq 0$. The corresponding linearization of (5.21) and (5.22) about that equilibrium configuration yields

$$\begin{bmatrix} \dot{\varsigma}_1(t) \\ \dot{\varsigma}_2(t) \end{bmatrix} = \begin{bmatrix} \frac{\partial \dot{\varsigma}_1}{\partial \varsigma_1} \big|_{\mathrm{eq}} & \frac{\partial \dot{\varsigma}_1}{\partial \varsigma_2} \big|_{\mathrm{eq}} \\ \frac{\partial \dot{\varsigma}_2}{\partial \varsigma_1} \big|_{\mathrm{eq}} & \frac{\partial \dot{\varsigma}_2}{\partial \varsigma_2} \big|_{\mathrm{eq}} \end{bmatrix} \begin{bmatrix} \varsigma_1(t) \\ \varsigma_2(t) \end{bmatrix}, \quad \varsigma(0) = \begin{bmatrix} \varsigma_1(0) & \varsigma_1(0) \end{bmatrix}^{\mathrm{T}}, \quad t \geq 0, \tag{5.26}$$

where

$$\left.\frac{\partial \dot{\varsigma}_1}{\partial \varsigma_1}\right|_{\mathrm{eq}} = \frac{m_4 u_{\mathrm{e}}}{m_5 - a m_4}, \qquad \left.\frac{\partial \dot{\varsigma}_1}{\partial \varsigma_2}\right|_{\mathrm{eq}} = \frac{1}{m_5 - a m_4}, \tag{5.27}$$

$$\left.\frac{\partial \dot{\varsigma}_2}{\partial \varsigma_1}\right|_{\mathrm{eq}} = \frac{u_{\mathrm{e}}}{m_5 - a m_4}\Big(m_4(l d_{\mathrm{l3}} + d_{\mathrm{l23}}) - m_5(l d_{\mathrm{l2}} + d_{\mathrm{l23}}) + u_{\mathrm{e}}(m_4(l m_1 + m_{23}) - m_5(m_2 - m_1))\Big), \tag{5.28}$$

$$\left.\frac{\partial \dot{\varsigma}_2}{\partial \varsigma_2}\right|_{\mathrm{eq}} = \frac{1}{m_5 - a m_4}\Big(l d_{\mathrm{l3}} + d_{\mathrm{l23}} - a(l d_{\mathrm{l2}} + d_{\mathrm{l23}}) + u_{\mathrm{e}}\left(m_1(l + a) + m_{23} - a m_2\right)\Big), \tag{5.29}$$

and $u_{\mathrm{e}} \triangleq \sqrt{x_{\mathrm{r21}}^2 + x_{\mathrm{r22}}^2}$.

Minimum Value of *a*

Studying the stability of the linear system (5.26), the range of values for a that would guarantee stability of the considered equilibrium point as a function of the various constant parameters characterizing the system's dynamics can be obtained. However, given the complexity of the obtained expressions, the presented analysis will be limited to a numerical estimation of the range of a using the values of the aforementioned constant parameters corresponding to the Silent Quick Unmanned Intelligent Diver 2 (SQUID-2, [104]). The values used are the following,

$$M = \begin{bmatrix} 53.1748 & 0 & 0 \\ 0 & 87.4858 & 12.254 \\ 0 & 12.254 & 7.3346 \end{bmatrix}, \tag{5.30}$$

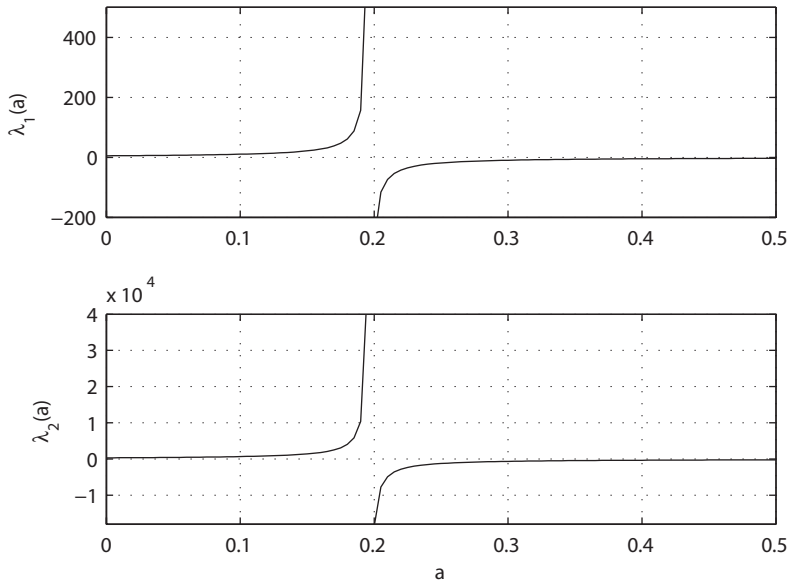

Figure 5.1: Eigenvalues of the Jacobian matrix in (5.26) versus a.

$$D(\nu) = \begin{bmatrix} 6.855 + 8.246|u| & 0 & 0 \\ 0 & 25.094 + 48.329|v| & 10.668 + 14.649|r| \\ 0 & 10.668 + 14.649|v| & 4.002 + 7.331|r| \end{bmatrix}, \qquad (5.31)$$

and $l = 0.5$. In addition, choose $u_{\mathrm{e}} = 1$.

As seen in Figure 5.1, the eigenvalues of the state matrix display a singular behavior at $a_{\mathrm{s}} = \frac{m_5}{m_4} \simeq 0.1964$. For $a < a_{\mathrm{s}}$, both eigenvalues λ_1 and λ_2 are positive and the considered equilibrium point is unstable. However, for $a > a_{\mathrm{s}}$, the eigenvalues are strictly negative. As emphasized earlier, the introduction of the maximum allowable position error a allowed to stabilize the zero-dynamics. Indeed, without this position error, the zero-dynamics equilibrium configuration of interest is unstable, while it becomes stable for $a > a_{\mathrm{s}}$.

5.4. Conclusion

The presented result addresses trajectory tracking in the horizontal plane for marine vehicles equipped with a fixed thruster and a rudder, or, equivalently, a vectored thruster. Such vehicles are characterized by a non-minimum phase type behavior. To overcome the unstable nature of the system's internal dynamics, special tracking errors were selected. A nonlinear control algorithm which guarantees global asymptotic stability of the tracking errors was introduced. Then, the impact of the chosen control strategy on the internal dynamics was assessed. It was shown that the proposed control framework, through design of a constant design parameter, guarantees local stability of the zero-dynamics for a simple maneuver.

Chapter 6

Adaptive Control of Non-Minimum Phase Autonomous Marine Vehicles [4–6]

The results featured in this chapter were presented at the 4$^{\text{th}}$ Asian Control Conference in 2002 ([4]), at the 2003 IEEE Conference on Decision and Control ([5]), and were the object of an article to appear in the International Journal of Adaptive Control and Signal Processing ([6]).

6.1. Introduction

The mathematical model of the system under consideration in this chapter remains the same as in Chapter 5. However, while the algorithm presented in the previous chapter assumed knowledge of the constant parameters characterizing the vehicle's model, the controllers introduced in this chapter will relax that assumption, using adaptive techniques. This additional challenge can be handled using the result from Theorem 4.3.2, however, the controller obtained in Chapter 5 depends nonlinearly on some of the unknown parameters,

and consequently, the certainty equivalence principle cannot be applied to derive a direct adaptive control law. This nonlinear parameterization is a direct result of the choice of tracking errors (5.7) and (5.8), which lead to a non-constant $\frac{\partial q_2(x,x_r,\chi)}{\partial \nu}$. This situation illustrates how critical the choice of tracking errors is when considering an adaptive control problem.

To allow derivation of a direct adaptive controller, Section 6.2 alters the control law from Section 5.2 in such a way that it becomes linear in the uncertain parameters. The resulting adaptive controller shows interesting performance in simulation. Alternatively, this nonlinear parametrization can be addressed using Dynamic Surface Control (DSC, [61], also see [5]). In this case, the tracking errors are modified, using filters designed in addition to the backstepping procedure. These filters not only simplify the expressions involved in the derivations, but also lead to a command linear in the uncertain parameters. Section 6.3 presents a step by step derivation of the control algorithm. Results of numerical simulations illustrating the performance of this particular adaptive controller are presented.

In the DSC case, proof of stability relies on an elaborate design of the time constant matrices of such filters (design omitted in Section 6.3, see [61]), to an extent that the technique can be of limited practical use. To remedy this situation, an indirect adaptive approach is proposed. The algorithm relies on a partial state predictor (similar to that used in [108]) to determine the appropriate command to the system, as opposed to relying on the uncertain portion of the actual model. As described in following sections, the use of this technique gives rise to a new issue. Indeed, the closed form of the control command includes the inverse of a matrix which is function of the estimates. To avoid singularity of this matrix, a projection algorithm ([109]) is used to constrain the estimates to acceptable values. Section 6.4 introduces an indirect adaptive control law, which guarantees Lyapunov stability and con-

vergence of the tracking errors in spite of parametric uncertainties, and details the projection algorithm used to avoid singularity of the command. Results of numerical simulations are presented. Section 6.5 concludes this chapter.

6.2. Direct Adaptive Control Algorithm for Linear in the Uncertain Parameters Control Law [4]

The system under consideration remains the same as that in the previous chapter; that is, using previously established notations,

$$\dot{\eta}(t) = J(\eta(t))\nu(t), \qquad \eta(0) = \eta_0, \quad t \geq 0, \tag{6.1}$$

$$\dot{\nu}(t) = -M^{-1}\left(C(\nu(t)) + D(\nu(t))\right)\nu(t) + M^{-1}B\tau(t), \quad \nu(0) = \nu_0. \tag{6.2}$$

The control law derived for this system in the previous chapter is of the form

$$\begin{aligned}\tau^*(t) = -(B_e(e_1(t))\Theta_2^*)^{-1}\Big(&J_{\mathrm{s}}^{\mathrm{T}}(\psi(t))(-\omega_0^2 x_{\mathrm{r}1}(t) + (r(t)S - 2\zeta\omega_0)x_{\mathrm{r}2}(t) + \omega_0^2 r_{\mathrm{s}}(t)) + r(t)Sq_2(t) \\ &- \dot{q}_{2\mathrm{des}}(e_1(t), e_2(t)) + e_2(t) + G_2^{-1}J_{\mathrm{s}}(\beta(t))\gamma(e_1(t)) + B_e(e_1(t))\Theta_1^*\varphi_1(\nu(t))\Big), \quad t \geq 0. \end{aligned} \tag{6.3}$$

The model of the system features parametric uncertainties, contained in matrices M, $C(\cdot)$, $D(\cdot)$ and B of (6.2). Consequently, the value of Θ_1^* and Θ_2^* in (6.3) are unknown, and the corresponding command can not be computed. To address this issue, a direct adaptive technique can be used. However, due to the presence of $(B_e(e_1(t))\Theta_2^*)^{-1}$, $t \geq 0$, in (6.3), the command is nonlinear in the uncertain parameters, which makes it difficult to apply classical direct adaptive techniques. As previously mentioned, this nonlinearity in the parameters is a direct consequence of the particular choice of tracking errors (5.7) and (5.8), which lead to the expression of $q_2(\cdot)$ given by (5.10). For this particular expression of $q_2(\cdot)$, it follows that $\frac{\partial q_2(x, x_{\mathrm{r}}, \chi)}{\partial \nu} = B_e(e_1)$, which is function of the tracking error e_1.

To simplify the problem, it will be assumed that the off-diagonal terms in M and $D(\nu(t))$, $t \geq 0$, are negligible. In addition, $\tau^*(t)$, $t \geq 0$, will be altered by substitution of $B_{e\mathrm{a}} \triangleq B_e(a,0)$ for $B_e(e_\mathrm{d}(t),\beta(t))$, $t \geq 0$. In order to assess the stability of the corresponding closed-loop system, consider the following Lyapunov function candidate,

$$V(e_1,e_2) \triangleq e_\mathrm{d}\sin^2(\beta/2) + \frac{1}{2}(e_\mathrm{d}-a)^2 + \frac{1}{2}e_2^\mathrm{T}G_2e_2. \tag{6.4}$$

The control command

$$\begin{aligned}\tau_\mathrm{a}^*(t) \triangleq & -(B_{e\mathrm{a}}\Theta_2^*)^{-1}\Big(B_{e\mathrm{a}}\Theta_1^*\varphi_1(\nu(t)) + J_\mathrm{s}^\mathrm{T}(\psi(t))(-\omega_0^2x_{\mathrm{r}1}(t) + (r(t)S - 2\zeta\omega_0)x_{\mathrm{r}2}(t) \\ & +\omega_0^2r_\mathrm{s}(t)) - \dot{q}_{2\mathrm{des}}(e_1(t),e_2(t)) + r(t)Sq_2(t) + G_2^{-1}J_\mathrm{s}(\beta(t))\gamma(e_1(t)) + e_2(t)\Big), \quad t \geq 0, \end{aligned} \tag{6.5}$$

results in the following time derivative of (6.4),

$$\begin{aligned}\dot{V}(t) = & -e_\mathrm{d}(t)\gamma^\mathrm{T}(e_1(t))G_1\gamma(e_1(t)) - e_2^\mathrm{T}(t)G_2e_2(t) + e_2^\mathrm{T}\begin{bmatrix} 0 & \frac{l}{m_3} \end{bmatrix}\tau_\mathrm{a}^*(t)S\begin{bmatrix} e_\mathrm{d}\cos(\beta) - a \\ e_\mathrm{d}\sin(\beta) \end{bmatrix}, \\ & t \geq 0. \end{aligned} \tag{6.6}$$

Note that, for small tracking errors, the third term on the right-hand side of (6.6) is also small. Consequently, manipulation of the right-hand side of (6.6), through completion of the squares, for instance, could allow to conclude ultimate boundedness of the tracking errors. Indeed, outside of a given domain, the sum of the first two negative quadratic terms in (6.6) can be shown to be greater in norm than the last term. This will not be shown rigorously at this time, as the objective is to design of a direct adaptive control algorithm performing adequately in simulation, providing insights which will allow the design of adaptive algorithms with rigorously proven stability guarantees in later sections.

Direct Adaptive Control Law

Following the notations of Chapter 4, the command (6.5) can be rewritten as

$$\tau_{\mathrm{a}}^{*}(t) \;=\; -\Theta^{*} w(t) - W^{*}\sigma(t), \qquad t \geq 0, \tag{6.7}$$

where $\sigma(t) = \varphi_1(t)$, $t \geq 0$,

$$\Theta^{*} \;=\; (B_{e\mathrm{a}}\Theta_2^{*})^{-1}, \tag{6.8}$$

$$W^{*} \;=\; (B_{e\mathrm{a}}\Theta_2^{*})^{-1} B_{e\mathrm{a}}\Theta_1^{*}, \tag{6.9}$$

$$\begin{aligned} w(t) \;=\; & J_{\mathrm{s}}^{\mathrm{T}}(\psi(t))(-\omega_0^2 x_{\mathrm{r}1}(t) + (r(t)S - 2\zeta\omega_0)x_{\mathrm{r}2}(t) + \omega_0^2 r_{\mathrm{s}}(t)) - \dot{q}_{2\mathrm{des}}(e_1(t), e_2(t)) \\ & + r(t)Sq_2(t) + G_2^{-1} J_{\mathrm{s}}(\beta(t))\gamma(e_1(t)) + e_2(t), \quad t \geq 0, \end{aligned} \tag{6.10}$$

Using Theorem 4.3.2, the control command (6.7) is replaced with the following,

$$\tau_{\mathrm{a}}(t) \;=\; -\Theta(t) w(t) - W(t)\sigma(t), \qquad t \geq 0, \tag{6.11}$$

where $\Theta(t)$ and $W(t)$, $t \geq 0$, are estimates of Θ^{*} and W^{*}, given by the update laws

$$\dot{\Theta}(t) \;=\; G_2 e_2(t) w^{\mathrm{T}}(t)\Gamma_1 - \sigma_1\Theta(t), \qquad \Theta(0) = \Theta_0, \quad t \geq 0, \tag{6.12}$$

$$\dot{W}(t) \;=\; G_2 e_2(t)\sigma^{\mathrm{T}}(t)\Gamma_2 - \sigma_2 W(t), \qquad W(0) = W_0. \tag{6.13}$$

The efficacy of the resulting control algorithm was tested through numerical simulations, as described in the following subsection.

Numerical Simulations

Circular Trajectory

The first maneuver attempted is a counterclockwise circle of radius 10m at a velocity 0.5m/s, with the following initial conditions,

$$\eta = \begin{bmatrix} 0 & 0 & 0 \end{bmatrix}^{\mathrm{T}}, \qquad \nu = \begin{bmatrix} 0 & 0 & 0 \end{bmatrix}^{\mathrm{T}}.$$

The natural frequency and damping of reference system (4.7) are chosen to be

$$w_0 = 0.2I_2, \qquad \zeta = 0.9I_2.$$

The initials conditions chosen for the estimates are

$$\Theta_0 = 200I_2, \qquad W_0 = \begin{bmatrix} 100I_2 & 50I_2 & 250I_2 & I_2 & I_2 \end{bmatrix}.$$

Furthermore, $\Gamma_1 = \Gamma_2 = 10I_2$, $a = 2.25$, and $G_1 = G_2 = I_2$. For the dynamic model of the vehicle, the numerical values provided in [110] were used. Finally, the initial position of the desired trajectory is

$$\eta_{\mathrm{ds}}(0) = \begin{bmatrix} 7.0711 & 7.0711 \end{bmatrix}^{\mathrm{T}}.$$

As shown in Figure 6.1, in spite of the controller modification, the tracking performance is excellent, and the vehicle is moving in a coherent fashion (the arrows show the orientation of the vehicle). The algorithm of Chapter 2 was used to enforce control amplitude and rate saturation, and was successful in keeping the control efforts at reasonable levels, as shown in Figure 6.1.

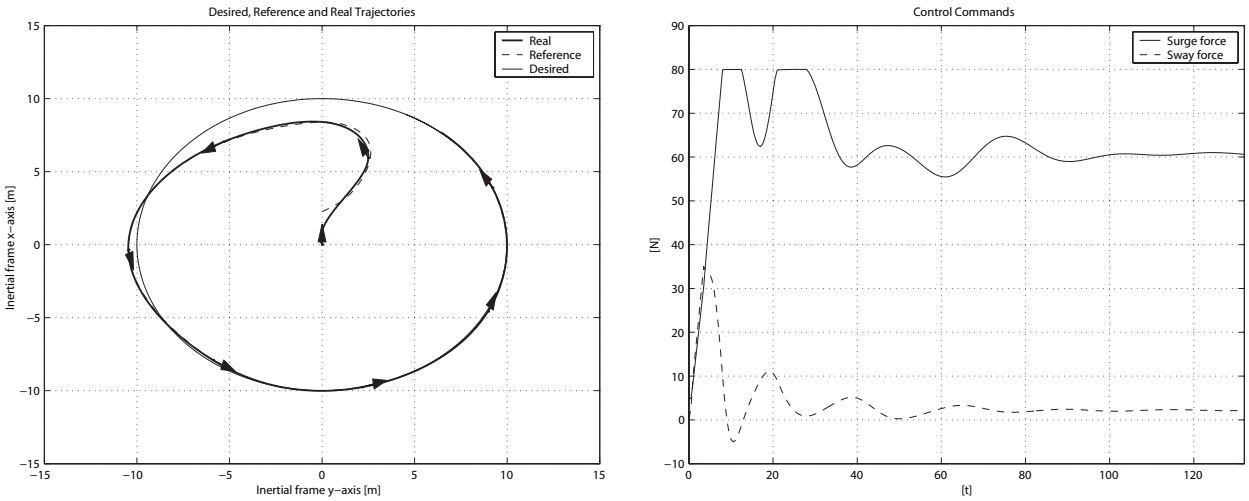

Figure 6.1: Circular trajectory and corresponding control commands.

Octomorphic Trajectory

For a second maneuver, consider an eight-shaped (octomorphic) trajectory. The initial conditions are the same as for the previous example. The desired trajectory is of the form

$$\eta_{\mathrm{d}}(t) = 10 \begin{bmatrix} \sin(\omega t) & \sin(\omega t/2) \end{bmatrix}^{\mathrm{T}}, \qquad t \geq 0, \tag{6.14}$$

with $\omega = 0.1$, with zero initial velocity and initial position $\eta_{\mathrm{d}}(0) = \begin{bmatrix} 0 & 0 \end{bmatrix}^{\mathrm{T}}$.

The result of this simulation are displayed in Figure 6.2. The tracking performance is very good, and the vehicle is still moving in a coherent fashion. The control efforts are shown in Figure 6.2.

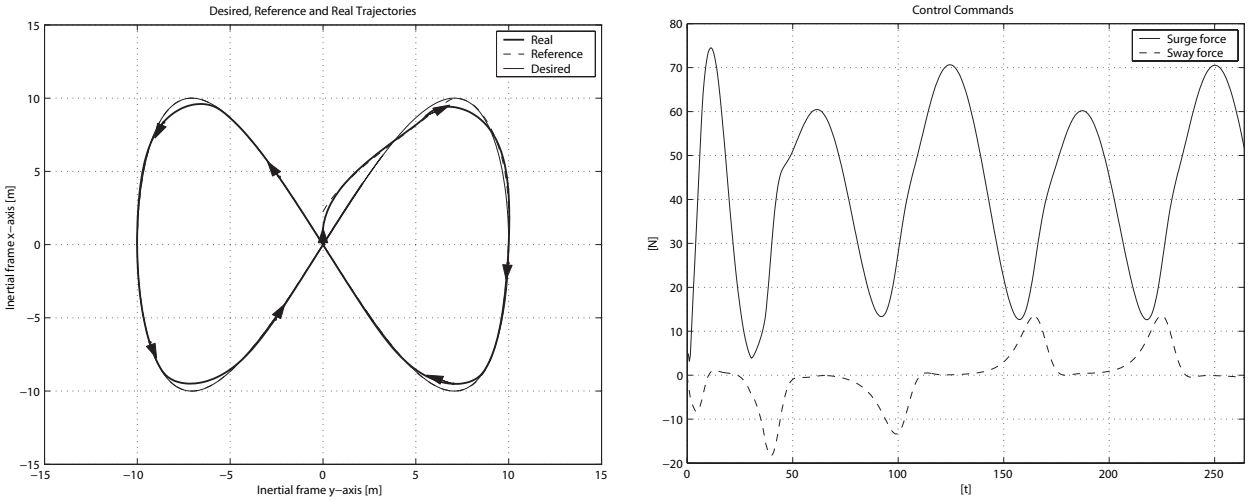

Figure 6.2: Octomorphic trajectory and corresponding control commands.

6.3. Direct Adaptive Control Law with Dynamic Surface Control [5]

Although the algorithm in the previous section showed interesting results in simulation, it does rely on the approximation that $B_e(e_{\mathrm{d}}(t), \beta(t)) \simeq B_{e\mathrm{a}}$, $t \geq 0$. This section presents an alternate control design, removing this approximation. In particular, derivations will follow the strategy presented in Section 5.2, and use a technique derived from DSC ([61]), following the same method that was used in Chapter 3.

Nonlinear Control Law

Consider the following Lyapunov function candidate,

$$V_s(e_1) = e_{\mathrm{d}} \sin^2(\beta/2) + \frac{1}{2}(e_{\mathrm{d}} - a)^2. \tag{6.15}$$

In this section, derivations will rely on a different choice of $q_2(t)$, $t \geq 0$, from that in Section 5.2. In particular, $Q_1(t)$ and $q_2(t)$, $t \geq 0$, are chosen as

$$Q_1(t) \triangleq \begin{bmatrix} 1 & 0 \\ 0 & 1/e_{\rm d}(t) \end{bmatrix} J_{\rm s}^{\rm T}(\beta(t)), \qquad t \geq 0, \tag{6.16}$$

$$q_2(t) \triangleq J_{\rm s}^{-1}(\psi(t))x_{\rm r2}(t) + B_0\nu(t) + \chi(t), \tag{6.17}$$

where

$$B_0 \triangleq \begin{bmatrix} -I_2 & 0_{2\times 1} \end{bmatrix}. \tag{6.18}$$

and $\chi(t)$, $t \geq 0$, is obtained from the filter

$$T\dot{\chi}(t) + \chi(t) = r(t)S \begin{bmatrix} e_{\rm d}(t)\cos(\beta(t)) & e_{\rm d}(t)\sin(\beta(t)) \end{bmatrix}^{\rm T}, \qquad t \geq 0, \tag{6.19}$$

with $T > 0$ a diagonal matrix whose elements are positive constants and constitute the filter's time constants.

The expression chosen for $q_2(t)$, $t \geq 0$, differs from the one used in the previous chapter (see (5.10)) so that $\frac{\partial q_2(x,x_{\rm r},\chi)}{\partial \nu} = B_0$ is constant. This was achieved by breaking up $B_e(e_1)$ into a constant part B_0, which remains in (6.17), and a time varying part, which is accounted for by $\chi(t)$, $t \geq 0$. This adjustment to $q_2(t)$, $t \geq 0$, leads to a constant $\frac{\partial q_2(x,x_{\rm r},\chi)}{\partial \nu}$, which, using Theorem 4.3.1, yields a control law that is linear in the unknown parameters. This modification allows to satisfy one of the most important assumptions in Theorem 4.3.2.

The velocity error corresponding to the above choice of $q_2(t)$, $t \geq 0$, is of the form

$$e_{2\rm f}(t) \triangleq J_{\rm s}^{-1}(\psi(t))x_{\rm r2}(t) + B_0\nu(t) + \chi(t) - q_{2\rm des}(e_1(t)), \qquad t \geq 0, \tag{6.20}$$

where $q_{2\rm des}(e_1(t))$ is given by (5.13). The time derivative of this velocity error is given by

$$\begin{aligned} \dot{e}_{2\rm f}(t) \;=\; & J_{\rm s}^{\rm T}(\psi(t))(-\omega_0^2 x_{\rm r1}(t) + (r(t)S - 2\zeta\omega_0)x_{\rm r2}(t) + \omega_0^2 r_{\rm s}(t)) + \dot{\chi}(t) - \dot{q}_{2\rm des}(t) \\ & + B_0(\Theta_1^*\varphi_1(t) + \Theta_2^*\tau(t)), \quad t \geq 0, \end{aligned} \tag{6.21}$$

The control law is designed using Theorem 4.3.1, and is of the form

$$\tau^*(t) = -(B_0\Theta_2^*)^{-1}\Big(J_{\rm s}^{\rm T}(\psi(t))(-\omega_0^2 x_{\rm r1}(t) + (r(t)S - 2\zeta\omega_0)x_{\rm r2}(t) + \omega_0^2 r_{\rm s}(t)) + \dot{\chi}(t) - \dot{q}_{\rm 2des}(t) + B_0\Theta_1^*\varphi_1(t) + e_{\rm 2f}(t) + G_2^{-1}J_{\rm s}(\beta(t))\left[\sin^2(\beta(t)/2) + e_{\rm d}(t),\ \frac{1}{2}\sin(\beta(t))\right]^{\rm T}\Big),\ t \geq 0. \quad (6.22)$$

Adaptive Control Law

Following a procedure similar to that used in the previous section, the command (6.22) is rewritten as

$$\tau^*(t) \ = \ -\Theta^* w(t) - W^*\sigma(t), \qquad t \geq 0, \quad (6.23)$$

where $\sigma(t) = \varphi_1(t)$, $t \geq 0$, and

$$\Theta^* = (B_0\Theta_2^*)^{-1}, \quad (6.24)$$

$$W^* = (B_0\Theta_2^*)^{-1}B_0\Theta_1^*, \quad (6.25)$$

$$w(t) = J_{\rm s}^{\rm T}(\psi(t))(-\omega_0^2 x_{\rm r1}(t) + (r(t)S - 2\zeta\omega_0)x_{\rm r2}(t) + \omega_0^2 r_{\rm s}(t)) + \dot{\chi}(t) - \dot{q}_{\rm 2des}(e_1(t), e_2(t)) + r(t)Sq_2(t) + G_2^{-1}J_{\rm s}(\beta(t))\left[\ \sin^2(\beta(t)/2) + e_{\rm d}(t) \quad \tfrac{1}{2}\sin(\beta(t))\ \right]^{\rm T} + e_2(t),\ t \geq 0. \quad (6.26)$$

Using Theorem 4.3.2, the control command (6.23) is replaced by

$$\tau(t) \ = \ -\Theta(t)w(t) - W(t)\sigma(t), \qquad t \geq 0. \quad (6.27)$$

where $\Theta(t)$ and $W(t)$, $t \geq 0$, are estimates of Θ^* and W^*, given by the update laws

$$\dot{\Theta}(t) \ = \ G_2 e_{\rm 2f}(t)w^{\rm T}(t)\Gamma_1 - \sigma_1\Theta(t), \qquad \Theta(0) = \Theta_0, \quad t \geq 0, \quad (6.28)$$

$$\dot{W}(t) \ = \ G_2 e_{\rm 2f}(t)\sigma^{\rm T}(t)\Gamma_2 - \sigma_2 W(t), \qquad W(0) = W_0. \quad (6.29)$$

The tracking performance of the resulting control algorithm was tested through numerical simulations, as described in the following subsection.

Numerical Simulations

As in the previous section, the first maneuver attempted is a counterclockwise circle of radius 10m, but here at a velocity of 1m/s, with the following initial conditions,

$$\eta = \begin{bmatrix} 0 & 0 & 0 \end{bmatrix}^{\mathrm{T}}, \qquad \nu = \begin{bmatrix} 0 & 0 & 0 \end{bmatrix}^{\mathrm{T}}. \tag{6.30}$$

The reference model's initial conditions are

$$x_{\mathrm{r}10} = \begin{bmatrix} 0.6 & 0 \end{bmatrix}^{\mathrm{T}}. \tag{6.31}$$

The initials conditions chosen for the estimates are

$$\Theta_0 = \begin{bmatrix} 15 & 0 \\ 0 & 50 \end{bmatrix}, \quad W = \begin{bmatrix} -5 & 0 & -5 & 0 & 40 & 0 & 1 & 0 & 1 & 0 \\ 0 & 10 & 0 & 10 & 0 & 10 & 0 & 1 & 0 & 1 \end{bmatrix}. \tag{6.32}$$

Furthermore, $\Gamma_i = I_2$, $i = 1, 2$, $a = 0.6$, and $G_1 = G_2 = I_2$. The dynamic model of the vehicle corresponds to the Silent Quick Unmanned Intelligent Diver [104]. The values for the constant parameters in M, $D(\nu)$ and $C(\nu)$ are given in (5.31). Finally, the initial position of the desired trajectory is

$$\eta_{\mathrm{ds}}(0) = \begin{bmatrix} 7.0711 & 7.0711 \end{bmatrix}^{\mathrm{T}}.$$

As shown in Figure 6.3, the tracking performances are excellent, and the vehicle is moving in a coherent fashion. In addition, the framework introduced in Chapter 2 was used to enforce command input amplitude saturation, and keep the control efforts at a reasonable level, as shown in Figure 6.3. Finally, the estimates converge quickly and remain stable (Figure 6.4).

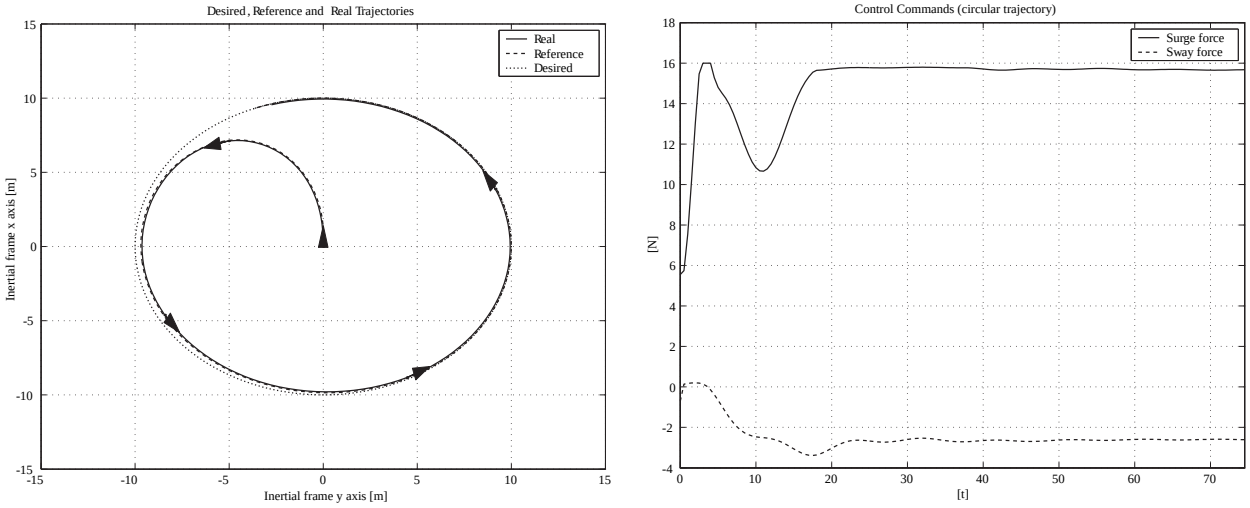

Figure 6.3: Circular trajectory and corresponding control efforts.

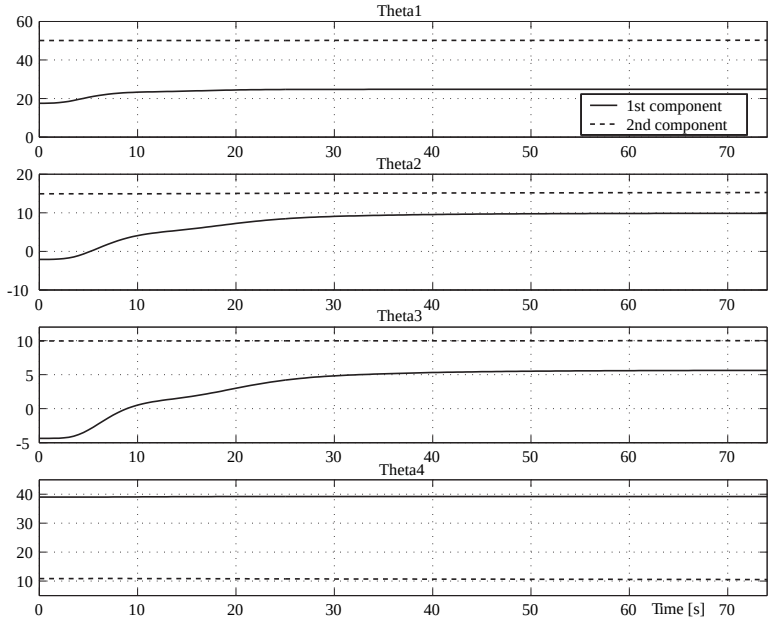

Figure 6.4: Relevant Θ gains .

6.4. Indirect Adaptive Algorithm [6]

It is clear from (6.3) that, in order to compute the value of the given control law, knowledge of the exact values of Θ_1^* and Θ_2^* would be required. Since this information is not necessarily available, it is desirable to obtain a control law only requiring estimates of these parameters. However, classical direct adaptive techniques rely on a linearly parameterized command (to allow the application of the equivalence certainty principle). As discussed in previous sections, the term $(B_e(e_1(t))\Theta_2^*)^{-1}$ is nonlinear in the uncertain parameters, which makes it difficult to apply direct adaptive techniques. In this section, this issue will be addressed using an indirect adaptive approach.

In particular, the presented approach makes use of the partial state predictor

$$\dot{\hat{\nu}}(t) = \Theta_1(t)\varphi_1(\nu(t)) + \tau_{\mathrm{d}}(t)\Theta_{2\mathrm{v}}(t) + u_{\mathrm{p}}(t), \qquad \hat{\nu}(0) = \nu_0, \qquad t \geq 0, \tag{6.33}$$

where $\Theta_1(t) \in \mathbb{R}^{3\times 10}$, and $\Theta_{2\mathrm{v}}(t) \triangleq \left[\begin{array}{ccc} \theta_{21}(t) & \theta_{22}(t) & \theta_{23}(t) \end{array}\right]^{\mathrm{T}} \in \mathbb{R}^{3\times 1}$, $t \geq 0$, are estimates of Θ_1^* and $\Theta_{2\mathrm{v}}^* \triangleq \left[\begin{array}{ccc} \theta_{21}^* & \theta_{22}^* & \theta_{23}^* \end{array}\right]^{\mathrm{T}}$, respectively, $\hat{\nu}(t) \triangleq \left[\begin{array}{ccc} \hat{u}(t) & \hat{v}(t) & \hat{r}(t) \end{array}\right]^{\mathrm{T}}$, $t \geq 0$, and finally $\tau_{\mathrm{d}}(t) \triangleq \mathrm{diag}(\left[\begin{array}{ccc} \tau_1(t) & \tau_2(t) & \tau_2(t) \end{array}\right])$, $t \geq 0$. The predictor signal $u_{\mathrm{p}}(t) \in \mathbb{R}^3$, $t \geq 0$, will be designed to improve performance of the predictor, allowing (6.33) to emulate the dynamics in (4.5).

Adaptive Control Command

Consider the error

$$e_\nu(t) \triangleq \nu(t) - \hat{\nu}(t), \qquad t \geq 0, \tag{6.34}$$

which reflects the difference between the vehicle's velocity and its estimate, provided by the state predictor (6.33). The time derivative of (6.34) is given by

$$\begin{aligned}\dot{e}_\nu(t) &= \Theta_1^*\varphi_1(\nu(t))+\Theta_2^*\tau(t)-\Theta_1(t)\varphi_1(\nu(t))-\Theta_2(t)\tau(t)-u_{\rm p}(t)\\ &= (\Theta_1^*-\Theta_1(t))\varphi_1(\nu(t))+\tau_{\rm d}(t)(\Theta_{2{\rm v}}^*-\Theta_{2{\rm v}}(t))-u_{\rm p}(t), \quad e_\nu(0)=\nu_0-\hat{\nu}_0, \quad t\geq 0. \end{aligned} \tag{6.35}$$

The velocity error defined by (5.15) is then modified so that the control algorithm relies on the fully known state predictor, instead of the actual system's dynamics, which are uncertain. To do so, define the new velocity error

$$\hat{e}_2(t) \triangleq \varphi_0(\eta(t),\hat{\nu}(t),x_{\rm r}(t))+e_{\rm d}(t)J_{\rm s}(\beta(t))G_1\gamma(e_1(t)), \qquad t\geq 0, \tag{6.36}$$

which is similar to (5.15), the only difference being its dependence upon $\hat{\nu}(t)$, $t \geq 0$, as opposed to $\nu(t)$, $t \geq 0$. Note that, using (5.11) and (6.34), it is possible to rewrite (6.36) as

$$\hat{e}_2(t) \triangleq \varphi_0(\eta(t),\nu(t),x_{\rm r}(t))-B_e(e_1(t))e_\nu(t)+e_{\rm d}(t)J_{\rm s}(\beta(t))G_1\gamma(e_1(t)), \qquad t\geq 0. \tag{6.37}$$

The time derivative of (6.36) is given by

$$\begin{aligned}\dot{\hat{e}}_2(t) &= J_{\rm s}^{\rm T}(\psi(t))(-\omega_0^2x_{\rm r1}(t)+(r(t)S-2\zeta\omega_0)x_{\rm r2}(t)+\omega_0^2r_{\rm s}(t))+B_e(e_1(t))\Theta_2(t)\tau(t)\\ &\quad +\hat{r}(t)S\varphi_0(t)+B_e(e_1(t))(\Theta_1(t)\varphi_1(\nu(t))+u_{\rm p}(t))+\varphi_2(e_1(t),e_2(t)), \quad t\geq 0, \end{aligned} \tag{6.38}$$

where

$$\Theta_2(t) \triangleq \left[\begin{array}{cc} \theta_{21}(t) & 0\\ 0 & \theta_{22}(t)\\ 0 & \theta_{23}(t)\end{array}\right], \qquad t\geq 0. \tag{6.39}$$

Note that (6.38) is similar to (5.16), however, a significant difference is that the uncertain parameters Θ_1^* and Θ_2^* have been replaced by their estimates $\Theta_1(t)$ and $\Theta_2(t)$, $t \geq 0$.

The following result presents commands $\tau(t)$ and $u_{\rm p}(t)$, $t \geq 0$, along with update laws $\dot{\Theta}_1(t)$ and $\dot{\Theta}_{2{\rm v}}(t)$, $t \geq 0$, that will guarantee Lyapunov stability of the error dynamics (5.9), (6.35) and (6.38), as well as convergence of $e_1(t)$, $t \geq 0$, to $\left[\begin{array}{cc} a & 0 \end{array} \right]^{\rm T}$, in spite of the parametric uncertainties in (4.5).

Theorem 6.4.1. Consider the system given by (5.9), (6.35) and (6.38), and assume that $B_e(e_1(t))\Theta_2(t)$, $t \geq 0$, is nonsingular. Then, the feedback control laws

$$u_{\rm p}(e_1, e_\nu) = B_e^{\rm T}(e_1) J_{\rm s}(\beta)\gamma(e_1) + G_\nu e_\nu, \tag{6.40}$$

$$\begin{aligned} \tau(t) = {} & (B_e(e_1(t))\Theta_2(t))^{-1}\Big(- B_e(e_1(t))(\Theta_1(t)\varphi_1(\nu(t)) + u_{\rm p}(t)) - J_{\rm s}^{\rm T}(\psi(t))(-\omega_0^2 x_{\rm r1}(t) \\ & + (r(t)S - 2\zeta\omega_0)x_{\rm r2}(t) + \omega_0^2 r_{\rm s}(t)) - \varphi_2(e_1(t), e_2(t)) - \hat{r}(t)S\varphi_0(\eta(t), \nu(t), x_{\rm r}(t)) \\ & - J_{\rm s}(\beta(t))\gamma(e_1(t)) - G_2\hat{e}_2(t)\Big), \quad t \geq 0, \end{aligned} \tag{6.41}$$

along with update laws

$$\dot{\Theta}_1(t) = e_\nu(t)\varphi_1^{\rm T}(\nu(t))\Gamma_1, \qquad \Theta_1(t) = \Theta_{10}, \qquad t \geq 0, \tag{6.42}$$

$$\dot{\Theta}_{2{\rm v}}(t) = \tau_{\rm d}(t) e_\nu(t)\Gamma_2, \qquad \Theta_{2{\rm v}}(t) = \Theta_{2{\rm v}0}, \tag{6.43}$$

where $\Gamma_1 \in \mathbb{R}^{10\times 10}$ is a positive definite matrix and $\Gamma_2 > 0$, guarantee Lyapunov stability of the solution $\left[\begin{array}{cc} e_{\rm d}(t) & \beta(t) \end{array} \right]^{\rm T} \equiv \left[\begin{array}{cc} a & 0 \end{array} \right]^{\rm T}$, $\hat{e}_2(t) \equiv 0$, $e_\nu(t) \equiv 0$, $\Theta_1(t) \equiv \Theta_1^*$, $\Theta_{2{\rm v}}(t) \equiv \Theta_{2{\rm v}}^*$, $t \geq 0$, of the dynamics given by (5.9), (6.38), (6.35), (6.42) and (6.43). In addition, $(e_{\rm d}(t), \beta(t)) \to (a, 0)$ and $(e_2(t), e_\nu(t)) \to (0, 0)$, as $t \to \infty$.

Proof. Substituting the feedback control law (6.41) into (6.38), we obtain

$$\dot{\hat{e}}_2(t) = -J_{\rm s}(\beta(t))\gamma(e_1(t)) - G_2\hat{e}_2(t), \qquad t \geq 0. \tag{6.44}$$

Next, consider the Lyapunov function candidate

$$V(e_1,\hat{e}_2,e_\nu,\Theta_1,\Theta_2) \triangleq e_{\rm d}\sin^2(\beta/2)+\frac{1}{2}(e_{\rm d}-a)^2+\frac{1}{2}\hat{e}_2^{\rm T}\hat{e}_2+\frac{1}{2}{\rm tr}\left[(\Theta_1-\Theta_1^*)\Gamma_1^{-1}(\Theta_1-\Theta_1^*)^{\rm T}\right]$$
$$+\frac{1}{2}e_\nu^{\rm T}e_\nu+\frac{1}{2}{\rm tr}\left[(\Theta_{2{\rm v}}-\Theta_{2{\rm v}}^*)\Gamma_2^{-1}(\Theta_{2{\rm v}}-\Theta_{2{\rm v}}^*)^{\rm T}\right], \qquad (6.45)$$

which is a positive definite function of $e_{\rm d}-a$, β, $\hat{e}_2$, e_ν, $\Theta_1-\Theta_1^*$, and $\Theta_{2{\rm v}}-\Theta_{2{\rm v}}^*$. The Lyapunov derivative along the closed-loop system trajectories is given by

$$\begin{aligned}
\dot{V}(t)=&-e_{\rm d}(t)\gamma^{\rm T}(e_1(t))G_1\gamma(e_1(t))+\gamma^{\rm T}(e_1(t))J_{\rm s}^{\rm T}(\beta(t))\hat{e}_2(t)-\hat{e}_2^{\rm T}(t)(J_{\rm s}(\beta(t))\gamma(e_1(t))\\
&+G_2\hat{e}_2(t))+\gamma^{\rm T}(e_1(t))J_{\rm s}^{\rm T}(\beta(t))B_e(e_1(t))e_\nu(t)-e_\nu^{\rm T}(t)((\Theta_1(t)-\Theta_1^*)\varphi_1(\nu(t))\\
&+B_e^{\rm T}(e_1(t))J_{\rm s}(\beta(t))\gamma(e_1(t))+\tau_{\rm d}(t)(\Theta_{2{\rm v}}^*-\Theta_{2{\rm v}}(t))+G_\nu e_\nu(t))+{\rm tr}[(\Theta_1(t)-\Theta_1^*)\Gamma_1^{-1}\dot{\Theta}_1^{\rm T}(t)]\\
&+{\rm tr}[(\Theta_{2{\rm v}}(t)-\Theta_{2{\rm v}}^*)\Gamma_2^{-1}\dot{\Theta}_{2{\rm v}}^{\rm T}(t)]\\
=&-e_{\rm d}(t)\gamma^{\rm T}(e_1(t))G_1\gamma(e_1(t))-\hat{e}_2^{\rm T}(t)G_2\hat{e}_2(t)-{\rm tr}[(\Theta_1(t)-\Theta_1^*)\varphi_1(\nu(t))e_\nu^{\rm T}(t)]\\
&-e_\nu^{\rm T}(t)G_\nu e_\nu(t)+{\rm tr}[(\Theta_1(t)-\Theta_1^*)\Gamma_1^{-1}\dot{\Theta}_1^{\rm T}(t)]-{\rm tr}[(\Theta_{2{\rm v}}(t)-\Theta_{2{\rm v}}^*)e_\nu^{\rm T}(t)\tau_{\rm d}(t)]\\
&+{\rm tr}[(\Theta_{2{\rm v}}(t)-\Theta_{2{\rm v}}^*)\Gamma_2^{-1}\dot{\Theta}_{2{\rm v}}^{\rm T}(t)]\\
=&-e_{\rm d}(t)\gamma^{\rm T}(e_1(t))G_1\gamma(e_1(t))+{\rm tr}[(\Theta_1(t)-\Theta_1^*)(\Gamma_1^{-1}\dot{\Theta}_1^{\rm T}(t)-\varphi_1(\nu(t))e_\nu^{\rm T}(t))]\\
&-\hat{e}_2^{\rm T}(t)G_2\hat{e}_2(t)-e_\nu^{\rm T}(t)G_\nu e_\nu(t)+{\rm tr}[(\Theta_{2{\rm v}}(t)-\Theta_{2{\rm v}}^*)(\Gamma_2^{-1}\dot{\Theta}_{2{\rm v}}^{\rm T}(t)-e_\nu^{\rm T}(t)\tau_{\rm d}(t))], \quad t\geq 0. \qquad (6.46)
\end{aligned}$$

Substituting update laws (6.42) and (6.43) into (6.46), we obtain

$$\dot{V}(t) = -e_{\rm d}(t)\gamma^{\rm T}(e_1(t))G_1\gamma(e_1(t))-\hat{e}_2^{\rm T}(t)G_2\hat{e}_2(t)-e_\nu^{\rm T}(t)G_\nu e_\nu(t)\leqslant 0, \qquad (6.47)$$

which, according to the LaSalle-Yoshizawa Theorem ([10, 44]), proves the final statement of the Theorem. □

Projection Algorithm

Note that in (6.41), the closed form of the command includes the term $(B_e(e_1)\Theta_2)^{-1}$, whose existence was one of the assumptions of Theorem 6.4.1. To remove this assumption, a projection algorithm ([109]) will be used. Note that

$$B_e(e_1)\Theta_2 = \begin{bmatrix} -\theta_{21} & -e_{\mathrm{d}}\sin(\beta)\theta_{23} \\ 0 & -\theta_{22} - e_{\mathrm{d}}\cos(\beta)\theta_{23} \end{bmatrix}, \tag{6.48}$$

whose eigenvalues are $-\theta_{21}$, and $-\theta_{22} - e_{\mathrm{d}}\cos(\beta)\theta_{23}$. Following the technique introduced in [109], define

$$f_\lambda(\Theta_{2\mathrm{v}}) = \frac{1}{r_{\mathrm{to}}^2 - r_{\mathrm{ti}}^2}\left((\theta_{21} - c_{\mathrm{t}})^2 + (\theta_{22} - c_{\mathrm{t}})^2 + (\theta_{23} - c_{\mathrm{t}})^2 - r_{\mathrm{ti}}^2\right), \qquad t \geq 0, \tag{6.49}$$

where $c_{\mathrm{t}} > 0$ and $0 < r_{\mathrm{ti}} < r_{\mathrm{to}}$. In addition, define the projection operator $P_{\mathrm{o}}(\zeta_0) : \mathcal{C}_n \to \mathcal{C}_n$, where $\mathcal{C}_n$ denotes the set of continuous $n-$valued functions, such that ([109])

$$P_{\mathrm{o}}(\zeta_0(t)) \triangleq \zeta_0(t) - \frac{f_\lambda'^{\mathrm{T}}(\Theta_{2\mathrm{v}}(t))}{\|f_\lambda'(\Theta_{2\mathrm{v}}(t))\|^2} f_\lambda'(\Theta_{2\mathrm{v}}(t))\zeta_0(t) f_\lambda(\Theta_{2\mathrm{v}}(t)), \qquad t \geq 0, \tag{6.50}$$

where $f_\lambda'(\Theta_{2\mathrm{v}})$ denotes the Fréchet derivative of $f_\lambda(\Theta_{2\mathrm{v}})$ with respect to $\Theta_{2\mathrm{v}}$. The update law for $\Theta_{2\mathrm{v}}(t)$, $t \geq 0$, is modified as follows ([109]),

$$\dot{\Theta}_{2\mathrm{v}}(t) = \begin{cases} P_{\mathrm{o}}(\zeta(t)), & \text{if } f_\lambda(\Theta_{2\mathrm{v}}(t)) \geq 0 \text{ and } f_\lambda'(\Theta_{2\mathrm{v}}(t))\zeta(t) > 0, \\ \zeta(t), & \text{otherwise,} \end{cases} \quad \Theta_{2\mathrm{v}}(t) = \Theta_{2\mathrm{v}0}, \quad t \geq 0, \tag{6.51}$$

where $\zeta(t) \triangleq \tau_{\mathrm{d}}(t) e_\nu(t)\Gamma_2$, $t \geq 0$. Since the update law (6.51) only adds a negative term to the Lyapunov derivative (6.46) ([109]), the stability properties established in Theorem 6.4.1 are not modified.

Numerical Simulations

This subsection presents results from numerical simulations illustrating the efficacy of the proposed control algorithm. In particular, results using the above indirect adaptive algorithm

are presented, which show convergence of the trajectory to the reference one, boundedness of the estimates, and behavior of the eigenvalues of $B_e(e_1)\Theta_2$. The control algorithm is used for tracking a circular trajectory and an octomorphic trajectory.

Circular Trajectory

The simulation uses initial estimates $\Theta_{10} = 0_{3\times 10}$ and

$$\Theta_{20} = \frac{1}{10}\begin{bmatrix} 1.3 & 0 \\ 0 & -1 \\ 0 & 1 \end{bmatrix}, \tag{6.52}$$

where Θ_{20} is chosen different from $0_{3\times 2}$ to avoid singularity of $B_e(e_1(0))\Theta_{20}$. To accommodate the values of the entries of Θ_2^*, while still being able to force the eigenvalues not to cross zero, set $c_{\rm t} = 10$, $r_{\rm ti} = c_{\rm t} - 10^{-3}$, $r_{\rm to} = c_{\rm t} - 2\times 10^{-3}$. The chosen desired trajectory is circular, of radius 10 meters, with a constant traveling speed of 1 meter per second. The vehicle's initial position is at the center of this circle, its initial velocity is zero. The reference trajectory's initial position is chosen slightly off of the vehicle's, to show convergence of the tracking errors, $x_{\rm r10} = \begin{bmatrix} 0.6\sqrt{2} & -0.6\sqrt{2} \end{bmatrix}^{\rm T}$. The gains are chosen as follows, $G_1 = 10I_2$, $G_2 = 0.1I_2$, $G_\nu = 10I_3$, $\Gamma_1 = 0.3I_{10}$, and $\Gamma_2 = 0.3I_2$. The reference signal is of the form

$$r_{\rm s}(t) = \omega_0^{-2}(\ddot{x}_{\rm d}(t) + \omega_0^2 x_{\rm d}(t) + 2\zeta\omega_0\dot{x}_{\rm d}(t)), \qquad t \geq 0, \tag{6.53}$$

where $x_{\rm d}(t)$ denotes the desired position in the xy-plane at time $t \geq 0$, $\zeta = 1.2I_2$ and $\omega_0 = 0.7I_2$. Finally, the constant parameters in M, $D(\nu)$ and $C(\nu)$ are given by (5.31), and $a = 0.2 > a_{\rm s}$.

The tracking errors converge smoothly to their expected steady state values. Figure 6.5 shows that the position error $e_{\rm d}(t)$, $t \geq 0$, converges to $a = 0.2$, while $\beta(t)$ and $e_2(t)$, $t \geq 0$, converge to zero. Figure 6.6 compares the actual and estimated body-fixed velocities,

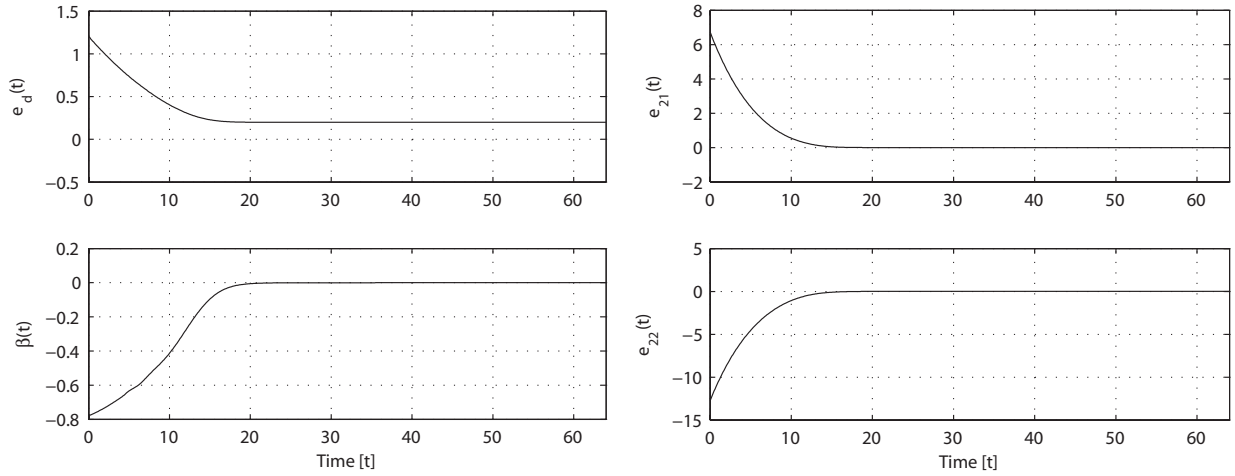

Figure 6.5: Tracking errors $e_1(t)$ and $e_2(t)$, $t \geq 0$, circular trajectory.

$\nu(t)$ and $\hat{\nu}(t)$, $t \geq 0$. Note that, the purpose of the state predictor (6.33) and update laws (6.42) and (6.43) is not necessarily to accurately estimate $\nu(t)$, $t \geq 0$, but rather to allow construction of the control command (6.41), in spite of parametric uncertainties. Nevertheless, Figure 6.6 shows that the estimated velocities match the actual ones.

Figure 6.7 shows the trajectory of the actual system (solid curve) converging smoothly to the reference (dashed), which in turn converges to the desired trajectory (dotted). Orientation of the vehicle is represented using black arrows, which demonstrate that the system moves in a coherent fashion. Indeed, the arrows indicate that the vehicle is moving bow first, which is corroborated by the fact that, as seen in Figure 6.6, the surge velocity $u(t)$, $t \geq 0$, remains positive throughout the simulation.

Figure 6.6 shows that the projection algorithm of Subsection 6.4 is effective in preventing the eigenvalues of $B_e(e_1(t))\Theta_2(t)$, $t \geq 0$, from crossing zero, thus ensuring that the inverse of this matrix is well defined. The effects of the projection algorithm are particularly evident for the first eigenvalue, which is constrained away from zero by the projection.

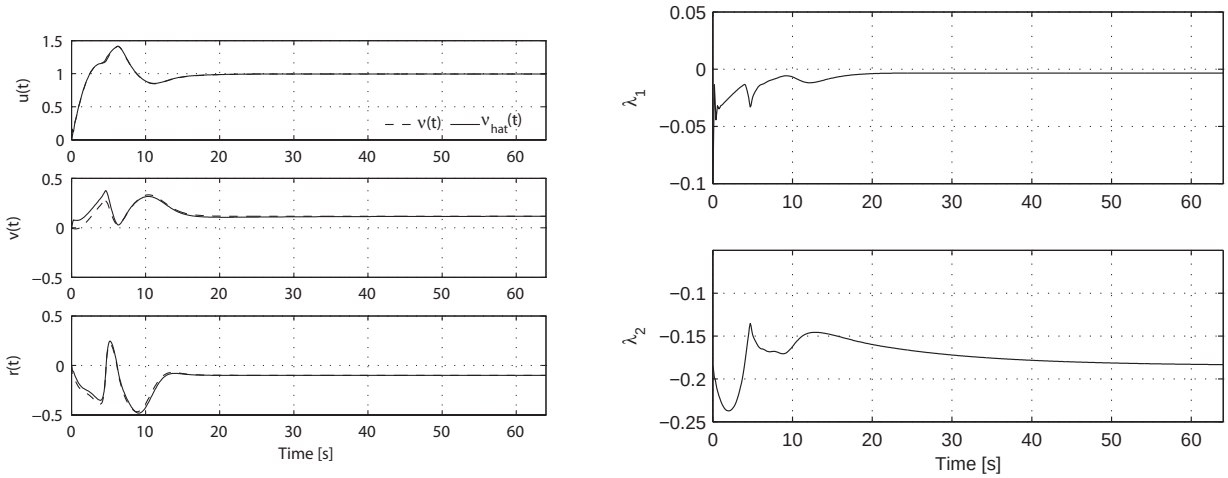

Figure 6.6: Actual and estimated body-fixed velocities, $\nu(t)$ and $\hat{\nu}(t)$, $t \geq 0$, left, and eigenvalues of $B_e(e_1(t))\Theta_2(t)$, $t \geq 0$, right (circular trajectory).

The control input is shown in Figure 6.7. The saturation technique discussed in Chapter 2 was applied to constrain the amplitude of the control effort to reasonable values. Figure 6.8 shows $\Theta_{2\mathrm{v}}(t)$, $t \geq 0$, and illustrates the boundedness of the estimates.

Octomorphic Trajectory

The second maneuver considered is an octomorphic trajectory, identical to that in Subsection 6.2. The initial position is $\eta_0 = \begin{bmatrix} -1 & 0 & 0 \end{bmatrix}^{\mathrm{T}}$, while the initial reference position is $x_{\mathrm{r}10} = \begin{bmatrix} 0.2 & 0 \end{bmatrix}^{\mathrm{T}}$. All other initial conditions, gains and parameters remain identical to what was chosen for the previous example.

As shown in Figure 6.9, the behavior is similar to that observed with a circular desired trajectory. The vehicle converges smoothly to the desired trajectory, and the orientation, still indicated by black arrows, remains appropriate. The control command can be found in Figure 6.9, and the estimate $\Theta_{2\mathrm{v}}(t)$, $t \geq 0$, in Figure 6.10.

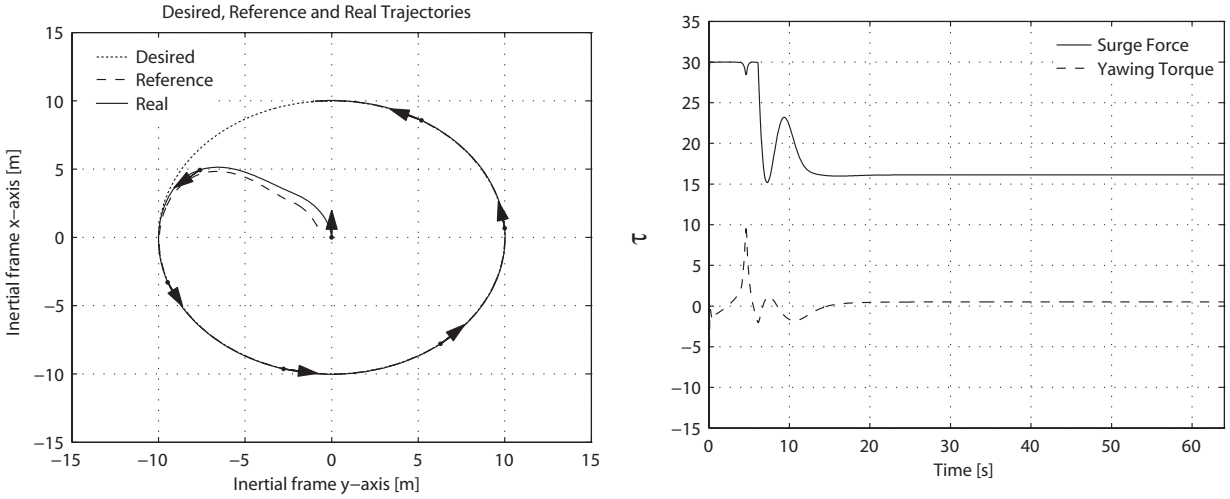

Figure 6.7: Actual, reference and desired trajectories, left, and corresponding control command $\tau(t)$, $t \geq 0$, right (circular trajectory).

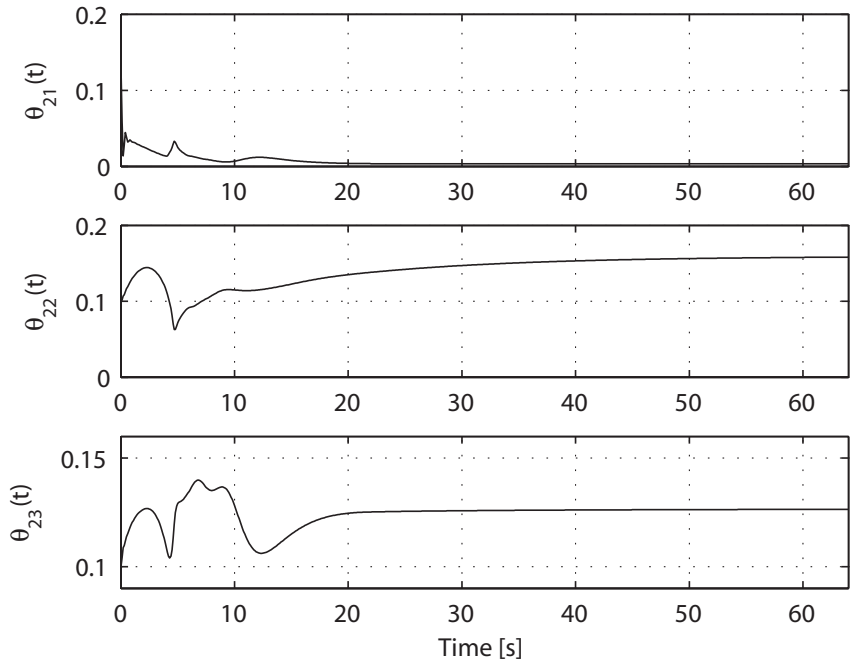

Figure 6.8: Elements of the parameter estimate vector $\Theta_{2v}(t)$, $t \geq 0$, circular trajectory.

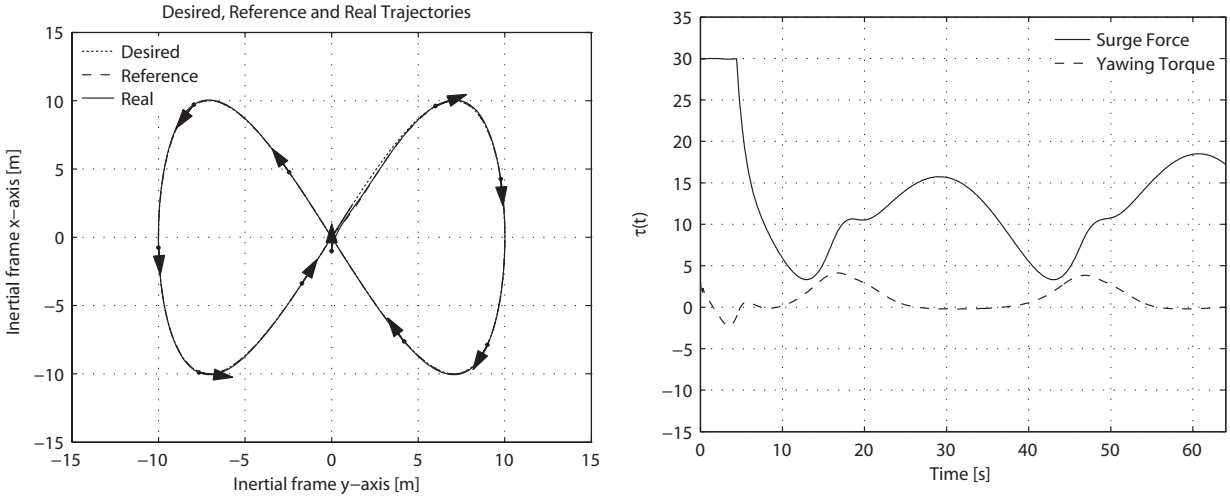

Figure 6.9: Actual, reference and desired trajectories, left, and corresponding control command $\tau(t)$, $t \geq 0$, right (octomorphic trajectory).

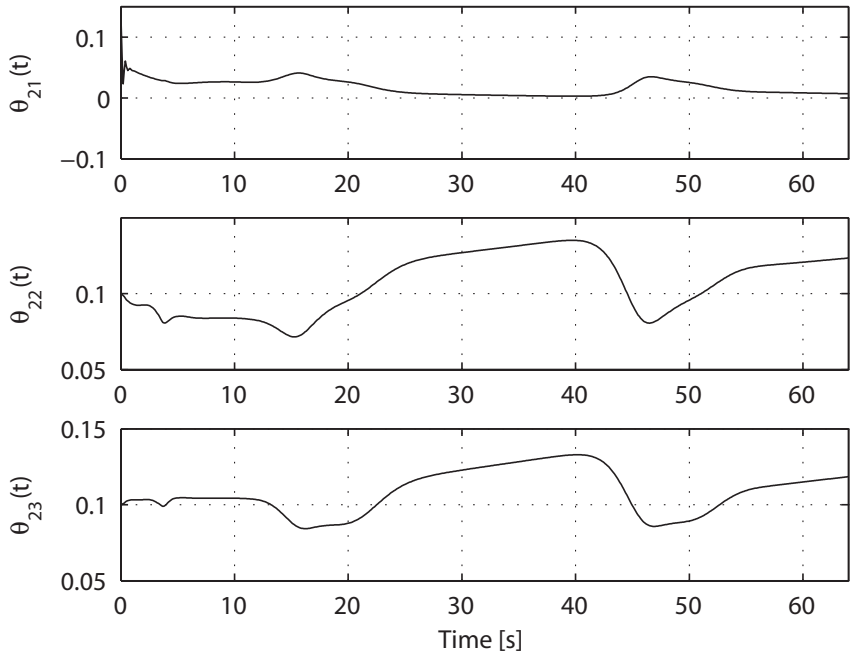

Figure 6.10: Elements of the parameter estimate vector $\Theta_{2v}(t)$, $t \geq 0$, octomorphic trajectory.

6.5. Conclusion

The results presented in this chapter build upon that in Chapter 5, which addressed trajectory tracking in the horizontal plane for a class of non-minimum phase marine vehicles. Since the control law obtained in Section 5.2 depends on uncertain parameters, adaptive control algorithms were derived. Furthermore, the unknown parameters appear nonlinearly in the command, which lead to difficulties in deriving a direct adaptive algorithm. This nonlinear parametrization was overcome using two different approaches; that is, linearization of the command with respect of the uncertain parameters, as described in Section 6.2, and DSC, as seen in Section 6.3. Both direct adaptive controllers showed interesting performance in simulations. Next, an indirect adaptive algorithm was presented. The obtained adaptive control algorithm guarantees convergence of the tracking errors and Lyapunov stability of the dynamics, in spite of the parametric uncertainties. Numerical simulations illustrate the excellent performance of the indirect adaptive control algorithm in the case of circular and octomorphic trajectories. In addition, simulation results correlate with the presented stability analysis of the zero-dynamics from the previous chapter, as they show the vehicle moving bow first, meaning that the system's velocity in surge remains positive.

Chapter 7

Prediction-based Observation of Nonlinear Systems Non-affine in the Unmeasured States [7]

The following result was the object of an article submitted to Automatica (currently under review) and a conference paper submitted to the 2009 IEEE Conference on Decision and Control (currently under review).

7.1. Introduction

The control algorithms presented in previous chapters require full state measurements. However, in practice, it is not uncommon that only partial state measurements are available. Accordingly, the following chapters will address the output feedback control problem, for a wide class of uncertain nonlinear systems. The final result in Chapter 9 relies on an output predictor, based upon the nonlinear observer introduced in the following.

More specifically, this chapter presents a novel nonlinear observer design which, while concerned with a smaller class of systems than the immersion and invariance based technique

introduced in [46], has the advantage of being systematic and relatively simple to apply. In a departure from high gain observation techniques such as those in [44, 45], the presented approach relaxes high gain requirements by using derivative estimates ([56,57]). The observer relies on a partial state predictor, which compares predictions on the measured states with actual measurements. The prediction error is then used to estimate the unmeasured states. The design of this predictor-observer relies on specific prediction-observation errors, designed using a backstepping technique ([10]). A Lyapunov stability analysis of the errors' dynamics shows that they are Lyapunov stable, and converge to a neighborhood of the origin. The size of this neighborhood depends upon the accuracy of the derivative estimate, as well as on a number of design constants. Accordingly, the errors can be made arbitrarily small by using a high performance derivative estimator, and/or selecting appropriate gains.

This chapter is structured as follows. Section 7.2 describes the class of systems considered and presents the observation strategy. The predictor-observer is then introduced in Section 7.3. Performance of the obtained observer was tested through numerical simulations for two different nonlinear oscillators, and a three degree of freedom helicopter model. Simulation results are presented in Section 7.4 and illustrate the efficacy of the proposed observer. The algorithm was also tested experimentally, on a three degree of freedom helicopter setup. Implementation results are given in Section 7.5. Section 7.6 concludes this chapter.

7.2. Problem Statement and Observation Strategy

Consider a system of the form

$$\dot{x}(t) = f(x(t), t), \quad x(0) = x_0, \quad t \geq 0, \tag{7.1}$$

$$y(t) = Cx(t), \tag{7.2}$$

where $x(t) \in \mathbb{R}^n$, $t \geq 0$, is the system's state vector, $y(t) \in \mathbb{R}^m$, $t \geq 0$, the measured output vector, with $m \geq n/2$, and $C = \left[\begin{array}{cc} I_m & 0_{m \times p} \end{array} \right]$, with $p = n - m \leq m$.

A sufficient condition for system (7.1)–(7.2) to be observable is that $\text{rank}[J(x(t), t)] = n$, $t \geq 0$, ([111, 112]), where

$$J(x(t), t) \triangleq \left[\begin{array}{c} \nabla y(t) \\ \nabla y^{(1)}(t) \\ \vdots \\ \nabla y^{(n-1)}(t) \end{array} \right], \quad t \geq 0, \tag{7.3}$$

with $\nabla g(x) \triangleq \frac{\mathrm{d}g(x)}{\mathrm{d}x}$, and $(\cdot)^{(i)}$ denotes the i^{th} derivative with respect to time. In the following, we focus on a subset of the set of observable systems as defined by the above condition. More specifically, we consider systems for which $\text{rank}[J_{\text{s}}(x(t), t)] = n$, $t \geq 0$, where

$$J_{\text{s}}(x(t), t) \triangleq \left[\begin{array}{c} \nabla y(t) \\ \nabla \dot{y}(t) \end{array} \right], \quad t \geq 0. \tag{7.4}$$

The goal of the presented work is to reconstruct the entire state vector $x(t)$, $t \geq 0$, using the information provided by the output measurement $y(t)$, $t \geq 0$, and partial knowledge of the form of the right-hand-side of (7.1). To reach this goal, we define $x_1(t) \triangleq y(t)$, $t \geq 0$, and decompose the state vector as $x(t) = \left[\begin{array}{cc} x_1^{\text{T}}(t) & x_2^{\text{T}}(t) \end{array} \right]^{\text{T}}$, $t \geq 0$, where $x_2(t) \in \mathbb{R}^p$, $t \geq 0$, denotes the unmeasured states which we attempt to reconstruct. Furthermore, the dynamics of the measured states are described by

$$\dot{x}_1(t) \, = \, f_1(x_1(t), x_2(t), t), \quad x_1(0) = Cx_0 \triangleq x_{10} = y(0), \quad t \geq 0, \tag{7.5}$$

where $f_1(x_1(t), x_2(t), t) \triangleq Cf(x(t), t)$, $t \geq 0$. Note that, using (7.2) and (7.5), we can rewrite (7.4) as

$$J_{\text{s}}(x, t) \triangleq \left[\begin{array}{cc} I_m & 0_{m \times p} \\ \frac{\partial f_1(x_1, x_2, t)}{\partial x_1} & \frac{\partial f_1(x_1, x_2, t)}{\partial x_2} \end{array} \right], \tag{7.6}$$

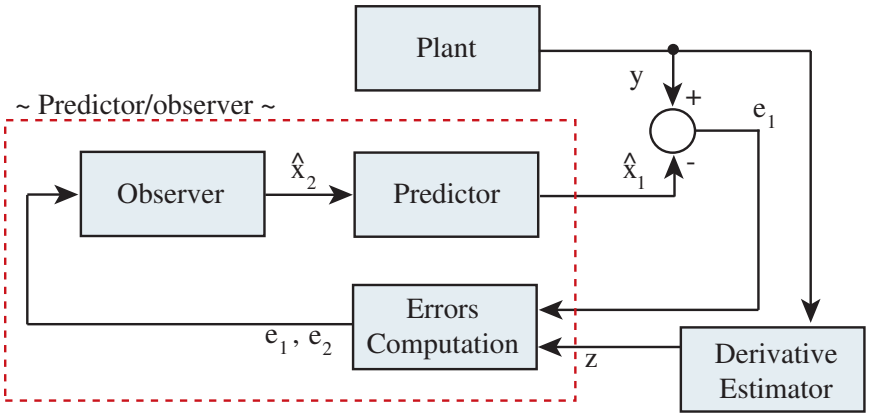

Figure 7.1: Block diagram of the presented observation algorithm.

and the above observability condition reduces to the condition that $\text{rank}[\partial f_1(x_1, x_2, t)/\partial x_2] = p$. In addition, from (7.2) and (7.5), we have that

$$\dot{y}(t) - f_1(y(t), x_2(t), t) = 0, \quad t \geq 0. \tag{7.7}$$

According to the implicit function theorem ([113]), if $\text{rank}[\partial f_1(x_1, x_2, t)/\partial x_2] = p$, there exists a unique function $g : \mathbb{R}^m \times \mathbb{R}^m \times \mathbb{R} \to \mathbb{R}^p$, such that $g(y, \dot{y}, t) = x_2$. However, obtaining a closed form expression of this function can prove challenging, and its existence can only be guaranteed locally. In addition, while $y(t)$, $t \geq 0$, is measured and hence known, $\dot{y}(t)$, $t \geq 0$, is not necessarily available. Thus, directly working in terms of the above $g(\cdot)$ does not constitute a viable option.

Instead, we will *indirectly* work in terms of $g(\cdot)$. In particular, we will construct an estimate $\hat{x}_2(t)$ of $x_2(t)$, $t \geq 0$, which uniformly converges to a neighborhood of $g(y(t), \dot{y}(t), t)$, $t \geq 0$. In addition, since $\dot{y}(t)$, $t \geq 0$, is not measured, we will estimate its value, using measured information (i.e. $y(t)$, $t \geq 0$) and a derivative estimator (such as those in [56, 57]). The resulting estimate $\hat{x}_2(t)$, $t \geq 0$, is then further refined by adjusting it according to a prediction error, as described in Figure 7.1. The latter is computed as the difference between

the measured output and a predicted $\hat{x}_1(t)$, $t \geq 0$, obtained by integrating a partial state predictor whose form is similar to (7.5), with $x_2(t)$ replaced by $\hat{x}_2(t)$, $t \geq 0$.

7.3. Nonlinear Observer Design

Following the approach delineated in Section 7.2, we construct a partial state predictor, with the following Luenberger form ([13]),

$$\dot{\hat{x}}_1(t) = f_1(x_1(t), \hat{x}_2(t), t) - De_1(t), \quad \hat{x}_1(0) = x_{10}, \quad t \geq 0, \tag{7.8}$$

where $D \in \mathbb{R}^{m \times m}$, $e_1(t) \triangleq x_1(t) - \hat{x}_1(t)$, $t \geq 0$, is a prediction error, and $\hat{x}_2(t) \in \mathbb{R}^p$, $t \geq 0$, is designed so that $\hat{x}_1(t) \in \mathbb{R}^m$, $t \geq 0$, provides a predicted value of $x_1(t)$, $t \geq 0$. In addition, to provide more flexibility in the design procedure, the algorithm will rely on an auxiliary signal $\omega(t) \in \mathbb{R}^m$, $t \geq 0$, obtained from

$$\dot{\omega}(t) = W_{\mathrm{a}}(x_1(t), \hat{x}_2(t), t)v(t), \quad \omega(0) = 0_m, \quad t \geq 0, \tag{7.9}$$

where $v(t) \in \mathbb{R}^{m-p}$, $t \geq 0$, and $W_{\mathrm{a}}(\cdot) \in \mathbb{R}^{m \times (m-p)}$ is designed so that $W_2(x_1, \hat{x}_2, t) \triangleq \left[\begin{array}{cc} \frac{\partial f_1(x_1, \hat{x}_2, t)}{\partial \hat{x}_2} & W_{\mathrm{a}}(x_1, \hat{x}_2, t) \end{array} \right] \in \mathbb{R}^{m \times m}$ is nonsingular for all $x_1 \in \mathbb{R}^m$, $\hat{x}_2 \in \mathbb{R}^p$, $t \geq 0$.

In the following, we will construct $\dot{\hat{x}}_{2\mathrm{a}}(t) \triangleq \left[\begin{array}{cc} \dot{\hat{x}}_2^{\mathrm{T}}(t) & v^{\mathrm{T}}(t) \end{array} \right]^{\mathrm{T}} \in \mathbb{R}^m$, $t \geq 0$, so that the origin of the prediction-observation error dynamics is Lyapunov stable and $e_1(t)$, $t \geq 0$, asymptotically converges to a neighborhood of the origin, uniformly in time.

For the statement of the following theorem, we will use the notations

$$W_1(x_1, \hat{x}_2, t) \triangleq \frac{\partial f_1(x_1, \hat{x}_2, t)}{\partial x_1}, \quad W_3(x_1, \hat{x}_2, t) \triangleq \frac{\partial f_1(x_1, \hat{x}_2, t)}{\partial t}, \tag{7.10}$$

as well as the following lemma,

Lemma 7.3.1. [114] Let $A, \Sigma \in \mathbb{R}^{m\times m}$ be Hurwitz, and $Q \triangleq R^{\mathrm{T}}R$, with $R \in \mathbb{R}^{m\times m}$ full rank. If

$$H \triangleq \left[\begin{array}{cc} A & \Sigma\Sigma^{\mathrm{T}} \\ -Q & -A^{\mathrm{T}} \end{array} \right], \tag{7.11}$$

has no eigenvalues on the imaginary axis, then there exists $P \geq 0$ such that

$$A^{\mathrm{T}}P + PA + Q + P\Sigma\Sigma^{\mathrm{T}}P = 0. \tag{7.12}$$

In addition, if (A, R) is observable, $P > 0$.

Theorem 7.3.1. Consider the system given by (7.1)–(7.2), and the partial state predictor (7.8). Assume that a continuously differentiable signal $z(t)$ is available such that $z(t) = \dot{y}(t) + \omega(t) - \epsilon(t)$, with $\|\epsilon(t)\| \leq \sqrt{\varepsilon/3}$, $\varepsilon > 0$, $t \geq 0$. Then, consider the estimated trajectory $\hat{x}_2(t)$, $t \geq 0$, generated by

$$\begin{aligned} \dot{\hat{x}}_{2\mathrm{a}}(t) = W_2^{-1}(x_1(t), \hat{x}_2(t), t)\Big[P_2^{-1}P_1e_1(t) - A_1((A_1 + P_1^{-1}K)e_1(t) - e_2(t)) + \dot{z}(t) + A_2e_2(t) \\ -W_1(x_1(t), \hat{x}_2(t), t)\Big(z(t) - \omega(t) + \frac{1}{2}W_1^{\mathrm{T}}(x_1(t), \hat{x}_2(t), t)P_2e_2(t)\Big) - W_3(x_1(t), \hat{x}_2(t), t)\Big], \\ \hat{x}_{2\mathrm{a}}(0) = 0_m, \quad t \geq 0, \end{aligned} \tag{7.13}$$

$$\hat{x}_2(t) = \left[\begin{array}{cc} I_p & 0_{p\times(m-p)} \end{array} \right] \hat{x}_{2\mathrm{a}}(t), \tag{7.14}$$

where A_1, A_2, and K are chosen Hurwitz, $e_2(t) \triangleq f_1(x_1(t), \hat{x}_2(t), t) + \omega(t) + A_1e_1(t) - z(t)$, $t \geq 0$, the matrices P_1, $P_2 \in \mathbb{R}^{m\times m}$ are obtained from the following Riccati equations,

$$A_1^{\mathrm{T}}P_1 + P_1A_1 + Q_1 + P_1^2 = 0, \tag{7.15}$$

$$A_2^{\mathrm{T}}P_2 + P_2A_2 + Q_2 + P_2A_1A_1^{\mathrm{T}}P_2 = 0, \tag{7.16}$$

and $Q_1 \triangleq R_1^{\mathrm{T}}R_1 > 0$, $Q_2 \triangleq R_2^{\mathrm{T}}R_2 > 0$, are chosen such that

$$H_1 \triangleq \left[\begin{array}{cc} A_1 & I_m \\ -Q_1 & -A_1^{\mathrm{T}} \end{array} \right], \quad H_2 \triangleq \left[\begin{array}{cc} A_2 & A_1A_1^{\mathrm{T}} \\ -Q_2 & -A_2^{\mathrm{T}} \end{array} \right], \tag{7.17}$$

have no eigenvalues on the imaginary axis and (A_1, R_1), (A_2, R_2) are observable. In addition, the auxiliary signal $\omega(t)$ is obtained from (7.9), with $v(t) \triangleq \left[\begin{array}{cc} 0_{(m-p)\times(p)} & I_{m-p} \end{array}\right] \dot{\hat{x}}_{2\mathrm{a}}(t)$, $t \geq 0$. Finally, choose $D = P_1^{-1}K$, define $\bar{Q}_1 \triangleq Q_1 - K - K^{\mathrm{T}}$,

$$M \triangleq \left[\begin{array}{cc} \bar{Q}_1^{-1}P_1 & 0_{m\times m} \\ 0_{m\times m} & Q_2^{-1}P_2 \end{array}\right], \tag{7.18}$$

and let $\lambda_{\max}(M)$ denote the maximum eigenvalue of M. The solution $\hat{x}_{2\mathrm{a}}(t)$, $t \geq 0$, to (7.13) guarantees uniform ultimate boundedness of $(e_1(t), e_2(t))$, $t \geq 0$, with an ultimate bound given by $\mathcal{D} \triangleq \left\{(e_1, e_2) : e_1^{\mathrm{T}}P_1e_1 + e_2^{\mathrm{T}}P_2e_2 \leq \varepsilon\lambda_{\max}(M)\right\}$.

Proof. The time derivative of the prediction error $e_1(t)$, $t \geq 0$, is given by

$$\dot{e}_1(t) = f_1(x_1(t), x_2(t), t) - f_1(x_1(t), \hat{x}_2(t), t) + P_1^{-1}Ke_1(t), \quad t \geq 0, \tag{7.19}$$

which, by definition of $e_2(t)$, $t \geq 0$, can be rewritten

$$\begin{aligned} \dot{e}_1(t) &= f_1(x_1(t), x_2(t), t) + \omega(t) + P_1^{-1}Ke_1(t) - z(t) + A_1e_1(t) - e_2(t) \\ &= (A_1 + P_1^{-1}K)e_1(t) - e_2(t) + \epsilon(t), \quad t \geq 0. \end{aligned} \tag{7.20}$$

In addition, the time derivative of the observation error $e_2(t)$, $t \geq 0$, is of the form

$$\begin{aligned} \dot{e}_2(t) &= A_1\dot{e}_1(t) + W_1(x_1(t), \hat{x}_2(t), t)\dot{x}_1(t) + W_2(x_1(t), \hat{x}_2(t), t)\dot{\hat{x}}_{2\mathrm{a}}(t) + W_3(x_1(t), \hat{x}_2(t), t) - \dot{z}(t) \\ &= A_1\epsilon(t) + A_1((A_1 + P_1^{-1}K)e_1(t) - e_2(t)) + W_1(x_1(t), \hat{x}_2(t), t)(z(t) - \omega(t) + \epsilon(t)) \\ &\quad -\dot{z}(t) + W_3(x_1(t), \hat{x}_2(t), t) + W_2(x_1(t), \hat{x}_2(t), t)\dot{\hat{x}}_{2\mathrm{a}}, \quad t \geq 0. \end{aligned} \tag{7.21}$$

Substituting (7.13) into (7.21), we obtain

$$\begin{aligned} \dot{e}_2(t) &= A_1\epsilon(t) + A_1((A_1 + P_1^{-1}K)e_1(t) - e_2(t)) + W_1(x_1(t), \hat{x}_2(t), t)(z(t) - \omega(t) + \epsilon(t)) \\ &\quad -\dot{z}(t) + W_3(x_1(t), \hat{x}_2(t), t) + P_2^{-1}P_1e_1(t) - A_1((A_1 + P_1^{-1}K)e_1(t) - e_2(t)) \end{aligned}$$

$$
\begin{aligned}
&+\dot{z}(t)+A_2e_2(t)-W_1(x_1(t),\hat{x}_2(t),t)\Big(z(t)-\omega(t)+\frac{1}{2}W_1^{\mathrm{T}}(x_1(t),\hat{x}_2(t),t)P_2e_2(t)\Big)\\
&-W_3(x_1(t),\hat{x}_2(t),t)\\
&=P_2^{-1}P_1e_1(t)+A_2e_2(t)+W_1(x_1(t),\hat{x}_2(t),t)\Big(\epsilon(t)-\frac{1}{2}W_1^{\mathrm{T}}(x_1(t),\hat{x}_2(t),t)P_2e_2(t)\Big)\\
&+A_1\epsilon(t),\quad t\geq 0. \qquad (7.22)
\end{aligned}
$$

Then, consider the following Lyapunov function candidate,

$$
V(e_1,e_2)\;=\;e_1^{\mathrm{T}}P_1e_1+e_2^{\mathrm{T}}P_2e_2, \qquad (7.23)
$$

where $P_1,\ P_2>0$ are obtained from (7.15) and (7.16), respectively. The time derivative of (7.23) along the trajectories of (7.20) and (7.22) is given by

$$
\begin{aligned}
\dot{V}(t)&=e_1^{\mathrm{T}}(t)(A_1^{\mathrm{T}}P_1+P_1A_1)e_1(t)+e_2^{\mathrm{T}}(t)(A_2^{\mathrm{T}}P_2+P_2A_2)e_2(t)+e_1^{\mathrm{T}}(t)(K+K^{\mathrm{T}})e_1(t)\\
&\quad+2e_2^{\mathrm{T}}(t)P_2\Big(A_1\epsilon(t)+W_1(x_1(t),\hat{x}_2(t),t)\Big(\epsilon(t)-\frac{1}{2}W_1^{\mathrm{T}}(x_1(t),\hat{x}_2(t),t)P_2e_2(t)\Big)\\
&\quad+P_2^{-1}P_1e_1(t)\Big)-2e_1^{\mathrm{T}}(t)P_1(e_2(t)-\epsilon(t))\\
&=2e_2^{\mathrm{T}}(t)P_2W_1(x_1(t),\hat{x}_2(t),t)\Big(\epsilon(t)-\frac{1}{2}W_1^{\mathrm{T}}(x_1(t),\hat{x}_2(t),t)P_2e_2(t)\Big)+2e_2^{\mathrm{T}}(t)P_2A_1\epsilon(t)\\
&\quad-e_1^{\mathrm{T}}(t)(Q_1-K-K^{\mathrm{T}}+P_1^2)e_1(t)-e_2^{\mathrm{T}}(t)(Q_2+P_2A_1A_1^{\mathrm{T}}P_2)e_2(t)+2e_1^{\mathrm{T}}(t)P_1\epsilon(t),t\geq 0. \qquad (7.24)
\end{aligned}
$$

Next, using the completion of the square rule, we obtain

$$
2e_1^{\mathrm{T}}P_1\epsilon\;=\;-(P_1e_1-\epsilon)^{\mathrm{T}}(P_1e_1-\epsilon)+e_1^{\mathrm{T}}P_1^2e_1+\epsilon^{\mathrm{T}}\epsilon, \qquad (7.25)
$$

$$
2e_2^{\mathrm{T}}P_2A_1\epsilon\;=\;-(A_1^{\mathrm{T}}P_2e_2-\epsilon)^{\mathrm{T}}(A_1^{\mathrm{T}}P_2e_2-\epsilon)+e_2^{\mathrm{T}}P_2A_1A_1^{\mathrm{T}}P_2e_2+\epsilon^{\mathrm{T}}\epsilon, \qquad (7.26)
$$

$$
\begin{aligned}
2e_2^{\mathrm{T}}P_2W_1(x_1,\hat{x}_2,t)\epsilon\;&=\;e_2^{\mathrm{T}}P_2W_1(x_1,\hat{x}_2,t)W_1^{\mathrm{T}}(x_1,\hat{x}_2,t)P_2e_2+\epsilon^{\mathrm{T}}\epsilon\\
&\quad-\left(W_1^{\mathrm{T}}(x_1,\hat{x}_2,t)P_2e_2-\epsilon\right)^{\mathrm{T}}\left(W_1^{\mathrm{T}}(x_1,\hat{x}_2,t)P_2e_2-\epsilon\right). \qquad (7.27)
\end{aligned}
$$

It follows that

$$
\dot{V}(t)\;\leq\;-e_1^{\mathrm{T}}(t)(\bar{Q}_1+P_1^2)e_1(t)+e_1^{\mathrm{T}}(t)P_1^2e_1(t)-e_2^{\mathrm{T}}(t)(Q_2+P_2A_1A_1^{\mathrm{T}}P_2)e_2(t)
$$

$$
\begin{aligned}
&+e_2^{\mathrm{T}}(t)P_2A_1A_1^{\mathrm{T}}P_2e_2(t)+e_2^{\mathrm{T}}(t)P_2W_1(x_1(t),\hat{x}_2(t),t)W_1^{\mathrm{T}}(x_1(t),\hat{x}_2(t),t)P_2e_2(t)\\
&-e_2^{\mathrm{T}}(t)P_2W_1(x_1(t),\hat{x}_2(t),t)W_1^{\mathrm{T}}(x_1(t),\hat{x}_2(t),t)P_2e_2(t)+3\epsilon^{\mathrm{T}}(t)\epsilon(t)\\
\leq\ &-e_1^{\mathrm{T}}(t)\bar{Q}_1e_1(t)-e_2^{\mathrm{T}}(t)Q_2e_2(t)+\varepsilon,\quad t\geq 0. \qquad (7.28)
\end{aligned}
$$

Hence, $\dot{V}(t)$, $t \geq 0$, is strictly negative outside of $\big\{(e_1, e_2) : e_1^{\mathrm{T}}\bar{Q}_1e_1 + e_2^{\mathrm{T}}Q_2e_2 \leq \varepsilon\big\}$, which allows to conclude ultimate boundedness of $(e_1(t), e_2(t))$, $t \geq 0$ ([44, 88]). In addition, the ultimate bound can be characterized by $\alpha \triangleq \min(e_1^{\mathrm{T}}P_1e_1 + e_2^{\mathrm{T}}P_2e_2)$, subject to the constraint $e_1^{\mathrm{T}}\bar{Q}_1e_1 + e_2^{\mathrm{T}}Q_2e_2 = \varepsilon$. This constrained minimization problem is easily solved using Lagrange multipliers, yielding $\alpha = \varepsilon\lambda_{\max}(M)$, which proves uniform convergence of the error trajectories to $\mathcal{D}$ and concludes this proof. □

Remark 7.3.1. Note that, in the ideal case that $\epsilon(t) \equiv 0$, $t \geq 0$, we would obtain that $(e_1(t), e_2(t)) \to 0$ as $t \to \infty$. Hence, from the definition of $e_2(t)$, $t \geq 0$, we would obtain convergence of $\hat{x}_2(t)$ to the implicit function $g(y(t), \dot{y}(t), t)$, $t \geq 0$, defined by (7.7).

Remark 7.3.2. In Theorem 7.3.1, it is assumed that $m \geq n/2$. In the particular case that $m = n/2$, the design procedure is simpler. Indeed, in such a situation, the auxiliary signal $\omega(t)$, $t \geq 0$, becomes superfluous, K can be chosen to be zero, and $\hat{x}_{2\mathrm{a}}(t) = \hat{x}_2(t)$, $t \geq 0$.

7.4. Illustrative Numerical Examples

To obtain an estimate $z(t)$ of $\dot{y}(t)+\omega(t)$, $t \geq 0$, we will use the Adaptive Integral Variable Structure Derivative Estimator (AIVSDE) described in [57]. The object of the technique is, using measurements of a signal $r(t)$, $t \geq 0$, to obtain an estimate of its time derivative $\dot{r}(t)$, $t \geq 0$. This is achieved by constructing a signal $\gamma(t)$, $t \geq 0$, which converges to $r(t)$, $t \geq 0$.

The signal $\gamma(t)$, $t \geq 0$, is obtained from

$$\dot{\gamma}(t) = k_r(t)\text{sign}(\sigma(t)) + k_b\sigma(t) - k_1k_2^{-1}\gamma(t), \qquad \gamma(0) = \gamma_0, \quad t \geq 0, \tag{7.29}$$

$$\sigma(t) = k_2(r(t) - \gamma(t)) + k_1\int_0^t (r(\tau) - \gamma(\tau))\mathrm{d}\tau, \tag{7.30}$$

where k_b, k_1, $k_2 \geq 0$, the adaptive gain $k_r(t)$, $t \geq 0$, is obtained from

$$\dot{k}_r(t) = \begin{cases} \alpha_r & \text{for} \|\sigma(t)\| \geq \mu, \\ 0 & \text{for} \|\sigma(t)\| < \mu, \end{cases}, \quad k_r(0) = k_{r0}, \quad t \geq 0, \tag{7.31}$$

where $\alpha_r \geq 0$ and $\mu \geq 0$. The estimate of $\dot{r}(t)$ is given by $\dot{\gamma}(t)$, $t \geq 0$. In our case, setting $r(t) = y(t) + \int_0^t \omega(\tau)\mathrm{d}\tau$, and $z(t) = \dot{\gamma}(t)$, $t \geq 0$, we obtain an estimate $z(t)$ of $\dot{y}(t) + \omega(t)$, $t \geq 0$.

In the following, we will apply the predictor-observer described in Section 7.3, in conjunction with the above AIVSDE technique, to address the observation problem for three distinct systems. In a first example, we consider a system with state $[x_1(t)\ x_2(t)]^{\mathrm{T}} \in \mathbb{R}^2$, $t \geq 0$, where $x_1(t)$, $t \geq 0$, is measured, and we attempt to construct an estimate $\hat{x}_2(t)$ of the unmeasured $x_2(t)$, $t \geq 0$. This example illustrates performance of the presented approach, and in particular, the domain of convergence obtained in Theorem 7.3.1 is shown to be conservative. In a second example, we apply the technique to a case where $m < p$; that is, a case in which there are more measured states than unmeasured ones. Finally, we address the same observation problem for a system with state $[\eta^{\mathrm{T}}(t)\ \nu^{\mathrm{T}}(t)]^{\mathrm{T}} \in \mathbb{R}^6$, $t \geq 0$, with output $\eta(t) \in \mathbb{R}^3$, $t \geq 0$. The estimate $\hat{\nu}(t)$ is shown to converge to neighborhood of the unmeasured $\nu(t)$, $t \geq 0$.

Example 7.4.1. Consider the following system,

$$\dot{x}_1(t) = a\sin(x_1(t) + x_2(t)) + b(\tanh(\pi x_2(t) - 2) + \tanh(x_2^3(t)/10) + x_2^3(t)/100),$$

$$x_1(0) = x_{10}, \quad t \geq 0, \quad (7.32)$$

$$\dot{x}_2(t) = c\tanh(x_1(t)) - dx_2^3(t), \qquad x_2(0) = x_{20}, \quad (7.33)$$

$$y(t) = x_1(t), \quad (7.34)$$

where $x_1(t)$, $x_2(t) \in \mathbb{R}$, $t \geq 0$, and a, b, c, $d \in \mathbb{R}$. Note that, for the above system, $m = p = 1$. It is therefore unnecessary to construct an auxiliary signal $\omega(t)$, $t \geq 0$, K can be chosen to be zero, and the design procedure is simplified. More specifically, we construct the following predictor-observer,

$$\dot{\hat{x}}_1(t) = a\sin(x_1(t) + \hat{x}_2(t)) + b(\tanh(\pi\hat{x}_2(t) - 2) + \tanh(\hat{x}_2^3(t)/10) + \hat{x}_2^3(t)/100),$$
$$\hat{x}_1(0) = x_{10}, \quad t \geq 0, \quad (7.35)$$

$$\dot{\hat{x}}_2(t) = \Big(p_1e_1(t)/p_2 - A_1(A_1e_1(t) - e_2(t)) + \dot{z}(t) + A_2e_2(t) - w_1(x_1(t), \hat{x}_2(t))z(t)$$
$$-\frac{1}{2}w_1(x_1(t), \hat{x}_2(t))w_1^{\mathrm{T}}(x_1(t), \hat{x}_2(t))p_2e_2(t)\Big)/w_2(x_1(t), \hat{x}_2(t)), \quad \hat{x}_2(0) = 0, \quad (7.36)$$

where $e_1(t) = x_1(t) - \hat{x}_1(t)$, $e_2(t) = \dot{\hat{x}}_1(t) + A_1e_1(t) - z(t)$, $t \geq 0$, $w_1(x_1, \hat{x}_2) \triangleq a\cos(x_1 + \hat{x}_2)$, $w_2(x_1, \hat{x}_2) \triangleq a\cos(x_1 + \hat{x}_2) + b(\pi\mathrm{sech}^2(\pi\hat{x}_2 - 2) + \mathrm{sech}^2(\hat{x}_2^3/10)(3\hat{x}_2^2/10) + 3\hat{x}_2^2/100)$. Note that $w_2(x_1, \hat{x}_2) > 0$, for all $x_1 \in \mathbb{R}$, $\hat{x}_2 \in \mathbb{R}$.

Since in this example $m = 1$, The Riccati equations (7.15)–(7.16) simplify to

$$p_1^2 + 2A_1p_1 + q_1 = 0, \quad (7.37)$$

$$A_1^2p_2^2 + 2A_2p_2 + q_2 = 0, \quad (7.38)$$

where A_i, p_i and q_i, $i = 1, 2$, are scalars. From (7.37)–(7.38), we obtain that $p_1 = (-A_1 \pm \sqrt{A_1^2 - q_1})$ and $p_2 = (-A_2 \pm \sqrt{A_2^2 - A_1^2q_2})/A_1^2$. We thus need to choose $q_1 \leq A_1^2$, and $q_2 \leq A_2^2/A_1^2$. We choose $A_1 = -10$, $A_2 = -100$, $q_1 = 10$, $q_2 = 80$, and obtain $p_1 = 0.5132$, $p_2 = 0.5528$. The parameters of the AIVSDE are chosen as follows, $k_1 = k_b = 10$, $k_2 = 20$, $\alpha_r = 0$, $\mu = 1$, $\gamma_0 = x_{10}$ and $k_{r0} = 145$.

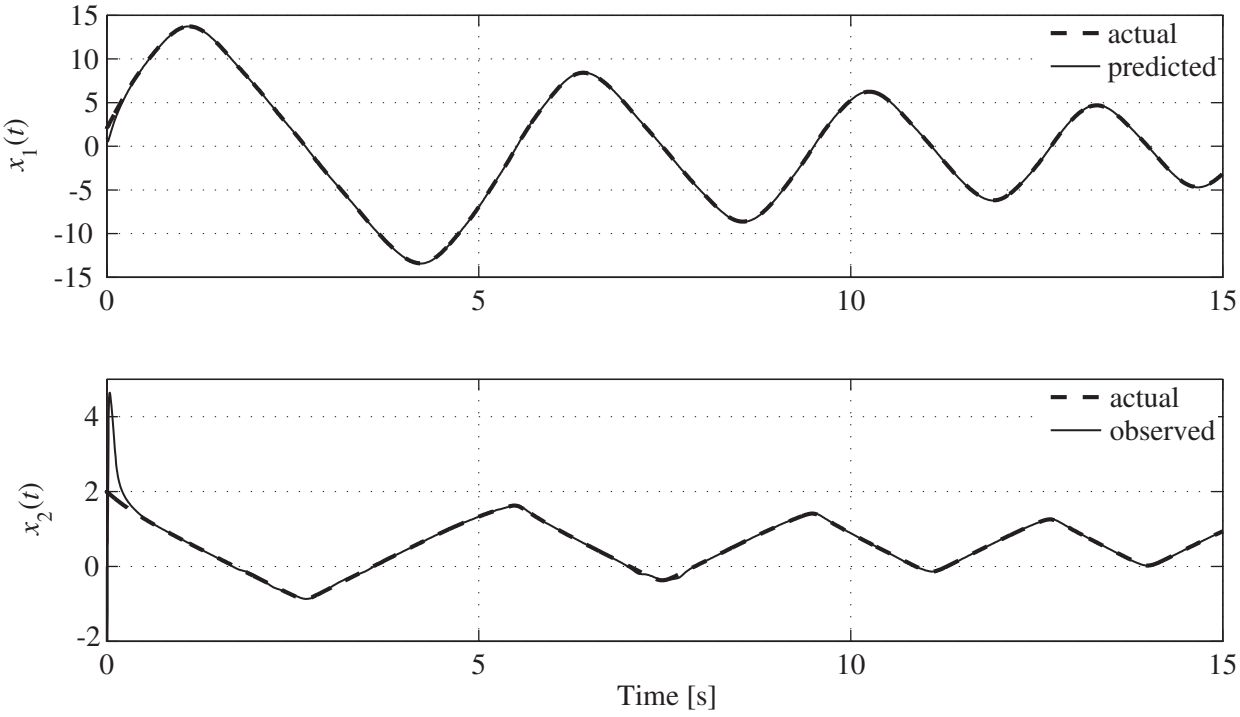

Figure 7.2: Actual and predicted/observed trajectories.

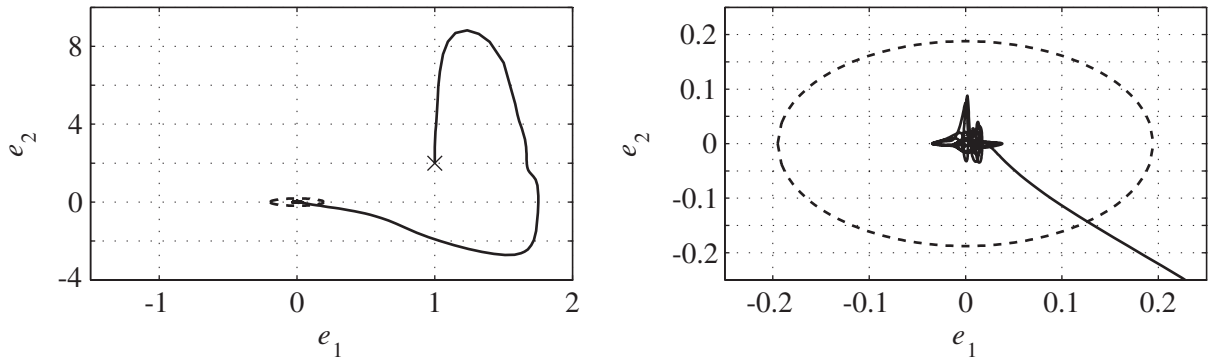

Figure 7.3: Prediction and observation error trajectories.

For the purpose of numerical simulation, we chose the following parameters for the system model, $a = 0.4$, $b = 10$, $c = -1$ and $d = 0.1$. Note that, with this choice of parameters, $w_2(x_1, \hat{x}_2) \neq 0$, for all $x_1, \hat{x}_2 \in \mathbb{R}$. In addition, we choose $x_{10} = x_{20} = 2$, $\hat{x}_{10} = 1$, $\hat{x}_{20} = 0$, and $z(0) = 0$. The resulting system and predictor-observer trajectories are shown in Figure 7.2.

The predicted $\hat{x}_1(t)$ closely matches the measured $x_1(t)$, $t \geq 0$, as seen in Figure 7.2. More interestingly, the observed $\hat{x}_2(t)$ also closely matches the unmeasured $x_2(t)$, $t \geq 0$, and converges as quickly as its predicted counterpart. Note that the initial condition for the prediction $\hat{x}_{10}$ could have been chosen as x_{10}, since $x_1(t)$, $t \geq 0$, is measured. This would have resulted in a decreased overshoot of $\hat{x}_2(t)$, $t \geq 0$. The initial prediction was however chosen different from x_{10} to illustrate convergence of $\hat{x}_1(t)$ to $x_1(t)$, $t \geq 0$.

The level of performance of the observer is intrinsically dependent upon that of the chosen numerical derivative estimator (through ε). The AIVSDE estimator performs well, with a maximum error of less than $\varepsilon = 0.38$ (discarding large early estimation errors due to arbitrary choice of initial condition $z_0 = 0$). In addition, from our choice of design parameters, we have that $\lambda_{\max}(M) = 0.051$. Hence, the predictor-observer designed as in Theorem 7.3.1 guarantees convergence of the error trajectories to $\mathcal{D} \triangleq \{(e_1, e_2) : e_1^{\mathrm{T}} P_1 e_1 + e_2^{\mathrm{T}} P_2 e_2 \leq 0.019\}$. The error trajectory is shown in Figure 7.3 (left), where the dashed ellipse delimits $\mathcal{D}$. As expected, the error trajectory enters and remains within $\mathcal{D}$. In addition, $\mathcal{D}$ itself appears to be a fairly conservative estimate of the actual domain of convergence (see Figure 7.3, right). This is in part due to the fact that non-positive terms in $\dot{V}(t)$, $t \geq 0$, resulting from the completion of the square, were omitted to facilitate estimation of the ultimate bound.

Example 7.4.2. Consider the system

$$\dot{x}_{11}(t) = -x_{11}^3(t) + \tanh(x_{12}(t)) + 3\sin(x_2(t)), \qquad x_{11}(0) = x_{110}, \quad t \geq 0, \tag{7.39}$$

$$\dot{x}_{12}(t) = 4\tanh(x_{11}(t)) - 2\tanh(x_{12}(t)) - 3\cos(x_2(t)), \quad x_{12}(0) = x_{120}, \tag{7.40}$$

$$\dot{x}_2(t) = -x_2^3(t) - 2\tanh((x_{11}(t) + x_{12}(t))^2), \qquad x_2(0) = x_{20}, \tag{7.41}$$

$$y(t) = x_1(t), \tag{7.42}$$

where $x_1(t) \triangleq \left[\begin{array}{cc} x_{11}(t) & x_{12}(t) \end{array}\right]^{\mathrm{T}} \in \mathbb{R}^2$, and $x_2(t) \in \mathbb{R}$, $t \geq 0$. Applying the technique described in Theorem 7.3.1, we construct the following predictor-observer,

$$\dot{\hat{x}}_1(t) = \left[\begin{array}{c} -x_{11}^3(t) + \tanh(x_{12}(t)) + 3\sin(\hat{x}_2(t)) \\ 4\tanh(x_{11}(t)) - 2\tanh(x_{12}(t)) - 3\cos(\hat{x}_2(t)) \end{array}\right] - P_1^{-1}Ke_1(t),$$
$$\hat{x}_1(0) = x_{10} \triangleq \left[\begin{array}{cc} x_{110} & x_{120} \end{array}\right]^{\mathrm{T}}, \quad t \geq 0, \tag{7.43}$$

$$\dot{\hat{x}}_{2\mathrm{a}}(t) = W_2^{-1}(x_2(t))\Big[P_2^{-1}P_1e_1(t) - A_1((A_1 - P_1^{-1}K)e_1(t) - e_2(t)) + \dot{z}(t) + A_2e_2(t)$$
$$-W_1(x_1(t))\Big(z(t) - \omega(t) + \frac{1}{2}W_1^{\mathrm{T}}(x_1(t))P_2e_2(t)\Big)\Big], \qquad \hat{x}_{2\mathrm{a}}(0) = \hat{x}_{2\mathrm{a}0}, \tag{7.44}$$

where $e_1(t) = x_1(t) - \hat{x}_1(t)$, $e_2(t) = \dot{\hat{x}}_1(t) + P_1^{-1}Ke_1(t) + \omega(t) - z(t) + A_1e_1(t)$, $t \geq 0$, the auxiliary signal $\omega(t)$, $t \geq 0$, is obtained from (7.9), with $W_{\mathrm{a}}(\hat{x}_2) = 3[\,-\sin(\hat{x}_2)\ \ \cos(\hat{x}_2)\,]^{\mathrm{T}}$, and $K = -150I_2$. In addition,

$$W_1(x_1) = \left[\begin{array}{cc} -3x_{11}^2 & \mathrm{sech}^2(x_{12}) \\ 4\mathrm{sech}^2(x_{11}) & -2\mathrm{sech}^2(x_{12}) \end{array}\right], \quad W_2(\hat{x}_2) = 3\left[\begin{array}{cc} \cos(\hat{x}_2) & -\sin(\hat{x}_2) \\ \sin(\hat{x}_2) & \cos(\hat{x}_2) \end{array}\right]. \tag{7.45}$$

Choosing $A_1 = -10I_2$, $Q_1 = 10I_2$, $A_2 = -30I_2$, and $Q_2 = 8I_2$, we obtain, from (7.15)–(7.16), $P_1 = 0.5132I_2$, $P_2 = 0.2I_2$. The parameters used for the AIVSDE are identical to that in the previous example. The initial conditions for the system are chosen as $x_{10} = \left[\begin{array}{cc} 2 & 2 \end{array}\right]^{\mathrm{T}}$, and $x_{20} = -1$. Finally, the initial prediction is $\hat{x}_{10} = \left[\begin{array}{cc} 0 & 0 \end{array}\right]^{\mathrm{T}}$, while the initial estimate is chosen as $\hat{x}_{20} = 0$. As seen in Figure 7.4, the predicted trajectory $\hat{x}_1(t)$, $t \geq 0$, quickly

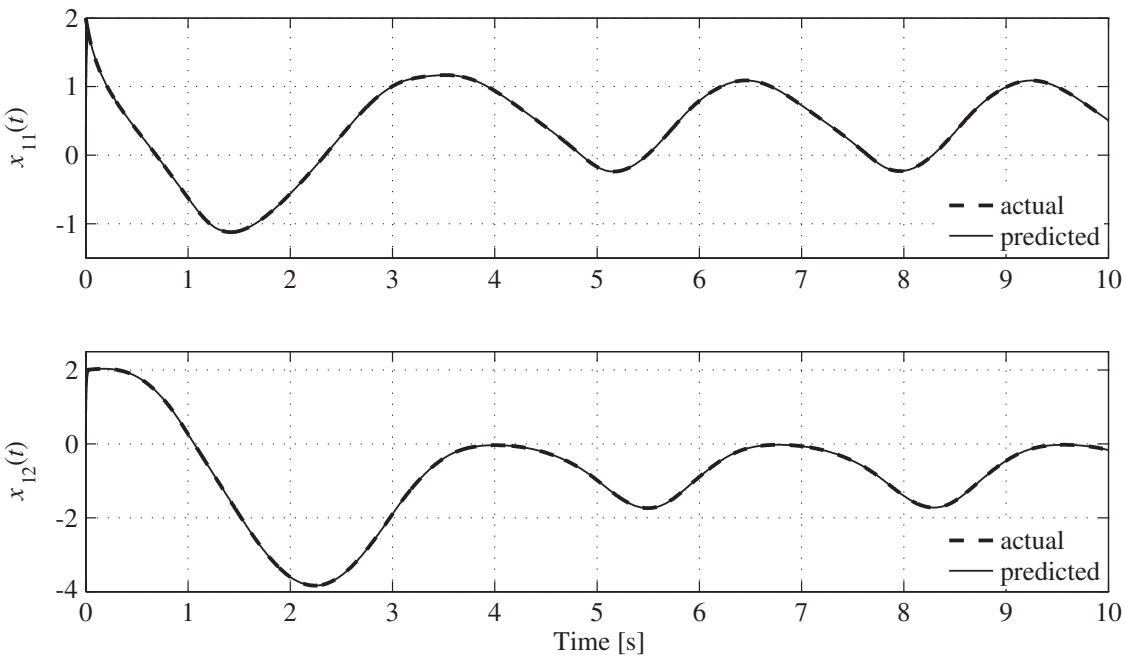

Figure 7.4: Actual and predicted trajectories.

converges to the actual trajectory $x_1(t)$, $t \geq 0$. Similarly, after a short transient, the observed trajectory $\hat{x}_2(t)$, $t \geq 0$, matches the unmeasured state $x_2(t)$, $t \geq 0$, very closely, as observed from Figure 7.5.

Example 7.4.3. Consider the system

$$\dot{\eta}(t) = J(\eta(t))\nu(t), \qquad \eta(0) = \eta_0, \quad t \geq 0, \tag{7.46}$$

$$\dot{\nu}(t) = \Theta_1^* \varphi(\eta(t)) + \Theta_2^* \tau(t), \quad \nu(0) = \nu_0, \tag{7.47}$$

$$y(t) = \eta(t), \tag{7.48}$$

where $\eta(t) \triangleq \left[\begin{array}{ccc} \phi(t) & \theta(t) & \psi(t) \end{array} \right]^{\mathrm{T}} \in \mathbb{R}^3$, $t \geq 0$, is the measured output, $\nu(t) \in \mathbb{R}^3$, $t \geq 0$, is not measured, and $\tau(t) \in \mathbb{R}^2$, $t \geq 0$, is the control input applied to the system. In addition,

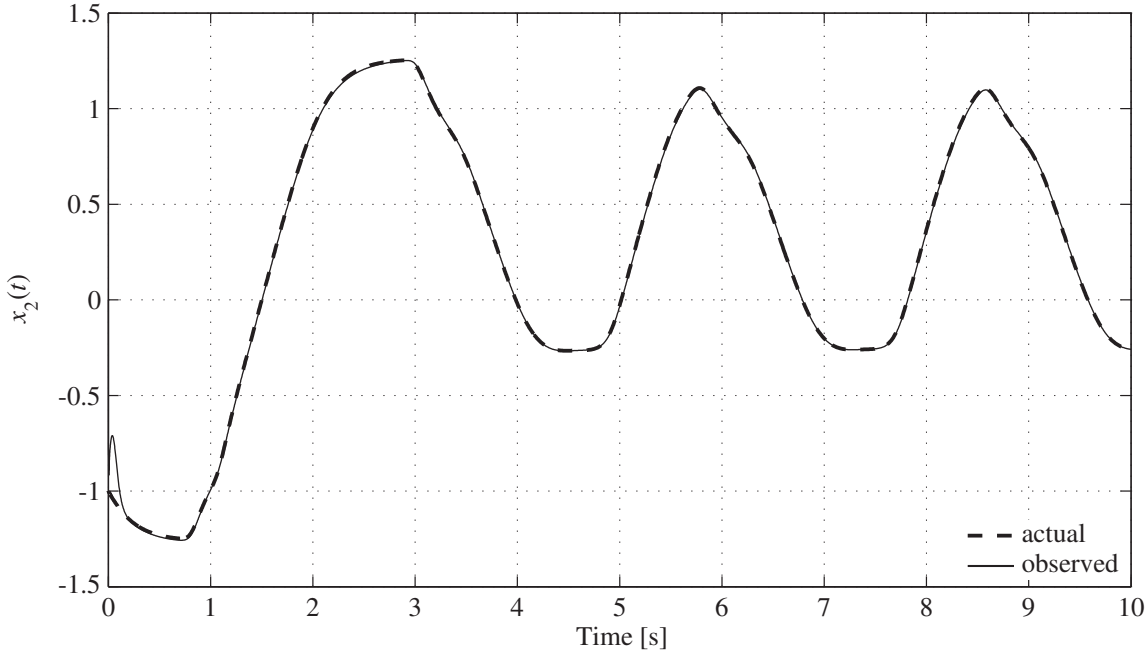

Figure 7.5: Actual and observed trajectories.

$\Theta_1^* \in \mathbb{R}^{3\times 2}$ and $\Theta_2^* \in \mathbb{R}^{3\times 2}$ are unknown constant matrices, and

$$J(\eta) \triangleq \begin{bmatrix} 1 & \tan(\theta)\sin(\phi) & \tan(\theta)\cos(\phi) \\ 0 & \cos(\phi) & -\sin(\phi) \\ 0 & \sin(\phi)/\cos(\theta) & \cos(\phi)/\cos(\theta) \end{bmatrix}, \tag{7.49}$$

$$\varphi(\eta) \triangleq \begin{bmatrix} \cos(\theta)\cos(\phi) & -\cos(\theta)\sin(\phi) \end{bmatrix}^{\mathrm{T}}. \tag{7.50}$$

Applying the technique described in Theorem 7.3.1, we construct the following predictor-observer,

$$\dot{\hat{\eta}}(t) = J(\eta(t))\hat{\nu}(t), \quad \hat{\eta}(0) = \eta_0, \quad t \geq 0, \tag{7.51}$$

$$\begin{aligned} \dot{\hat{\nu}}(t) = {} & J^{-1}(\eta(t))\Big(P_2^{-1}P_1 e_1(t) - A_1(A_1 e_1(t) - e_2(t)) + \dot{z}(t) + A_2 e_2(t) - W_1(\eta(t),\hat{\nu}(t))z(t) \\ & -\frac{1}{2}W_1(\eta(t),\hat{\nu}(t))W_1^{\mathrm{T}}(\eta(t),\hat{\nu}(t))P_2 e_2(t)\Big), \quad \hat{\nu}(0) = \hat{\nu}_0, \end{aligned} \tag{7.52}$$

where $e_1(t) \triangleq \eta(t) - \hat{\eta}(t)$, $e_2(t) \triangleq A_1 e_1(t) - z(t) + J(\eta(t))\hat{\nu}(t)$, $t \geq 0$, and $W_1(\eta,\hat{\nu}) \triangleq \frac{\partial J(\eta)\hat{\nu}}{\partial \eta}$.

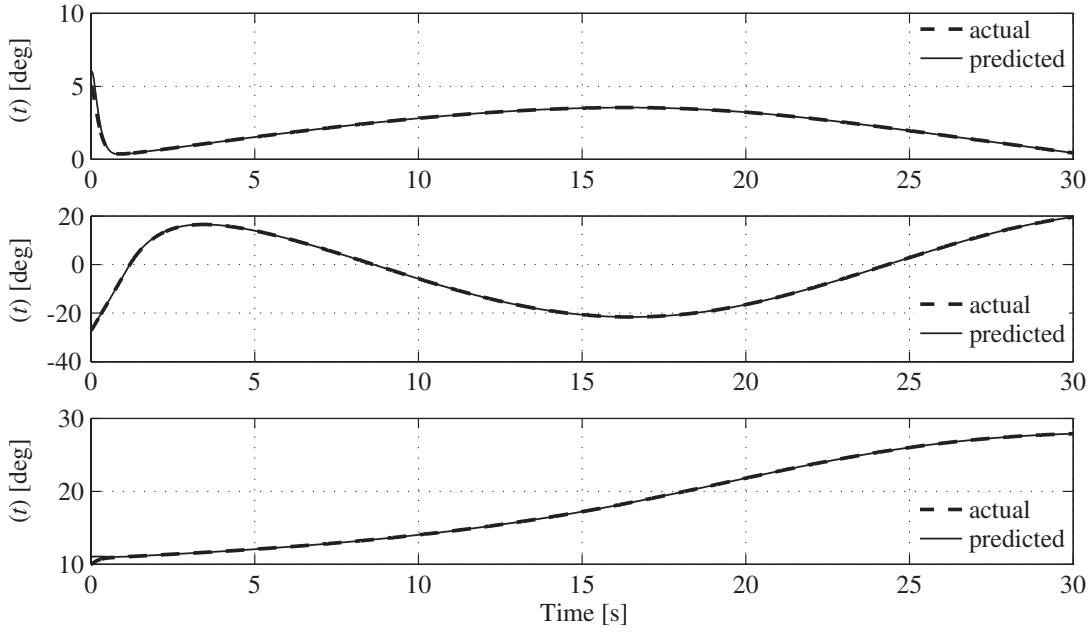

Figure 7.6: Actual and predicted trajectories of $\eta(t)$, $t \geq 0$.

We choose $A_1 = -4I_3$, $A_2 = -40I_3$, $Q_1 = 12I_3$, $Q_2 = 40I_3$, and obtain, from (7.15) and (7.16), $P_1 = 6I_3$, $P_2 = (2.5 + \sqrt{15}/2)I_3$. The AIVSDE parameters are chosen as follows, $k_1 = 10$, $k_2 = 15$, $k_b = 1/2$, $\alpha_r = 0$, $\mu = 1$, $\gamma_0 = x_{10}$ and $k_{r0} = 1$.

In addition, we use the following for plant parameters,

$$\Theta_1^* = \begin{bmatrix} -2.6828 & 3.2966 \\ 9.8298 & 9.9455 \\ 0 & -20 \end{bmatrix}, \quad \Theta_2^* = \begin{bmatrix} 0.25 & 0 \\ 0 & -0.575 \\ 0 & 0 \end{bmatrix}. \tag{7.53}$$

The initial conditions are chosen as $\eta_0 = [\, 5 \;\; -27 \;\; 10 \,]^{\mathrm{T}}$, $\nu_0 = 0_3$, $\hat{\eta}_0 = \eta_0 + [\, 1 \;\; 1 \;\; 1 \,]^{\mathrm{T}}$, $\hat{\nu}_0 = [\, 5 \; 5 \; 5 \,]^{\mathrm{T}}$, and $z(0) = 0_3$. The trajectories $\eta(t)$ and $\nu(t)$, $t \geq 0$, are shown in Figure 7.6 and Figure 7.7, respectively. As was the case with Example 7.4.1, the algorithm performs admirably. The predicted and observed trajectories closely match the real ones, with a short transient.

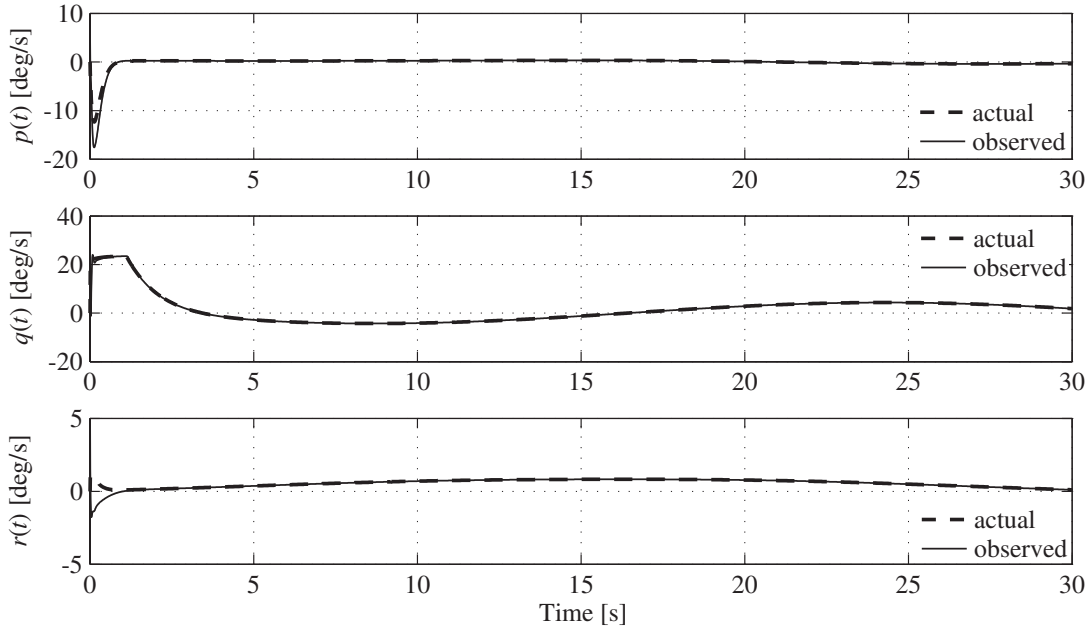

Figure 7.7: Actual and observed trajectories of $\nu(t)$, $t \geq 0$.

7.5. Experimental Test

The previous section presented numerical simulation results, illustrating the performance of the algorithm. Performance was further tested by implementing the presented predictor-observer algorithm on the Quanser "3DOF helicopter" setup. Equations (7.46)–(7.48) provide a model of the setup's dynamics. Hence, we will apply the algorithm as designed for Example 7.4.3. However, a significant hurdle in the way of implementation is the fact that the measurements provided by the experimental setup are discrete and quantized, with quantization intervals of $\pi/2048$.

The observation of systems with quantized outputs constitutes a challenging problem (as discussed in [115]), which remains essentially open. The presented predictor-observer technique does not account for quantization of the measurements, and application of the

technique as is to such a system yields poor results. This poor performance is mainly due to the difficulty in obtaining a signal $z(t)$, $t \geq 0$, providing a reasonable approximation of $\dot{y}(t)$, $t \geq 0$. In particular, when the measurements change from a level of quantization to the next, most numerical derivation techniques lead to large spikes in the estimate of the derivative. In an attempt to compensate for this issue, we used a second order low-pass filter to smooth-out the measurements. This filter has a damping coefficient $\zeta = \sqrt{2}/2$ and a natural frequency $\omega_{\mathrm{n}} = 10$. This simple addition to the algorithm significantly improved experimental results, to an extent that performance of the algorithm when subjected to quantized measurements became comparable to that without quantization (see Figure 7.8 for simulation results showing actual and observed $\nu(t)$, $t \geq 0$, with quantized measurements), and allowed implementation of the presented algorithm.

Experimental results are shown in Figure 7.9. Note that the body fixed velocity vector $\nu(t)$, $t \geq 0$, is not measured. Hence, to assess performance of the presented algorithm, we compare the observed $\hat{\nu}(t)$, $t \geq 0$, to an estimate of $\nu(t)$, $t \geq 0$, obtained from the output of the AIVSDE, $z(t)$, $t \geq 0$. Since $z(t)$ is an estimate of $\dot{\eta}(t)$, $t \geq 0$, it can be pre-multiplied by $J^{-1}(\eta(t))$, $t \geq 0$, to obtain an estimate of $\nu(t)$, $t \geq 0$. As seen in Figure 7.9, the observed trajectories are in practice significantly noisier than in simulation. The algorithm however yields promising results. In particular, the transient shows that the observer reacts more quickly than the output of the AIVSDE to large changes in velocity.

7.6. Conclusion

This chapter presented a prediction-based observer, relevant to a wide class of nonlinear systems, including systems whose unmeasured states appear nonlinearly in the system dy-

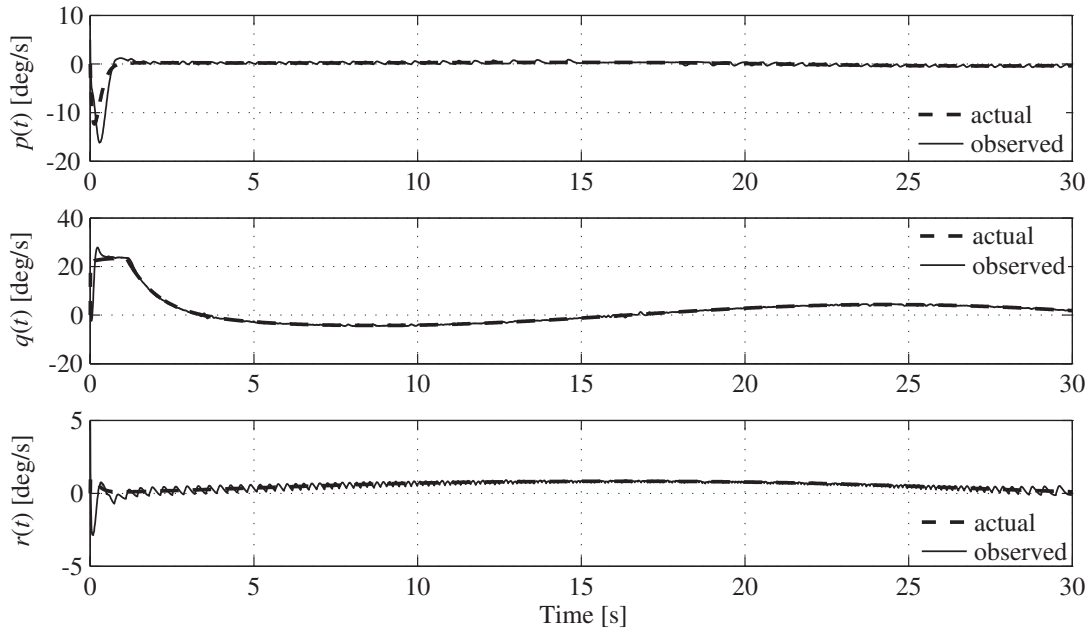

Figure 7.8: Numerical simulation with measurement quantization, actual and observed trajectories of $\nu(t)$, $t \geq 0$.

namics. The algorithm relies on a pair of prediction-observation errors, constructed using a backstepping technique. Lyapunov's second method was used to prove Lyapunov stability of these errors, as well as their convergence to a neighborhood of the origin. The algorithm makes use of a derivative estimator, which allows to relax high gain requirements commonly found in observation techniques for nonlinear systems. In addition, the relationship between the ultimate bound on the prediction-observation errors and the derivative estimator's level of performance, as well as a number of relevant design constants, was made explicit. While the algorithm is itself of interest, it essentially constitutes toward solving the output feedback problem. In following chapters, the observer presented here will be modified and complemented with control laws to solve the problem.

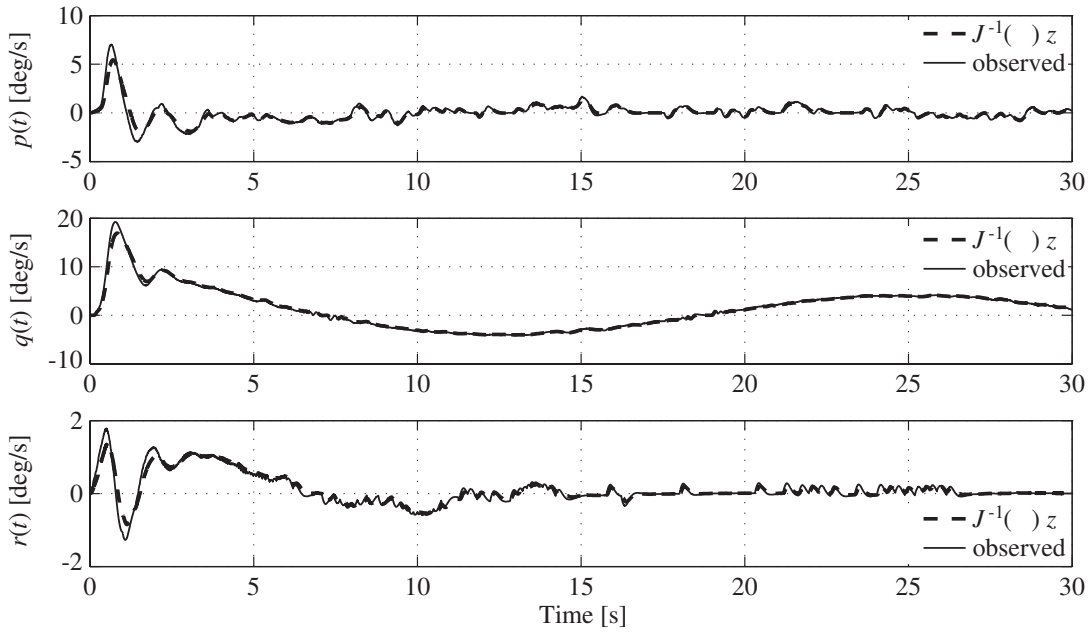

Figure 7.9: Experimental results, observed trajectory of $\nu(t)$, $t \geq 0$, compared to a numerical derivative.

Chapter 8

Observer-Based Output Feedback Control of Nonlinear Systems Non-Affine in the Unmeasured States [8]

The following results were the object of a conference paper submitted to the 2009 ASME Dynamic Systems and Control Conference (currently under review). In addition, it will be submitted for consideration to the IEEE Transactions on Control Systems Technology.

8.1. Introduction

The work presented in this chapter builds upon the nonlinear observer introduced in Chapter 7 to solve the output feedback control for a class of nonlinear systems. The result aims to alleviate a number of issues inherent to separation-based algorithms. It relies on the same premise of *dividing to rule*, in the sense that the output feedback control problem is split into the two simpler problems of observer and state feedback design. However, in a departure from classical procedures, the control law is not designed to control the system's output, but

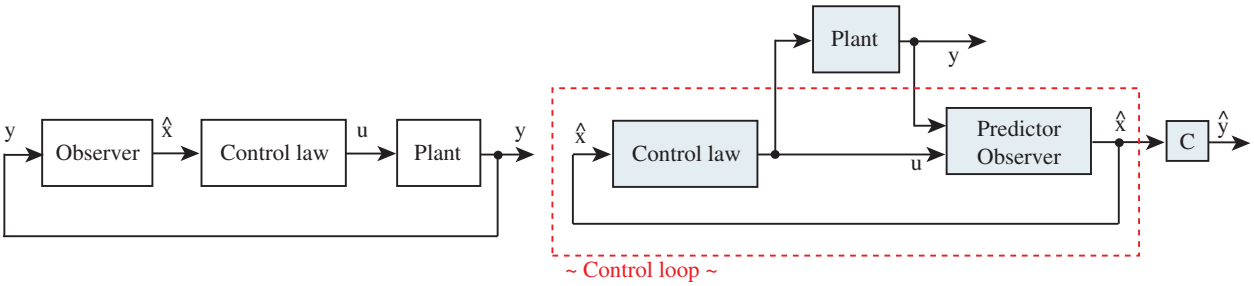

Figure 8.1: Scheme comparison between separation based algorithms (left), and the proposed indirect approach (right).

rather that of the observer, as described in Figure 8.1. Existing separation-based techniques use estimates in the stead of unmeasured states, hence pursuing a "certainty equivalence" design similar to that used in adaptive control ([10]). The output feedback algorithm presented, although sharing a similar observer/controller structure, distinguishes itself from separation-based approaches in the extent that the control law's form is dependent upon that of the observer, hence breaking separation. While design flexibility is accordingly reduced, any "certainty equivalence" (or lack thereof) related issue is effectively circumvented. In particular, this scheme significantly alleviates the pressure placed upon the observer. The only requirement on such an observer is that it must be capable of predicting the actual system's output to a given accuracy for all admissible control inputs and is controllable. The approach shares similarities with that presented in [62, 64], where a neural network is employed to emulate the system's dynamics, which is comparable to the role of the observer in the approach presented here.

This observer is designed as an extension of that introduced in Chapter 7. The latter relies on predictions of the measured output to observe the unmeasured states of a wide class of nonlinear systems. The observer designed here shares the same overall structure, but is

capable of handling controlled systems. As previously mentioned, the observer-predictor is a dynamical system which is constructed in such a way that its output converges to an arbitrarily small neighborhood of the actual system's output, for any admissible control input. Once that is achieved, a backstepping-based ([10]) control algorithm is designed for the obtained observer system. Ultimately, it is shown that the observer's structure guarantees convergence of its output to a neighborhood of the output of the actual system, while the control input guarantees convergence of the same observer output to a neighborhood of a given desired trajectory. It follows that the actual system's output approaches the desired trajectory. This *indirect* control technique, in which one does not directly control the actual system but rather an observer (or predictor), constitutes an extension of that used in [6,108], where the input is designed to control a state predictor. The approach presented here is conceptually similar, with the difference that the input is designed to control a predictor-observer, in an extension from state feedback to output feedback.

This chapter is structured as follows. Section 8.2 describes the class of nonlinear systems considered and provides further details on the control strategy employed. Design of the observer-predictor is presented in Section 8.3, followed by that of the control law in Section 8.4. Numerical simulation results are provided in Section 8.5 for three examples and illustrate the efficacy of the control scheme. Section 8.6 concludes this chapter.

8.2. Problem Statement and Control Strategy

Consider a system of the form

$$\dot{x}(t) = f(x(t),t) + g(x(t),t)u(t), \quad x(0) = x_0, \quad t \geq 0, \tag{8.1}$$

$$y(t) = Cx(t), \tag{8.2}$$

where $x(t) \in \mathbb{R}^n$, $t \geq 0$, is the system's state vector, $y(t) \in \mathbb{R}^m$, $t \geq 0$, the measured output vector, with $m \geq n/2$, $u(t) \in \mathbb{R}^m$, $t \geq 0$, the control input, and $C = \left[\begin{array}{cc} I_m & 0_{m \times p} \end{array} \right]$, with $p = n - m \leq m$. The object of the presented work is to design the control input $u(t)$, $t \geq 0$, such that the output $y(t)$, $t \geq 0$, uniformly converges to an arbitrarily small neighborhood of a given $y_{\mathrm{d}}(t) \in \mathbb{R}^m$, $t \geq 0$. In order to simplify the notation, define $\Lambda_i \triangleq \left[\begin{array}{cc} I_i & 0_{i \times (m-i)} \end{array} \right]$ and $\bar{\Lambda}_i \triangleq \left[\begin{array}{cc} 0_{(m-i) \times i} & I_{m-i} \end{array} \right]$, $i = 1, \ldots, m-1$.

Let $x_1(t) \triangleq y(t)$, $t \geq 0$, denote the measured states, and $x_2(t) \in \mathbb{R}^p$, $t \geq 0$, denote the unmeasured states. In the following, we will assume that the system's outputs have well defined relative degrees one or two. The technique can be extended to handle greater relative degrees, but we will limit ourselves to this case for ease of exposition. More specifically, assume that $q \leq m$ of the m measured states are of relative degree one. Ordering the measured states vector $x_1(t)$, $t \geq 0$, by increasing relative degree, we can rewrite (8.1) as

$$\dot{x}_1(t) = f_1(x_1(t), x_2(t), t) + g_1(x_1(t), x_2(t), t) u_1(t), \quad x_1(0) = x_{10}, \quad t \geq 0, \tag{8.3}$$

$$\dot{x}_2(t) = f_2(x_1(t), x_2(t), t) + g_2(x_1(t), x_2(t), t) u_2(t), \quad x_2(0) = x_{20}, \tag{8.4}$$

where $g_1(x_1(t), x_2(t), t) \triangleq \Lambda_q^{\mathrm{T}} g_{1\mathrm{s}}(x_1(t), x_2(t), t)$, $u_1(t) \in \mathbb{R}^q$ and $u_2(t) \in \mathbb{R}^{m-q}$, $t \geq 0$, so that $u(t) = \left[\begin{array}{cc} u_1^{\mathrm{T}}(t) & u_2^{\mathrm{T}}(t) \end{array} \right]^{\mathrm{T}}$, $t \geq 0$.

In the following, we will first design a predictor-based observer for system (8.3)–(8.4), building upon the technique introduced in Chapter 7. The intent is to construct a system, with the same input $u(t)$, $t \geq 0$, as (8.3)–(8.4), and whose state $\hat{x}(t) \triangleq \left[\begin{array}{cc} \hat{x}_1^{\mathrm{T}}(t) & \hat{x}_2^{\mathrm{T}}(t) \end{array} \right]^{\mathrm{T}} \in \mathbb{R}^n$, $t \geq 0$, is such that $\hat{x}_1(t) \in \mathbb{R}^m$, $t \geq 0$, converges to an arbitrarily small neighborhood of $x_1(t)$, $t \geq 0$, for any admissible control signal $u(t)$, $t \geq 0$. Next, we will design the control input $u(t)$, $t \geq 0$, so that $\hat{x}_1(t)$, $t \geq 0$, asymptotically converges to a given $y_{\mathrm{d}}(t)$, $t \geq 0$, uniformly in time. As a result, we will obtain that $\hat{x}_1(t)$ will simultaneously converge to

both $x_1(t)$ *and* $\hat{x}_1(t)$, $t \geq 0$. Hence, we will obtain that $x_1(t) \to y_{\rm d}(t)$, $t \to \infty$. The results presented in the following sections rely on several assumptions. In particular, in the design of the observer, we will assume that $\mathrm{rank}[W_{2\rm s}(x_1, \hat{x}_2, t)] = p$ for all $x_1 \in \mathbb{R}^m$, $\hat{x}_2 \in \mathbb{R}^p$, and $t \geq 0$, where $W_{2\rm s}(x_1, \hat{x}_2, t) \triangleq \partial f_1(x_1, \hat{x}_2, t)/\partial \hat{x}_2$. This assumption implies that the class of systems considered is a subset of the set of all observable systems ([7, 111, 112]). In addition, we assume that $g_{1\rm s}(x_1, \hat{x}_2, t) \in \mathbb{R}^{q \times q}$ is nonsingular for all $x_1 \in \mathbb{R}^m$, $\hat{x}_2 \in \mathbb{R}^p$, and $t \geq 0$. Finally, we require that there exists a constant matrix $B \in \mathbb{R}^{p \times (m-q)}$, such that $\bar{\Lambda}_q W_{2\rm s}(x_1, \hat{x}_2, t)B$ is nonsingular for all $x_1 \in \mathbb{R}^m$, $\hat{x}_2 \in \mathbb{R}^p$, $t \geq 0$. The latter assumption is equivalent to assuming that the system is controllable through backstepping ([10]), and is needed to ensure controllability of the observer-predictor to be designed.

8.3. Nonlinear Observer Design

Building upon the approach in Chapter 7, we construct a partial state predictor, with the following Luenberger form ([13]),

$$\dot{\hat{x}}_1(t) = f_1(x_1(t), \hat{x}_2(t), t) + g_1(x_1(t), \hat{x}_2(t), t)u_1(t) - De_{1\rm o}(t), \quad \hat{x}_1(0) = x_{10}, \quad t \geq 0, \tag{8.5}$$

where $D \in \mathbb{R}^{m \times m}$ is chosen Hurwitz, $e_{1\rm o}(t) \triangleq x_1(t) - \hat{x}_1(t)$, $t \geq 0$, is a prediction error, and $\hat{x}_2(t) \in \mathbb{R}^p$, $t \geq 0$, is designed so that $\hat{x}_1(t) \in \mathbb{R}^m$, $t \geq 0$, provides a predicted value of $x_1(t)$, $t \geq 0$. In addition, to provide more flexibility in the design procedure, the observer-predictor will rely on an auxiliary signal $\omega(t) \in \mathbb{R}^m$, $t \geq 0$, obtained from

$$\dot{\omega}(t) = W_{\rm a}(x_1(t), \hat{x}_2(t), t)v(t), \quad \omega(0) = 0_m, \quad t \geq 0, \tag{8.6}$$

where $v(t) \in \mathbb{R}^{m-p}$, $t \geq 0$, and the matrix $W_{\rm a}(\cdot) \in \mathbb{R}^{m \times (m-p)}$ is designed such that $W_2(x_1, \hat{x}_2, t) \triangleq \left[\begin{array}{cc} W_{2\rm s}(x_1, \hat{x}_2, t) & W_{\rm a}(x_1, \hat{x}_2, t) \end{array} \right] \in \mathbb{R}^{m \times m}$ is nonsingular for all $x_1 \in \mathbb{R}^m$,

$\hat{x}_2 \in \mathbb{R}^p$, $t \geq 0$. In the following, we will construct $\dot{\hat{x}}_{2\mathrm{a}}(t) \triangleq \left[\begin{array}{cc} \dot{\hat{x}}_2^{\mathrm{T}}(t) & v^{\mathrm{T}}(t) \end{array} \right]^{\mathrm{T}} \in \mathbb{R}^m$, $t \geq 0$, so that the origin of the observation error dynamics is Lyapunov stable and $e_{1\mathrm{o}}(t)$, $t \geq 0$, asymptotically converges to a neighborhood of the origin, uniformly in time.

Theorem 8.3.1. Consider the system given by (8.1)–(8.2), and the partial state predictor (8.5). Assume that a continuously differentiable signal $z(t)$ is available such that $z(t) = \dot{y}(t) + \omega(t) - \dot{\hat{x}}_u(t) - \epsilon(t)$, with $\|\epsilon(t)\| \leq \sqrt{\varepsilon/3}$, $\varepsilon > 0$, $t \geq 0$, where $\dot{\hat{x}}_u(t) \triangleq \dot{\hat{x}}_{u1}(t) + \dot{\hat{x}}_{u2}(t)$, $t \geq 0$, and $\hat{x}_{u1}(t)$ and $\hat{x}_{u2}(t)$, $t \geq 0$, are obtained from

$$\dot{\hat{x}}_{u1}(t) = g_1(x_1(t), \hat{x}_2(t), t)u_1(t) - \alpha_1 \hat{x}_{u1}(t), \qquad \hat{x}_{u1}(0) = 0_m, \quad t \geq 0, \tag{8.7}$$

$$\ddot{\hat{x}}_{u2}(t) = W_{2\mathrm{s}}(x_1(t), \hat{x}_2(t), t)Bu_2(t) - \alpha_2 \dot{\hat{x}}_{u2}(t) - \alpha_3 \hat{x}_{u2}(t), \quad \dot{\hat{x}}_{u2}(0) = \hat{x}_{u2}(0) = 0_m, \tag{8.8}$$

where $\alpha_i > 0$, $i = 1, 2, 3$, and the matrix $B \in \mathbb{R}^{p \times (m-q)}$ is chosen so that $\bar{\Lambda}_q W_{2\mathrm{s}}(x_1(t), \hat{x}_2(t), t)$ $B \in \mathbb{R}^{(m-q)\times(m-q)}$ is nonsingular for all $t \geq 0$. Then, consider the estimated trajectory $\hat{x}_2(t)$, $t \geq 0$, generated by

$$\begin{aligned} \dot{\hat{x}}_{2\mathrm{a}}(t) = {} & W_2^{-1}(x_1(t), \hat{x}_2(t), t)\Big[P_{2\mathrm{o}}^{-1} P_{1\mathrm{o}} e_{1\mathrm{o}}(t) - A_{1\mathrm{o}}((A_{1\mathrm{o}} + P_{1\mathrm{o}}^{-1}K)e_{1\mathrm{o}}(t) - e_{2\mathrm{o}}(t)) + \dot{z}(t) \\ & + A_{2\mathrm{o}} e_{2\mathrm{o}}(t) - W_1(x_1(t), \hat{x}_2(t), t)\Big(z(t) + \dot{\hat{x}}_u(t) - \omega(t) + \frac{1}{2} W_1^{\mathrm{T}}(x_1(t), \hat{x}_2(t), t) P_{2\mathrm{o}} e_{2\mathrm{o}}(t)\Big) \\ & - \alpha_1 \dot{\hat{x}}_{u1}(t) - \alpha_2 \dot{\hat{x}}_{u2}(t) - \alpha_3 \hat{x}_{u2}(t) - W_3(x_1(t), \hat{x}_2(t), t) + W_{2\mathrm{s}}(x_1(t), \hat{x}_2(t), t)Bu_2(t)\Big], \\ & \hat{x}_{2\mathrm{a}}(0) = 0_m, \quad t \geq 0, \end{aligned} \tag{8.9}$$

$$\hat{x}_2(t) = \Lambda_p \hat{x}_{2\mathrm{a}}(t), \tag{8.10}$$

where $A_{1\mathrm{o}}$, $A_{2\mathrm{o}}$, and K are chosen Hurwitz,

$$e_{1\mathrm{o}}(t) \triangleq x_1(t) - \hat{x}_1(t), \quad t \geq 0, \tag{8.11}$$

$$e_{2\mathrm{o}}(t) \triangleq f_1(x_1(t), \hat{x}_2(t), t) + \omega(t) - \dot{\hat{x}}_{u2}(t) + \alpha_1 \hat{x}_{u1}(t) + A_{1\mathrm{o}} e_{1\mathrm{o}}(t) - z(t), \tag{8.12}$$

the matrices $P_{1\mathrm{o}}$, $P_{2\mathrm{o}} \in \mathbb{R}^{m\times m}$ are obtained from the following Riccati equations,

$$A_{1\mathrm{o}}^{\mathrm{T}}P_{1\mathrm{o}} + P_{1\mathrm{o}}A_{1\mathrm{o}} + Q_{1\mathrm{o}} + P_{1\mathrm{o}}^2 = 0, \tag{8.13}$$

$$A_{2\mathrm{o}}^{\mathrm{T}}P_{2\mathrm{o}} + P_{2\mathrm{o}}A_{2\mathrm{o}} + Q_{2\mathrm{o}} + P_{2\mathrm{o}}A_{1\mathrm{o}}A_{1\mathrm{o}}^{\mathrm{T}}P_{2\mathrm{o}} = 0, \tag{8.14}$$

and $Q_{1\mathrm{o}} \triangleq R_1^{\mathrm{T}}R_1 > 0$, $Q_{2\mathrm{o}} \triangleq R_2^{\mathrm{T}}R_2 > 0$, are chosen such that

$$H_{1\mathrm{o}} \triangleq \left[\begin{array}{cc} A_{1\mathrm{o}} & I_m \\ -Q_{1\mathrm{o}} & -A_{1\mathrm{o}}^{\mathrm{T}} \end{array}\right], \quad H_{2\mathrm{o}} \triangleq \left[\begin{array}{cc} A_{2\mathrm{o}} & A_{1\mathrm{o}}A_{1\mathrm{o}}^{\mathrm{T}} \\ -Q_{2\mathrm{o}} & -A_{2\mathrm{o}}^{\mathrm{T}} \end{array}\right], \tag{8.15}$$

have no eigenvalues on the imaginary axis and $(A_{1\mathrm{o}}, R_1)$, $(A_{2\mathrm{o}}, R_2)$ are both observable. In addition, the auxiliary signal $\omega(t)$, $t \geq 0$, is obtained from (8.6), with $v(t) \triangleq \bar{\Lambda}_p\dot{\hat{x}}_{2\mathrm{a}}(t)$, $t \geq 0$. Finally, choose $D = P_{1\mathrm{o}}^{-1}K$, define $\bar{Q}_{1\mathrm{o}} \triangleq Q_{1\mathrm{o}} - K - K^{\mathrm{T}}$,

$$N_{\mathrm{o}} \triangleq \left[\begin{array}{cc} \bar{Q}_{1\mathrm{o}}^{-1}P_{1\mathrm{o}} & 0_{m\times m} \\ 0_{m\times m} & Q_{2\mathrm{o}}^{-1}P_{2\mathrm{o}} \end{array}\right], \tag{8.16}$$

and let $\lambda_{\max}(N_{\mathrm{o}})$ denote the maximum eigenvalue of N_{o}. The solution $\hat{x}_{2\mathrm{a}}(t)$, $t \geq 0$, to (8.9) guarantees uniform ultimate boundedness of (8.11)–(8.12) with an ultimate bound given by $\mathcal{D}_{\mathrm{o}} \triangleq \{(e_{1\mathrm{o}}, e_{2\mathrm{o}}) : e_{1\mathrm{o}}^{\mathrm{T}}P_{1\mathrm{o}}e_{1\mathrm{o}} + e_{2\mathrm{o}}^{\mathrm{T}}P_{2\mathrm{o}}e_{2\mathrm{o}} \leq \varepsilon\lambda_{\max}(N_{\mathrm{o}})\}$.

Proof. The time derivative of the prediction error $e_{1\mathrm{o}}(t)$, $t \geq 0$, is given by

$$\begin{aligned}\dot{e}_{1\mathrm{o}}(t) = {} & f_1(x_1(t), x_2(t), t) + g_1(x_1(t), x_2(t), t)u_1(t) - f_1(x_1(t), \hat{x}_2(t), t) - g_1(x_1(t), \hat{x}_2(t), t)u_1(t) \\ & + P_{1\mathrm{o}}^{-1}Ke_{1\mathrm{o}}(t), \quad t \geq 0, \end{aligned} \tag{8.17}$$

which, using $\dot{y}(t) = z(t) + \dot{\hat{x}}_u(t) - \omega(t) + \epsilon(t)$, $\dot{\hat{x}}_u(t) = \dot{\hat{x}}_{u1}(t) + \dot{\hat{x}}_{u2}(t)$, $t \geq 0$, and (8.7), can be rewritten as

$$\begin{aligned}\dot{e}_{1\mathrm{o}}(t) &= z(t) + \dot{\hat{x}}_u(t) + \epsilon(t) + P_{1\mathrm{o}}^{-1}Ke_{1\mathrm{o}}(t) - (f_1(x_1(t), \hat{x}_2(t), t) + \omega(t)) - g_1(x_1(t), \hat{x}_2(t), t)u_1(t) \\ &= z(t) + \dot{\hat{x}}_{u2}(t) - \alpha_1\hat{x}_{u1}(t) + P_{1\mathrm{o}}^{-1}Ke_{1\mathrm{o}}(t) + \epsilon(t) - (f_1(x_1(t), \hat{x}_2(t), t) + \omega(t)), \quad t \geq 0. \end{aligned} \tag{8.18}$$

Furthermore, substituting (8.12) into (8.18), we obtain

$$\dot{e}_{1\mathrm{o}}(t) \,=\, (A_{1\mathrm{o}} + P_{1\mathrm{o}}^{-1}K)e_{1\mathrm{o}}(t) - e_{2\mathrm{o}}(t) + \epsilon(t), \quad t \geq 0. \tag{8.19}$$

The time derivative of the observation error $e_{2\mathrm{o}}(t)$, $t \geq 0$, is of the form

$$\begin{aligned}
\dot{e}_{2\mathrm{o}}(t) \,=\, & A_{1\mathrm{o}}\dot{e}_{1\mathrm{o}}(t) + W_1(x_1(t), \hat{x}_2(t), t)\dot{x}_1(t) + W_2(x_1(t), \hat{x}_2(t), t)\dot{\hat{x}}_{2\mathrm{a}}(t) + W_3(x_1(t), \hat{x}_2(t), t) \\
& -\dot{z}(t) - W_{2\mathrm{s}}(x_1(t), \hat{x}_2(t), t)Bu_2(t) + \alpha_1\hat{x}_{u1}(t) + \alpha_2\dot{\hat{x}}_{u2}(t) + \alpha_3\hat{x}_{u2}(t) \\
= \, & A_{1\mathrm{o}}\epsilon(t) + A_{1\mathrm{o}}((A_{1\mathrm{o}} + P_{1\mathrm{o}}^{-1}K)e_{1\mathrm{o}}(t) - e_{2\mathrm{o}}(t)) - \dot{z}(t) + W_1(x_1(t), \hat{x}_2(t), t)(z(t) - \omega(t) \\
& +\dot{\hat{x}}_u(t)+\epsilon(t))+W_3(x_1(t), \hat{x}_2(t), t)-W_{2\mathrm{s}}(x_1(t), \hat{x}_2(t), t)Bu_2(t) + \alpha_1\dot{\hat{x}}_{u1}(t) + \alpha_2\dot{\hat{x}}_{u2}(t) \\
& +\alpha_3\hat{x}_{u2}(t) + W_2(x_1(t), \hat{x}_2(t), t)\dot{\hat{x}}_{2\mathrm{a}}(t), \quad t \geq 0.
\end{aligned} \tag{8.20}$$

Substituting (8.9) into (8.20), we obtain

$$\begin{aligned}
\dot{e}_{2\mathrm{o}}(t) = \, & A_{1\mathrm{o}}\epsilon(t) + A_{1\mathrm{o}}((A_{1\mathrm{o}} + P_{1\mathrm{o}}^{-1}K)e_{1\mathrm{o}}(t) - e_{2\mathrm{o}}(t)) - \dot{z}(t) + W_1(x_1(t), \hat{x}_2(t), t)(z(t) - \omega(t) \\
& +\dot{\hat{x}}_u(t)+\epsilon(t))+W_3(x_1(t), \hat{x}_2(t), t)-W_{2\mathrm{s}}(x_1(t), \hat{x}_2(t), t)Bu_2(t)+P_{2\mathrm{o}}^{-1}P_{1\mathrm{o}}e_{1\mathrm{o}}(t)+\dot{z}(t) \\
& +\alpha_1\dot{\hat{x}}_{u1}(t) + \alpha_2\dot{\hat{x}}_{u2}(t) + \alpha_3\hat{x}_{u2}(t) - W_3(x_1(t), \hat{x}_2(t), t)-W_1(x_1(t), \hat{x}_2(t), t)\Big(z(t) \\
& +\dot{\hat{x}}_u(t)-\omega(t)+\frac{1}{2}W_1^{\mathrm{T}}(x_1(t), \hat{x}_2(t), t)P_{2\mathrm{o}}e_{2\mathrm{o}}(t)\Big)+A_{2\mathrm{o}}e_{2\mathrm{o}}(t)+W_{2\mathrm{s}}(x_1(t), \hat{x}_2(t), t)Bu_2(t) \\
& -A_{1\mathrm{o}}((A_{1\mathrm{o}} + P_{1\mathrm{o}}^{-1}K)e_{1\mathrm{o}}(t) - e_{2\mathrm{o}}(t)) - \alpha_1\dot{\hat{x}}_{u1}(t) - \alpha_2\dot{\hat{x}}_{u2}(t) - \alpha_3\hat{x}_{u2}(t) \\
= \, & P_{2\mathrm{o}}^{-1}P_{1\mathrm{o}}e_{1\mathrm{o}}(t) + A_{2\mathrm{o}}e_{2\mathrm{o}}(t) - W_1(x_1(t), \hat{x}_2(t), t)\Big(\frac{1}{2}W_1^{\mathrm{T}}(x_1(t), \hat{x}_2(t), t)P_{2\mathrm{o}}e_{2\mathrm{o}}(t) - \epsilon(t)\Big) \\
& +A_{1\mathrm{o}}\epsilon(t), \quad t \geq 0.
\end{aligned} \tag{8.21}$$

Next, we consider the following Lyapunov function candidate,

$$V(e_{1\mathrm{o}}, e_{2\mathrm{o}}) \,=\, e_{1\mathrm{o}}^{\mathrm{T}}P_{1\mathrm{o}}e_{1\mathrm{o}} + e_{2\mathrm{o}}^{\mathrm{T}}P_{2\mathrm{o}}e_{2\mathrm{o}}, \tag{8.22}$$

where $P_{1\mathrm{o}}$, $P_{2\mathrm{o}} > 0$ are obtained from (8.13) and (8.14), respectively. The time derivative of

(8.22) along the trajectories of (8.19) and (8.21) is given by

$$\begin{aligned}\dot{V}(t)=&e_{1\mathrm{o}}^{\mathrm{T}}(t)(A_{1\mathrm{o}}^{\mathrm{T}}P_{1\mathrm{o}}+P_{1\mathrm{o}}A_{1\mathrm{o}})e_{1\mathrm{o}}(t)+e_{2\mathrm{o}}^{\mathrm{T}}(t)(A_{2\mathrm{o}}^{\mathrm{T}}P_{2\mathrm{o}}+P_{2\mathrm{o}}A_{2\mathrm{o}})e_{2\mathrm{o}}(t)+e_{1\mathrm{o}}^{\mathrm{T}}(t)(K+K^{\mathrm{T}})e_{1\mathrm{o}}(t)\\&+2e_{2\mathrm{o}}^{\mathrm{T}}(t)P_{2\mathrm{o}}\Big[A_{1\mathrm{o}}\epsilon(t)+W_1(x_1(t),\hat{x}_2(t),t)\Big(\epsilon(t)-\frac{1}{2}W_1^{\mathrm{T}}(x_1(t),\hat{x}_2(t),t)P_{2\mathrm{o}}e_{2\mathrm{o}}(t)\Big)\\&+P_{2\mathrm{o}}^{-1}P_{1\mathrm{o}}e_{1\mathrm{o}}(t)\Big]-2e_{1\mathrm{o}}^{\mathrm{T}}(t)P_{1\mathrm{o}}(e_{2\mathrm{o}}(t)-\epsilon(t))\\=&2e_{2\mathrm{o}}^{\mathrm{T}}(t)P_{2\mathrm{o}}W_1(x_1(t),\hat{x}_2(t),t)\Big(\epsilon(t)-\frac{1}{2}W_1^{\mathrm{T}}(x_1(t),\hat{x}_2(t),t)P_{2\mathrm{o}}e_{2\mathrm{o}}(t)\Big)+2e_{2\mathrm{o}}^{\mathrm{T}}(t)P_{2\mathrm{o}}A_{1\mathrm{o}}\epsilon(t)\\&-e_{1\mathrm{o}}^{\mathrm{T}}(t)(\bar{Q}_{1\mathrm{o}}+P_{1\mathrm{o}}^2)e_{1\mathrm{o}}(t)-e_{2\mathrm{o}}^{\mathrm{T}}(t)(Q_{2\mathrm{o}}+P_{2\mathrm{o}}A_{1\mathrm{o}}A_{1\mathrm{o}}^{\mathrm{T}}P_{2\mathrm{o}})e_{2\mathrm{o}}(t)+2e_{1\mathrm{o}}^{\mathrm{T}}(t)P_{1\mathrm{o}}\epsilon(t),\ t\geq 0. \end{aligned}\tag{8.23}$$

Using the completion of the square rule, we obtain

$$2e_{1\mathrm{o}}^{\mathrm{T}}P_{1\mathrm{o}}\epsilon=-(P_{1\mathrm{o}}e_{1\mathrm{o}}-\epsilon)^{\mathrm{T}}(P_{1\mathrm{o}}e_{1\mathrm{o}}-\epsilon)+e_{1\mathrm{o}}^{\mathrm{T}}P_{1\mathrm{o}}^2e_{1\mathrm{o}}+\epsilon^{\mathrm{T}}\epsilon,\tag{8.24}$$

$$2e_{2\mathrm{o}}^{\mathrm{T}}P_{2\mathrm{o}}A_{1\mathrm{o}}\epsilon=-(A_{1\mathrm{o}}^{\mathrm{T}}P_{2\mathrm{o}}e_{2\mathrm{o}}-\epsilon)^{\mathrm{T}}(A_{1\mathrm{o}}^{\mathrm{T}}P_{2\mathrm{o}}e_{2\mathrm{o}}-\epsilon)+e_{2\mathrm{o}}^{\mathrm{T}}P_{2\mathrm{o}}A_{1\mathrm{o}}A_{1\mathrm{o}}^{\mathrm{T}}P_{2\mathrm{o}}e_{2\mathrm{o}}+\epsilon^{\mathrm{T}}\epsilon,\tag{8.25}$$

$$\begin{aligned}2e_{2\mathrm{o}}^{\mathrm{T}}P_{2\mathrm{o}}W_1(x_1,\hat{x}_2,t)\epsilon=&e_{2\mathrm{o}}^{\mathrm{T}}P_{2\mathrm{o}}W_1(x_1,\hat{x}_2,t)W_1^{\mathrm{T}}(x_1,\hat{x}_2,t)P_{2\mathrm{o}}e_{2\mathrm{o}}+\epsilon^{\mathrm{T}}\epsilon\\&-\left(W_1^{\mathrm{T}}(x_1,\hat{x}_2,t)P_{2\mathrm{o}}e_{2\mathrm{o}}-\epsilon\right)^{\mathrm{T}}\left(W_1^{\mathrm{T}}(x_1,\hat{x}_2,t)P_{2\mathrm{o}}e_{2\mathrm{o}}-\epsilon\right).\end{aligned}\tag{8.26}$$

Substituting (8.24)–(8.26) in (8.23), it follows that

$$\begin{aligned}\dot{V}(t)\ \leq\ &-e_{1\mathrm{o}}^{\mathrm{T}}(t)(\bar{Q}_{1\mathrm{o}}+P_{1\mathrm{o}}^2)e_{1\mathrm{o}}(t)+e_{1\mathrm{o}}^{\mathrm{T}}(t)P_{1\mathrm{o}}^2e_{1\mathrm{o}}(t)-e_{2\mathrm{o}}^{\mathrm{T}}(t)(Q_{2\mathrm{o}}+P_{2\mathrm{o}}A_{1\mathrm{o}}A_{1\mathrm{o}}^{\mathrm{T}}P_{2\mathrm{o}})e_{2\mathrm{o}}(t)\\&+e_{2\mathrm{o}}^{\mathrm{T}}(t)P_{2\mathrm{o}}A_{1\mathrm{o}}A_{1\mathrm{o}}^{\mathrm{T}}P_{2\mathrm{o}}e_{2\mathrm{o}}(t)+e_{2\mathrm{o}}^{\mathrm{T}}(t)P_{2\mathrm{o}}W_1(x_1(t),\hat{x}_2(t),t)W_1^{\mathrm{T}}(x_1(t),\hat{x}_2(t),t)P_{2\mathrm{o}}e_{2\mathrm{o}}(t)\\&-e_{2\mathrm{o}}^{\mathrm{T}}(t)P_{2\mathrm{o}}W_1(x_1(t),\hat{x}_2(t),t)W_1^{\mathrm{T}}(x_1(t),\hat{x}_2(t),t)P_{2\mathrm{o}}e_{2\mathrm{o}}(t)+3\epsilon^{\mathrm{T}}(t)\epsilon(t)\\\leq\ &-e_{1\mathrm{o}}^{\mathrm{T}}(t)\bar{Q}_{1\mathrm{o}}e_{1\mathrm{o}}(t)-e_{2\mathrm{o}}^{\mathrm{T}}(t)Q_{2\mathrm{o}}e_{2\mathrm{o}}(t)+\varepsilon,\quad t\geq 0.\end{aligned}\tag{8.27}$$

Hence, $\dot{V}(t)$, $t\geq 0$, is strictly negative outside of $\big\{(e_{1\mathrm{o}},e_{2\mathrm{o}}):e_{1\mathrm{o}}^{\mathrm{T}}\bar{Q}_{1\mathrm{o}}e_{1\mathrm{o}}+e_{2\mathrm{o}}^{\mathrm{T}}Q_{2\mathrm{o}}e_{2\mathrm{o}}\leq\varepsilon\big\}$, which allows to conclude ultimate boundedness of $(e_{1\mathrm{o}}(t),e_{2\mathrm{o}}(t))$, $t\geq 0$ ([44,88]). In addition, the ultimate bound can be characterized by $\alpha\triangleq\min(e_{1\mathrm{o}}^{\mathrm{T}}P_{1\mathrm{o}}e_{1\mathrm{o}}+e_{2\mathrm{o}}^{\mathrm{T}}P_{2\mathrm{o}}e_{2\mathrm{o}})$, subject to the constraint $e_{1\mathrm{o}}^{\mathrm{T}}\bar{Q}_{1\mathrm{o}}e_{1\mathrm{o}}+e_{2\mathrm{o}}^{\mathrm{T}}Q_{2\mathrm{o}}e_{2\mathrm{o}}=\varepsilon$. This constrained minimization problem is easily solved

using Lagrange multipliers, yielding $\alpha = \varepsilon\lambda_{\max}(N_{\mathrm{o}})$, which proves convergence of the error trajectories to $\mathcal{D}_{\mathrm{o}}$ and concludes this proof. $\square$

8.4. Nonlinear Controller Design

In the previous section, we designed an observer-predictor, which provides a prediction $\hat{x}_1(t)$ of $x_1(t)$, $t \geq 0$. This prediction can be made arbitrarily accurate, for any admissible input $u(t)$, $t \geq 0$. Next, we will design the input $u(t)$, $t \geq 0$, so that the origin of the tracking error dynamics is Lyapunov stable and $e_{1\mathrm{t}}(t) \triangleq y_{\mathrm{d}} - \hat{x}_1(t)$, $t \geq 0$, asymptotically converges to a neighborhood of the origin, uniformly in time. More specifically, we design a controller for the following system,

$$\dot{\hat{x}}_1(t) = f_1(x_1(t), \hat{x}_2(t), t) - De_{1\mathrm{o}}(t) + g_1(x_1(t), \hat{x}_2(t), t)u_1(t), \quad \hat{x}_1(0) = x_{10}, \quad t \geq 0, \tag{8.28}$$

$$\dot{\hat{x}}_2(t) = \Lambda_p W_2^{-1}(x_1(t), \hat{x}_2(t), t)\gamma(t) + Bu_2(t), \qquad \hat{x}_2(0) = 0_p, \tag{8.29}$$

where $D = P_{1\mathrm{o}}^{-1}K$ and

$$\begin{aligned}\gamma(t) \triangleq\ & P_{2\mathrm{o}}^{-1}P_{1\mathrm{o}}e_{1\mathrm{o}}(t) - A_{1\mathrm{o}}((A_{1\mathrm{o}} + P_{1\mathrm{o}}^{-1}K)e_{1\mathrm{o}}(t) - e_{2\mathrm{o}}(t)) + \dot{z}(t) + A_{2\mathrm{o}}e_{2\mathrm{o}}(t) - W_3(x_1(t), \hat{x}_2(t), t) \\ & - W_1(x_1(t), \hat{x}_2(t), t)\Big(z(t) + \dot{\hat{x}}_u(t) - \omega(t) + \frac{1}{2}W_1^{\mathrm{T}}(x_1(t), \hat{x}_2(t), t)P_{2\mathrm{o}}e_{2\mathrm{o}}(t)\Big) - \alpha_1\dot{\hat{x}}_{u1}(t) \\ & - \alpha_2\dot{\hat{x}}_{u2}(t) - \alpha_3\hat{x}_{u2}(t), \quad t \geq 0. \end{aligned} \tag{8.30}$$

In the following, we require that the contribution of the control signal $u_2(t)$, $t \geq 0$, to the observer's dynamics be topologically equivalent to its contribution to the actual system's dynamics. This is achieved by requiring that $u_2^{\mathrm{T}}B^{\mathrm{T}}g_2(x_1, x_2, t)u_2 > 0$, for all $u_2 \in \mathbb{R}^{m-q}\backslash\{0\}$, $x_1 \in \mathbb{R}^m$, $x_2 \in \mathbb{R}^p$, and $t \geq 0$. This requirement is verified if B is constructed such that the symmetric part of $B^{\mathrm{T}}g_2(x_1, x_2, t)$ is positive definite for all $x_1 \in \mathbb{R}^m$, $x_2 \in \mathbb{R}^p$, and $t \geq 0$.

Note that in the scalar case, this is equivalent to assuming that B and $g_2(x_1, x_2, t)$ share the same sign for all $x_1 \in \mathbb{R}^m$, $x_2 \in \mathbb{R}^p$, and $t \geq 0$. This assumption is similar to that introduced in [58], where the authors assume knowledge of the signs of the leading minors of $g_2(x_1, x_2, t)$.

The problem of designing a control algorithm for system (8.28)–(8.29) can be solved using a backstepping procedure, as described in [10]. This type of approach leads to the following result.

Theorem 8.4.1. Consider system (8.28)–(8.29), and the control input $u(t) = [\, u_1^{\mathrm{T}}(t), u_2^{\mathrm{T}}(t)\,]^{\mathrm{T}}$, $t \geq 0$, given by

$$u_1(t) = g_{1\mathrm{s}}^{-1}(x_1(t), \hat{x}_2(t), t)\Lambda_q(\dot{y}_{\mathrm{d}}(t) - f_1(x_1(t), \hat{x}_2(t), t) + De_{1\mathrm{o}}(t) - A_{1\mathrm{t}}e_{1\mathrm{t}}(t)),\ t \geq 0, \quad (8.31)$$

$$\begin{aligned} u_2(t) = {} & (\bar{\Lambda}_q W_{2\mathrm{s}}(x_1(t), \hat{x}_2(t), t)B)^{-1}[\bar{\Lambda}_q(-W_1(x_1(t), \hat{x}_2(t), t)(z(t) - \omega(t) + \dot{\hat{x}}_u(t)) \\ & + \ddot{y}_{\mathrm{d}}(t) - W_{2\mathrm{s}}(x_1(t), \hat{x}_2(t), t)\Lambda_p W_2^{-1}(x_1(t), \hat{x}_2(t), t)\gamma(t) - W_3(x_1(t), \hat{x}_2(t), t) \\ & + D((A_{1\mathrm{o}} + D)e_{1\mathrm{o}}(t) - e_{2\mathrm{o}}(t)) - A_{1\mathrm{t}}(A_{1\mathrm{t}}e_{1\mathrm{t}}(t) - \bar{\Lambda}_q^{\mathrm{T}}e_{2\mathrm{t}}(t))) + P_{2\mathrm{t}}^{-1}\bar{\Lambda}_q P_{1\mathrm{t}}e_{1\mathrm{t}}(t) + A_{2\mathrm{t}}e_{2\mathrm{t}}(t) \\ & - \frac{1}{2}\bar{\Lambda}_q(W_1(x_1(t), \hat{x}_2(t), t) - D)(W_1(x_1(t), \hat{x}_2(t), t) - D)^{\mathrm{T}}\bar{\Lambda}_q^{\mathrm{T}}P_{2\mathrm{t}}e_{2\mathrm{t}}(t)], \end{aligned} \quad (8.32)$$

where $y_{\mathrm{d}}(t) \in \mathbb{R}^m$, $t \geq 0$, is a given desired output, $\omega(t)$, $t \geq 0$, is obtained from (8.6), $\hat{x}_u(t) = \hat{x}_{u1}(t) + \hat{x}_{u2}(t)$, $t \geq 0$, is obtained from (8.7)–(8.8), $\gamma(t)$, $t \geq 0$, is given by (8.30), $e_{2\mathrm{t}}(t) \triangleq \bar{\Lambda}_q f_1(x_1(t), \hat{x}_2(t), t) - \bar{\Lambda}_q(\dot{y}_{\mathrm{d}}(t) + De_{1\mathrm{o}}(t) - A_{1\mathrm{t}}e_{1\mathrm{t}}(t))$, the matrices $A_{1\mathrm{t}}$ and $A_{2\mathrm{t}}$ are chosen Hurwitz, and $P_{1\mathrm{t}}$, $P_{2\mathrm{t}} > 0$, are solutions to

$$A_{1\mathrm{t}}^{\mathrm{T}}P_{1\mathrm{t}} + P_{1\mathrm{t}}A_{1\mathrm{t}} + Q_{1\mathrm{t}} = 0, \quad A_{2\mathrm{t}}^{\mathrm{T}}P_{2\mathrm{t}} + P_{2\mathrm{t}}A_{2\mathrm{t}} + Q_{2\mathrm{t}} = 0, \quad (8.33)$$

where $Q_{1\mathrm{t}}$ and $Q_{2\mathrm{t}}$ are chosen positive definite. Finally, define

$$N_{\mathrm{t}} \triangleq \begin{bmatrix} Q_{1\mathrm{t}}^{-1}P_{1\mathrm{t}} & 0_{m\times m} \\ 0_{m\times m} & Q_{2\mathrm{t}}^{-1}P_{2\mathrm{t}} \end{bmatrix}. \quad (8.34)$$

Then, the control input (8.31)–(8.32) guarantees uniform ultimate boundedness of the tracking errors $(e_{1\mathrm{t}}(t), e_{2\mathrm{t}}(t))$, $t \geq 0$, with an ultimate bound given by $\mathcal{D}_{\mathrm{t}} \triangleq \{(e_{1\mathrm{t}}, e_{2\mathrm{t}}) : e_{1\mathrm{t}}^{\mathrm{T}} P_{1\mathrm{t}} e_{1\mathrm{t}} + e_{2\mathrm{t}}^{\mathrm{T}} P_{2\mathrm{t}} e_{2\mathrm{t}} \leq \varepsilon \lambda_{\max}(N_{\mathrm{t}})/3\}$.

Proof. The time derivative of the tracking error $e_{1\mathrm{t}}(t)$, $t \geq 0$, is given by

$$\dot{e}_{1\mathrm{t}}(t) = \dot{y}_{\mathrm{d}}(t) - f_1(x_1(t), \hat{x}_2(t), t) - g_1(x_1(t), \hat{x}_2(t), t)u_1(t) + De_{1\mathrm{o}}(t), \quad t \geq 0. \tag{8.35}$$

Note that

$$\Lambda_q \dot{e}_{1\mathrm{t}}(t) = \Lambda_q(\dot{y}_{\mathrm{d}}(t) - f_1(x_1(t), \hat{x}_2(t), t) + De_{1\mathrm{o}}(t)) - g_{1\mathrm{s}}(x_1(t), \hat{x}_2(t), t)u_1(t), \quad t \geq 0. \tag{8.36}$$

Substituting (8.31) in the above, we obtain

$$\Lambda_q \dot{e}_{1\mathrm{t}}(t) = \Lambda_q A_{1\mathrm{t}} e_{1\mathrm{t}}(t), \quad t \geq 0. \tag{8.37}$$

In addition, by definition of $e_{2\mathrm{t}}(t)$, $t \geq 0$,

$$\bar{\Lambda}_q \dot{e}_{1\mathrm{t}}(t) = \bar{\Lambda}_q A_{1\mathrm{t}} e_{1\mathrm{t}}(t) - e_{2\mathrm{t}}(t), \quad t \geq 0. \tag{8.38}$$

Combining (8.37) and (8.38), and observing that $[\, \Lambda_q^{\mathrm{T}} \ \bar{\Lambda}_q^{\mathrm{T}} \,] = I_m$, we obtain

$$\dot{e}_{1\mathrm{t}}(t) = A_{1\mathrm{t}} e_{1\mathrm{t}}(t) - \bar{\Lambda}_q^{\mathrm{T}} e_{2\mathrm{t}}(t), \quad t \geq 0. \tag{8.39}$$

The time derivative of $e_{2\mathrm{t}}(t)$, $t \geq 0$, is given by

$$\begin{aligned}
\dot{e}_{2\mathrm{t}}(t) = \bar{\Lambda}_q &(W_1(x_1(t), \hat{x}_2(t), t)\dot{x}_1(t) + W_{2\mathrm{s}}(x_1(t), \hat{x}_2(t), t)\dot{\hat{x}}_2(t) + W_3(x_1(t), \hat{x}_2(t), t) - \ddot{y}_{\mathrm{d}}(t) \\
&+ A_{1\mathrm{t}}\dot{e}_{1\mathrm{t}}(t) - D\dot{e}_{1\mathrm{o}}(t)) \\
= \bar{\Lambda}_q \Big(&W_1(x_1(t), \hat{x}_2(t), t)(z(t) - \omega(t) + \dot{\hat{x}}_u(t) + \epsilon(t)) + W_3(x_1(t), \hat{x}_2(t), t) - \ddot{y}_{\mathrm{d}}(t) \\
&+ W_{2\mathrm{s}}(x_1(t), \hat{x}_2(t), t)\Lambda_p W_2^{-1}(x_1(t), \hat{x}_2(t), t)\gamma(t) + A_{1\mathrm{t}}(A_{1\mathrm{t}} e_{1\mathrm{t}}(t) - \bar{\Lambda}_q^{\mathrm{T}} e_{2\mathrm{t}}(t)) \\
&- D((A_{1\mathrm{o}} + D)e_{1\mathrm{o}}(t) - e_{2\mathrm{o}}(t) + \epsilon(t)) \Big) + \bar{\Lambda}_q W_{2\mathrm{s}}(x_1(t), \hat{x}_2(t), t) B u_2(t), \quad t \geq 0.
\end{aligned} \tag{8.40}$$

Substituting (8.32) in (8.40) yields

$$\dot{e}_{2\mathrm{t}}(t) = -\frac{1}{2}\bar{\Lambda}_q(W_1(x_1(t),\hat{x}_2(t),t)-D)(W_1(x_1(t),\hat{x}_2(t),t)-D)^{\mathrm{T}}\bar{\Lambda}_q^{\mathrm{T}}P_{2\mathrm{t}}e_{2\mathrm{t}}(t)$$
$$+A_{2\mathrm{t}}e_{2\mathrm{t}}(t)+P_{2\mathrm{t}}^{-1}\bar{\Lambda}_qP_{1\mathrm{t}}e_{1\mathrm{t}}(t)+\bar{\Lambda}_q(W_1(x_1(t),\hat{x}_2(t),t)-D)\epsilon(t),\quad t\geq 0. \tag{8.41}$$

Next, we consider the following Lyapunov function candidate,

$$V(e_{1\mathrm{t}},e_{2\mathrm{t}}) = e_{1\mathrm{t}}^{\mathrm{T}}P_{1\mathrm{t}}e_{1\mathrm{t}}+e_{2\mathrm{t}}^{\mathrm{T}}P_{2\mathrm{t}}e_{2\mathrm{t}}, \tag{8.42}$$

where $P_{1\mathrm{t}},\ P_{2\mathrm{t}}>0$ are obtained from (8.33). The time derivative of (8.42) along the trajectories of (8.39) and (8.41) is given by

$$\begin{aligned}\dot{V}(t) &= e_{1\mathrm{t}}^{\mathrm{T}}(t)(A_{1\mathrm{t}}^{\mathrm{T}}P_{1\mathrm{t}}+P_{1\mathrm{t}}A_{1\mathrm{t}})e_{1\mathrm{t}}(t)+e_{2\mathrm{t}}^{\mathrm{T}}(t)(A_{2\mathrm{t}}^{\mathrm{T}}P_{2\mathrm{t}}+P_{2\mathrm{t}}A_{2\mathrm{t}})e_{2\mathrm{t}}(t)-2e_{1\mathrm{t}}^{\mathrm{T}}(t)P_{1\mathrm{t}}\bar{\Lambda}_q^{\mathrm{T}}e_{2\mathrm{t}}(t)\\
&\quad -2e_{2\mathrm{t}}^{\mathrm{T}}(t)P_{2\mathrm{t}}\Big(\frac{1}{2}\bar{\Lambda}_q(W_1(x_1(t),\hat{x}_2(t),t)-D)(W_1(x_1(t),\hat{x}_2(t),t)-D)^{\mathrm{T}}\bar{\Lambda}_q^{\mathrm{T}}P_{2\mathrm{t}}e_{2\mathrm{t}}(t)\\
&\quad -P_{2\mathrm{t}}^{-1}\bar{\Lambda}_qP_{1\mathrm{t}}e_{1\mathrm{t}}(t)-\bar{\Lambda}_q(W_1(x_1(t),\hat{x}_2(t),t)-D)\epsilon(t)\Big)\\
&= -e_{1\mathrm{t}}^{\mathrm{T}}(t)Q_{1\mathrm{t}}e_{1\mathrm{t}}(t)-e_{2\mathrm{t}}^{\mathrm{T}}(t)Q_{2\mathrm{t}}e_{2\mathrm{t}}(t)+2e_{2\mathrm{t}}^{\mathrm{T}}(t)P_{2\mathrm{t}}\bar{\Lambda}_q(W_1(x_1(t),\hat{x}_2(t),t)-D)\epsilon(t)\\
&\quad -e_{2\mathrm{t}}^{\mathrm{T}}(t)P_{2\mathrm{t}}\bar{\Lambda}_q(W_1(x_1(t),\hat{x}_2(t),t)-D)(W_1(x_1(t),\hat{x}_2(t),t)-D)^{\mathrm{T}}\bar{\Lambda}_q^{\mathrm{T}}P_{2\mathrm{t}}e_{2\mathrm{t}}(t),\ t\geq 0.\end{aligned} \tag{8.43}$$

Note that

$$\begin{aligned}2e_{2\mathrm{t}}^{\mathrm{T}}P_{2\mathrm{t}}\bar{\Lambda}_q(D-W_1(x_1,\hat{x}_2,t))\epsilon &= e_{2\mathrm{t}}^{\mathrm{T}}P_{2\mathrm{t}}\bar{\Lambda}_q(D-W_1(x_1,\hat{x}_2,t))(D-W_1(x_1,\hat{x}_2,t))^{\mathrm{T}}\bar{\Lambda}_q^{\mathrm{T}}P_{2\mathrm{t}}e_{2\mathrm{t}}\\
&\quad -\big((D-W_1(x_1,\hat{x}_2,t))^{\mathrm{T}}\bar{\Lambda}_q^{\mathrm{T}}P_{2\mathrm{t}}e_{2\mathrm{t}}-\epsilon\big)^{\mathrm{T}}\big((D-W_1(x_1,\hat{x}_2,t))^{\mathrm{T}}\bar{\Lambda}_q^{\mathrm{T}}P_{2\mathrm{t}}e_{2\mathrm{t}}-\epsilon\big)+\epsilon^{\mathrm{T}}\epsilon.\end{aligned} \tag{8.44}$$

Substituting (8.44) into (8.43), we obtain that

$$\begin{aligned}\dot{V}(t) &\leq -e_{1\mathrm{t}}^{\mathrm{T}}(t)Q_{1\mathrm{t}}e_{1\mathrm{t}}(t)-e_{2\mathrm{t}}^{\mathrm{T}}(t)Q_{2\mathrm{t}}e_{2\mathrm{t}}(t)+\epsilon^{\mathrm{T}}(t)\epsilon(t)\\
&\leq -e_{1\mathrm{t}}^{\mathrm{T}}(t)Q_{1\mathrm{t}}e_{1\mathrm{t}}(t)-e_{2\mathrm{t}}^{\mathrm{T}}(t)Q_{2\mathrm{t}}e_{2\mathrm{t}}(t)+\frac{\varepsilon}{3},\quad t\geq 0.\end{aligned} \tag{8.45}$$

Following the same reasoning as that at the end of the proof of Theorem 8.3.1, we conclude that $(e_{1\mathrm{t}}(t),e_{2\mathrm{t}}(t))$, $t\geq 0$, is ultimately bounded and uniformly converges to $\mathcal{D}_{\mathrm{t}}$. □

8.5. Illustrative Numerical Examples

As in the preceding chapter, the predictor-observer will use the Adaptive Integral Variable Structure Derivative Estimator (AIVSDE) described in [57]. However, in this chapter, we set $r(t) = y(t) - \hat{x}_u(t) + \int_0^t \omega(\tau)\mathrm{d}\tau$, to obtain an estimate $z(t)$ of $\dot{y}(t) + \omega(t) - \dot{\hat{x}}_u(t)$, $t \geq 0$.

Example 8.5.1. Consider the following system,

$$\dot{x}_1(t) = a\sin(x_1(t) + x_2(t)) + b(\tanh(\pi x_2(t) - 2) + \tanh(x_2^3(t)/10) + x_2^3(t)/100), \quad x_1(0) = x_{10}, \quad t \geq 0, \tag{8.46}$$

$$\dot{x}_2(t) = c\tanh(x_1(t)) - dx_2^3(t) + u(t), \qquad x_2(0) = x_{20}, \tag{8.47}$$

$$y(t) = x_1(t), \tag{8.48}$$

where $x_1(t)$, $x_2(t)$, $u(t) \in \mathbb{R}$, $t \geq 0$, and a, b, c, $d \in \mathbb{R}$. Note that, for the above system, $m = p = 1$. It is therefore unnecessary to construct an auxiliary signal $\omega(t)$, $t \geq 0$, and the design procedure is simplified. More specifically, we construct the following predictor-observer,

$$\dot{\hat{x}}_1(t) = a\sin(x_1(t) + \hat{x}_2(t)) + b(\tanh(\pi\hat{x}_2(t) - 2) + \tanh(\hat{x}_2^3(t)/10) + \hat{x}_2^3(t)/100), \quad \hat{x}_1(0) = \hat{x}_{10}, \quad t \geq 0, \tag{8.49}$$

$$\dot{\hat{x}}_2(t) = \gamma(t)/w_2(x_1(t), \hat{x}_2(t)) + u(t), \qquad \hat{x}_2(0) = 0, \tag{8.50}$$

where

$$\gamma(t) = p_{1\mathrm{o}}e_{1\mathrm{o}}(t)/p_{2\mathrm{o}} - w_1(x_1(t), \hat{x}_2(t))(z(t) + \dot{\hat{x}}_u(t) + w_1^{\mathrm{T}}(x_1(t), \hat{x}_2(t))p_{2\mathrm{o}}e_{2\mathrm{o}}(t)/2) + A_{2\mathrm{o}}e_{2\mathrm{o}}(t) - A_{1\mathrm{o}}(A_{1\mathrm{o}}e_{1\mathrm{o}}(t) - e_{2\mathrm{o}}(t)) + \dot{z}(t) - \dot{\hat{x}}_u(t) - \hat{x}_u(t), \quad t \geq 0, \tag{8.51}$$

$$e_{1\mathrm{o}}(t) = x_1(t) - \hat{x}_1(t), \tag{8.52}$$

$$e_{2\mathrm{o}}(t) = \dot{\hat{x}}_1(t) + A_{1\mathrm{o}}e_{1\mathrm{o}}(t) - z(t) - \dot{\hat{x}}_u(t) + \hat{x}_u(t), \tag{8.53}$$

$$w_1(x_1, \hat{x}_2) = a\cos(x_1 + \hat{x}_2), \tag{8.54}$$

$$w_2(x_1, \hat{x}_2) = a\cos(x_1 + \hat{x}_2) + b(\pi\mathrm{sech}^2(\pi\hat{x}_2 - 2) + \mathrm{sech}^2(\hat{x}_2^3/10)(3\hat{x}_2^2/10) + 3\hat{x}_2^2/100). \tag{8.55}$$

Choosing $A_{1\mathrm{o}} = -10$, $A_{2\mathrm{o}} = -100$, $q_{1\mathrm{o}} = 10$, $q_{2\mathrm{o}} = 80$, we obtain $p_{1\mathrm{o}} = 0.5132$, $p_{2\mathrm{o}} = 0.5528$ from (8.13)–(8.14). The parameters of the AIVSDE are chosen as follows, $k_1 = 10$, $k_2 = 20$, $k_b = 30$, $\alpha_r = 0.1$, $\mu = 0.2$, $\gamma_{r0} = x_{10}$ and $k_{r0} = 10$. In accordance with the form of system (8.49)–(8.50), the control law is given by

$$\begin{aligned} u(t) = [&- w_1(x_1(t), \hat{x}_2(t))(z(t) + \dot{\hat{x}}_u(t)) + \ddot{y}_{\mathrm{d}}(t) - \gamma(t) - A_{1\mathrm{t}}(A_{1\mathrm{t}}e_{1\mathrm{t}}(t) - e_{2\mathrm{t}}(t)) + A_{2\mathrm{t}}e_{2\mathrm{t}}(t) \\ &+ p_{1\mathrm{t}}e_{1\mathrm{t}}(t)/p_{2\mathrm{t}} - w_1(x_1(t), \hat{x}_2(t))w_1^{\mathrm{T}}(x_1(t), \hat{x}_2(t))p_{2\mathrm{t}}e_{2\mathrm{t}}(t)/2]/w_2(x_1(t), \hat{x}_2(t)), \ t \geq 0, \end{aligned} \tag{8.56}$$

where $e_{1\mathrm{t}}(t) = y_{\mathrm{d}} - \hat{x}_1(t)$, $e_{2\mathrm{t}}(t) = \dot{\hat{x}}_1(t) - \dot{y}_{\mathrm{d}}(t) + A_{1\mathrm{t}}e_{1\mathrm{t}}(t)$, $t \geq 0$. In addition, we chose $A_{1\mathrm{t}} = -5$, $A_{2\mathrm{t}} = -1$, $q_{1\mathrm{t}} = 5$, $q_{2\mathrm{t}} = 1$, and obtain from (8.33), $p_{1\mathrm{t}} = p_{2\mathrm{t}} = 1/2$. Finally, $\dot{\hat{x}}_u(t)$, $t \geq 0$, is obtained from (8.8) with $B = \alpha_2 = \alpha_3 = 1$, and $u_2(t)$, $t \geq 0$, given by (8.56). The desired output trajectory is chosen to be $y_{\mathrm{d}}(t) = -5\cos(t)$, $t \geq 0$.

For the purpose of numerical simulation, we chose the following parameters for the system model, $a = 0.4$, $b = 10$, $c = -1$ and $d = 0.1$. Note that, with this choice of parameters, $w_2(x_1, \hat{x}_2) \neq 0$, for all $x_1, \hat{x}_2 \in \mathbb{R}$. In addition, we choose $x_{10} = x_{20} = 2$, $\hat{x}_{10} = 1$, $\hat{x}_{20} = 0$, and $z(0) = 0$. The resulting system and predictor-observer trajectories are shown in Figure 8.2.

The predicted $\hat{x}_1(t)$ closely matches the measured $x_1(t)$, $t \geq 0$, as seen in Figure 8.2. In addition, the observed $\hat{x}_2(t)$ also closely matches the unmeasured $x_2(t)$, $t \geq 0$, and converges as quickly as its predicted counterpart. Note that the initial condition for the prediction $\hat{x}_{10}$ could have been chosen as x_{10}, since $x_1(t)$, $t \geq 0$, is measured. This would have resulted

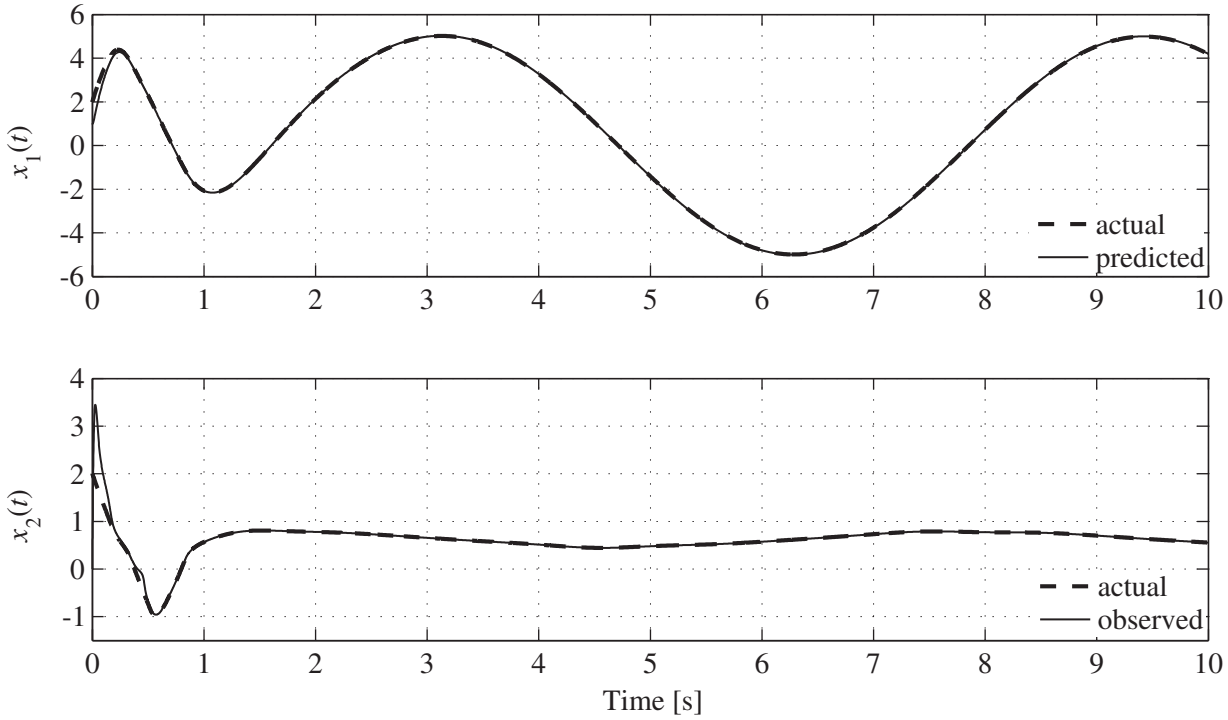

Figure 8.2: Actual and predicted/observed trajectories.

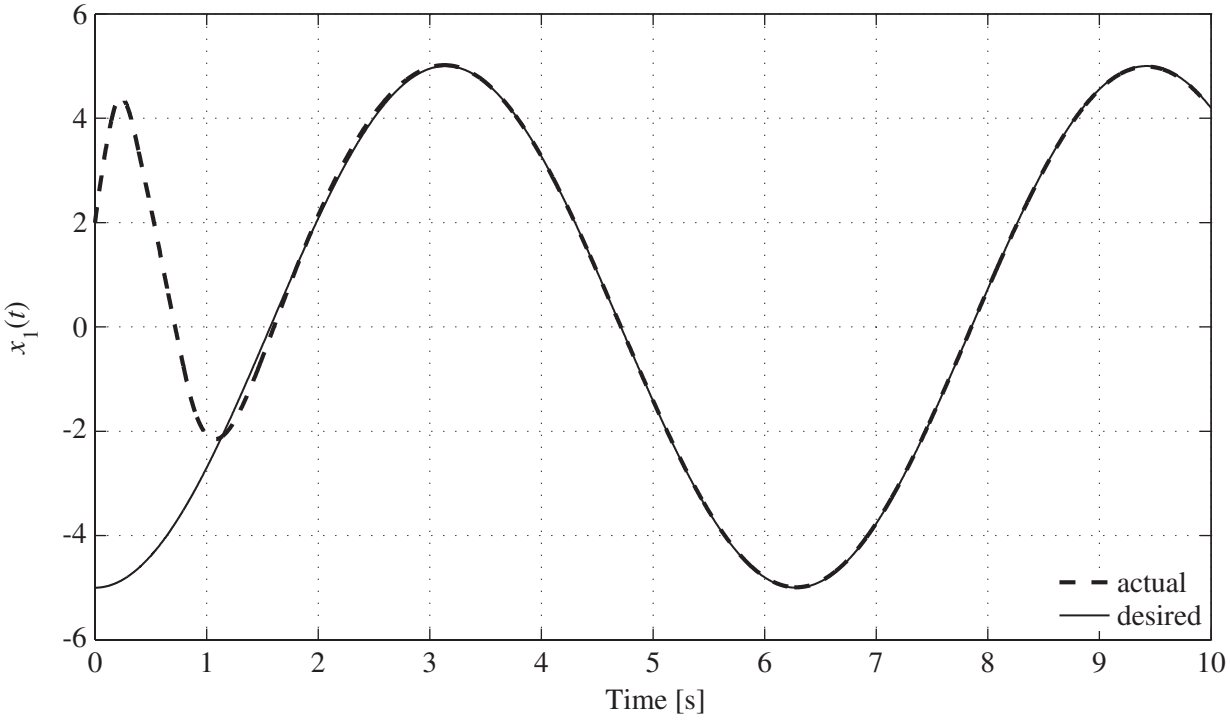

Figure 8.3: Actual and desired output trajectories.

in a decreased initial overshoot of $\hat{x}_2(t)$, $t \geq 0$. The initial prediction was however chosen different from x_{10} to illustrate convergence of $\hat{x}_1(t)$ to $x_1(t)$, $t \geq 0$. The efficacy of the control law (8.56) is illustrated by Figure 8.3, which shows the real trajectory converging to the desired $y_{\rm d}(t)$, $t \geq 0$. The control input is shown in Figure 8.4. Note that we have employed the saturation algorithm presented in [1] to limit the command in amplitude.

Example 8.5.2. Consider the system

$$\dot{x}_{11}(t) = -x_{11}^3(t) + \tanh(x_{12}(t)) + \frac{1+x_{11}^2(t)}{1+x_2^2(t)}u_1(t), \qquad x_{11}(0) = x_{110},\ t \geq 0, \tag{8.57}$$

$$\dot{x}_{12}(t) = 4\tanh(x_{11}(t)) - 2\tanh(x_{12}(t)) + x_2(t) + \cos(x_2^2(t))/2, \quad x_{12}(0) = x_{120}, \tag{8.58}$$

$$\dot{x}_2(t) = -x_2^3(t) - 2\tanh((x_{11}(t)+x_{12}(t))^3) + \frac{1+x_{11}^2(t)}{1+x_2^2(t)}u_2(t), \qquad x_2(0) = x_{20}, \tag{8.59}$$

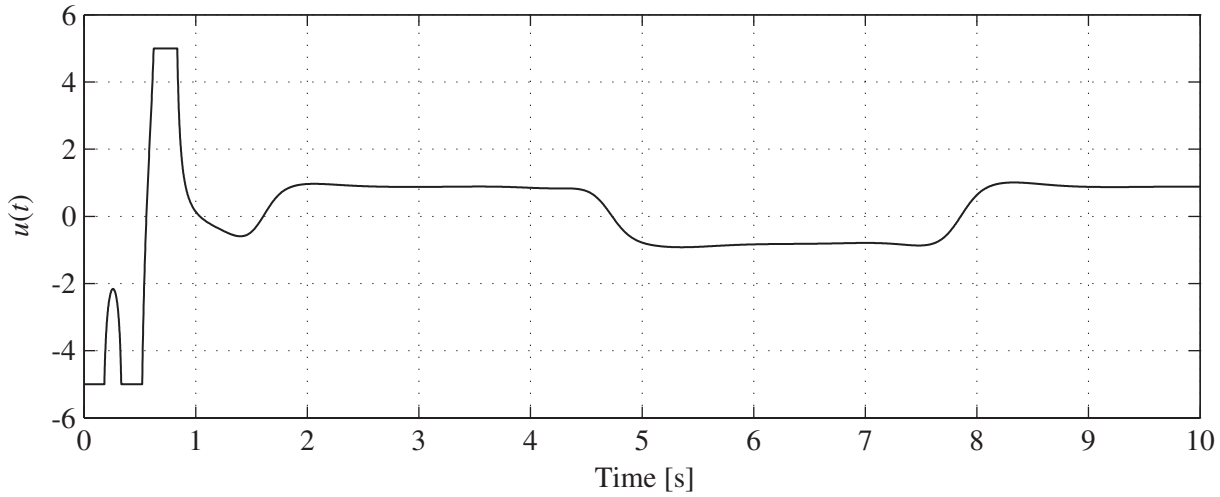

Figure 8.4: Control effort.

$$y(t) = x_1(t), \tag{8.60}$$

where $x_1(t) \triangleq \begin{bmatrix} x_{11}(t) & x_{12}(t) \end{bmatrix}^{\mathrm{T}} \in \mathbb{R}^2$, and $x_2(t) \in \mathbb{R}$, $t \geq 0$. Applying the technique described in Theorem 8.3.1, we construct the following predictor-observer,

$$\dot{\hat{x}}_1(t) = f_1(x_1(t), \hat{x}_2(t)) + g_1(x_1(t), \hat{x}_2(t))u_1(t) - De_{1\mathrm{o}}(t), \quad \hat{x}_1(0) = x_{10} \triangleq \begin{bmatrix} x_{110} & x_{120} \end{bmatrix}^{\mathrm{T}},$$
$$t \geq 0, \tag{8.61}$$

$$\dot{\hat{x}}_{2\mathrm{a}}(t) = W_2^{-1}(x_2(t))(\gamma(t) + W_{2\mathrm{s}}u_2(t)), \qquad \hat{x}_{2\mathrm{a}}(0) = \hat{x}_{2\mathrm{a}0}, \tag{8.62}$$

where

$$\gamma(t) = P_{2\mathrm{o}}^{-1}P_{1\mathrm{o}}e_{1\mathrm{o}}(t) - A_{1\mathrm{o}}((A_{1\mathrm{o}} + P_{1\mathrm{o}}^{-1}K)e_{1\mathrm{o}}(t) - e_{2\mathrm{o}}(t)) + \dot{z}(t) + A_{2\mathrm{o}}e_{2\mathrm{o}}(t) - \dot{\hat{x}}_{u1}(t) - \hat{x}_{u2}(t)$$
$$-\dot{\hat{x}}_{u2}(t) - W_1(x_1(t))\Big(z(t) - \omega(t) + \dot{\hat{x}}_u(t) + W_1^{\mathrm{T}}(x_1(t))P_{2\mathrm{o}}e_{2\mathrm{o}}(t)/2\Big), \quad t \geq 0, \tag{8.63}$$

$$e_{1\mathrm{o}}(t) = x_1(t) - \hat{x}_1(t), \tag{8.64}$$

$$e_{2\mathrm{o}}(t) = f_1(x_1(t), \hat{x}_2(t)) - \dot{\hat{x}}_{u2}(t) + \hat{x}_{u1}(t) + \omega(t) - z(t) + A_{1\mathrm{o}}e_{1\mathrm{o}}(t), \tag{8.65}$$

the auxiliary signals $\omega(t)$ is obtained from (8.6), with $v(t) \triangleq \begin{bmatrix} 0 & 1 \end{bmatrix} \dot{\hat{x}}_{2\mathrm{a}}(t)$, $t \geq 0$, and $W_{\mathrm{a}} = \begin{bmatrix} 1 \, 0 \end{bmatrix}^{\mathrm{T}}$. In addition, $K = -5I_2$,

$$f_1(x_1, \hat{x}_2) = \begin{bmatrix} -x_{11}^3 + \tanh(x_{12}) + 3\sin(\hat{x}_2) \\ 4\tanh(x_{11}) - 2\tanh(x_{12}) - 3\cos(\hat{x}_2) \end{bmatrix}, \quad g_1(x_1, \hat{x}_2) = \begin{bmatrix} \frac{1+x_{11}^2}{1+\hat{x}_2^2} \\ 0 \end{bmatrix}, \tag{8.66}$$

$$W_1(x_1) = \begin{bmatrix} -3x_{11}^2 & \mathrm{sech}^2(x_{12}) \\ 4\mathrm{sech}^2(x_{11}) & -2\mathrm{sech}^2(x_{12}) \end{bmatrix}, \qquad W_2(\hat{x}_2) = \begin{bmatrix} 0 & 1 \\ 1 - \sin(2\hat{x}_2)/2 & 0 \end{bmatrix}. \tag{8.67}$$

Choosing $A_{1\mathrm{o}} = -35I_2$, $Q_{1\mathrm{o}} = 35I_2$, $A_{2\mathrm{o}} = -500I_2$, and $Q_{2\mathrm{o}} = 160I_2$, we obtain, from (8.13)–(8.14), $P_{1\mathrm{o}} = 0.5036I_2$, $P_{2\mathrm{o}} = 0.2185I_2$. The parameters used for the AIVSDE are identical to that in the previous example. The initial conditions for the system and the observer are chosen as $x_{10} = \begin{bmatrix} 2 & 2 \end{bmatrix}^{\mathrm{T}}$, $x_{20} = -1$, and $\hat{x}_{2\mathrm{a}0} = 0_2$. The control command is of the form

$$u_1(t) = \frac{1 + \hat{x}_2^2(t)}{1 + x_{11}^2(t)} \Lambda_1 (\dot{y}_{\mathrm{d}}(t) - f_1(x_1(t), \hat{x}_2(t)) + De_{1\mathrm{o}}(t) - A_{1\mathrm{t}} e_{1\mathrm{t}}(t)), \quad t \geq 0, \tag{8.68}$$

$$\begin{aligned} u_2(t) = {} & \frac{2}{2 - \sin(2\hat{x}_2(t))} \Big(\bar{\Lambda}_1 (-W_1(x_1(t))(z(t) - \omega(t) + \dot{\hat{x}}_u(t)) + \ddot{y}_{\mathrm{d}}(t) - \gamma(t) \\ & + D((A_{1\mathrm{o}} + D)e_{1\mathrm{o}}(t) - e_{2\mathrm{o}}(t)) - A_{1\mathrm{t}}(A_{1\mathrm{t}} e_{1\mathrm{t}}(t) - \bar{\Lambda}_1^{\mathrm{T}} e_{2\mathrm{t}}(t))) + A_{2\mathrm{t}} e_{2\mathrm{t}}(t) \\ & + P_{2\mathrm{t}}^{-1} \bar{\Lambda}_1 P_{1\mathrm{t}} e_{1\mathrm{t}}(t) - \frac{1}{2} \bar{\Lambda}_1 (W_1(x_1(t)) - D)(W_1(x_1(t)) - D)^{\mathrm{T}} \bar{\Lambda}_1^{\mathrm{T}} P_{2\mathrm{t}} e_{2\mathrm{t}}(t) \Big), \end{aligned} \tag{8.69}$$

with $e_{1\mathrm{t}}(t) = y_{\mathrm{d}} - \hat{x}_1(t)$, $e_{2\mathrm{t}}(t) = \bar{\Lambda}_1 f_1(x_1(t), \hat{x}_2(t)) - \bar{\Lambda}_1 (\dot{y}_{\mathrm{d}}(t) + De_{1\mathrm{o}}(t) - A_{1\mathrm{t}} e_{1\mathrm{t}}(t))$, $t \geq 0$. In addition, we choose $A_{1\mathrm{t}} = -10I_2$, $A_{2\mathrm{t}} = -10$, $Q_{1\mathrm{t}} = 10I_2$, $Q_{2\mathrm{t}} = 10$, and obtain from (8.33), $P_{1\mathrm{t}} = I_2/2$, $P_{2\mathrm{t}} = 1/2$. Finally, $\dot{\hat{x}}_u(t)$, $t \geq 0$, is obtained from (8.7)–(8.8) with $B = \alpha_i = 1$, $i = 1, 2, 3$, $W_{2\mathrm{s}} = [0, \; 1 - \sin(2\hat{x}_2)/2]^{\mathrm{T}}$, and $g_{1\mathrm{s}}(x_1, \hat{x}_2) = \Lambda_1 g_1(x_1, \hat{x}_2)$. The desired trajectory is chosen to be $y_{\mathrm{d}}(t) = [\, 2\sin(2t), \; 1 + \sin(2t)/2 \,]^{\mathrm{T}}$, $t \geq 0$.

As seen in Figure 8.5, the predicted trajectory $\hat{x}_1(t)$, $t \geq 0$, quickly converges to the actual trajectory $x_1(t)$, $t \geq 0$. Similarly, after a short transient, the observed trajectory $\hat{x}_2(t)$, $t \geq 0$, matches the unmeasured state $x_2(t)$, $t \geq 0$, very closely, as observed from Figure 8.6. Furthermore, the command (8.68)–(8.69), shown in Figure 8.7, proves effective,

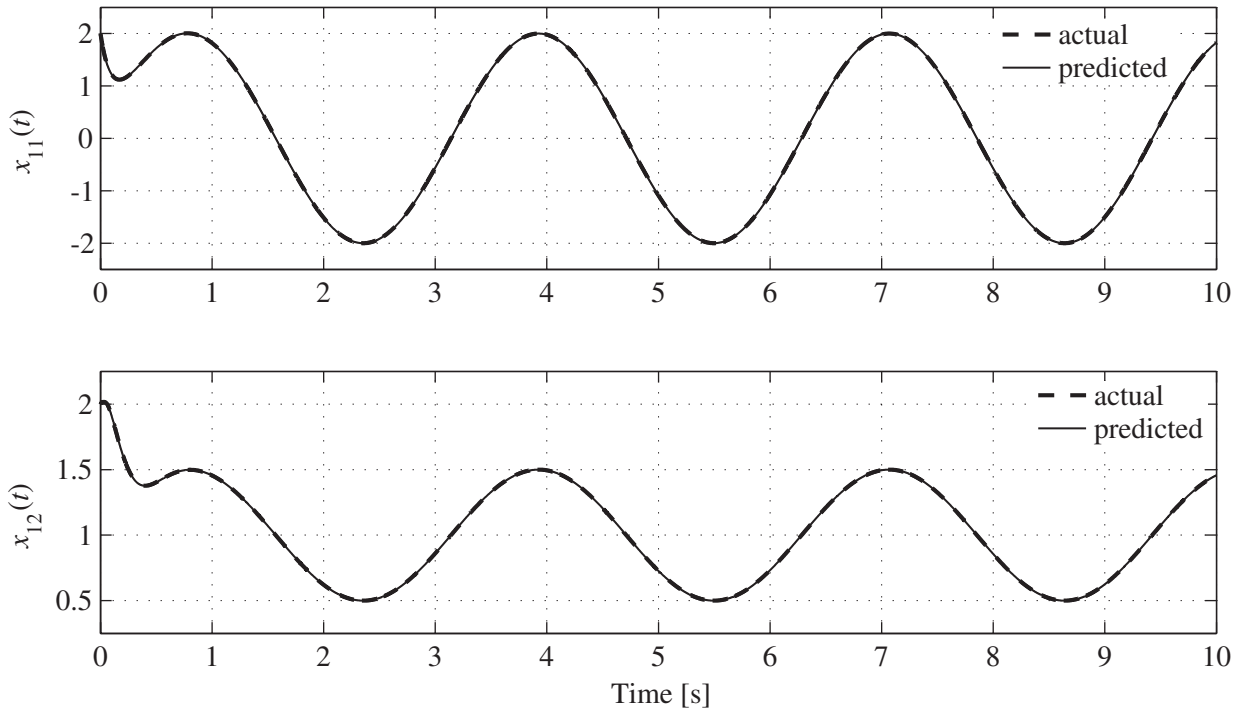

Figure 8.5: Actual and predicted trajectories.

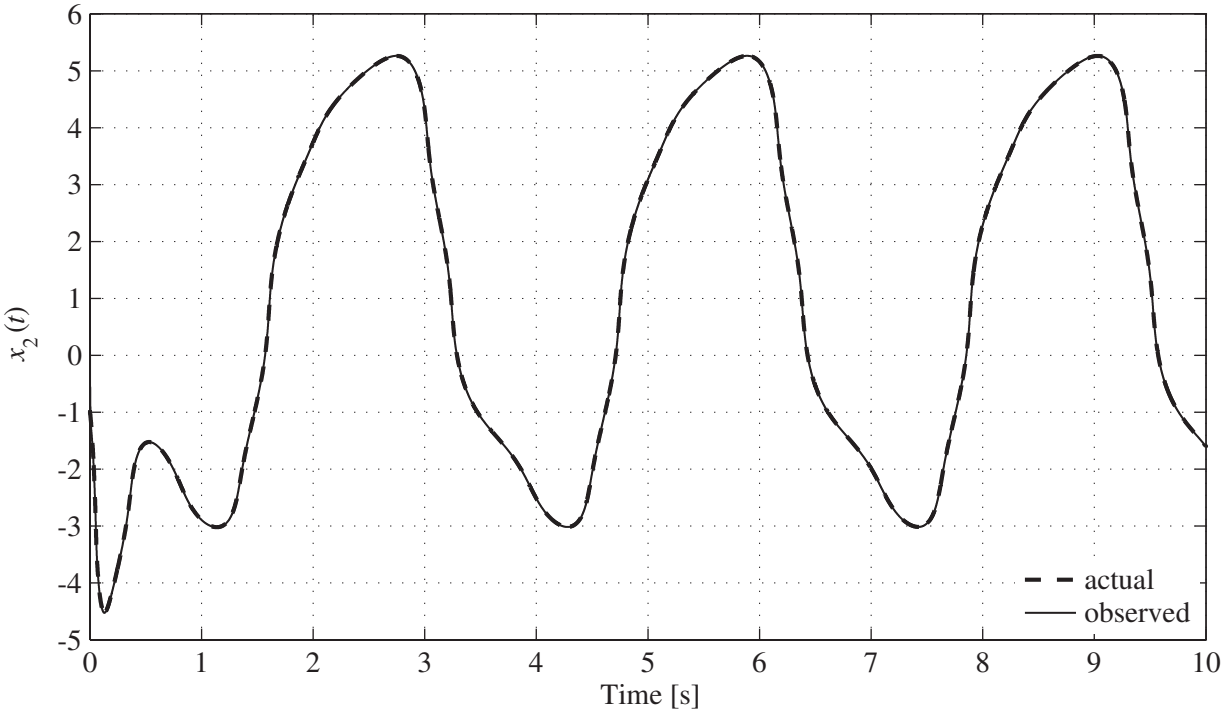

Figure 8.6: Actual and observed trajectories.

and $x_1(t)$, $t \geq 0$, converges to the desired $y_{\mathrm{d}}(t)$, $t \geq 0$, as shown in Figure 8.8.

Example 8.5.3. Consider the system

$$\dot{\eta}(t) = J(\eta(t))\nu(t), \qquad \eta(0) = \eta_0, \quad t \geq 0, \tag{8.70}$$

$$\dot{\nu}(t) = \Theta_1^* \varphi(\eta(t)) + \Theta_2^* u(t), \quad \nu(0) = \nu_0, \tag{8.71}$$

$$y(t) = \eta(t), \tag{8.72}$$

where $\eta(t) \triangleq \left[\begin{array}{ccc} \phi(t) & \theta(t) & \psi(t) \end{array} \right]^{\mathrm{T}} \in \mathbb{R}^3$, $t \geq 0$, is the measured output, $\nu(t) \in \mathbb{R}^3$, $t \geq 0$, is not measured, and $u(t) \in \mathbb{R}^2$, $t \geq 0$, is the control input applied to the system. In addition,

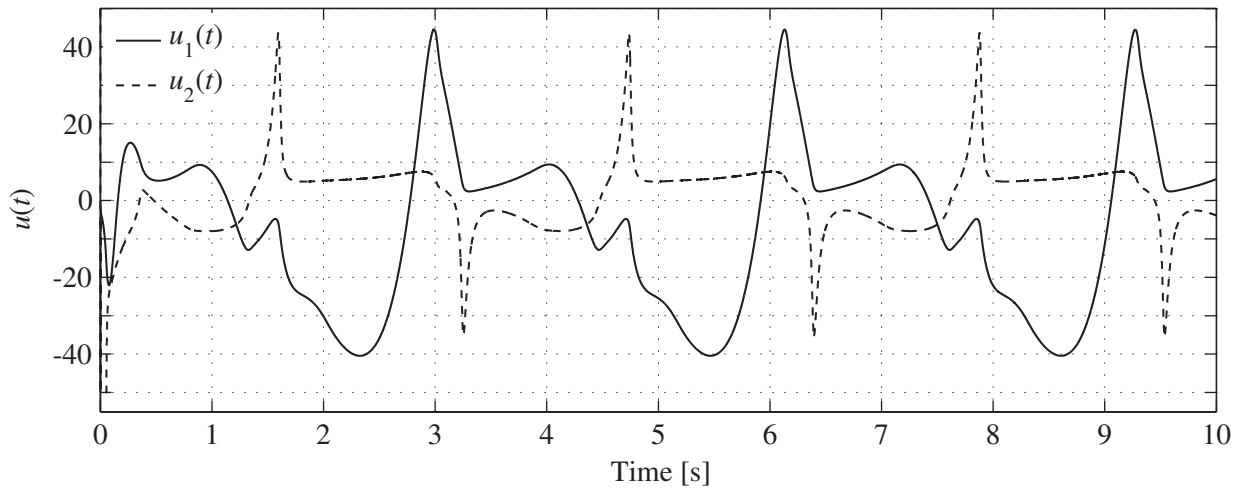

Figure 8.7: Control input.

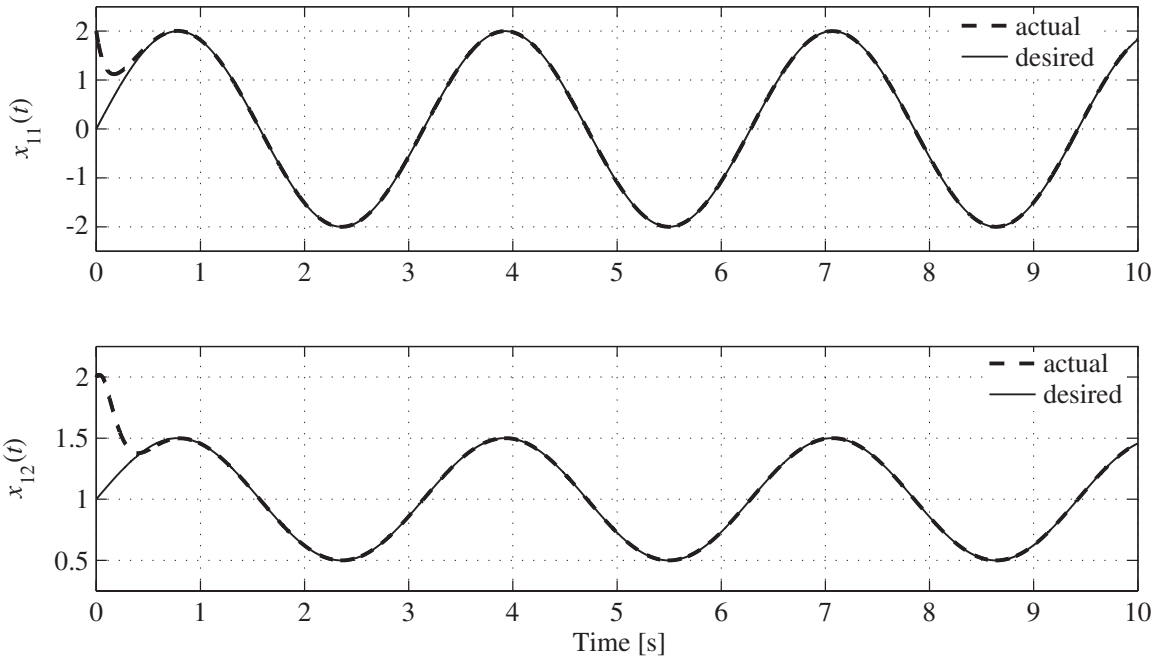

Figure 8.8: Actual and desired output trajectories.

$\Theta_1^* \in \mathbb{R}^{3\times 2}$ and $\Theta_2^* \in \mathbb{R}^{3\times 2}$ are unknown constant matrices, and

$$J(\eta) \triangleq \begin{bmatrix} 1 & \tan(\theta)\sin(\phi) & \tan(\theta)\cos(\phi) \\ 0 & \cos(\phi) & -\sin(\phi) \\ 0 & \sin(\phi)/\cos(\theta) & \cos(\phi)/\cos(\theta) \end{bmatrix}, \ \varphi(\eta) \triangleq \begin{bmatrix} \cos(\theta)\cos(\phi) \\ -\cos(\theta)\sin(\phi) \end{bmatrix}. \tag{8.73}$$

Applying the technique described in Theorem 8.3.1, we construct the following predictor-observer,

$$\dot{\hat{\eta}}(t) = J(\eta(t))\hat{\nu}(t), \qquad \hat{\eta}(0) = \eta_0, \quad t \geq 0, \tag{8.74}$$

$$\dot{\hat{\nu}}(t) = J^{-1}(\eta(t))\gamma(t) + Bu(t), \quad \hat{\nu}(0) = \hat{\nu}_0, \tag{8.75}$$

where

$$\begin{aligned} \gamma(t) = {} & P_{2\mathrm{o}}^{-1}P_{1\mathrm{o}}e_{1\mathrm{o}}(t) - A_{1\mathrm{o}}(A_{1\mathrm{o}}e_{1\mathrm{o}}(t) - e_{2\mathrm{o}}(t)) + \dot{z}(t) + A_{2\mathrm{o}}e_{2\mathrm{o}}(t) - \hat{x}_u(t) - \dot{\hat{x}}_u(t) \\ & -W_1(\eta(t),\hat{\nu}(t))(z(t) + \dot{\hat{x}}_u(t) + W_1^{\mathrm{T}}(\eta(t),\hat{\nu}(t))P_{2\mathrm{o}}e_{2\mathrm{o}}(t)/2), \quad t \geq 0, \end{aligned} \tag{8.76}$$

$$e_{1\mathrm{o}}(t) = \eta(t) - \hat{\eta}(t), \tag{8.77}$$

$$e_{2\mathrm{o}}(t) = A_{1\mathrm{o}}e_{1\mathrm{o}}(t) - z(t) + J(\eta(t))\hat{\nu}(t) - \dot{\hat{x}}_u(t), \tag{8.78}$$

$$W_1(\eta,\hat{\nu}) = \frac{\partial J(\eta)\hat{\nu}}{\partial \eta}, \tag{8.79}$$

and we choose

$$B \triangleq \begin{bmatrix} 1 & 0 & 0 \\ 0 & -1 & 0 \end{bmatrix}^{\mathrm{T}}. \tag{8.80}$$

In addition, we choose $A_{1\mathrm{o}} = -\mathrm{diag}([\ 20\ \ 10\ \ 10\ ])$, $A_{2\mathrm{o}} = 10A_{1\mathrm{o}}$, $Q_{1\mathrm{o}} = -A_{1\mathrm{o}}$, $Q_{2\mathrm{o}} = \mathrm{diag}([\ 80\ 60\ 60\ ])$, and obtain, from (8.13) and (8.14), $P_{1\mathrm{o}} = \mathrm{diag}([\ 0.5064,\ 0.5132,\ 0.5132\ ])$, $P_{2\mathrm{o}} = \mathrm{diag}([0.2764, 0.3675, 0.3675])$. The AIVSDE parameters are chosen as follows, $k_1 = 10$, $k_2 = 15$, $k_b = 1$, $\alpha_r = 0$, $\mu = 0.2$, $\gamma_{r0} = x_{10}$ and $k_{r0} = 2$.

In addition, we use the following for plant parameters,

$$\Theta_1^* = \begin{bmatrix} -2.6828 & 3.2966 \\ 9.8298 & 9.9455 \\ 0 & -20 \end{bmatrix}, \quad \Theta_2^* = \begin{bmatrix} 0.25 & 0 \\ 0 & -0.575 \\ 0 & 0 \end{bmatrix}. \tag{8.81}$$

Note that $B^{\mathrm{T}}\Theta_2^* > 0$. In addition, since $u(t) \in \mathbb{R}^2$, $t \geq 0$, we will here limit ourselves to controlling two of the three degrees of freedom of the system. In particular, we will control $\eta_{\mathrm{s}}(t) \triangleq [\, \phi(t)\ \theta(t)\,]^{\mathrm{T}}$, $t \geq 0$. This can be achieved by adjusting the control law (8.31)–(8.32) as follows,

$$u(t) = B_{\mathrm{s}} J_1^{-1}(\eta(t)) \Big(-W_{1\mathrm{s}}(\eta(t), \hat{\nu}(t)) \Lambda_2 (z(t) + \dot{\hat{x}}_u(t)) - J_3(\eta(t))\gamma(t) - j_2(t)\dot{\hat{r}}(t) + \ddot{y}_{\mathrm{d}}(t) + A_{2\mathrm{t}} e_{2\mathrm{t}}(t) - A_{1\mathrm{t}}(A_{1\mathrm{t}} e_{1\mathrm{t}}(t) - e_{2\mathrm{t}}(t)) + P_{2\mathrm{t}}^{-1} P_{1\mathrm{t}} e_{1\mathrm{t}}(t) - W_{1\mathrm{s}}(\eta(t), \hat{\nu}(t)) W_{1\mathrm{s}}^{\mathrm{T}}(\eta(t), \hat{\nu}(t)) P_{2\mathrm{t}} e_{2\mathrm{t}}(t)/2 \Big), \quad t \geq 0, \tag{8.82}$$

where $e_{1\mathrm{t}}(t) \triangleq y_{\mathrm{d}}(t) - \hat{\eta}_{\mathrm{s}}(t)$, $e_{2\mathrm{t}}(t) \triangleq J_1(\eta(t))\hat{\nu}_{\mathrm{s}}(t) - \dot{y}_{\mathrm{d}} + j_2(\eta(t))\hat{r}(t) + A_{1\mathrm{t}} e_{1\mathrm{t}}(t)$, $t \geq 0$,

$$B_{\mathrm{s}} \triangleq \begin{bmatrix} 1 & 0 \\ 0 & -1 \end{bmatrix}, \qquad J_1(\eta) \triangleq \begin{bmatrix} 1 & \tan(\theta)\sin(\phi) \\ 0 & \cos(\phi) \end{bmatrix}, \qquad \Lambda_2 \triangleq \begin{bmatrix} I_2 & 0_2 \end{bmatrix},$$

$$W_{1\mathrm{s}}(\eta, \hat{\nu}) \triangleq \begin{bmatrix} \hat{q}\tan(\theta)\cos(\phi) - \hat{r}\tan(\theta)\sin(\phi) & \hat{q}(1+\tan^2(\theta))\sin(\phi) + \hat{r}(1+\tan^2(\theta))\cos(\phi) \\ -\hat{q}\sin(\phi) - \hat{r}\cos(\phi) & 0 \end{bmatrix},$$

$$J_3(\eta) \triangleq \begin{bmatrix} 1 & \tan(\theta)\sin(\phi) & -\sin(\theta)\cos^2(\phi) \\ 0 & \cos^2(\phi) & \sin(2\phi)\cos(\theta)/2 \end{bmatrix}, \ j_2(t) \triangleq \begin{bmatrix} \tan(\theta)\cos(\phi) & -\sin(\phi) \end{bmatrix}^{\mathrm{T}}. \tag{8.83}$$

In addition, we choose $A_{1\mathrm{t}} = -5I_2$, $A_{2\mathrm{t}} = -1I_2$, $Q_{1\mathrm{t}} = 5I_2$, $Q_{2\mathrm{t}} = 5I_2$, and obtain from (8.33), $P_{1\mathrm{t}} = P_{2\mathrm{t}} = I_2/2$. Finally, $\dot{\hat{x}}_u(t)$, $t \geq 0$, is obtained from (8.8) with $W_{2\mathrm{s}}(\eta) = J(\eta)$, $\alpha_2 = \alpha_3 = 1$, and we choose $y_{\mathrm{d}}(t) = [\, 3.3\sin(t/8),\ -22\cos(t/4)\,]^{\mathrm{T}}$, $t \geq 0$. Note that the control law (8.82) is based on (8.32). The latter had to be modified for this example as the system features fewer control inputs than outputs.

The initial conditions are chosen as $\eta_0 = [\, 4\ \ -27\ 10\,]^{\mathrm{T}}$, $\nu_0 = 0_3$, $\hat{\nu}_0 = [\, 1\ 1\ 1\,]^{\mathrm{T}}$, and $z(0) = 0_3$. The trajectories $\eta(t)$ and $\nu(t)$, $t \geq 0$, are shown in Figure 8.9 and Figure 8.10, respectively. As was the case with Example 8.5.1, the observer performs well. The predicted and observed trajectories closely match the real ones, with a short transient. The command is shown in Figure 8.12. It is effective, and $\eta_{\mathrm{s}}(t)$ converges to the desired $y_{\mathrm{d}}(t)$, $t \geq 0$, as can be seen in Figure 8.11.

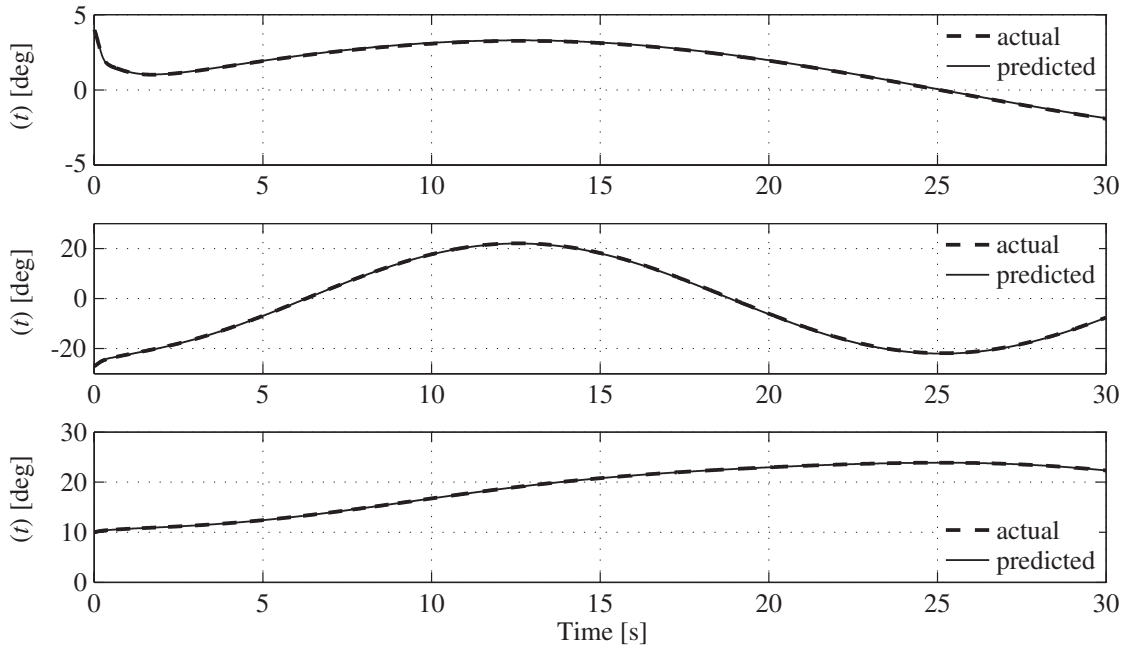

Figure 8.9: Actual and predicted trajectories of $\eta(t)$, $t \geq 0$.

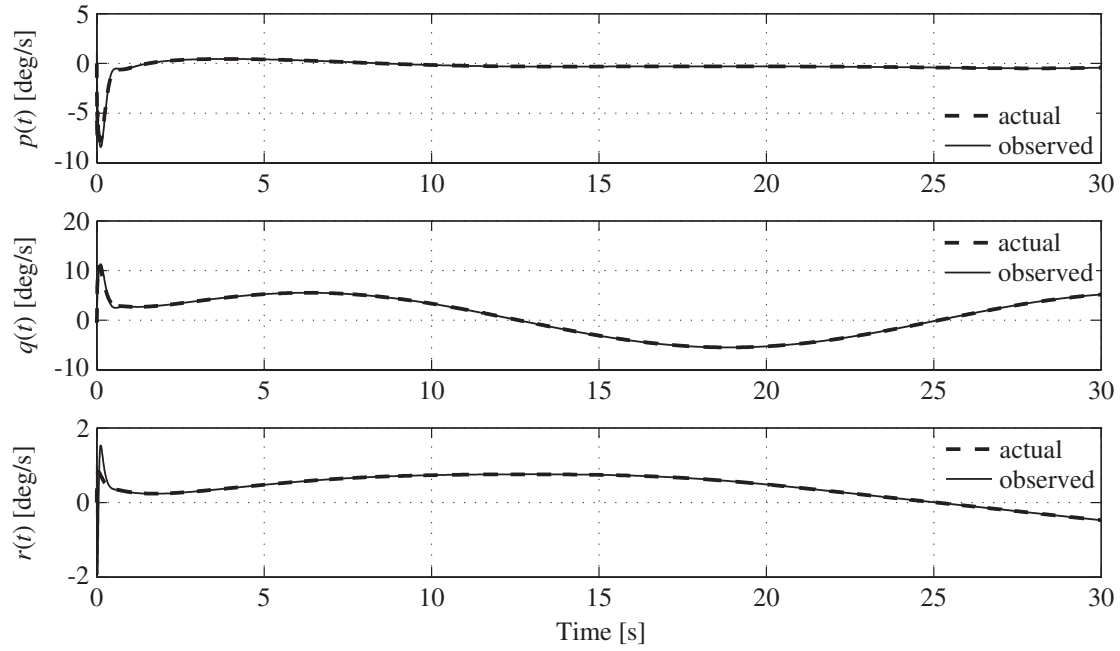

Figure 8.10: Actual and observed trajectories of $\nu(t)$, $t \geq 0$.

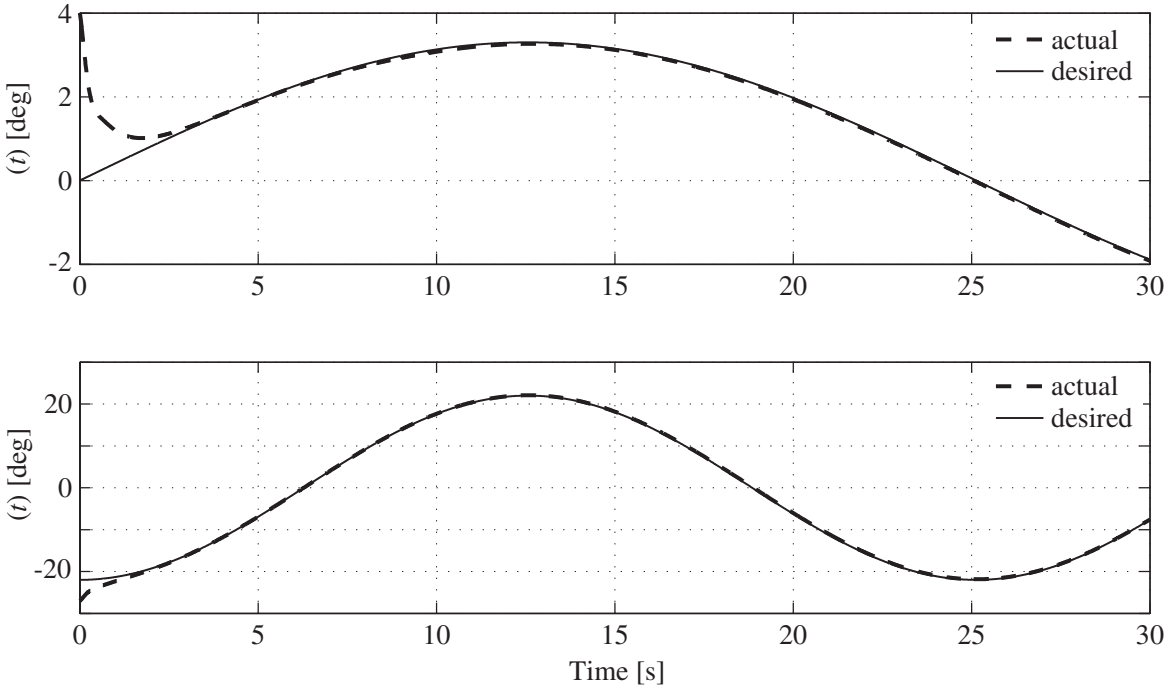

Figure 8.11: Actual and desired trajectories of $\eta_s(t)$, $t \geq 0$.

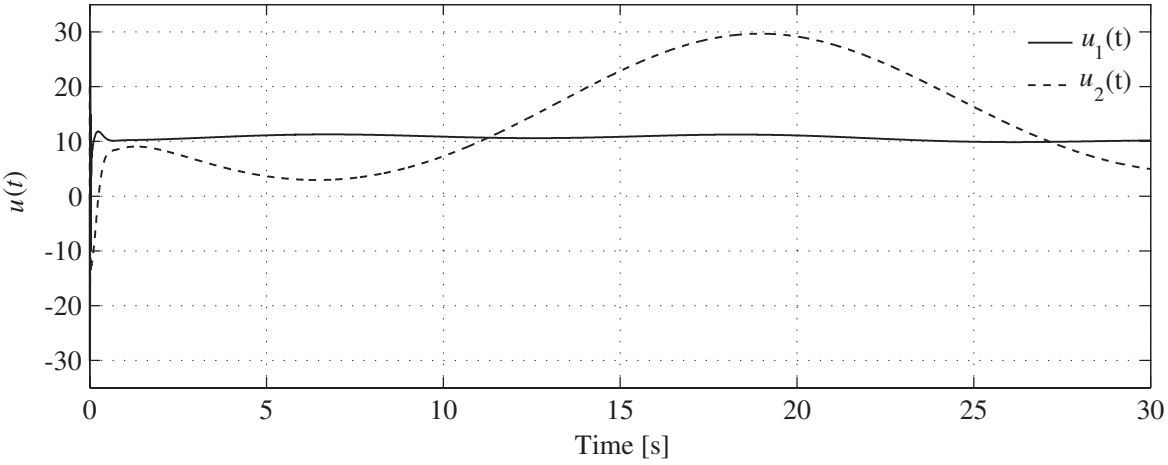

Figure 8.12: Control input.

8.6. Conclusion

This chapter presented a novel output feedback control scheme, combining an observer-predictor and a state feedback control law. In a first step, the observer-predictor is designed so that its output converges to an arbitrarily small neighborhood of the actual system's output, for any admissible control input. In a second step, a control algorithm is derived, using backstepping, to control the observer-predictor's output. The latter is shown to converge to an arbitrarily small neighborhood of a given desired trajectory. It thus follows that the actual system's output converges to the desired output. Note that the algorithm requires knowledge of the system's dynamics. This requirement will be relaxed in the following chapter.

Chapter 9

Nonlinear Predictor-Based Output Feedback Control for a Class of Uncertain Nonlinear Systems

The following results will be submitted for consideration to the 2010 IEEE American Control Conference and Transactions on Automatic Control.

9.1. Introduction

In the following, we build upon the observer-based output feedback algorithm introduced in the previous chapter. The knowledge requirements the observer in Chapter 8 relied on will be relaxed by reducing the predictor-observer to an output predictor. The approach is comparable to that introduced in [59], in which the author rely on an adaptive output predictor to solve the output feedback problem. However, we avoid resorting to an adaptive technique. More specifically, we construct an output predictor, similar to that in Chapter 8, capable of predicting the actual system's output with arbitrary accuracy, for any admissible control input. The prediction relies on a derivative estimator such as those found in [54, 56,

57], which is used to allow accurate predictions in spite of limited knowledge of the system's dynamics. Subsequently, since the predictor's state and dynamics are constructed and hence known, a simple state feedback control law is designed to control the predictor's output using backstepping. Ultimately, it is shown that the predictor's output is made to converge to the actual system's outputs and to the desired output simultaneously. It thus follows that the actual system's output approaches the desired output. Lyapunov's direct method is used to show uniform ultimate boundedness of both prediction and tracking errors.

This chapter is structured as follows. Section 9.2 describes the type of system considered. The output predictor is introduced in Section 9.3. Design of a control algorithm for this predictor is then presented in Section 9.4. Results of numerical simulations are presented in Section 9.5 and illustrate the efficacy of the algorithm. Section 9.6 concludes this chapter.

9.2. Problem Statement and Control Strategy

Consider a system of the form

$$\dot{x}(t) = f(x(t),t) + g(x(t),t)u(t), \quad x(0) = x_0, \quad t \geq 0, \tag{9.1}$$

$$y(t) = Cx(t), \tag{9.2}$$

where $x(t) \in \mathbb{R}^n$, $t \geq 0$, is the system's state vector, $y(t) \in \mathbb{R}^m$, $t \geq 0$, the measured output vector, with $m < n$, $u(t) \in \mathbb{R}^m$, $t \geq 0$, the control input, and $C = \left[\begin{array}{cc} I_m & 0_{m\times p} \end{array} \right]$, with $p = n - m$. In order to simplify the notation, define $\Lambda_i \triangleq \left[\begin{array}{cc} I_i & 0_{i\times(m-i)} \end{array} \right]$ and $\bar{\Lambda}_i \triangleq \left[\begin{array}{cc} 0_{(m-i)\times i} & I_{m-i} \end{array} \right]$, $i = 1, \ldots, m-1$. The object of the presented work is, using output measurements, to design the control input $u(t)$, $t \geq 0$, such that the output $y(t)$, $t \geq 0$, uniformly converges to an arbitrarily small neighborhood of a given $y_{\mathrm{d}}(t) \in \mathbb{R}^m$, $t \geq 0$, in

spite of limited knowledge of both $f(\cdot)$ and $g(\cdot)$.

Let $x_1(t) \triangleq y(t)$, $t \geq 0$, denote the measured states, and $x_2(t) \in \mathbb{R}^p$, $t \geq 0$, denote the unmeasured states. In the following, we will assume that the system's outputs have well defined relative degrees one or two. The technique can be extended to handle greater relative degrees, but we will limit ourselves to this case for ease of exposition. More specifically, assume that $q \leq m$ of the m measured states are of relative degree one. Ordering the measured states vector $x_1(t)$, $t \geq 0$, by increasing relative degree, we can rewrite (9.1) as

$$\dot{x}_1(t) = f_1(x_1(t), x_2(t), t) + g_1(x_1(t), x_2(t), t)u_1(t), \quad x_1(0) = x_{10}, \quad t \geq 0, \tag{9.3}$$

$$\dot{x}_2(t) = f_2(x_1(t), x_2(t), t) + g_2(x_1(t), x_2(t), t)u_2(t), \quad x_2(0) = x_{20}, \tag{9.4}$$

where $g_1(x_1(t), x_2(t), t) \triangleq \Lambda_q^{\mathrm{T}} g_{1\mathrm{s}}(x_1(t), x_2(t), t)$, $u_1(t) \in \mathbb{R}^q$ and $u_2(t) \in \mathbb{R}^{m-q}$, $t \geq 0$, so that $u(t) = \left[\begin{array}{cc} u_1^{\mathrm{T}}(t) & u_2^{\mathrm{T}}(t) \end{array} \right]^{\mathrm{T}}$, $t \geq 0$.

To solve the output feedback problem, we will construct an output predictor. This predictor is constructed so that its output approaches an arbitrarily small neighborhood of the actual system's output for any admissible control signal. In addition, we design the predictor in such a fashion that it is controllable. Then, we construct a full state feedback controller using a backstepping design. The controller is designed to drive the predictor's output to an arbitrarily small neighborhood of a given desired output trajectory.

9.3. Output Predictor Design

Building upon the approach in Chapter 8, we construct a partial state predictor of the form

$$\dot{\hat{x}}_1(t) = \varphi_1(x_1(t), v(t), t) + \gamma_1(x_1(t), v(t), t)u_1(t), \quad \hat{x}_1(0) = x_{10}, \quad t \geq 0, \tag{9.5}$$

where $\varphi_1(x_1, v, t) \in \mathbb{R}^m$ is designed so that $W_2(x_1, v, t) \triangleq \partial\varphi_1(x_1, v, t)/\partial v \in \mathbb{R}^{m\times m}$ is nonsingular for all $x_1 \in \mathbb{R}^m$, $v \in \mathbb{R}^m$ and $t \geq 0$, the matrix $\gamma_1(x_1, v, t) \triangleq \Lambda_q^{\mathrm{T}}\gamma_{1\mathrm{s}}(x_1(t), x_2(t), t) \in \mathbb{R}^{m\times q}$ is designed such that $\gamma_{1\mathrm{s}}(x_1, v, t) \in \mathbb{R}^{q\times q}$ is nonsingular for all $x_1 \in \mathbb{R}^m$, $v \in \mathbb{R}^m$ and $t \geq 0$, and the signal $v(t) \in \mathbb{R}^m$, $t \geq 0$, is to be designed so that $\hat{x}_1(t) \in \mathbb{R}^m$, $t \geq 0$, provides a predicted value of $x_1(t)$, $t \geq 0$.

For the statement of the following result, we will use the notations

$$W_1(x_1, v, t) \triangleq \frac{\partial\varphi_1(x_1, v, t)}{\partial x_1}, \qquad W_3(x_1, v, t) \triangleq \frac{\partial\varphi_1(x_1, v, t)}{\partial t}. \tag{9.6}$$

Theorem 9.3.1. Consider the system given by (9.1)–(9.2). Assume that a continuously differentiable signal $z(t)$ is available such that $z(t) = \dot{y}(t) - \dot{\hat{x}}_u(t) - \epsilon(t)$, with $\|\epsilon(t)\| \leq \sqrt{\varepsilon/3}$, $\varepsilon > 0$, $t \geq 0$, where $\dot{\hat{x}}_u(t) \triangleq \dot{\hat{x}}_{u1}(t) + \dot{\hat{x}}_{u2}(t)$, $t \geq 0$, and $\hat{x}_{u1}(t)$ and $\hat{x}_{u2}(t)$, $t \geq 0$, are obtained from

$$\dot{\hat{x}}_{u1}(t) = \gamma_1(x_1(t), v(t), t)u_1(t) - \alpha_1\hat{x}_{u1}(t), \qquad \hat{x}_{u1}(0) = 0_m, \quad t \geq 0, \tag{9.7}$$

$$\ddot{\hat{x}}_{u2}(t) = W_2(x_1(t), v(t), t)\gamma_2(x_1(t), v(t), t)u_2(t) - \alpha_2\dot{\hat{x}}_{u2}(t) - \alpha_3\hat{x}_{u2}(t),\ \dot{\hat{x}}_{u2}(0) = \hat{x}_{u2}(0) = 0_m, \tag{9.8}$$

where α_1, α_2, $\alpha_3 > 0$, the matrix $\gamma_2(x_1, v, t) \in \mathbb{R}^{p\times(m-q)}$ is chosen so that $\bar{\Lambda}_q W_2(x_1(t), v(t), t)$ $\gamma_2(x_1(t), v(t), t) \in \mathbb{R}^{(m-q)\times(m-q)}$ is nonsingular for all $x_1 \in \mathbb{R}^m$, $v \in \mathbb{R}^m$, and $t \geq 0$. Then, consider the following state predictor,

$$\dot{\hat{x}}_1(t) = \varphi_1(x_1(t), v(t), t) + \gamma_1(x_1(t), v(t), t)u_1(t), \quad \hat{x}_1(0) = x_{10}, \quad t \geq 0, \tag{9.9}$$

$$\dot{v}(t) = \varphi_2(t) + \gamma_2(x_1(t), v(t), t)u_2(t), \qquad v(0) = 0_m, \tag{9.10}$$

where

$$\varphi_2(t) \triangleq W_2^{-1}(x_1(t), v(t), t)\Big[P_{2\mathrm{o}}^{-1}P_{1\mathrm{o}}e_{1\mathrm{o}}(t) - A_{1\mathrm{o}}(A_{1\mathrm{o}}e_{1\mathrm{o}}(t) - e_{2\mathrm{o}}(t)) + \dot{z}(t) - W_3(x_1(t), v(t), t)$$

$$-W_1(x_1(t),v(t),t)\Big(z(t)+\dot{\hat{x}}_u(t)+\frac{1}{2}W_1^{\mathrm{T}}(x_1(t),v(t),t)P_{2\mathrm{o}}e_{2\mathrm{o}}(t)\Big)+A_{2\mathrm{o}}e_{2\mathrm{o}}(t)-\alpha_1\dot{\hat{x}}_{u1}(t)$$
$$-\alpha_2\dot{\hat{x}}_{u2}(t)-\alpha_3\hat{x}_{u2}(t)\Big],\quad t\geq 0, \tag{9.11}$$

with $A_{1\mathrm{o}}$ and $A_{2\mathrm{o}}$ chosen Hurwitz,

$$e_{1\mathrm{o}}(t)\triangleq x_1(t)-\hat{x}_1(t),\quad t\geq 0, \tag{9.12}$$

$$e_{2\mathrm{o}}(t)\triangleq \varphi_1(x_1(t),v(t),t)-\dot{\hat{x}}_{u2}(t)+\alpha_1\hat{x}_{u1}(t)+A_{1\mathrm{o}}e_{1\mathrm{o}}(t)-z(t), \tag{9.13}$$

the matrices $P_{1\mathrm{o}}$, $P_{2\mathrm{o}}\in\mathbb{R}^{m\times m}$ are obtained from the following Riccati equations,

$$A_{1\mathrm{o}}^{\mathrm{T}}P_{1\mathrm{o}}+P_{1\mathrm{o}}A_{1\mathrm{o}}+Q_{1\mathrm{o}}+P_{1\mathrm{o}}^2=0, \tag{9.14}$$

$$A_{2\mathrm{o}}^{\mathrm{T}}P_{2\mathrm{o}}+P_{2\mathrm{o}}A_{2\mathrm{o}}+Q_{2\mathrm{o}}+P_{2\mathrm{o}}A_{1\mathrm{o}}A_{1\mathrm{o}}^{\mathrm{T}}P_{2\mathrm{o}}=0, \tag{9.15}$$

and $Q_{1\mathrm{o}}\triangleq R_1^{\mathrm{T}}R_1>0$, $Q_{2\mathrm{o}}\triangleq R_2^{\mathrm{T}}R_2>0$, are chosen such that

$$H_{1\mathrm{o}}\triangleq\begin{bmatrix}A_{1\mathrm{o}} & I_m\\ -Q_{1\mathrm{o}} & -A_{1\mathrm{o}}^{\mathrm{T}}\end{bmatrix},\quad H_{2\mathrm{o}}\triangleq\begin{bmatrix}A_{2\mathrm{o}} & A_{1\mathrm{o}}A_{1\mathrm{o}}^{\mathrm{T}}\\ -Q_{2\mathrm{o}} & -A_{2\mathrm{o}}^{\mathrm{T}}\end{bmatrix}, \tag{9.16}$$

have no eigenvalues on the imaginary axis and $(A_{1\mathrm{o}},R_1)$, $(A_{2\mathrm{o}},R_2)$ are both observable. Finally, define

$$N_{\mathrm{o}}\triangleq\begin{bmatrix}Q_{1\mathrm{o}}^{-1}P_{1\mathrm{o}} & 0_{m\times m}\\ 0_{m\times m} & Q_{2\mathrm{o}}^{-1}P_{2\mathrm{o}}\end{bmatrix}, \tag{9.17}$$

and let $\lambda_{\max}(N_{\mathrm{o}})$ denote the maximum eigenvalue of N_{o}. Then the solution $v(t)$, $t\geq 0$, to (9.10) guarantees uniform ultimate boundedness of (9.12)–(9.13) with an ultimate bound given by $\mathcal{D}_{\mathrm{o}}\triangleq\{(e_{1\mathrm{o}},e_{2\mathrm{o}}):e_{1\mathrm{o}}^{\mathrm{T}}P_{1\mathrm{o}}e_{1\mathrm{o}}+e_{2\mathrm{o}}^{\mathrm{T}}P_{2\mathrm{o}}e_{2\mathrm{o}}\leq\varepsilon\ \lambda_{\max}(N_{\mathrm{o}})\}$.

Proof. The time derivative of the prediction error $e_{1\mathrm{o}}(t)$, $t\geq 0$, is given by

$$\dot{e}_{1\mathrm{o}}(t)=f_1(x_1(t),x_2(t),t)+g_1(x_1(t),x_2(t),t)u_1(t)-\varphi_1(x_1(t),v(t),t)-\gamma_1(x_1(t),v(t),t)u_1(t),$$
$$t\geq 0, \tag{9.18}$$

which, using $\dot{y}(t) = z(t) + \dot{\hat{x}}_u(t) + \epsilon(t)$, $\dot{\hat{x}}_u(t) = \dot{\hat{x}}_{u1}(t) + \dot{\hat{x}}_{u2}(t)$, $t \geq 0$, and (9.7), can be rewritten as

$$\begin{aligned}\dot{e}_{1\mathrm{o}}(t) &= z(t) + \dot{\hat{x}}_u(t) + \epsilon(t) - \varphi_1(x_1(t), v(t), t) - \gamma_1(x_1(t), v(t), t)u_1(t)\\ &= z(t) + \dot{\hat{x}}_{u2}(t) - \alpha_1\hat{x}_{u1}(t) + \epsilon(t) - \varphi_1(x_1(t), v(t), t), \quad t \geq 0. \end{aligned} \tag{9.19}$$

Furthermore, using (9.13), we obtain

$$\begin{aligned}\dot{e}_{1\mathrm{o}}(t) &= z(t) + \dot{\hat{x}}_{u2}(t) - \alpha_1\hat{x}_{u1}(t) + \epsilon(t) - e_{2\mathrm{o}}(t) - \dot{\hat{x}}_{u2}(t) + \alpha_1\hat{x}_{u1}(t) + A_{1\mathrm{o}}e_{1\mathrm{o}}(t) - z(t)\\ &= A_{1\mathrm{o}}e_{1\mathrm{o}}(t) - e_{2\mathrm{o}}(t) + \epsilon(t), \quad t \geq 0. \end{aligned} \tag{9.20}$$

The time derivative of the error $e_{2\mathrm{o}}(t)$, $t \geq 0$, is of the form

$$\begin{aligned}\dot{e}_{2\mathrm{o}}(t) &= A_{1\mathrm{o}}\dot{e}_{1\mathrm{o}}(t) + W_1(x_1(t), v(t), t)\dot{x}_1(t) + W_2(x_1(t), v(t), t)\dot{v}(t) + W_3(x_1(t), v(t), t)\\ &\quad -\dot{z}(t) - W_2(x_1(t), v(t), t)\gamma_2(x_1(t), v(t), t)u_2(t) + \alpha_1\dot{\hat{x}}_{u1}(t) + \alpha_2\dot{\hat{x}}_{u2}(t) + \alpha_3\hat{x}_{u2}(t)\\ &= A_{1\mathrm{o}}\epsilon(t) + A_{1\mathrm{o}}(A_{1\mathrm{o}}e_{1\mathrm{o}}(t) - e_{2\mathrm{o}}(t)) - \dot{z}(t) + W_1(x_1(t), v(t), t)(z(t) + \dot{\hat{x}}_u(t) + \epsilon(t))\\ &\quad +W_3(x_1(t), v(t), t) - W_2(x_1(t), v(t), t)\gamma_2(x_1(t), v(t), t)u_2(t) + W_2(x_1(t), v(t), t)\dot{v}(t)\\ &\quad +\alpha_1\dot{\hat{x}}_{u1}(t) + \alpha_2\dot{\hat{x}}_{u2}(t) + \alpha_3\hat{x}_{u2}(t), \quad t \geq 0. \end{aligned} \tag{9.21}$$

Substituting (9.10) into (9.21), we obtain

$$\begin{aligned}\dot{e}_{2\mathrm{o}}(t) &= A_{1\mathrm{o}}\epsilon(t) + A_{1\mathrm{o}}(A_{1\mathrm{o}}e_{1\mathrm{o}}(t) - e_{2\mathrm{o}}(t)) - \dot{z}(t) + W_1(x_1(t), v(t), t)(z(t) + \dot{\hat{x}}_u(t) + \epsilon(t))\\ &\quad +W_3(x_1(t), v(t), t) - W_2(x_1(t), v(t), t)\gamma_2(x_1(t), v(t), t)u_2(t) + P_{2\mathrm{o}}^{-1}P_{1\mathrm{o}}e_{1\mathrm{o}}(t) + \dot{z}(t)\\ &\quad +\alpha_1\dot{\hat{x}}_{u1}(t) + \alpha_2\dot{\hat{x}}_{u2}(t) + \alpha_3\hat{x}_{u2}(t) - A_{1\mathrm{o}}(A_{1\mathrm{o}}e_{1\mathrm{o}}(t) - e_{2\mathrm{o}}(t)) - W_3(x_1(t), v(t), t)\\ &\quad -W_1(x_1(t), v(t), t)\Big(z(t) + \dot{\hat{x}}_u(t) + \frac{1}{2}W_1^{\mathrm{T}}(x_1(t), v(t), t)P_{2\mathrm{o}}e_{2\mathrm{o}}(t)\Big) + A_{2\mathrm{o}}e_{2\mathrm{o}}(t)\\ &\quad -\alpha_1\dot{\hat{x}}_{u1}(t) - \alpha_2\dot{\hat{x}}_{u2}(t) - \alpha_3\hat{x}_{u2}(t) + W_2(x_1(t), v(t), t)\gamma_2(x_1(t), v(t), t)u_2(t)\\ &= P_{2\mathrm{o}}^{-1}P_{1\mathrm{o}}e_{1\mathrm{o}}(t) + A_{2\mathrm{o}}e_{2\mathrm{o}}(t) - \frac{1}{2}W_1(x_1(t), v(t), t)W_1^{\mathrm{T}}(x_1(t), v(t), t)P_{2\mathrm{o}}e_{2\mathrm{o}}(t)\\ &\quad +(W_1(x_1(t), v(t), t) + A_{1\mathrm{o}})\epsilon(t), \quad t \geq 0. \end{aligned} \tag{9.22}$$

Next, we consider the following Lyapunov function candidate,

$$V(e_{1o}, e_{2o}) = e_{1o}^{T} P_{1o} e_{1o} + e_{2o}^{T} P_{2o} e_{2o}, \tag{9.23}$$

where P_{1o}, $P_{2o} > 0$ are obtained from (9.14) and (9.15), respectively. The time derivative of (9.23) along the trajectories of (9.20) and (9.22) is given by

$$\begin{aligned}
\dot{V}(t) =& e_{1o}^{T}(t)(A_{1o}^{T}P_{1o} + P_{1o}A_{1o})e_{1o}(t) + e_{2o}^{T}(t)(A_{2o}^{T}P_{2o} + P_{2o}A_{2o})e_{2o}(t) - 2e_{1o}^{T}(t)P_{1o}(e_{2o}(t) - \epsilon(t)) \\
&+ 2e_{2o}^{T}(t)P_{2o}\Big[(W_1(x_1(t), v(t), t) + A_{1o})\epsilon(t) - W_1(x_1(t), v(t), t)W_1^{T}(x_1(t), v(t), t)P_{2o}e_{2o}(t)/2 \\
&+ P_{2o}^{-1}P_{1o}e_{1o}(t)\Big] \\
=& e_{2o}^{T}(t)P_{2o}W_1(x_1(t), v(t), t)(2\epsilon(t) - W_1^{T}(x_1(t), v(t), t)P_{2o}e_{2o}(t)) + 2e_{2o}^{T}(t)P_{2o}A_{1o}\epsilon(t) \\
&- e_{1o}^{T}(t)(Q_{1o} + P_{1o}^{2})e_{1o}(t) - e_{2o}^{T}(t)(Q_{2o} + P_{2o}A_{1o}A_{1o}^{T}P_{2o})e_{2o}(t) + 2e_{1o}^{T}(t)P_{1o}\epsilon(t),\ t \geq 0.
\end{aligned} \tag{9.24}$$

Using the completion of the square rule, we obtain

$$2e_{1o}^{T}P_{1o}\epsilon = -(P_{1o}e_{1o} - \epsilon)^{T}(P_{1o}e_{1o} - \epsilon) + e_{1o}^{T}P_{1o}^{2}e_{1o} + \epsilon^{T}\epsilon, \tag{9.25}$$

$$2e_{2o}^{T}P_{2o}A_{1o}\epsilon = -(A_{1o}^{T}P_{2o}e_{2o} - \epsilon)^{T}(A_{1o}^{T}P_{2o}e_{2o} - \epsilon) + e_{2o}^{T}P_{2o}A_{1o}A_{1o}^{T}P_{2o}e_{2o} + \epsilon^{T}\epsilon, \tag{9.26}$$

$$\begin{aligned}
2e_{2o}^{T}P_{2o}W_1(x_1, v, t)\epsilon =& e_{2o}^{T}P_{2o}W_1(x_1, v, t)W_1^{T}(x_1, v, t)P_{2o}e_{2o} + \epsilon^{T}\epsilon \\
&- \left(W_1^{T}(x_1, v, t)P_{2o}e_{2o} - \epsilon\right)^{T}\left(W_1^{T}(x_1, v, t)P_{2o}e_{2o} - \epsilon\right).
\end{aligned} \tag{9.27}$$

It follows that

$$\begin{aligned}
\dot{V}(t) \leq& -e_{1o}^{T}(t)(Q_{1o} + P_{1o}^{2})e_{1o}(t) + e_{1o}^{T}(t)P_{1o}^{2}e_{1o}(t) - e_{2o}^{T}(t)(Q_{2o} + P_{2o}A_{1o}A_{1o}^{T}P_{2o})e_{2o}(t) \\
&+ e_{2o}^{T}(t)P_{2o}A_{1o}A_{1o}^{T}P_{2o}e_{2o}(t) + e_{2o}^{T}(t)P_{2o}W_1(x_1(t), v(t), t)W_1^{T}(x_1(t), v(t), t)P_{2o}e_{2o}(t) \\
&- e_{2o}^{T}(t)P_{2o}W_1(x_1(t), v(t), t)W_1^{T}(x_1(t), v(t), t)P_{2o}e_{2o}(t) + 3\epsilon^{T}(t)\epsilon(t) \\
\leq& -e_{1o}^{T}(t)Q_{1o}e_{1o}(t) - e_{2o}^{T}(t)Q_{2o}e_{2o}(t) + \varepsilon, \quad t \geq 0.
\end{aligned} \tag{9.28}$$

Hence, $\dot{V}(t)$, $t \geq 0$, is strictly negative outside of $\left\{(e_{1\mathrm{o}}, e_{2\mathrm{o}}) : e_{1\mathrm{o}}^{\mathrm{T}} Q_{1\mathrm{o}} e_{1\mathrm{o}} + e_{2\mathrm{o}}^{\mathrm{T}} Q_{2\mathrm{o}} e_{2\mathrm{o}} \leq \varepsilon\right\}$, which allows to conclude ultimate boundedness of $(e_{1\mathrm{o}}(t), e_{2\mathrm{o}}(t))$, $t \geq 0$ ([44,88]). In addition, the ultimate bound can be characterized by $\alpha \triangleq \min(e_{1\mathrm{o}}^{\mathrm{T}} P_{1\mathrm{o}} e_{1\mathrm{o}} + e_{2\mathrm{o}}^{\mathrm{T}} P_{2\mathrm{o}} e_{2\mathrm{o}})$, subject to the constraint $e_{1\mathrm{o}}^{\mathrm{T}} Q_{1\mathrm{o}} e_{1\mathrm{o}} + e_{2\mathrm{o}}^{\mathrm{T}} Q_{2\mathrm{o}} e_{2\mathrm{o}} = \varepsilon$. This constrained minimization problem is easily solved using Lagrange multipliers, yielding $\alpha = \varepsilon \lambda_{\max}(N_{\mathrm{o}})$, which proves convergence of the error trajectories to $\mathcal{D}_{\mathrm{o}}$ and concludes this proof. $\square$

Remark 9.3.1. Note that the result in Theorem 9.3.1 does not require knowledge of the dimension of the system state, n.

Theorem 9.3.1 proposes a fairly general form of output predictor, given by (9.9)–(9.10). Provided that the assumptions are verified, it is guaranteed to generate an arbitrarily accurate prediction $\hat{x}_1(t)$ of $x_1(t)$, $t \geq 0$, for any admissible input signal $u(t)$, $t \geq 0$. The prediction algorithm is designed to handle a wide class of nonlinear systems, and, as a consequence, is somewhat complex. It can however be specialized and accordingly simplified, as described in the following corollary.

Corollary 9.3.1. Consider the system given by (9.1)–(9.2), and assume that a continuously differentiable signal $z(t)$ is available such that $z(t) = \dot{y}(t) - \dot{\hat{x}}_u(t) - \epsilon(t)$, with $\|\epsilon(t)\| \leq \sqrt{\varepsilon/2}$, $\varepsilon > 0$, $t \geq 0$, where $\dot{\hat{x}}_u(t) \triangleq \dot{\hat{x}}_{u1}(t) + \dot{\hat{x}}_{u2}(t)$, $t \geq 0$, and $\hat{x}_{u1}(t)$ and $\hat{x}_{u2}(t)$, $t \geq 0$, are obtained from

$$\dot{\hat{x}}_{u1}(t) = B_1 u_1(t) - \alpha_1 \hat{x}_{u1}(t), \qquad \hat{x}_{u1}(0) = 0_m, \qquad t \geq 0, \tag{9.29}$$

$$\ddot{\hat{x}}_{u2}(t) = B_2 u_2(t) - \alpha_2 \dot{\hat{x}}_{u2}(t) - \alpha_3 \hat{x}_{u2}(t), \quad \dot{\hat{x}}_{u2}(0) = \hat{x}_{u2}(0) = 0_m, \tag{9.30}$$

where α_1, α_2, $\alpha_3 > 0$, $B_1 \triangleq \left[\begin{array}{cc} B_{1\mathrm{s}}^{\mathrm{T}} & 0_{q \times (m-q)} \end{array}\right]^{\mathrm{T}} \in \mathbb{R}^{m \times q}$ and $B_2 \in \mathbb{R}^{m \times (m-q)}$, are designed so that $B_{1\mathrm{s}} \in \mathbb{R}^{q \times q}$ and $\bar{\Lambda}_q B_2 \in \mathbb{R}^{(m-q) \times (m-q)}$ are nonsingular. Consider the following output

predictor,

$$\dot{\hat{x}}_1(t) = v(t) + B_1 u_1(t), \quad \hat{x}_1(0) = x_{10}, \quad t \geq 0, \tag{9.31}$$

$$\dot{v}(t) = \varphi_2(t) + B_2 u_2(t), \quad v(0) = 0_m, \tag{9.32}$$

with

$$\varphi_2(t) = P_{2\mathrm{o}}^{-1} P_{1\mathrm{o}} e_{1\mathrm{o}}(t) - A_{1\mathrm{o}}(A_{1\mathrm{o}} e_{1\mathrm{o}}(t) - e_{2\mathrm{o}}(t)) + \dot{z}(t) + A_{2\mathrm{o}} e_{2\mathrm{o}}(t) - \alpha_1 \dot{\hat{x}}_{u1}(t) - \alpha_2 \dot{\hat{x}}_{u2}(t)$$
$$-\alpha_3 \hat{x}_{u2}(t), \quad t \geq 0, \tag{9.33}$$

where $e_{1\mathrm{o}}(t)$, $e_{2\mathrm{o}}(t)$, $t \geq 0$, are given by (9.12)–(9.13), with $\varphi_1(v) \triangleq v$, $A_{1\mathrm{o}}$, $A_{2\mathrm{o}}$ are chosen Hurwitz, the matrices $P_{1\mathrm{o}}$, $P_{2\mathrm{o}} \in \mathbb{R}^{m \times m}$ are obtained from (9.14)–(9.15), with $Q_{1\mathrm{o}}$, $Q_{2\mathrm{o}}$, chosen as described in Theorem 9.3.1. The solution $v(t)$, $t \geq 0$, to (9.32) guarantees ultimate boundedness of the tracking errors $(e_{1\mathrm{o}}(t), e_{2\mathrm{o}}(t))$ with an ultimate bound given by $\mathcal{D}_{\mathrm{o}}$.

Proof. After appropriate substitutions, the time derivative of (9.12)–(9.13) yields the following error dynamics,

$$\dot{e}_{1\mathrm{o}}(t) = A_{1\mathrm{o}} e_{1\mathrm{o}}(t) - e_{2\mathrm{o}}(t) + \epsilon(t), \qquad e_{1\mathrm{o}}(0) = 0_m, \quad t \geq 0. \tag{9.34}$$

$$\dot{e}_{2\mathrm{o}}(t) = P_{2\mathrm{o}}^{-1} P_{1\mathrm{o}} e_{1\mathrm{o}}(t) + A_{2\mathrm{o}} e_{2\mathrm{o}}(t) + A_{1\mathrm{o}} \epsilon(t), \quad e_{2\mathrm{o}}(0) = e_{2\mathrm{o}0}. \tag{9.35}$$

Selecting the Lyapunov function candidate given by (9.23), its time derivative long the trajectories of (9.34)–(9.35) is given by

$$\dot{V}(t) = -e_{1\mathrm{o}}^{\mathrm{T}}(t)(Q_{1\mathrm{o}} + P_{1\mathrm{o}}^2) e_{1\mathrm{o}}(t) - e_{2\mathrm{o}}^{\mathrm{T}}(t)(Q_{2\mathrm{o}} + P_{2\mathrm{o}} A_{1\mathrm{o}} A_{1\mathrm{o}}^{\mathrm{T}} P_{2\mathrm{o}}) e_{2\mathrm{o}}(t) + 2 e_{1\mathrm{o}}^{\mathrm{T}}(t) P_{1\mathrm{o}} \epsilon(t)$$
$$+2 e_{2\mathrm{o}}^{\mathrm{T}}(t) P_{2\mathrm{o}} A_{1\mathrm{o}} \epsilon(t), \quad t \geq 0. \tag{9.36}$$

Substituting (9.25)–(9.26) into (9.36), we obtain

$$\dot{V}(t) \leq -e_{1\mathrm{o}}^{\mathrm{T}}(t) Q_{1\mathrm{o}} e_{1\mathrm{o}}(t) - e_{2\mathrm{o}}^{\mathrm{T}}(t) Q_{2\mathrm{o}} e_{2\mathrm{o}}(t) + \varepsilon, \quad t \geq 0, \tag{9.37}$$

which, following the same reasoning as that at the conclusion of the proof of Theorem 9.3.1, allows to conclude ultimate boundedness of $(e_{1\mathrm{o}}(t), e_{2\mathrm{o}}(t))$, $t \geq 0$, and convergence of the error trajectories to $\mathcal{D}_{\mathrm{o}}$. $\square$

9.4. Nonlinear Controller Design

In the previous section, we designed an output predictor, which provides a prediction $\hat{x}_1(t)$ of $x_1(t)$, $t \geq 0$. This prediction can be made arbitrarily accurate, for any admissible input $u(t)$, $t \geq 0$. Next, we will design the input $u(t)$, $t \geq 0$, so that the origin of the tracking error dynamics is Lyapunov stable and $e_{1\mathrm{t}}(t) \triangleq y_{\mathrm{d}} - \hat{x}_1(t)$, $t \geq 0$, asymptotically converges to a neighborhood of the origin, uniformly in time. More specifically, we design a controller for the following system,

$$\dot{\hat{x}}_1(t) = \varphi_1(x_1(t), v(t), t) + \gamma_1(x_1(t), v(t), t)u_1(t), \quad \hat{x}_1(0) = x_{10}, \quad t \geq 0, \tag{9.38}$$

$$\dot{v}(t) = \varphi_2(t) + \gamma_2(x_1(t), v(t), t)u_2(t), \qquad v(0) = 0_m, \tag{9.39}$$

where $\varphi_2(t)$, $t \geq 0$, is given by (9.11). In the following, we require that the contribution of the control signal $u(t)$, $t \geq 0$, to the predictor's dynamics be topologically equivalent to its contribution to the actual system's dynamics. This is achieved by requiring that $u_1^{\mathrm{T}}\gamma_1^{\mathrm{T}}(x_1, v, t)g_1(x_1, x_2, t)u_1 > 0$ and $u_2\gamma_2^{\mathrm{T}}(x_1, v, t)W_2^{\mathrm{T}}(x_1, v, t)(\partial f_1(x_1, x_2, t)/\partial x_2)g_2(x_1, x_2, t)$ $u_2 > 0$, for all $u \in \mathbb{R}^m \setminus \{0\}$, $x_1 \in \mathbb{R}^m$, $x_2 \in \mathbb{R}^p$, $v \in \mathbb{R}^m$, and $t \geq 0$. This requirement is verified if $\gamma_1(\cdot)$ and $\gamma_2(\cdot)$ are constructed such that the symmetric part of both $\gamma_1^{\mathrm{T}}(x_1, v, t)g_1(x_1, x_2, t) \in \mathbb{R}^{q\times q}$ and $\gamma_2^{\mathrm{T}}(x_1, v, t)W_2^{\mathrm{T}}(x_1, v, t)(\partial f_1(x_1, x_2, t)/\partial x_2)g_2(x_1, x_2, t) \in \mathbb{R}^{(m-q)\times(m-q)}$ is positive definite for all $x_1 \in \mathbb{R}^m$, $x_2 \in \mathbb{R}^p$, $v \in \mathbb{R}^m$, and $t \geq 0$. Note that in the scalar case, the assumption on $\gamma_1(\cdot)$ is equivalent to assuming that $\gamma_1(x_1, v, t)$ and

$g_1(x_1, x_2, t)$ share the same sign for all $x_1 \in \mathbb{R}^m$, $x_2 \in \mathbb{R}^p$, $v \in \mathbb{R}^m$, and $t \geq 0$. This assumption is similar to that introduced in [58], where the authors assume knowledge of the signs of the leading minors of $g(x, t)$.

The problem of designing a control algorithm for system (9.38)–(9.39) can be solved using a backstepping procedure, as described in [10]. This type of approach leads to the following result.

Theorem 9.4.1. Consider system (9.38)–(9.39), and the control input $u(t) = [\, u_1^{\mathrm{T}}(t), u_2^{\mathrm{T}}(t)\,]^{\mathrm{T}}$, $t \geq 0$, given by

$$u_1(t) = \gamma_{1\mathrm{s}}^{-1}(x_1(t), v(t), t)\Lambda_q(\dot{y}_{\mathrm{d}}(t) - A_{1\mathrm{t}}e_{1\mathrm{t}}(t) - \varphi_1(x_1(t), v(t), t)), \quad t \geq 0, \tag{9.40}$$

$$\begin{aligned} u_2(t) = {} & (\bar{\Lambda}_q W_2(x_1(t), v(t), t)\gamma_2(x_1(t), v(t), t))^{-1}\Big[P_{2\mathrm{t}}^{-1}\bar{\Lambda}_q P_{1\mathrm{t}}e_{1\mathrm{t}}(t) - \bar{\Lambda}_q\Big(W_3(x_1(t), v(t), t) \\ & + W_2(x_1(t), v(t), t)\varphi_2(t) + W_1(x_1(t), v(t), t)(\dot{\hat{x}}_u(t) + W_1^{\mathrm{T}}(x_1(t), v(t), t)\bar{\Lambda}_q^{\mathrm{T}}P_{2\mathrm{t}}e_{2\mathrm{t}}(t)/2 \\ & + z(t)) - \ddot{y}_{\mathrm{d}}(t) + A_{1\mathrm{t}}(A_{1\mathrm{t}}e_{1\mathrm{t}}(t) - \bar{\Lambda}_q^{\mathrm{T}}e_{2\mathrm{t}}(t))\Big) + A_{2\mathrm{t}}e_{2\mathrm{t}}(t)\Big], \end{aligned} \tag{9.41}$$

where $y_{\mathrm{d}}(t) \in \mathbb{R}^m$, $t \geq 0$, is a given desired output, $\hat{x}_u(t) = \hat{x}_{u1}(t) + \hat{x}_{u2}(t)$, $t \geq 0$, is obtained from (9.7)–(9.8), $\varphi_2(t)$, $t \geq 0$, is given by (9.11), $e_{2\mathrm{t}}(t) \triangleq \bar{\Lambda}_q\varphi_1(x_1(t), v(t), t) - \bar{\Lambda}_q(\dot{y}_{\mathrm{d}}(t) - A_{1\mathrm{t}}e_{1\mathrm{t}}(t))$, the matrices $A_{1\mathrm{t}}$ and $A_{2\mathrm{t}}$ are chosen Hurwitz, and $P_{1\mathrm{t}}$, $P_{2\mathrm{t}} > 0$, are solutions to

$$A_{1\mathrm{t}}^{\mathrm{T}}P_{1\mathrm{t}} + P_{1\mathrm{t}}A_{1\mathrm{t}} + Q_{1\mathrm{t}} = 0, \quad A_{2\mathrm{t}}^{\mathrm{T}}P_{2\mathrm{t}} + P_{2\mathrm{t}}A_{2\mathrm{t}} + Q_{2\mathrm{t}} = 0, \tag{9.42}$$

where $Q_{1\mathrm{t}}$ and $Q_{2\mathrm{t}}$ are chosen positive definite. Finally, define

$$N_{\mathrm{t}} \triangleq \begin{bmatrix} Q_{1\mathrm{t}}^{-1}P_{1\mathrm{t}} & 0_{m\times m} \\ 0_{m\times m} & Q_{2\mathrm{t}}^{-1}P_{2\mathrm{t}} \end{bmatrix}. \tag{9.43}$$

Then, the control input (9.40)–(9.41) guarantees uniform ultimate boundedness of the tracking errors $(e_{1\mathrm{t}}(t), e_{2\mathrm{t}}(t))$, $t \geq 0$, with an ultimate bound given by $\mathcal{D}_{\mathrm{t}} \triangleq \{(e_{1\mathrm{t}}, e_{2\mathrm{t}}) : e_{1\mathrm{t}}^{\mathrm{T}}P_{1\mathrm{t}}e_{1\mathrm{t}} + e_{2\mathrm{t}}^{\mathrm{T}}P_{2\mathrm{t}}e_{2\mathrm{t}} \leq \varepsilon\lambda_{\max}(N_{\mathrm{t}})/3\}$.

Proof. The time derivative of the tracking error $e_{1\mathrm{t}}(t)$, $t \geq 0$, is given by

$$\dot{e}_{1\mathrm{t}}(t) \,=\, \dot{y}_{\mathrm{d}}(t) - \varphi_1(x_1(t), v(t), t) - \gamma_1(x_1(t), v(t), t)u_1(t), \quad t \geq 0. \tag{9.44}$$

Note that

$$\Lambda_q \dot{e}_{1\mathrm{t}}(t) \,=\, \Lambda_q(\dot{y}_{\mathrm{d}}(t) - \varphi_1(x_1(t), v(t), t)) - \gamma_{1\mathrm{s}}(x_1(t), v(t), t)u_1(t), \quad t \geq 0. \tag{9.45}$$

Substituting (9.40) in the above, we obtain

$$\Lambda_q \dot{e}_{1\mathrm{t}}(t) \,=\, \Lambda_q A_{1\mathrm{t}} e_{1\mathrm{t}}(t), \quad t \geq 0. \tag{9.46}$$

In addition, by definition of $e_{2\mathrm{t}}(t)$, $t \geq 0$,

$$\bar{\Lambda}_q \dot{e}_{1\mathrm{t}}(t) \,=\, \bar{\Lambda}_q A_{1\mathrm{t}} e_{1\mathrm{t}}(t) - e_{2\mathrm{t}}(t), \quad t \geq 0. \tag{9.47}$$

Combining (9.46) and (9.47), and observing that $[\, \Lambda_q^{\mathrm{T}} \; \bar{\Lambda}_q^{\mathrm{T}} \,] = I_m$, we obtain

$$\dot{e}_{1\mathrm{t}}(t) \,=\, A_{1\mathrm{t}} e_{1\mathrm{t}}(t) - \bar{\Lambda}_q^{\mathrm{T}} e_{2\mathrm{t}}(t), \quad t \geq 0. \tag{9.48}$$

The time derivative of $e_{2\mathrm{t}}(t)$, $t \geq 0$, is given by

$$\begin{aligned}
\dot{e}_{2\mathrm{t}}(t) =& \bar{\Lambda}_q(W_1(x_1(t), v(t), t)\dot{x}_1(t) + W_2(x_1(t), v(t), t)\dot{v}(t) + W_3(x_1(t), v(t), t) - \ddot{y}_{\mathrm{d}}(t) + A_{1\mathrm{t}}\dot{e}_{1\mathrm{t}}(t)) \\
=& \bar{\Lambda}_q\Big(W_1(x_1(t), v(t), t)(z(t) + \dot{\hat{x}}_u(t) + \epsilon(t)) + W_3(x_1(t), v(t), t) + W_2(x_1(t), v(t), t)\varphi_2(t) \\
& - \ddot{y}_{\mathrm{d}}(t) + A_{1\mathrm{t}}(A_{1\mathrm{t}} e_{1\mathrm{t}}(t) - \bar{\Lambda}_q^{\mathrm{T}} e_{2\mathrm{t}}(t))\Big) + \bar{\Lambda}_q W_2(x_1(t), v(t), t)\gamma_2(x_1(t), v(t), t)u_2(t), \; t \geq 0.
\end{aligned} \tag{9.49}$$

Substituting (9.41) in (9.49) yields

$$\begin{aligned}
\dot{e}_{2\mathrm{t}}(t) \,=\, & P_{2\mathrm{t}}^{-1}\bar{\Lambda}_q P_{1\mathrm{t}} e_{1\mathrm{t}}(t) + A_{2\mathrm{t}} e_{2\mathrm{t}}(t) - \frac{1}{2}\bar{\Lambda}_q W_1(x_1(t), v(t), t) W_1^{\mathrm{T}}(x_1(t), v(t), t)\bar{\Lambda}_q^{\mathrm{T}} P_{2\mathrm{t}} e_{2\mathrm{t}}(t) \\
& + \bar{\Lambda}_q W_1(x_1(t), v(t), t)\epsilon(t), \quad t \geq 0.
\end{aligned} \tag{9.50}$$

Next, we consider the following Lyapunov function candidate,

$$V(e_{1\mathrm{t}}, e_{2\mathrm{t}}) = e_{1\mathrm{t}}^{\mathrm{T}} P_{1\mathrm{t}} e_{1\mathrm{t}} + e_{2\mathrm{t}}^{\mathrm{T}} P_{2\mathrm{t}} e_{2\mathrm{t}}, \tag{9.51}$$

where $P_{1\mathrm{t}}$, $P_{2\mathrm{t}} > 0$ are obtained from (9.42). The time derivative of (9.51) along the trajectories of (9.48) and (9.50) is given by

$$\begin{aligned}
\dot{V}(t) &= e_{1\mathrm{t}}^{\mathrm{T}}(t)(A_{1\mathrm{t}}^{\mathrm{T}} P_{1\mathrm{t}} + P_{1\mathrm{t}} A_{1\mathrm{t}}) e_{1\mathrm{t}}(t) + e_{2\mathrm{t}}^{\mathrm{T}}(t)(A_{2\mathrm{t}}^{\mathrm{T}} P_{2\mathrm{t}} + P_{2\mathrm{t}} A_{2\mathrm{t}}) e_{2\mathrm{t}}(t) - 2e_{1\mathrm{t}}^{\mathrm{T}}(t) P_{1\mathrm{t}} \bar{\Lambda}_q^{\mathrm{T}} e_{2\mathrm{t}}(t) \\
&\quad + 2e_{2\mathrm{t}}^{\mathrm{T}}(t) P_{2\mathrm{t}} \Big(- \bar{\Lambda}_q W_1(x_1(t), v(t), t) W_1^{\mathrm{T}}(x_1(t), v(t), t) \bar{\Lambda}_q^{\mathrm{T}} P_{2\mathrm{t}} e_{2\mathrm{t}}(t) + P_{2\mathrm{t}}^{-1} \bar{\Lambda}_q P_{1\mathrm{t}} e_{1\mathrm{t}}(t) \\
&\quad + \bar{\Lambda}_q W_1(x_1(t), v(t), t) \epsilon(t) \Big) \\
&= -e_{1\mathrm{t}}^{\mathrm{T}}(t) Q_{1\mathrm{t}} e_{1\mathrm{t}}(t) - e_{2\mathrm{t}}^{\mathrm{T}}(t) Q_{2\mathrm{t}} e_{2\mathrm{t}}(t) + 2e_{2\mathrm{t}}^{\mathrm{T}}(t) P_{2\mathrm{t}} \bar{\Lambda}_q W_1(x_1(t), v(t), t) \epsilon(t) \\
&\quad - e_{2\mathrm{t}}^{\mathrm{T}}(t) P_{2\mathrm{t}} \bar{\Lambda}_q W_1(x_1(t), v(t), t) W_1^{\mathrm{T}}(x_1(t), v(t), t) \bar{\Lambda}_q^{\mathrm{T}} P_{2\mathrm{t}} e_{2\mathrm{t}}(t), \quad t \geq 0.
\end{aligned} \tag{9.52}$$

Note that

$$\begin{aligned}
2e_{2\mathrm{t}}^{\mathrm{T}} P_{2\mathrm{t}} \bar{\Lambda}_q W_1(x_1, v, t) \epsilon &= e_{2\mathrm{t}}^{\mathrm{T}} P_{2\mathrm{t}} \bar{\Lambda}_q W_1(x_1, v, t) W_1^{\mathrm{T}}(x_1, v, t) \bar{\Lambda}_q^{\mathrm{T}} P_{2\mathrm{t}} e_{2\mathrm{t}} + \epsilon^{\mathrm{T}} \epsilon \\
&\quad - \left(W_1^{\mathrm{T}}(x_1, v, t) \bar{\Lambda}_q^{\mathrm{T}} P_{2\mathrm{t}} e_{2\mathrm{t}} - \epsilon \right)^{\mathrm{T}} \left(W_1^{\mathrm{T}}(x_1, v, t) \bar{\Lambda}_q^{\mathrm{T}} P_{2\mathrm{t}} e_{2\mathrm{t}} - \epsilon \right).
\end{aligned} \tag{9.53}$$

Substituting (9.53) into (9.52), we obtain that

$$\begin{aligned}
\dot{V}(t) &\leq -e_{1\mathrm{t}}^{\mathrm{T}}(t) Q_{1\mathrm{t}} e_{1\mathrm{t}}(t) - e_{2\mathrm{t}}^{\mathrm{T}}(t) Q_{2\mathrm{t}} e_{2\mathrm{t}}(t) + \epsilon^{\mathrm{T}}(t) \epsilon(t) \\
&\leq -e_{1\mathrm{t}}^{\mathrm{T}}(t) Q_{1\mathrm{t}} e_{1\mathrm{t}}(t) - e_{2\mathrm{t}}^{\mathrm{T}}(t) Q_{2\mathrm{t}} e_{2\mathrm{t}}(t) + \frac{\varepsilon}{3}, \quad t \geq 0.
\end{aligned} \tag{9.54}$$

Following the same reasoning as that at the end of the proof of Theorem 9.3.1, we conclude that $(e_{1\mathrm{t}}(t), e_{2\mathrm{t}}(t))$, $t \geq 0$, is ultimately bounded and uniformly converges to $\mathcal{D}_{\mathrm{t}}$. □

In a similar fashion as was done in Corollary 9.3.1, the following corollary presents a simpler control algorithm than that in Theorem 9.4.1.

Corollary 9.4.1. Consider the system given by (9.31)–(9.32), and assume that there exists $B_1 \triangleq \left[\begin{array}{cc} B_{1\mathrm{s}}^{\mathrm{T}} & 0_{q\times(m-q)} \end{array} \right]^{\mathrm{T}} \in \mathbb{R}^{m\times q}$ and $B_2 \in \mathbb{R}^{m\times(m-q)}$ such that the symmetric part of $B_1^{\mathrm{T}} g_1(x_1, x_2, t) \in \mathbb{R}^{q\times q}$ and that of $B_2^{\mathrm{T}}(\partial f_1(x_1, x_2, t)/\partial x_2) g_2(x_1, x_2, t) \in \mathbb{R}^{(m-q)\times(m-q)}$ is positive definite for all $x_1 \in \mathbb{R}^m$, $x_2 \in \mathbb{R}^p$ and $t \geq 0$. Then consider the control input $u(t) = \left[\begin{array}{cc} u_1^{\mathrm{T}}(t) & u_2^{\mathrm{T}}(t) \end{array} \right]^{\mathrm{T}}$, $t \geq 0$, given by

$$u_1(t) = B_{1\mathrm{s}}^{-1} \Lambda_q (\dot{y}_{\mathrm{d}}(t) - A_{1\mathrm{t}} e_{1\mathrm{t}}(t) - v(t)), \quad t \geq 0, \tag{9.55}$$

$$u_2(t) = (\bar{\Lambda}_q B_2)^{-1} \Big[P_{2\mathrm{t}}^{-1} \bar{\Lambda}_q P_{1\mathrm{t}} e_{1\mathrm{t}}(t) + A_{2\mathrm{t}} e_{2\mathrm{t}}(t) - \bar{\Lambda}_q \Big(\varphi_2(t) - \ddot{y}_{\mathrm{d}}(t) + A_{1\mathrm{t}}(A_{1\mathrm{t}} e_{1\mathrm{t}}(t) - \bar{\Lambda}_q^{\mathrm{T}} e_{2\mathrm{t}}(t)) \Big) \Big], \tag{9.56}$$

where $y_{\mathrm{d}}(t) \in \mathbb{R}^m$, $t \geq 0$, is a given desired output, $\hat{x}_u(t) \triangleq \hat{x}_{u1}(t) + \hat{x}_{u2}(t)$, $t \geq 0$, is obtained from (9.29)–(9.30), $\varphi_2(t) = P_{2\mathrm{o}}^{-1} P_{1\mathrm{o}} e_{1\mathrm{o}}(t) - A_{1\mathrm{o}}(A_{1\mathrm{o}} e_{1\mathrm{o}}(t) - e_{2\mathrm{o}}(t)) + \dot{z}(t) + A_{2\mathrm{o}} e_{2\mathrm{o}}(t) - \alpha_1 \dot{\hat{x}}_{u1}(t) - \alpha_2 \dot{\hat{x}}_{u2}(t) - \alpha_3 \hat{x}_{u2}(t)$, $e_{2\mathrm{t}}(t) \triangleq \bar{\Lambda}_q v(t) - \bar{\Lambda}_q(\dot{y}_{\mathrm{d}}(t) - A_{1\mathrm{t}} e_{1\mathrm{t}}(t))$, the matrices $A_{1\mathrm{t}}$ and $A_{2\mathrm{t}}$ are chosen Hurwitz, and $P_{1\mathrm{t}}$, $P_{2\mathrm{t}} > 0$, are solutions to (9.42), with $Q_{1\mathrm{t}}$ and $Q_{2\mathrm{t}}$ chosen positive definite.

Then, the control input (9.55)–(9.56) guarantees Lyapunov stability and exponential convergence to the origin of the tracking errors $(e_{1\mathrm{t}}, e_{2\mathrm{t}})$.

Proof. The error dynamics are of the form

$$\dot{e}_{1\mathrm{t}}(t) = A_{1\mathrm{t}} e_{1\mathrm{t}}(t) - \bar{\Lambda}_q^{\mathrm{T}} e_{2\mathrm{t}}(t), \qquad e_{1\mathrm{t}}(0) = e_{1\mathrm{t}0}, \quad t \geq 0. \tag{9.57}$$

$$\dot{e}_{2\mathrm{t}}(t) = P_{2\mathrm{t}}^{-1} \bar{\Lambda}_q P_{1\mathrm{t}} e_{1\mathrm{t}}(t) + A_{2\mathrm{t}} e_{2\mathrm{t}}(t), \quad e_{2\mathrm{t}}(0) = e_{2\mathrm{t}0}. \tag{9.58}$$

The time derivative of Lyapunov function candidate (9.51) along the trajectories of (9.57)–(9.58) is of the form

$$\dot{V}(t) = -e_{1\mathrm{t}}^{\mathrm{T}}(t) Q_{1\mathrm{t}} e_{1\mathrm{t}}(t) - e_{2\mathrm{t}}^{\mathrm{T}}(t) Q_{2\mathrm{t}} e_{2\mathrm{o}}(t), \quad t \geq 0, \tag{9.59}$$

which satisfies the assumptions of Theorem 4.10 in [44], and thus allows to conclude exponential stability of the origin of system (9.57)–(9.58). □

9.5. Illustrative Numerical Examples

As in preceding chapters, the output predictor will use the Adaptive Integral Variable Structure Derivative Estimator (AIVSDE) described in [57]. However, in this chapter, we set $r(t) = y(t) - \hat{x}_u(t)$, to obtain an estimate $z(t)$ of $\dot{y}(t) - \dot{\hat{x}}_u(t)$, $t \geq 0$.

Example 9.5.1. Consider the following system,

$$\dot{x}_1(t) = a\sin(x_1(t) + x_2(t)) + b(\tanh(\pi x_2(t) - 2) + \tanh(x_2^3(t)/10) + x_2^3(t)/100), \quad x_1(0) = x_{10}, \quad t \geq 0, \tag{9.60}$$

$$\dot{x}_2(t) = c\tanh(x_1(t)) - dx_2^3(t) + u(t), \qquad x_2(0) = x_{20}, \tag{9.61}$$

$$y(t) = x_1(t), \tag{9.62}$$

where $x_1(t)$, $x_2(t)$, $u(t) \in \mathbb{R}$, $t \geq 0$, and a, b, c, $d \in \mathbb{R}$. Following the result in Corollary 9.3.1, we construct the following predictor,

$$\dot{\hat{x}}_1(t) = v(t), \qquad \hat{x}_1(0) = \hat{x}_{10}, \quad t \geq 0, \tag{9.63}$$

$$\dot{v}(t) = \varphi_2(t) + Bu(t), \quad \hat{v}(0) = 0, \tag{9.64}$$

where

$$e_{1o}(t) = x_1(t) - \hat{x}_1(t), \quad t \geq 0, \tag{9.65}$$

$$e_{2o}(t) = v(t) + A_{1o}e_{1o}(t) - z(t) - \dot{\hat{x}}_u(t), \tag{9.66}$$

$$\varphi_2(t) = p_{1o}e_{1o}(t)/p_{2o} - A_{1o}(A_{1o}e_{1o}(t) - e_{2o}(t)) + \dot{z}(t) + A_{2o}e_{2o}(t) - \alpha_2\dot{\hat{x}}_u(t) - \alpha_3\hat{x}_u(t). \tag{9.67}$$

In addition, we choose $B = 5$, and $\dot{\hat{x}}_u(t)$, $t \geq 0$, is obtained from (9.30) with $B_2 = B$, $\alpha_2 = \alpha_3 = 10$, and $u_2(t) = u(t)$, $t \geq 0$, given by

$$u(t) = p_{1\mathrm{t}} e_{1\mathrm{t}}(t)/p_{2\mathrm{t}} + A_{2\mathrm{t}} e_{2\mathrm{t}}(t) - \varphi_2(t) + \ddot{y}_{\mathrm{d}}(t) - A_{1\mathrm{t}}(A_{1\mathrm{t}} e_{1\mathrm{t}}(t) - e_{2\mathrm{t}}(t)), \quad t \geq 0, \quad (9.68)$$

where $e_{1\mathrm{t}}(t) = y_{\mathrm{d}} - \hat{x}_1(t)$, $e_{2\mathrm{t}}(t) = v(t) - \dot{y}_{\mathrm{d}}(t) + A_{1\mathrm{t}} e_{1\mathrm{t}}(t)$, $t \geq 0$. Choosing $A_{1\mathrm{o}} = -10$, $A_{2\mathrm{o}} = -20$, $q_{1\mathrm{o}} = 10$, $q_{2\mathrm{o}} = 3$, we obtain $p_{1\mathrm{o}} = 0.5132$, $p_{2\mathrm{o}} = 0.1$ from (9.14)–(9.15). The parameters of the AIVSDE are chosen as follows, $k_1 = 5$, $k_2 = 10$, $k_b = 5$, $\alpha_r = 0$, $\mu = 0.2$, $\gamma_{r0} = x_{10}$ and $k_{r0} = 5$. In addition, we chose $A_{1\mathrm{t}} = -5$, $A_{2\mathrm{t}} = -1$, $q_{1\mathrm{t}} = 5$, $q_{2\mathrm{t}} = 1$, and obtain from (9.42), $p_{1\mathrm{t}} = p_{2\mathrm{t}} = 1/2$. Finally, the desired output trajectory is chosen to be $y_{\mathrm{d}}(t) = -5\cos(t)$, $t \geq 0$.

For the purpose of numerical simulation, we chose the following parameters for the system model, $a = 0.4$, $b = 10$, $c = -1$ and $d = 0.1$. In addition, we choose $x_{10} = x_{20} = 2$, $\hat{x}_{10} = 1$, $\hat{x}_{20} = 0$, and $z(0) = 0$. The resulting system and predictor trajectories are shown in Figure 9.1 (top).

The predicted $\hat{x}_1(t)$ closely matches the measured $x_1(t)$, $t \geq 0$, as seen in Figure 9.1 (top). Note that the initial condition for the prediction $\hat{x}_{10}$ could have been chosen as x_{10}, since $x_1(t)$, $t \geq 0$, is measured. The initial prediction was however chosen different from x_{10} to illustrate convergence of $\hat{x}_1(t)$ to $x_1(t)$, $t \geq 0$. The efficacy of the control law (9.68) is also illustrated by Figure 9.1 (top), which shows the real trajectory converging to the desired $y_{\mathrm{d}}(t)$, $t \geq 0$. The control input is shown in Figure 9.1 (bottom). Note that we have employed the saturation algorithm presented in [1] to limit the command in amplitude.

Furthermore, note that $\partial f_1(x_1(t), x_2(t), t)/\partial x_2(t) = a\cos(x_1 + \hat{x}_2) + b(\pi \mathrm{sech}^2(\pi \hat{x}_2 - 2) + \mathrm{sech}^2(\hat{x}_2^3/10)\,(3\hat{x}_2^2/10) + 3\hat{x}_2^2/100)$, $t \geq 0$. With the selected a, b, c and d parameters, we have that $\partial f_1(x_1(t), x_2(t), t)/\partial x_2(t) > 0$ for all $x_1, \hat{x}_2 \in \mathbb{R}$ and $t \geq 0$. In addition, in the nota-

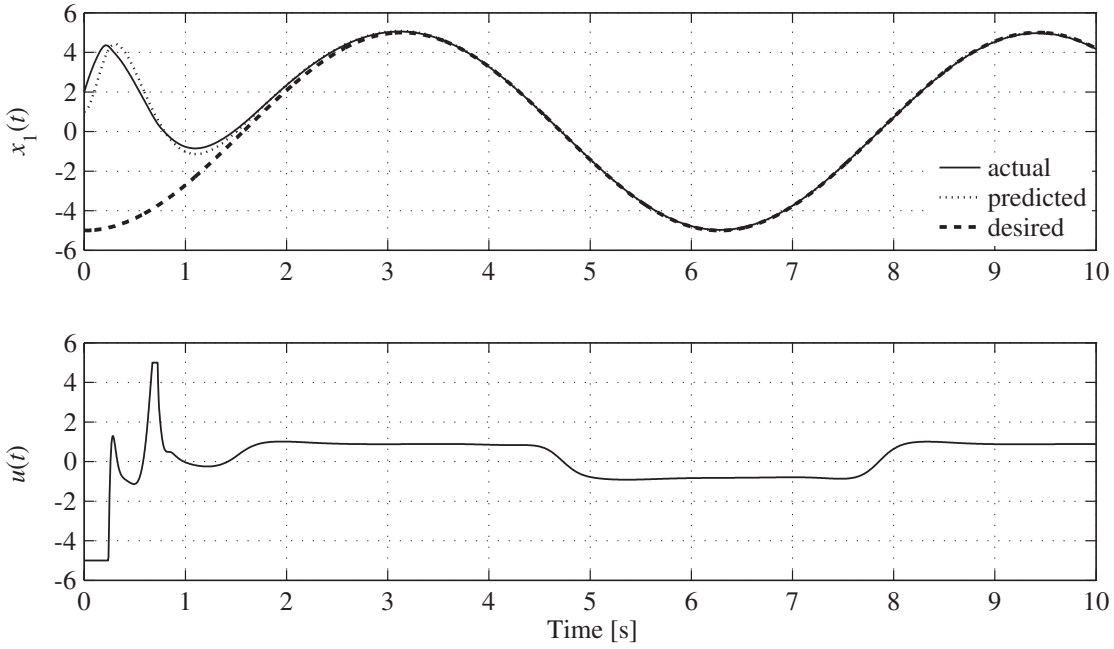

Figure 9.1: Actual, predicted and desired trajectories (top); control effort (bottom).

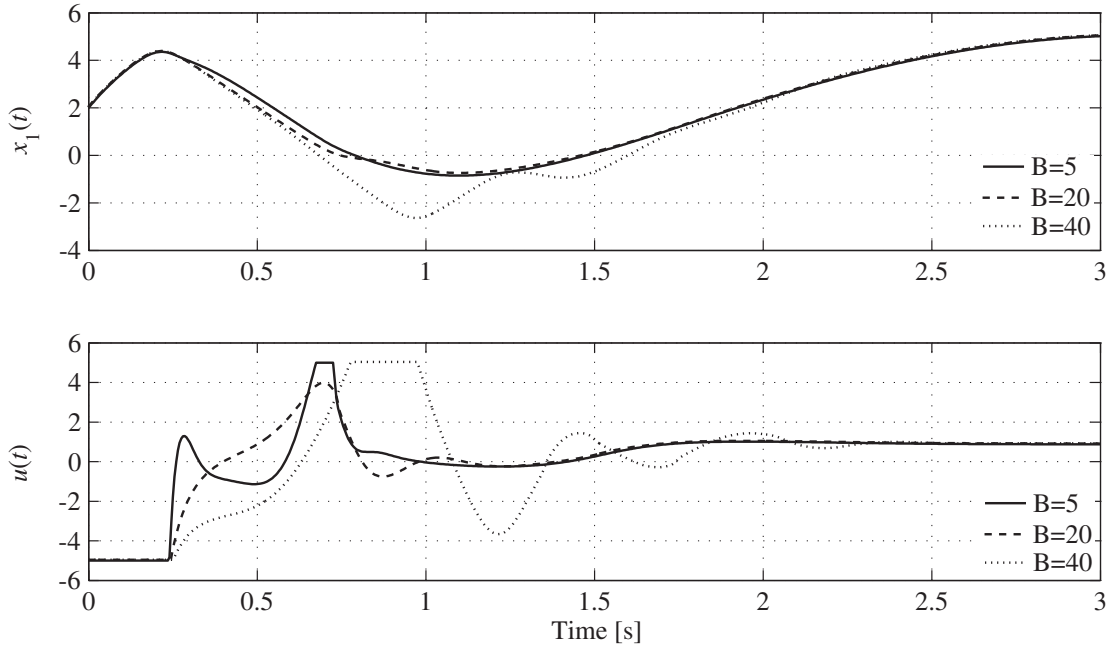

Figure 9.2: Actual trajectories (top); control effort (bottom).

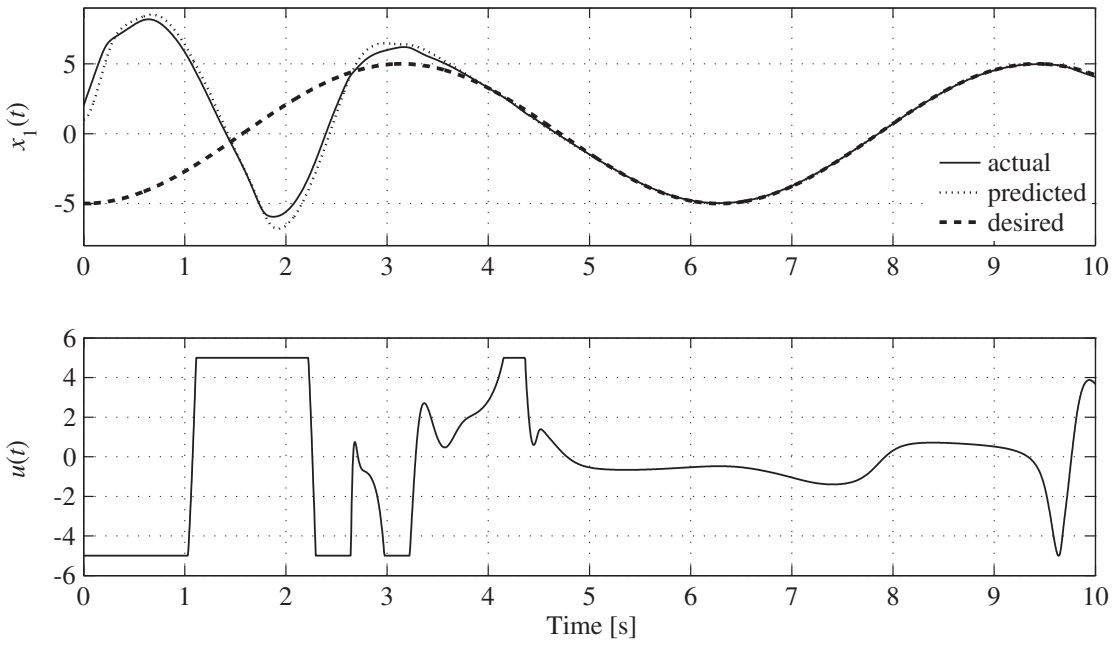

Figure 9.3: Actual, predicted and desired trajectories (top); control effort (bottom).

tions of Corollary 9.4.1, $g_2(x_1(t), x_2(t), t) \equiv 1$, $t \geq 0$. Hence, $B_2^{\mathrm{T}}(\partial f_1(x_1(t), x_2(t), t)/\partial x_2(t))$ $g_2(x_1(t), x_2(t), t)^{\mathrm{T}} > 0$ for any $B > 0$. In other words, the algorithm is guaranteed to perform well for any positive choice of B. This flexibility is illustrated by Figure 9.2, which shows the system output and control signal for various choices of B. While the transient changes for different values of B, the system output converges to the given desired trajectory in all cases.

In addition, note that the algorithm does not rely on knowledge of the form of the right-hand-side of (9.60)–(9.61). This means that the algorithm is not directly dependent upon the form of the system's dynamics. The same predictor-controller (9.63)–(9.68) provides the same stability guarantees for any particular form of the system's dynamics, provided that the system is controllable. To illustrate this point, we modify the right-hand-side of (9.60)

as follows,

$$\dot{x}_1(t) = a\sin(x_1(t) + x_2(t)) + b(\tanh(\pi x_2(t) - 2) + \tanh(x_2^3(t)/10) + x_2^3(t)/100) + 2x_1(t),$$
$$x_1(0) = x_{10}, \quad t \geq 0. \tag{9.69}$$

This new system is identical to the previous one, except for the addition of the (qualitatively) destabilizing term $2x_1(t)$, $t \geq 0$, in (9.69). Applying the same predictor-controller to this new system yielded the result shown in Figure 9.3. Due to the addition of the destabilizing term, the transient is extended by a few seconds. However, performance of the algorithm is ultimately identical. More specifically, we observe that $\hat{x}_1(t)$ converges to $x_1(t)$, $t \geq 0$, and that the system's output converges to the desired $y_{\mathrm{d}}(t)$, $t \geq 0$.

Example 9.5.2. Consider the system

$$\dot{x}_{11}(t) = -x_{11}^3(t) + \tanh(x_{12}(t)) + \frac{1 + x_{11}^2(t)}{1 + x_2^2(t)}u_1(t), \qquad x_{11}(0) = x_{110},\ t \geq 0, \tag{9.70}$$

$$\dot{x}_{12}(t) = 4\tanh(x_{11}(t)) - 2\tanh(x_{12}(t)) + x_2(t) + \cos(x_2^2(t))/2, \quad x_{12}(0) = x_{120}, \tag{9.71}$$

$$\dot{x}_2(t) = -x_2^3(t) - 2\tanh((x_{11}(t) + x_{12}(t))^3) + \frac{1 + x_{11}^2(t)}{1 + x_2^2(t)}u_2(t), \qquad x_2(0) = x_{20}, \tag{9.72}$$

$$y(t) = x_1(t), \tag{9.73}$$

where $x_1(t) \triangleq \begin{bmatrix} x_{11}(t) & x_{12}(t) \end{bmatrix}^{\mathrm{T}} \in \mathbb{R}^2$, and $x_2(t) \in \mathbb{R}$, $t \geq 0$. Applying the technique described in Corollary 9.3.1, we construct the following predictor,

$$\dot{\hat{x}}_1(t) = v(t) + B_1 u_1(t), \quad \hat{x}_1(0) = \hat{x}_{10}, \quad t \geq 0, \tag{9.74}$$

$$\dot{v}(t) = \varphi_2(t) + B_2 u_2(t), \quad v(0) = 0_2, \tag{9.75}$$

where

$$e_{1\mathrm{o}}(t) = x_1(t) - \hat{x}_1(t), \quad t \geq 0, \tag{9.76}$$

$$e_{2\mathrm{o}}(t) = v(t) - \dot{\hat{x}}_{u2}(t) + \alpha_1 \hat{x}_{u1}(t) - z(t) + A_{1\mathrm{o}} e_{1\mathrm{o}}(t), \tag{9.77}$$

$$\varphi_2(t) = P_{2\mathrm{o}}^{-1} P_{1\mathrm{o}} e_{1\mathrm{o}}(t) - A_{1\mathrm{o}}(A_{1\mathrm{o}} e_{1\mathrm{o}}(t) - e_{2\mathrm{o}}(t)) + \dot{z}(t) + A_{2\mathrm{o}} e_{2\mathrm{o}}(t) - \alpha_1 \dot{\hat{x}}_{u1}(t) - \alpha_2 \dot{\hat{x}}_{u2}(t) - \alpha_3 \hat{x}_{u1}(t). \tag{9.78}$$

In addition, we select $\alpha_i = 10$, $i = 1, 2, 3$, $B_1 = [\, 4,\ 0\,]^{\mathrm{T}}$, $B_2 = [\, 0,\ 2\,]^{\mathrm{T}}$, $A_{1\mathrm{o}} = -10 I_2$, $Q_{1\mathrm{o}} = 10 I_2$, $A_{2\mathrm{o}} = -20 I_2$, and $Q_{2\mathrm{o}} = 3 I_2$. We obtain, from (9.14)–(9.15), $P_{1\mathrm{o}} = 0.5132 I_2$, $P_{2\mathrm{o}} = 0.1 I_2$. The parameters used for the AIVSDE are identical to that in the previous example. The initial conditions for the system and the predictor are chosen as $x_{10} = \begin{bmatrix} 2 & 2 \end{bmatrix}^{\mathrm{T}}$, $x_{20} = -1$, and $\hat{x}_{10} = \begin{bmatrix} 1 & 1 \end{bmatrix}^{\mathrm{T}}$. The control command is of the form

$$u_1(t) = \Lambda_1(\dot{y}_{\mathrm{d}}(t) - v(t) - A_{1\mathrm{t}} e_{1\mathrm{t}}(t))/4, \quad t \geq 0, \tag{9.79}$$

$$u_2(t) = \Big[P_{2\mathrm{t}}^{-1} \bar{\Lambda}_1 P_{1\mathrm{t}} e_{1\mathrm{t}}(t) + A_{2\mathrm{t}} e_{2\mathrm{t}}(t) - \bar{\Lambda}_1 \Big(\varphi_2(t) - \ddot{y}_{\mathrm{d}}(t) - A_{1\mathrm{t}}(A_{1\mathrm{t}} e_{1\mathrm{t}}(t) - \bar{\Lambda}^{\mathrm{T}} e_{2\mathrm{t}}(t))\Big)\Big]/2, \tag{9.80}$$

with $e_{1\mathrm{t}}(t) = y_{\mathrm{d}} - \hat{x}_1(t)$, $e_{2\mathrm{t}}(t) = \bar{\Lambda}_1 v(t) - \bar{\Lambda}_1(\dot{y}_{\mathrm{d}}(t) - A_{1\mathrm{t}} e_{1\mathrm{t}}(t))$, $t \geq 0$. In addition, we choose $A_{1\mathrm{t}} = -10 I_2$, $A_{2\mathrm{t}} = -10$, $Q_{1\mathrm{t}} = 10 I_2$, $Q_{2\mathrm{t}} = 10$, and obtain from (9.42), $P_{1\mathrm{t}} = I_2/2$, $P_{2\mathrm{t}} = 1/2$. Finally, $\dot{\hat{x}}_u(t)$, $t \geq 0$, is obtained from (9.29)–(9.29). The desired trajectory is chosen to be $y_{\mathrm{d}}(t) = [\, 2\sin(2t),\ 1 + \sin(2t)/2\,]^{\mathrm{T}}$, $t \geq 0$.

As seen in Figure 9.4, the predicted trajectory $\hat{x}_1(t)$, $t \geq 0$, quickly converges to the actual trajectory $x_1(t)$, $t \geq 0$. Furthermore, the command (9.79)–(9.80), shown in Figure 9.5, proves effective, and $x_1(t)$, $t \geq 0$, converges to the desired $y_{\mathrm{d}}(t)$, $t \geq 0$, as shown in Figure 9.4.

Example 9.5.3. Consider the system

$$\dot{\eta}(t) = J(\eta(t))\nu(t), \qquad \eta(0) = \eta_0, \quad t \geq 0, \tag{9.81}$$

$$\dot{\nu}(t) = \Theta_1^* \varphi(\eta(t)) + \Theta_2^* u(t), \quad \nu(0) = \nu_0, \tag{9.82}$$

$$y(t) = \begin{bmatrix} I_2 & 0_2 \end{bmatrix} \eta(t), \tag{9.83}$$

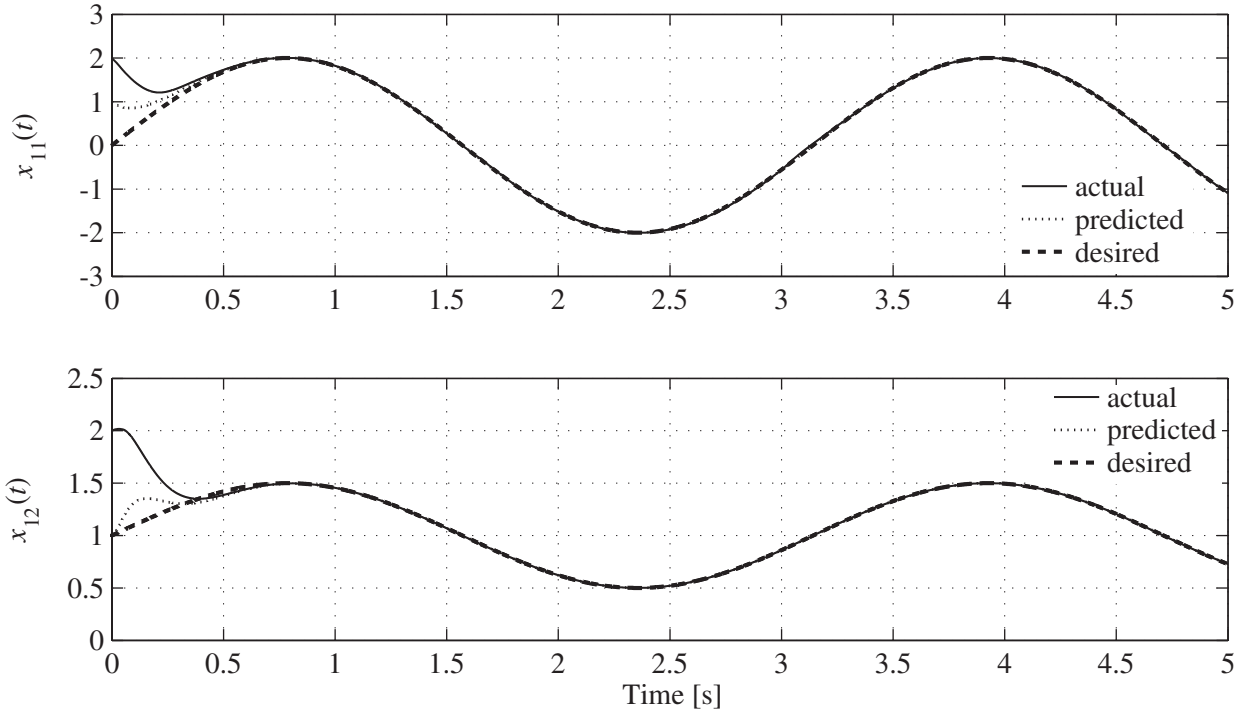

Figure 9.4: Actual, predicted and desired output trajectories.

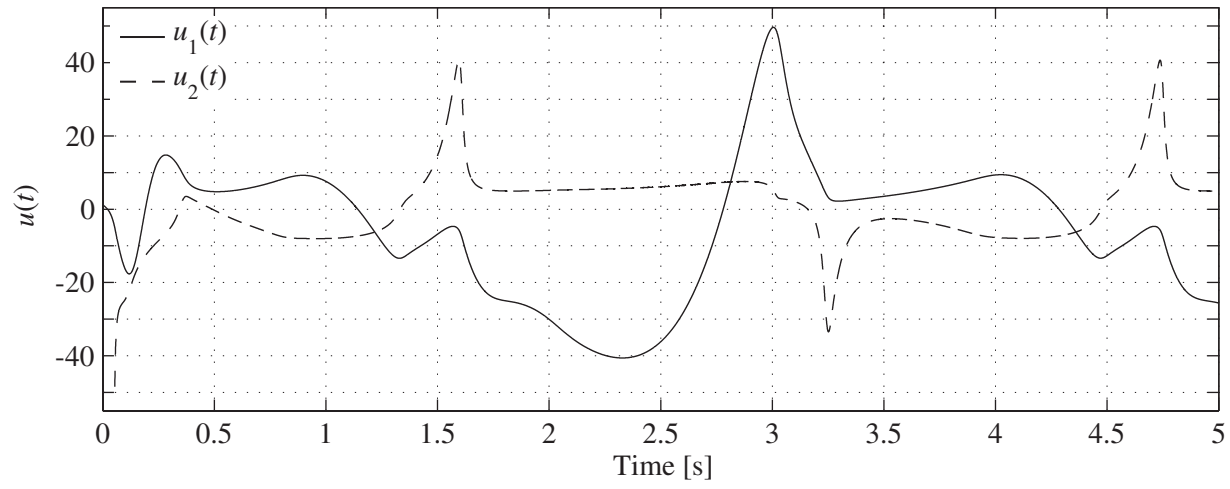

Figure 9.5: Control effort.

where $\eta(t) \triangleq \left[\begin{array}{ccc} \phi(t) & \theta(t) & \psi(t) \end{array}\right]^{\mathrm{T}} \in \mathbb{R}^3$, $\nu(t) \triangleq \left[\begin{array}{ccc} p(t) & q(t) & r(t) \end{array}\right]^{\mathrm{T}} \in \mathbb{R}^3$, and $u(t) \in \mathbb{R}^2$, $t \geq 0$, is the control input applied to the system. In addition, $\Theta_1^* \in \mathbb{R}^{3\times 2}$ and $\Theta_2^* \in \mathbb{R}^{3\times 2}$ are unknown constant matrices, and

$$J(\eta) \triangleq \left[\begin{array}{ccc} 1 & \tan(\theta)\sin(\phi) & \tan(\theta)\cos(\phi) \\ 0 & \cos(\phi) & -\sin(\phi) \\ 0 & \sin(\phi)/\cos(\theta) & \cos(\phi)/\cos(\theta) \end{array}\right], \ \varphi(\eta) \triangleq \left[\begin{array}{c} \cos(\theta)\cos(\phi) \\ -\cos(\theta)\sin(\phi) \end{array}\right]. \tag{9.84}$$

Applying the technique described in Theorem 9.3.1, we construct the following predictor,

$$\dot{\hat{x}}_1(t) = v(t), \qquad \hat{x}_1(0) = y(0), \quad t \geq 0, \tag{9.85}$$

$$\dot{v}(t) = \varphi_2(t) + B(y(t))u(t), \quad v(0) = v_0, \tag{9.86}$$

where

$$e_{1\mathrm{o}}(t) = x_1(t) - \hat{x}_1(t), \quad t \geq 0, \tag{9.87}$$

$$e_{2\mathrm{o}}(t) = v(t) - \dot{\hat{x}}_u(t) + \alpha_1 \hat{x}_{u1}(t) z(t) + A_{1\mathrm{o}} e_{1\mathrm{o}}(t), \tag{9.88}$$

$$\varphi_2(t) = P_{2\mathrm{o}}^{-1} P_{1\mathrm{o}} e_{1\mathrm{o}}(t) + A_{2\mathrm{o}} e_{2\mathrm{o}}(t) - A_{1\mathrm{o}}(A_{1\mathrm{o}} e_{1\mathrm{o}}(t) - e_{2\mathrm{o}}(t)) + \dot{z}(t) - \alpha_2 \dot{\hat{x}}_u(t) - \alpha_3 \hat{x}_u(t), \tag{9.89}$$

$$B(y(t)) = \left[\begin{array}{cc} 1 & -\tan(\theta)\sin(\phi) \\ 0 & -\cos(\phi) \end{array}\right]. \tag{9.90}$$

In addition, we choose $A_{1\mathrm{o}} = -\mathrm{diag}([\, 20 \ 10 \,])$, $A_{2\mathrm{o}} = 2A_{1\mathrm{o}}$, $Q_{1\mathrm{o}} = -A_{1\mathrm{o}}$, $Q_{2\mathrm{o}} = 3I_2$, and obtain, from (9.14) and (9.15), $P_{1\mathrm{o}} = \mathrm{diag}([\, 0.5064, \ 0.5132 \,])$, $P_{2\mathrm{o}} = \mathrm{diag}([\, 0.05, \ 0.1 \,])$. The AIVSDE parameters are chosen as follows, $k_1 = 10$, $k_2 = 15$, $k_b = 1$, $\alpha_r = 0$, $\mu = 0.2$, $\gamma_{r0} = x_{10}$ and $k_{r0} = 2$.

For simulation purposes, we use the following for plant parameters,

$$\Theta_1^* = \left[\begin{array}{cc} -2.6828 & 3.2966 \\ 9.8298 & 9.9455 \\ 0 & -20 \end{array}\right], \quad \Theta_2^* = \left[\begin{array}{cc} 0.25 & 0 \\ 0 & -0.575 \\ 0 & 0 \end{array}\right]. \tag{9.91}$$

The control law given (9.40)–(9.41) is of the form

$$u(t) = B^{-1}(y(t))(-\varphi_2(t) - A_{1\mathrm{t}}(A_{1\mathrm{t}} e_{1\mathrm{t}}(t) - e_{2\mathrm{t}}(t)) + \ddot{y}_{\mathrm{d}}(t) + A_{2\mathrm{t}} e_{2\mathrm{t}}(t) + P_{2\mathrm{t}}^{-1} P_{1\mathrm{t}} e_{1\mathrm{t}}(t)), \, t \geq 0, \tag{9.92}$$

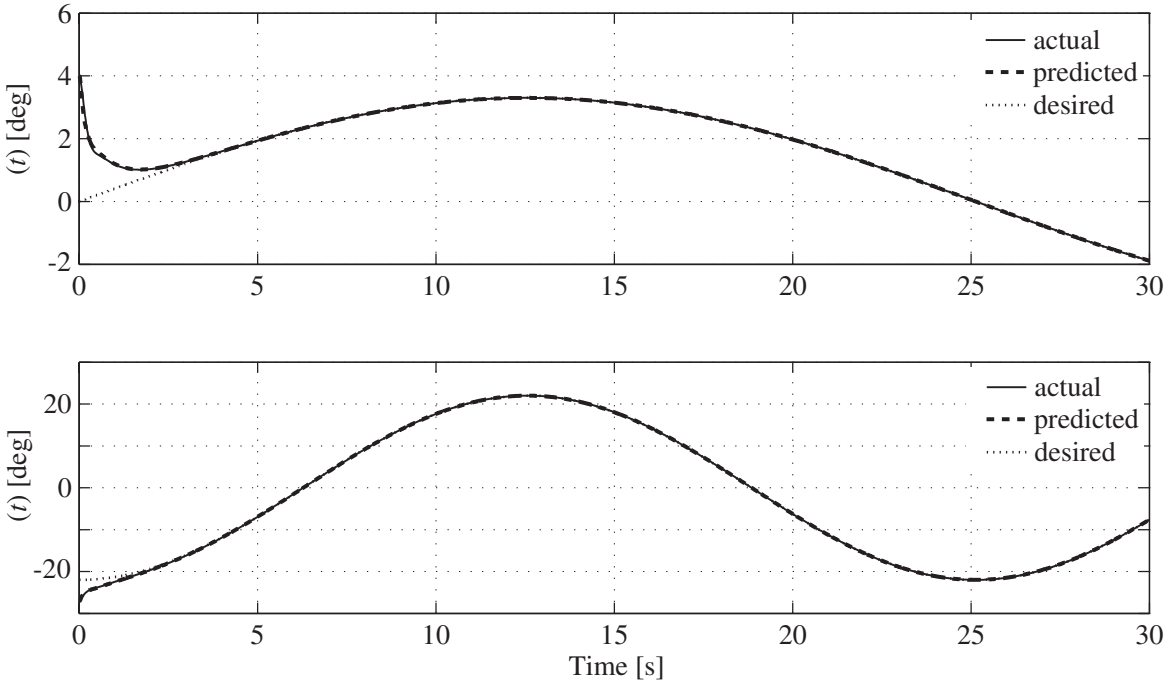

Figure 9.6: Actual, predicted and desired trajectories of $\eta_{\rm s}(t)$, $t \geq 0$.

where $e_{1{\rm t}}(t) \triangleq y_{\rm d}(t) - \hat{x}_1(t)$, and $e_{2{\rm t}}(t) \triangleq v(t) - \dot{y}_{\rm d} + A_{1{\rm t}} e_{1{\rm t}}(t)$, $t \geq 0$. In addition, we choose $A_{1{\rm t}} = -5I_2$, $A_{2{\rm t}} = -1I_2$, $Q_{1{\rm t}} = 5I_2$, $Q_{2{\rm t}} = 5I_2$, and obtain from (9.42), $P_{1{\rm t}} = P_{2{\rm t}} = I_2/2$. Finally, $\dot{\hat{x}}_u(t)$, $t \geq 0$, is obtained from (9.8) with $W_2\gamma_2(y) = B(y)$, $\alpha_2 = \alpha_3 = 10$, and we choose $y_{\rm d}(t) = [\, 3.3\sin(t/8),\ -22\cos(t/4)\,]^{\rm T}$, $t \geq 0$.

The initial conditions are chosen as $\eta_0 = [\, 4 \ \ -27 \ \ 10\,]^{\rm T}$, $\nu_0 = 0_3$, $v_0 = [\, 1 \ \ 1\,]^{\rm T}$, and $z(0) = 0_2$. As was the case with Example 9.5.1, the predictor performs well. The predicted trajectory closely matches the real one, as seen in Figure 9.6. The command is shown in Figure 9.7. It is effective, and the output $y(t)$ converges to the desired $y_{\rm d}(t)$, $t \geq 0$, as can be seen in Figure 9.6.

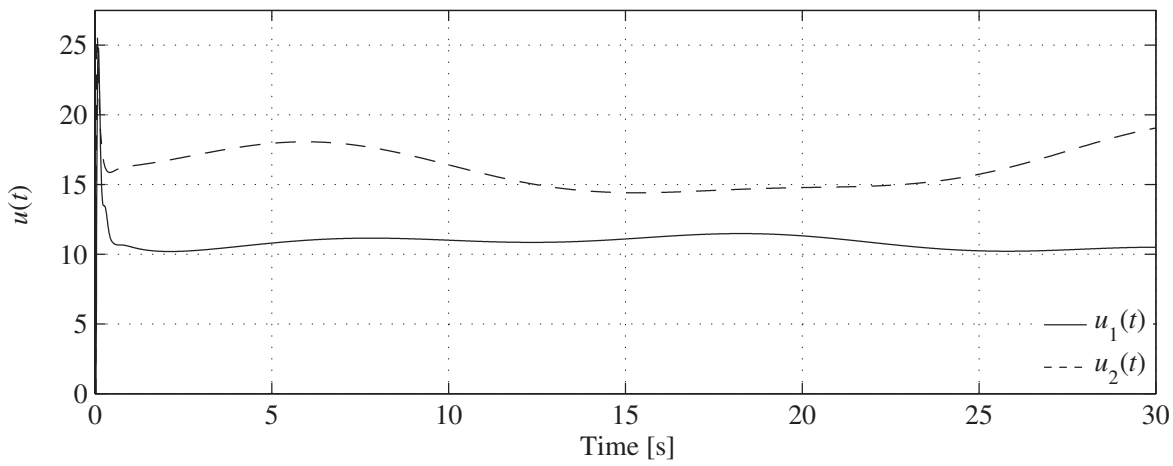

Figure 9.7: Control effort.

9.6. Conclusion

This chapter presented a novel output feedback control scheme for a class of uncertain nonlinear systems. The algorithm relies on an output predictor, designed to predict the actual system's output with arbitrary accuracy for any admissible control signal. A derivative estimator is used to construct the output predictor, and allows to relax most knowledge requirements on the system model. The predictor is complemented by a backstepping-based state feedback control algorithm. In a departure from more classical separation based algorithms, the control law is designed to control the predictor's output, as opposed to the actual system's output. Lyapunov's direct method was used to show ultimate boundedness of both the prediction and tracking errors, with an ultimate bound depending upon specific design constants. Appropriate choice of these constants allows to obtain arbitrarily accurate predictions and tracking performance.

Chapter 10

Indirect Collaborative Control of Autonomous Vehicles with Limited Communication Bandwidth [9]

The result featured in this chapter was presented at the 2005 IARP International Workshop on Underwater Robotics in November 2005 ([9]).

10.1. Introduction

While preceding chapters were concerned with motion control of a unmanned single vehicle, this chapter presents a technique allowing collaboration of a group of such vehicles. The current possible applications of collaborative controls are numerous, including search and rescue missions, mine detection, and surveying. Development of cooperative control theory and utilization of teams of autonomous vehicles will in the future allow the performance of missions impossible to accomplish thus far, such as mapping the ocean floor, recovering archeological artifacts, or disposing of space debris orbiting Earth. This chapter introduces a general framework for cooperative control of autonomous vehicles, complying with

limited communication bandwidth, short range and asynchronous communication requirements. Such requirements are inherent to underwater environments. However, application of the presented work is not limited to heterogeneous teams of Autonomous Underwater Vehicles, and can be effectively applied to any team of autonomous vehicles spanning any environments, provided that they satisfy minimal communication requirements.

The presented approach does not pertain to the decision making process of a cooperative control algorithm, but rather provides a general framework for such an algorithm, allowing a team of vehicles to cooperatively work together in spite of poor communication channels. In qualitative terms, the framework relies on the principle of trading computational time for communication bandwidth. More specifically, each vehicle continuously estimates the position of its peers in the team. It will be shown that this approach allows to drastically reduce vehicle to vehicle communication, and efficiently addresses issues related to asynchronous communications and communication delays. The proposed framework only requires vehicle to vehicle communication in specific instances, such as occurrences significantly affecting the mission. On such occasions, the decision making algorithm issues appropriate commands, which are relayed to the vehicles. As mentioned above, the proposed framework is meant to operate in symbiosis with such a decision making algorithm. The underlying concepts and mechanisms of the framework were tested through numerical simulation, the results of which are presented to illustrate the philosophy of the approach and the benefits in using it.

Numerous engineering problems have been addressed using robotic solutions. The rise in complexity of these problems has motivated exploration of innovative solutions. About two decades ago, researchers began investigating multiple-robot systems as a possible alternative to conventional, single-robot systems ([116]). The notion of using multiple robots to solve

engineering problems has triggered a significant research effort in the areas of biologically inspired robot swarms ([117, 118]) and team oriented cooperative approaches ([68]).

An extensive survey on cooperative control of mobile robots is presented in [67]. The authors define the concept of *cooperative behavior* as follows, "Given some task specified by a designer, a multiple-robot system displays cooperative behavior if, due to some underlying mechanism (i.e., the 'mechanism of cooperation'), there is an increase in the total utility of the system." The flexibility in this definition accommodates the wide range of 'mechanisms of cooperation' explored in recent years.

Although offering perspectives of advantageous solutions, the field of cooperative autonomous mobile robotics remains largely undeveloped and a majority of the associated techniques are considered far from mature ([116]). Controlling multiple robots poses challenges beyond those encountered when dealing with single-robot systems. Unfortunately, design of a traditional, single-robot control system can already prove a perplexing endeavor. It however constitutes but a starting point toward controlling multiple vehicles, added difficulties stemming from factors such as communication requirements, an increased uncertainty in the interaction with the environment and interferences between teammates ([119]). These engineering challenges call for more advanced control techniques.

Particular care has to be given to communication related issues. Indeed, communication requirements and bandwidth limitations prove to be a limiting factor for many cooperative control approaches available in the literature. In [120], the author introduces a decentralized control approach which uses the average and variance of the position of a school of Autonomous Underwater Vehicles (AUVs) to control their position. Access for each vehicle to these average position and variance information requires each and every vehicle to

continuously broadcast their position to all others. However, underwater acoustic communication is particularly onerous, and schools of AUVs have *very* limited communication range and bandwidth, which could become a limiting factor when implementing the framework introduced in [120].

Embedded computers see their computing power steadily increase and cost decrease. The proposition of trading computing power for bandwidth is thus particularly enticing. This chapter proposes the design of a collaborative control framework based on the above premise, aiming to use additional computing power to allow for a significantly reduced bandwidth utilization. Following a Model Reference Control (MRC) approach, each vehicle is assigned a reference system. Each autonomous vehicle, keeping track not only of its own reference system, but also of that associated will all other vehicles, has knowledge of the doings of its teammates, without requiring all vehicles to continuously broadcast position information. Coupling all reference systems through the desired trajectories they are tracking, vehicles find themselves indirectly coupled, allowing the team of autonomous vehicles to exhibit a cooperative behavior. This technique of introducing coupling through a reference system is referred to as indirect cooperation. It has been successfully applied to the control of dynamically interconnected systems ([71–73]), but has yet to be applied to cooperative control of autonomous vehicles.

The presented framework does not address decision making, but functions in conjunction with any arbitrary decision making algorithm. It could, for instance, operate within the cooperative control architecture presented in [121] (replacing the Vehicle Agents, block one, Figure 1, page 638). Note that, although vehicle to vehicle communications are drastically reduced using the proposed framework, communications still occur in specific situations. In

particular, when the decision making entity chooses to alter the mission, or when occurrences of important significance are met, updated directives have to be communicated to the relevant vehicles, thus closing the cooperative control loop. In the presented framework, this can be achieved by, for example, altering the desired trajectory followed by a vehicle or modifying its reference system.

The presented framework is designed to rely on a Model Reference Adaptive Controller (MRAC, [11]) to handle motion control. This choice is in part motivated by the fact that the framework relies on computation of reference systems, which a MRAC is naturally associated with. In addition, as previously mentioned, characterizing the dynamical behavior of marine vehicles, which constitute the intended application of the presented research, is particularly difficult, due to hydrodynamic phenomenons such as skin friction about the vehicle's hull and propeller induced cavitation. As the considered vehicles' mathematical model can thus be uncertain, an adaptive approach, such as that presented in previous chapters, is well suited. Note that using reference systems the motion and behavior of the team of vehicles can easily be adjusted, and enforcing features such as, for example, obstacle and collision avoidance becomes fairly simple.

Section 10.2 provides a description of the governing mechanisms of the proposed framework, along with results of numerical simulations illustrating the performance and key features of this framework in Section 10.3. Particular attention is given to the effect of communication delays on performance.

10.2. Indirect Collaborative Control Framework

Any mission to be accomplished by a team of autonomous vehicles can be divided into a succession of tasks, transition between tasks being triggered by appropriate conditions. Such tasks include search and rescue assignments, surveying of a prescribed area, but can also consist of global behaviors based on local relationships ([122]) leading to more conceptually abstract tasks, such as displacement of a passive object from one location to another ([123]). These assignments can naturally translate into specific formations for the team of vehicles to conform to ([124]). Solutions to the problem of formation keeping available in the literature typically require high-bandwidth communications. As mentioned previously, a Model Reference Control approach is adopted, each vehicle being assigned a reference system, which corresponds to a virtual vehicle whose trajectory the actual vehicle will have to track. These reference systems are chosen in such a way that the position of that virtual vehicle can easily and accurately track a prescribed desired trajectory. From a motion control perspective, the remaining task is to generate the actual vehicle's control input, guaranteeing convergence of the actual vehicle's trajectory to that of the virtual vehicle's. What the presented framework aims to accomplish is to take advantage of this MRC approach to decrease the amount of communication required for a team of vehicles to operate cooperatively.

10.2.1. Assumptions and Governing Principle

The proposed approach requires each vehicle to not only integrate the reference system it is tracking, but also the ones associated with all other vehicles, as seen in Figure 10.1. Assuming that each vehicle has knowledge of

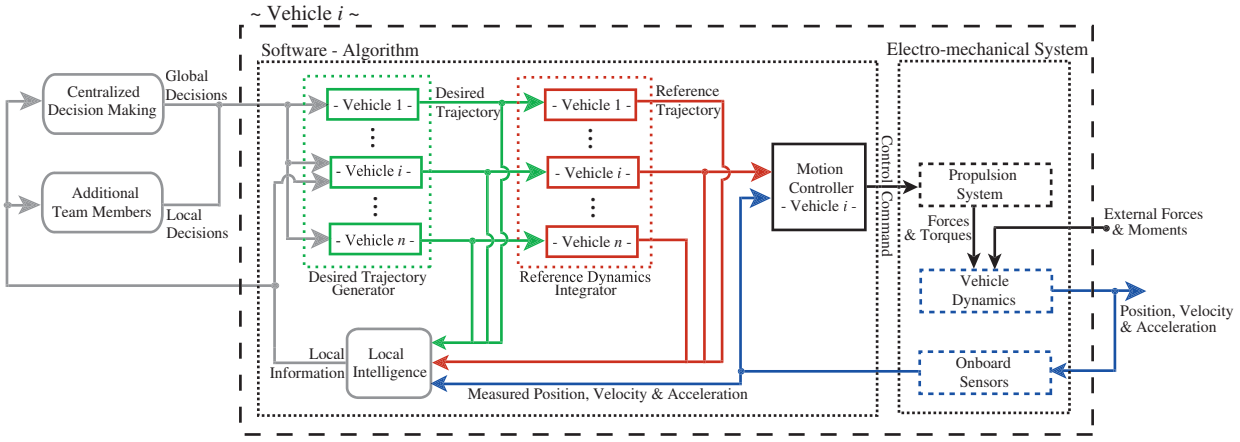

Figure 10.1: Block Diagram of the Algorithm for the i^{th} Vehicle in a Team of n.

- the predetermined desired trajectories for all vehicles corresponding to each task in a considered mission,

- the initial reference state and expression of the dynamics of all reference systems,

and assuming that each vehicle's motion controller provides perfect tracking of the reference trajectory, a specific vehicle can obtain a close estimate of any other vehicle's position by locally integrating its reference system, *without* requiring communication of position information. Transition from a task to another can be decided upon either by an individual, predetermined decision maker, if the decision making process is centralized ([125–127]), or by just about any vehicle in the team if it is decentralized ([67, 128–132]). This type of decision, as it affects all vehicles in the team, will be referred to as `Global Decision`. Advent of such a decision, which in general affects all vehicles, will require communication to all members of the team. The information systematically required to be passed along is limited to a `Task Number`, uniquely identifying the new task to be pursued, and a `Time Stamp` specifying the time at which the decision was taken. Upon reception of such a message, each vehicle

modifies, in accordance with the newly appointed task, the desired trajectories tracked by the reference systems it is locally integrating, or the reference systems themselves. The `Time Stamp` ensures that, upon reception of a `Global Decision` message by all vehicles, they are able to appropriately compute the reference trajectory of other team members in spite of time delays.

Note that, as mentioned above, `Time Stamp` and `Task Number` constitute the only information *systematically* required in a `Global Decision` message, but that, depending on the nature of the newly pursued task, additional information, such as position of a detected target to be intercepted or investigated (as seen in Subsection 10.3.3), might be necessary. Additionally, if a centralized decision making process is used, events witnessed locally by a specific member of the team that can potentially affect `Global Decisions`, such as detection of a target to be intercepted or investigated, should be relayed to the `Global Decision` making entity, requiring added communications, as illustrated in Subsection 10.3.3. Also note that the framework is essentially unrelated to the decision making process. Although lending itself well to decentralized approaches, it is flexible enough to seamlessly accommodate centralized decision making algorithms. Figure 10.1 reflects this flexibility and illustrates the fact that decisions affecting a specific vehicle's desired trajectory can be taken either locally (Local Intelligence block), or come from a centralized decision maker (Centralized Decision Making block). Note that cooperation between vehicles in the team is made possible by the communications from and to each vehicle, as represented in Figure 10.1.

In addition, note that knowledge of reference positions does not continuously provide knowledge of the actual position of the vehicles. In particular, during the transition periods following emission of a `Global Decision` message and preceding reception of this message

by all vehicles and convergence of the reference trajectories to the newly appointed desired trajectories, there exists a discrepancy in current desired and reference trajectories across the team. During this transition period, knowledge of the reference position of a vehicle only provides an estimate of its actual position, as seen in Subsection 10.3.1. Furthermore, in a realistic setting, perfect tracking of the reference trajectories by the actual vehicles is not achievable. To address this issue and avoid vehicle collisions, the framework relies on reference systems of a particular form, which enforces separation between vehicles' reference positions. This separation can be adjusted in function of the tracking performance of the motion controller to guarantee that vehicles do not collide.

The knowledge assumptions the framework relies on are equivalent to requirements in terms of memory available for each vehicle's electronic control system, and, as such, are trivially justifiable. As mentioned above, the perfect tracking assumption is not satisfied in realistic settings. However, a wealth of motion controllers providing accurate tracking for most types of autonomous vehicles can be found in the literature ([3, 5, 66, 133–135]). In addition, the reference systems can include terms guaranteeing strict vehicle to vehicle separation, as detailed in Section 10.3. An additional implicit assumption is that the control system onboard each vehicle has sufficient computational power to integrate, with arbitrary precision, a number of differential equations proportional to the considered number of vehicles in the team. Most modern embedded computers satisfy this requirement.

10.2.2. Advantages of the Proposed Framework

Note that no communication pertaining to vehicles' position is necessary, which considerably reduces bandwidth usage. A team of vehicles using the presented framework can

effectively maintain a formation without communication of relative positions or handshaking protocol. Furthermore, as a benefit of the inclusion of the `Time Stamp`, the punctual communications required for propagation of `Global Decisions` throughout the team of vehicles need not be synchronous or assumed instantaneous. In other words, the effect of communication time delays on team performance are minimal. Knowledge of all desired trajectories, reference dynamics and `Time Stamps` allows any vehicle to compute the reference trajectories of all other vehicles corresponding to the currently pursued task upon reception of a `Global Decision` message, regardless of delays in reception of this message. As mentioned earlier, a potential discrepancy between vehicles' trajectories computed locally on different vehicles does exist. Time delays render such discrepancies inevitable, regardless of the framework chosen. However, following the proposed approach, the time window of existence of these discrepancies is reduced to a short transient. Subsection 10.3.1 illustrates the approach proficiency in handling time delays.

Additionally, the proposed approach allows for a high level of flexibility in the way missions are handled. For instance, considering a target detection and identification mission, if a vehicle detects a potential target, it can either notify the `Global Decision` making entity and let it decide how this information should affect the mission, choose to investigate the target itself before notification, thus reducing the likelihood of false alarms affecting the whole team, or even take upon itself the task of identifying this specific target without notifying anyone (see Subsection 10.3.3). The approach removes the requirement commonly seen in formation control problems that each vehicle observes, measures, or receives the state of the entire team. The presented approach allows for a level of flexibility superior to that offered by traditional formation control frameworks.

In addition, the presented approach provides an interesting degree of robustness to occurrences that are commonly seen as unsurmountable, such as partial or total failure of one or several vehicles. Were a vehicle to be lost, this event can be communicated either to the `Global Decision` making entity, or to all other vehicles, allowing the team to adjust its behavior by switching to a different set of desired trajectories. The remaining vehicles, knowing that they cannot rely on the lost vehicle any longer, can modify the desired trajectories accordingly. In the case of a survey mission, for instance, the loss of one or several team members can potentially be made up for by increasing vehicle to vehicle spacing, allowing to cover the same area.

Finally, modifying the vehicles' reference systems allows to directly affect their behavior. This was taken advantage of in preliminary simulations to enforce obstacle and collision avoidance.

10.3. Numerical Simulations

The performance of the indirect collaborative control framework presented in Section 10.2 was tested using a simple numerical simulation. Subsection 1.2.1 will assume a centralized decision making process. A single vehicle in the team will have `Global Decision` making authority and will be referred to as `Master`, the remaining vehicles being referred to as `Slaves`. Subsection 10.3.3 provides an example of application of the proposed framework in the context of decentralized decision making process.

Assuming perfect tracking control performance, only desired and reference position of each vehicle are considered. It is assumed that motion is limited to the horizontal plane. The reference systems of the n considered vehicles are based on second order oscillators,

generating the position $\eta_{\mathrm{r}i}(t) \triangleq \begin{bmatrix} x_{\mathrm{r}i}(t) & y_{\mathrm{r}i}(t) \end{bmatrix}^{\mathrm{T}} \in \mathbb{R}^2$, $t \geqslant 0$, of the corresponding i^{th} virtual vehicle along the x and y axis of an inertial frame of reference of arbitrary origin. The dynamic equation corresponding to the i^{th} oscillators is of the form

$$\ddot{\eta}_{\mathrm{r}i}(t) + A_{\mathrm{r}}\dot{\eta}_{\mathrm{r}i}(t) + \Omega_{0i}^2\eta_{\mathrm{r}i}(t) = \Omega_{0i}^2\, r_i(t), \quad \eta_{\mathrm{r}i}(0) = \eta_{\mathrm{r}i0}, \quad t \geqslant 0, \quad i=1,2,...,n, \quad (10.1)$$

where

$$A_{\mathrm{r}} \triangleq 2\,\zeta_i\,\omega_{0i}\,I_{\mathrm{d}2}, \qquad \Omega_{0i}^2 = \omega_{0i}^2 I_{\mathrm{d}2}, \qquad i = 1,2,...,n, \quad (10.2)$$

where ζ_i and ω_{0i} represent the damping coefficient and natural frequency, respectively, for the oscillators of the i^{th} reference system, $r_i(t)$ corresponds to the reference signal controlling it and $I_{\mathrm{d}2}$ denotes the two dimensional identity matrix. All reference systems are chosen to have identical damping and natural frequency,

$$\zeta_i = 0.9, \qquad \omega_{0i} = 0.7, \qquad i = 1,2,...,n, \quad (10.3)$$

and the reference signals are computed as

$$r_i(t) \triangleq \Omega_{0i}^{-2}\left(\ddot{\eta}_{\mathrm{d}i}(t) + A_{\mathrm{r}}\dot{\eta}_{\mathrm{d}i}(t) + \Omega_{0i}^2\eta_{\mathrm{d}i}(t)\right), \quad t \geqslant 0, \quad i = 1,2,...,n, \quad (10.4)$$

where $\eta_{\mathrm{d}i}(t)$ represents the desired position of the i^{th} vehicle expressed in the aforementioned inertial frame of reference. This reference signal allows the reference system to track a desired trajectory. The above oscillators were augmented with two additional terms, handling collision and obstacle avoidance. Let $x_{\mathrm{r}i}(t) \triangleq \begin{bmatrix} \eta_{\mathrm{r}i}^{\mathrm{T}}(t) & \dot{\eta}_{\mathrm{r}i}^{\mathrm{T}}(t) \end{bmatrix}^{\mathrm{T}}$, $t \geqslant 0$. The complete reference system associated with each vehicle is of the form

$$\dot{x}_{\mathrm{r}i}(t) = A_{\mathrm{r}4}x_{\mathrm{r}i}(t) + B_{\mathrm{r}}r_i(t) + f_{\mathrm{c}}(x_{\mathrm{r}}(t)) + f_{\mathrm{o}}(x_{\mathrm{r}i}(t)), \quad t \geqslant 0, \quad i = 1,2,...,n, \quad (10.5)$$

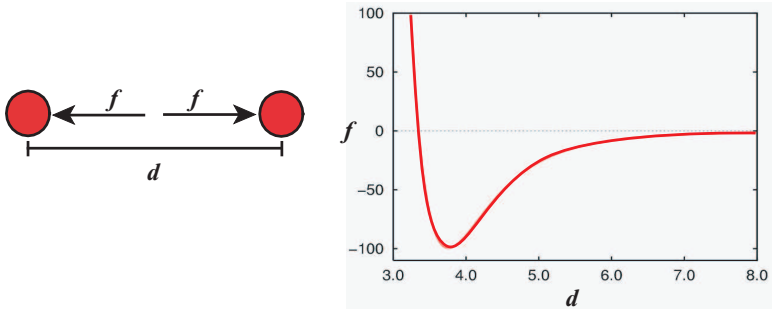

Figure 10.2: Interaction between molecules subjected to Van der Waals forces (left), force as a function of the intermolecular distance (right).

where

$$A_{\mathrm{r}4} \triangleq \begin{bmatrix} -\Omega_{0i}^2 & 0 \\ 0 & -A_{\mathrm{r}} \end{bmatrix}, \qquad B_{\mathrm{r}} \triangleq \begin{bmatrix} 0 \\ -\Omega_{0i}^2 \end{bmatrix}, \tag{10.6}$$

the vector x_{r} regroups the $x_{\mathrm{r}i}$ for all i, $f_{\mathrm{c}}(\cdot)$ and $f_{\mathrm{o}}(\cdot)$ are virtual forces enforcing collision and obstacle avoidance, respectively. To avoid collision, each reference system is subjected to virtual repulsion forces from all current reference positions in the team. More concretely, a force of the form

$$f_{\mathrm{c}}(x_{\mathrm{r}}(t)) \triangleq \frac{\alpha}{d^6(x_{\mathrm{r}}(t))} + \frac{\beta}{d^{12}(x_{\mathrm{r}}(t))}, \qquad t \geq 0, \tag{10.7}$$

where $\alpha,\ \beta \in \mathbb{R}$, $d(x_{\mathrm{r}}(t))$, $t \geq 0$, represents the distance between reference positions, is applied to the reference system for each additional team member. Such forces, which are similar to atomic interaction forces as modeled by Van der Waals, as described in Figure 10.2, allow to avoid vehicle collisions. The value of β can be adjusted to increase or decrease vehicle to vehicle separation. Finally, to enforce obstacle avoidance, the term f_{o} is composed of virtual forces of the form

$$f_{\mathrm{o}j}(x_{\mathrm{r}i}(t)) \triangleq \frac{\gamma}{d_{\mathrm{o}j}^2(x_{\mathrm{r}i}(t))}, \qquad t \geq 0, \tag{10.8}$$

where $\gamma \in \mathbb{R}$, and $d_{oj}(x_{ri}(t))$ represents the distance between vehicle i's reference position to the j^{th} detected obstacle.

10.3.1. Time delays

This first simulation illustrates how the presented framework handles communication delays. Four vehicles follow a desired trajectory traveling along a straight path, with a desired velocity $\dot{\eta}_{\text{d}}(t) = \begin{bmatrix} 1 & 0 \end{bmatrix}^{\text{T}}$. Their reference positions has them located randomly in a neighborhood of the initial desired position (at the origin). Global Decision making responsibilities are assigned to the first vehicle (`Master`), vehicles two to four being the `Slaves`. The formation is maintained up to a time $t_1 = 15$ seconds, time at which the `Master` decides to increase vehicle to vehicle spacing.

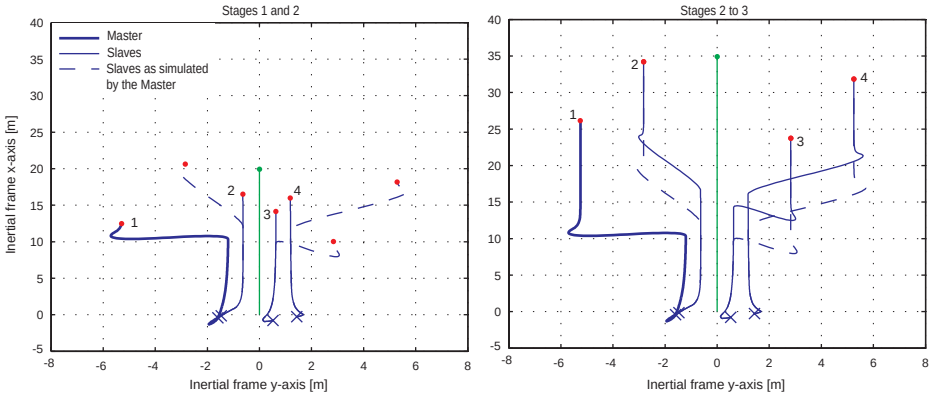

Figure 10.3: Formation Change under the Influence of Homogeneous Time Delay.

To clearly illustrate how time delays affect motion, consider an exaggerated communication delay of 5 seconds between the time t_1 at which the `Master` decides the change of formation and the time t_2 at which all `Slaves` receive that information. During the time period going from t_1 to t_2, the `Slaves` still maintain the previously defined separation while the `Master` makes the transition to the new one. Note that from the perspective of the `Master`,

the `Slaves`' reference trajectories transition to the newly defined formation instantly (trajectories of the `Slaves` from the perspective of the `Master` are represented using dashed lines in Figure 10.3). Similarly, from the perspective of the `Slaves`, the `Master` is still following the previous formation.

Upon reaching time t_2, the `Slaves` receive the formation-change order and modify their desired trajectories accordingly. Upon reception of the message by the `Slaves`, the discrepancy between trajectories from `Master`'s and `Slaves`' perspectives is rapidly shifted out, as seen on Figure 10.3. The actual reference trajectories of the `Slaves` soon match their reference trajectories as seen from the `Master`'s perspective.

Note that the time delay was greatly exaggerated to clearly illustrate its influence on the behavior of the system following the occurrence of a `Global Decision`. The duration of this transition, essentially corresponding to the time delay of 5 seconds, should realistically be reduced to a fraction of a second, thus reducing the discrepancy between trajectories as seen from `Master`'s and `Slaves`' perspectives to a hardly noticeable level.

As seen on Figure 10.3, all vehicles are attempting to track a single desired trajectory (in green). However, the collision avoidance term in the reference dynamics generates a separation between vehicles, such that no one vehicle perfectly tracks the desired trajectory, but the team follows the desired position in a compact cloud. On Figure 10.3, red dots represent reference position of vehicles, blue curves the reference trajectories, blue crosses the initial reference positions, the green dot is the desired position, and the green line if the desired trajectory.

10.3.2. Collision avoidance

In addition to allow for collision avoidance, the reference systems enforces obstacle avoidance, under the assumption that vehicles are equipped with sensors allowing detection of the aforementioned obstacles. In the following simulation, a sinusoidal desired trajectory, with a velocity along the $x-$axis of 1 meter per second crosses a region containing obstacles (represented by black dots in Figure 10.4). The first simulation features a group of four vehicles, with initial conditions located randomly about the origin. It can be seen on Figure 10.4 that the team of vehicles crosses the region while avoiding the obstacles. The team follows the desired position to the best of its possibilities, but gives priority to collision and obstacle avoidance. The motion of the team is difficult to adequately illustrate using a still figure. In particular, it can be seen that some of the reference trajectories cross each other. Collision avoidance is however strictly enforced, which is easily observed from animations representing the evolution of the trajectories. A second simulation illustrating the collision and obstacle avoidance properties of the framework has two groups of three and five vehicles following sinusoidal desired trajectories similar to the previous simulation, but with different phase. This results in two desired trajectories that repeatedly collide. This simulation includes obstacles as well. It can be seen on Figure 10.4 that the reference trajectories avoid all obstacles. Movies available at the above address show that vehicle collisions are successfully avoided.

10.3.3. Target Detection

This subsection considers a slightly more complex case. A team of four vehicles is given the mission to survey an area, detect targets in this area and identify them. All vehicles are

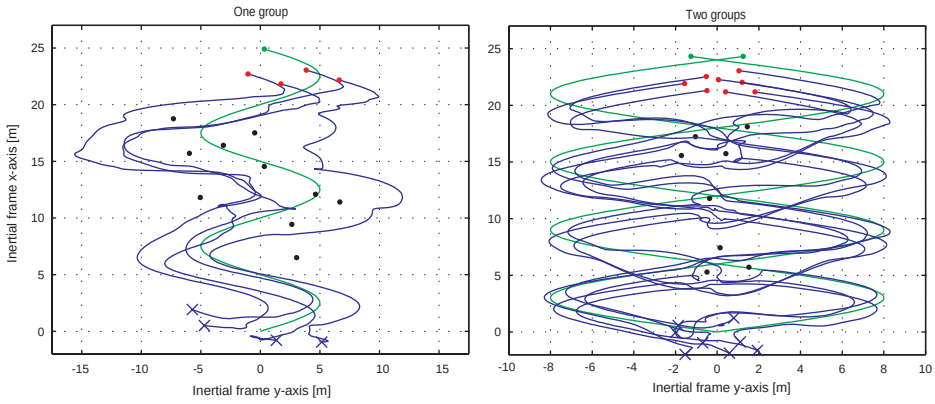

Figure 10.4: Collision avoidance.

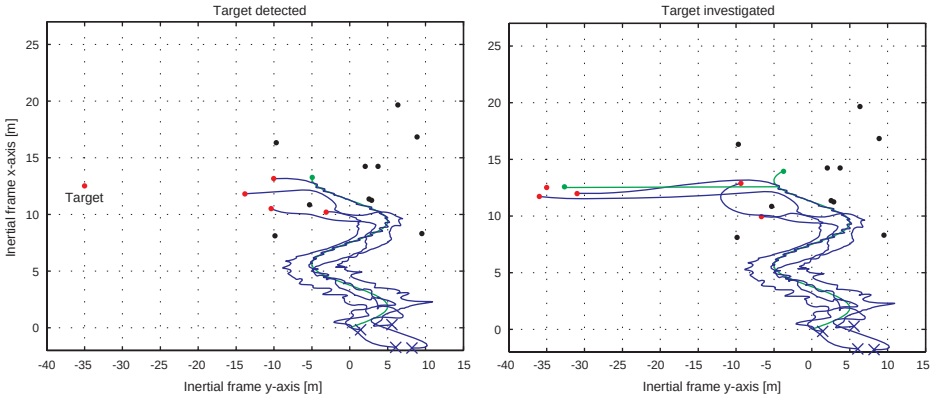

Figure 10.5: Target detection.

assumed to have onboard the appropriate sensing instrumentation to detect any target in a radius of 20 meters. In addition, obstacles in the area are to be avoided.

The mission is split in two distinct tasks. The first one consists in surveying the area, avoiding obstacle and detecting the presence of any target. Vehicles are arbitrarily set to follow a sinusoidal desired trajectory similar to that in previous simulations. The second task consists in identifying a target once it is detected. This is accomplished by traveling towards the detected target, and coming within half a meter of this target.

As seen in Figure 10.5, all vehicles have initial reference position randomly distributed

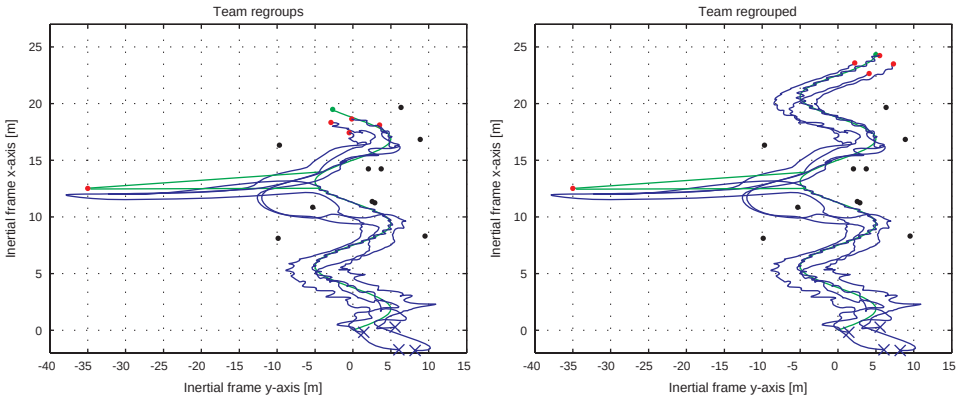

Figure 10.6: Target investigated.

about the origin. The vehicles follow the desired trajectory (in green), avoid collisions and obstacles, until a vehicle comes within 20 meters from the target (represented as an isolated red dot in Figure 10.5). As detection occurs, the vehicle which detected the target propagates this information to the decision making entity, and the decision of sending a pair of vehicles to investigate the target is taken. As a result, as seen on Figure 10.5, the two vehicles closest to the target follow a second desired trajectory leading them to the target. The two remaining vehicles in the team follow the original desired trajectory, in search of additional targets.

Once identification of the target is accomplished, the two vehicles regroup with the remaining team members and pursue the mission, as seen in Figure 10.6.

Note that if only one vehicle is required to identify a target, or if the vehicle detecting this target takes upon itself the responsibility of verifying the target before notifying the decision making entity and the target detection actually was a false alarm, this vehicle need not pass along notification of the event. All remaining team members would thus keep following the desired trajectory, while this particular vehicle would briefly assess the target, before

catching up with the remaining team members.

10.4. Conclusion

The presented framework presents a unifying basis upon which cooperative control algorithms for a team of autonomous vehicles can be built. This framework allows cooperative control of teams of autonomous vehicles with very limited communication capabilities in a hostile environment, and, when augmented with an adaptive motion control algorithm such as those presented in previous chapters, with uncertain or unknown dynamics. The possible applications of collaborative control include search and rescue, mine detection, and surveying. In addition, application of the framework is not limited to underwater vehicles, but also relevant to ground, air, and space vehicles.

Chapter 11

Conclusions and Future Research

This dissertation presents a number of results pertaining to control of unmanned vehicles. In Chapter 2, a general direct adaptive control framework, allowing to account for amplitude and rate saturation of the control command, was introduced. Chapter 3 presented a direct adaptive control algorithm designed for a class of VTOL vehicles. Chapter 4 introduced a neural-based direct adaptive control algorithm for a general class of AMVs, which is specialized to a particular (although commonly encountered) class of non-minimum phase AMVs in Chapters 5 and 6. Chapter 5 presents a nonlinear control algorithm for the considered system, and presents an analysis of the system's resulting internal dynamics. Chapter 6 builds upon this result and introduces a pair of direct adaptive algorithms, as well as an indirect adaptive controller. The control algorithms in Chapters 2 to 6 rely on the assumption that full state measurements are available for feedback. Chapters 7 to 9 present an alternate control strategy, which solves the output feedback control problem for a wide class of nonlinear systems. The approach is based on the nonlinear observer introduced in Chapter 7. This observer is extended in Chapter 8 to hand le controlled systems, and complemented by a simple backstepping-based state feedback control law. The resulting algorithm allows

to simultaneously solve the observation and output feedback control problem for nonlinear systems non-affine in the unmeasured states. The approach is further extended in Chapter 9, to handle a more general class of nonlinear systems and address issues related to model uncertainties. The approach appears promising, as the resulting control algorithm only requires limited knowledge of the system to guarantee arbitrarily accurate tracking. In addition, the final algorithm is practical and reasonably simple. In Chapter 10, a cooperative control framework, designed to handle limited inter-vehicular communication requirements was presented, extending the scope of the results from motion control of a single vehicle, to cooperative control of a group of vehicles.

Future Research

The output feedback scheme introduced in Chapters 7 to 9 could be extended to a larger class of observable systems, by working in terms of the derivatives up to the order q of the output $y(t)$, $t \geq 0$, where $q \leq n-1$ is the smallest integer such that $\text{rank}([\nabla y^{\text{T}}(t),\ \nabla \dot{y}^{\text{T}}(t),\ \ldots,\ \nabla y^{(q)\text{T}}(t)]^{\text{T}}) = n$. Obtaining estimates of these successive derivative could be achieved using the HOSMD introduced in [54]. Furthermore, the algorithms in Chapters 8 to 9 are designed to handle systems whose outputs have a relative degree of two at most, yet they could be fairly easily extended to handle systems whose outputs have greater relative degree. In addition, while knowledge of the system's state dimension is not required to apply the result in Chapter 9, the structure of the state predictor emulates that of the real system. As a result, knowledge of the vector relative degree of the output is necessary. However, one could investigate the ability of an output predictor to predict a given system's output in the case that the predictor's output relative degree does not match that of the system, e.g. can

a predictor with an output of relative degree one accurately predict the output of a system with relative degree two, three, or four, etc? Design of a predictor with such capacity would allow to relax the assumption that the system's output vector relative degree is known.

In addition, the control algorithms presented in this dissertation, as well as the majority of adaptive control algorithms found in the literature, address continuous-time scenarii. However, controllers for unmanned vehicles are typically implemented on digital computers, which only allow discrete-time computations, and thus do not directly allow execution of continuous algorithms. Nevertheless, continuous-time control algorithms have been successfully implemented on such media and have proved to perform adequately, in particular for fast sampling frequencies. While modern computers are digital in nature and can not execute an algorithm continuously but rather at a finite frequency, they can reach ever greater operating speeds. To such an extent that, although it remains impossible, for instance, to continuously compute the value of a control command on a digital computer, it is possible to discretely evaluate at a high frequency this continuous command with accuracy. Most physical systems are of a continuous nature. However, the interface between the control algorithm and the system to be controlled is oftentimes discrete, as sensor information and actuator updates can, depending on the hardware used, occur at arbitrary sampling times.

A possible extension of the presented work could be the adjustment of the presented control algorithms to allow performance in discrete-time environments, thus facilitating future implementation on real systems. That extension would require an effort on two fronts. Since the observer in Chapter 7 is only able to reconstruct the state from continuous output measurements, its use would require conversion of discrete-time output measurements to a continuous signal, which implies the need of reconstructing inter-sample output trajectories.

There exists a wide variety of techniques allowing to achieve this reconstruction, with varying levels of accuracy. It has for instance been shown in the past that simplistic approaches, such as linear interpolation of the raw, noisy measurements, can in practice provide sufficient inter-sample information, if only for systems with relatively low time constants ([136]). On the other end of the problem, the interface from control algorithm to the environment could be handled using the saturation algorithm of Chapter 2. The algorithm can indeed theoretically be used to enforce constant commands in between control updates, by virtue of inter-sample rate saturation.

Appendix A

Stability Theory Results

The results introduced in this dissertation rely on a number of classical stability theorems, which are presented here for completeness. More specifically, Theorem 2.2.1 considers a system of the general form

$$\dot{x}(t) = f(x(t)), \quad x(0) = x_0, \quad t \geq 0, \tag{A-1}$$

where $x(t) \in \mathbb{R}^n$, and $f : \mathcal{D} \to \mathbb{R}^n$ is locally Lipschitz. In addition, we will use the following definitions.

Definition A.1. [44] The equilibrium point $x = 0$ of (A-1) is

- stable if, for each $\epsilon > 0$, there is $\delta = \delta(\epsilon) > 0$ such that

$$\|x(0)\| < \delta \Rightarrow \|x(t)\| < \epsilon, \quad \forall t \geq 0, \tag{A-2}$$

- unstable if it is not stable,

- asymptotically stable if it is stable and δ can be chosen such that

$$\|x(0)\| < \delta \Rightarrow \lim_{t \to \infty} x(t) = 0. \tag{A-3}$$

Stability of an equilibrium point of (A-1) can be established using Lyapunov's stability theorem, as stated below.

Theorem A.1. [44] Let $x = 0$ be an equilibrium point for (A-1) and $\mathcal{D} \subset \mathbb{R}^n$ be a domain containing $x = 0$. Let $V : \mathcal{D} \to R$ be a continuously differentiable function such that

$$V(0) = 0 \quad \text{and} \quad V(x) > 0, x \in \mathcal{D} \setminus \{0\}, \tag{A-4}$$

$$\dot{V}(x) \leq 0, x \in \mathcal{D}, \tag{A-5}$$

then $x = 0$ is stable. Moreover, if

$$\dot{V}(x) < 0, x \in \mathcal{D} \setminus \{0\}, \tag{A-6}$$

then $x = 0$ is asymptotically stable.

Stability of adaptive systems can oftentimes be conveniently analyzed using the LaSalle-Yoshizawa theorem. The class of system considered is given by

$$\dot{x}(t) = f(x(t), t), \quad x(0) = x_0, \quad t \geq 0, \tag{A-7}$$

where $x(t) \in \mathbb{R}^n$, and $f : \mathcal{D} \times \mathbb{R} \to \mathbb{R}^n$ is locally Lipschitz in x and piecewise continuous in t. Statement of the theorem also requires the following definition.

Definition A.2. [44] A continuous function $\gamma : [\, 0,\, a\,) \to [\, 0,\, \infty\,)$ is said to belong to class $\mathcal{K}$ if it is strictly increasing and $\gamma(0) = 0$. It is said to belong to class $\mathcal{K}_\infty$ if $a = \infty$ and $\gamma(r) \to \infty$ as $r \to \infty$.

The stability of an equilibrium point of (A-7) can then be established using the LaSalle-Yoshizawa theorem, as stated below.

Theorem A.2. [10, 44] Let $x = 0$ be an equilibrium point of (A-7) and suppose $f(x,t)$ is locally Lipschitz in x uniformly in t. Let $V : \mathbb{R}^n \times \mathbb{R} \to \mathbb{R}$ be a continuously differentiable function such that

$$\gamma_1(|x|) \leq V(x,t) \leq \gamma_2(|x|), \tag{A-8}$$

$$\dot{V} = \frac{\partial V}{\partial t} + \frac{\partial V}{\partial x} f(x,t) \leq -W(x) \leq 0, \tag{A-9}$$

for all $t \geq 0$ and $x \in \mathbb{R}^n$, where γ_1 and γ_2 are class $\mathcal{K}_\infty$ functions and W is a continuous function. Then, all solutions of (A-7) are globally uniformly bounded and satisfy

$$\lim_{t \to \infty} W(x) = 0. \tag{A-10}$$

In addition, if $W(x)$ is positive definite, then the equilibrium $x = 0$ is globally uniformly asymptotically stable.

Finally, a number of results in this dissertation make use of the notion of ultimate boundedness, which is defined as follows.

Definition A.3. [88] The solution $x(t)$, $t \geq 0$, of (A-7) is ultimately bounded if there exists $b > 0$ and $T > 0$ such that $\|x(t)\| < b$ for all $t > T$.

Ultimate boundedness can be established using the following theorem, which is owed to LaSalle.

Theorem A.3. [88] Let $V(x)$ be a scalar function which for all x has continuous first partial derivatives with the property that $V(x) \to \infty$ as $\|x\| \to \infty$. If $\dot{V}(x) \leq -\epsilon < 0$ for all x outside of some closed and bounded set $\mathcal{M}$, then x is ultimately bounded.

References

[1] A. Leonessa, W. M. Haddad, T. Hayakawa, and Y. Morel, "Adaptive control for nonlinear uncertain systems with actuator amplitude and rate saturation constraints," *Int. Journ. of Adaptive Control and Signal Processing*, vol. 23, no. 1, pp. 73–96, 2009.

[2] Y. Morel and A. Leonessa, "Direct adaptive tracking control of quadrotor aerial vehicles," in *Proc. 2006 ASME Int. Mech. Eng. Congress and Exposition*, (Chicago, IL), 2006.

[3] A. Leonessa, T. S. VanZwieten, and Y. Morel, "Neural network model reference adaptive control of marine vehicles," *Current Trends in Nonlinear Systems and Control, Birkhäuser*, 2004.

[4] Y. Morel and A. Leonessa, "Adaptive nonlinear heading control of an underactuated non-minimum phase model of a marine vehicle," in *Proc. 4th Asian Contr. Conf.*, (Singapore), pp. 117–122, 2002.

[5] Y. Morel and A. Leonessa, "Adaptive nonlinear tracking control of an underactuated nonminimum phase model of a marine vehicle using ultimate boundedness," in *Proc. 42nd IEEE Conf. Dec. Contr.*, (Hawaii), 2003.

[6] Y. Morel and A. Leonessa, "Indirect adaptive control of a class of marine vehicles," *Int. Journ. of Adaptive Control and Signal Processing*, to appear.

[7] Y. Morel and A. Leonessa, "Prediction-based observation of nonlinear systems non-affine in the unmeasured states," *Automatica*, submitted, 2009.

[8] Y. Morel and A. Leonessa, "Observer-based output feedback control of nonlinear systems non-affine in the unmeasured states," in *Proc. 2009 ASME Dynamic Systems and Contr. Conf.*, (Los Angeles, CA), 2009.

[9] A. Leonessa and Y. Morel, "Indirect collaborative control of autonomous vehicles with limited communication bandwidth," in *Proc. of the IARP Int. Workshop on Underwater Robotics*, (Genoa, Italy), pp. 233–240, November 2005.

[10] M. Krstić, I. Kanellakopoullos, and P. Kokotović, *Nonlinear and Adaptive Control Design*. New York, NY: John Wiley and Sons, Inc, 1995.

[11] P. A. Ioannou and J. Sun, *Robust Adaptive Control*. Prentice-Hall, Upper Saddle River, NJ, 1996.

[12] A. L. Fradkov, I. V. Miroshnik, and V. O. Nikiforov, *Nonlinear and Adaptive Control of Complex Systems*. Kluwer Academic, 1999.

[13] K. S. Narendra and A. M. Annaswamy, *Stable Adaptive Systems*. Prentice Hall, 1989.

[14] K. J. Åström and B. Wittenmark, *Adaptive Control*. Addison-Wesley, 1995.

[15] J. T. Spooner, M. Maggiore, R. Ordòñez, and K. M. Passino, *Stable Adaptive Control and Estimation for Nonlinear Systems*. New York, NY: John Wiley and Sons, Inc, 2002.

[16] G. Tao, *Adaptive Control Design*. New York, NY: John Wiley and Sons, Inc, 2003.

[17] J. Sarangapani, *Neural Network Control of Nonlinear Discrete-Time Systems*. Boca Raton, FL: Taylor and Francis, 2006.

[18] K. Zhou, J. C. Doyle, and K. Glover, *Robust and Optimal Control*. Upper Saddle River, NJ: Prentice-Hall, 1995.

[19] C. W. Scherer, "Robust generalized H_2 control for uncertain and LPV systems with generalized scalings," in *Proc. 35th IEEE Conf. Dec. Contr.*, (Kobe, Japan), 1996.

[20] E. Feron, P. Apkarian, and P. Gahinet, "Analysis and synthesis of robust control systems via parameter-dependent lyapunov functions," *IEEE Trans. on Autom. Contr.*, vol. 41, no. 7, pp. 1041–1046, 1996.

[21] K. Zhou and J. C. Doyle, *Essentials of Robust Control*. Upper Saddle River, NJ: Prentice-Hall, 1997.

[22] J. Ackermann, *Robust Control: The Parameter Space Approach*. Springer, 2002.

[23] C. Kravaris and S. Palanki, "Robust nonlinear state feedback under structured uncertainty," *American Inst. of Chem. Eng. Journ.*, vol. 34, no. 7, pp. 1119–1127, 1988.

[24] H. Ito, "Robust control for nonlinear systems with structured $\mathcal{L}_2$-gain bounded uncertainty," *Sys. Contr. Lett.*, vol. 28, pp. 167–172, 1996.

[25] F. Ohkawa and Y. Yonezawa, "A discrete model reference adaptive control system for a plant with input amplitude constraints," *Int. J. Contr.*, vol. 36, pp. 747–753, 1982.

[26] D. Y. Abramovitch, R. L. Kosut, and G. F. Franklin, "Adaptive control with saturating inputs," *Proc. IEEE Conf. Dec. Contr.*, pp. 848–852, Athens, Greece, 1986.

[27] A. N. Payne, "Adaptive one-step-ahead control subject to an input-amplitude constraint," *Int. J. Contr.*, vol. 43, pp. 1257–1269, 1986.

[28] C. Zhang and R. J. Evans, "Amplitude constrained adaptive control," *Int. J. Contr.*, vol. 46, pp. 53–64, 1987.

[29] S. P. Kárason and A. M. Annaswamy, "Adaptive control in the presence of input constraints," *IEEE Trans. Autom. Contr.*, vol. 39, pp. 2325–2330, 1994.

[30] A. M. Annaswamy and S. P. Kárason, "Discrete-time adaptive control in the presence of input constraints," *Automatica*, vol. 31, pp. 1421–1431, 1995.

[31] E. Lavretsky and N. Hovakimyan, "Positive μ-modification for stable adaptation in the presence of input constraints," *Proc. Amer. Contr. Conf.*, pp. 2545–2550, Boston, MA, June 2004.

[32] E. Lavretsky and N. Hovakimyan, "Stable adaptation in the presence of input constraints," *Systems and Contr. Letters*, vol. 56, pp. 722–729, 2007.

[33] E. Lavretsky and N. Hovakimyan, "Positive μ-modification for stable adaptation in dynamic inversion based adaptive control with input saturation," *Proc. Amer. Contr. Conf.*, pp. 3373–3378, Portland, OR, June 2005.

[34] National Research Council, *Aviation Safety and Pilot Control: Understanding and Preventing Unfavorable Pilot-Vehicle Interactions*. Washington, DC: National Academy Press, 1997.

[35] R. A. Hess and S. A. Snell, "Flight control design with rate saturating actuators," *AIAA J. Guid. Contr. Dyn.*, vol. 20, pp. 90–96, 1997.

[36] A. Isidori, *Nonlinear Control Systems*. New York, NY: Springer-Verlag, 1995.

[37] R. E. Kalman, "A new approach to linear filtering and prediction problems," *Trans. of the ASME Journal of Basic Engineering*, vol. 82, no. Series D, pp. 35–45, 1960.

[38] R. E. Kalman and R. Bucy, "New results in linear filtering and prediction theory," *Trans. of the ASME Journal of Basic Engineering*, vol. 83, no. Series D, pp. 95–108, 1961.

[39] D. G. Luenberger, "Observer for multivariable systems," *IEEE Trans. on Automatic Control*, vol. AC-11, no. 2, pp. 190–197, 1966.

[40] D. G. Luenberger, "An introduction to observers," *IEEE Trans. on Automatic Control*, vol. AC-16, no. 6, pp. 596–602, 1971.

[41] M. S. Grewal and A. P. Andrews, *Kalman Filtering*. Upper Saddle River, NJ: Prentice-Hall, 1993.

[42] S. J. Julier and J. K. Uhlmann, "A new extension of the kalman filter to nonlinear systems," in *Int. Symp. Aerospace/Defense Sensing, Simul. and Controls*, pp. 182–193, 1997.

[43] F. L. Lewis, L. Xie, and D. Popa, *Optimal and Robust Estimation*. Boca Raton, FL: Taylor and Francis, 2008.

[44] H. K. Khalil, *Nonlinear Systems*. Upper Saddle River, NJ: Prentice Hall, third ed., 2002.

[45] S. Nazrulla and H. K. Khalil, "Robust stabilization of non-minimum phase nonlinear systems using extended high gain observers," in *Proc. 2008 Amer. Contr. Conf.*, (Seattle, WA), pp. 1734–1739, 2008.

[46] D. Karagiannis and A. Astolfi, "Nonlinear observer design using invariant manifolds and applications," in *Proc. 44th IEEE Conf. Dec. Contr.*, (Seville, Spain), pp. 7775–7780, 2005.

[47] A. Astolfi and R. Ortega, "Immersion and invariance: a new tool for stabilization and adaptive control of nonlinear systems," *IEEE Trans. on Automatic Control*, vol. 48, no. 4, pp. 590–606, 2003.

[48] P. Dorato, C. T. Abdallah, and V. Cerone, *Linear Quadratic Control, An Introduction*. Malabar, FL: Krieger, 2000.

[49] A. N. Atassi and H. K. Khalil, "A separation principle for the stabilization of a class of nonlinear systems," *IEEE Trans. on Automatic Control*, vol. 44, no. 9, pp. 1672–1687, 1999.

[50] A. N. Atassi and H. K. Khalil, "Separation results for the stabilization of nonlinear systems using different high-gain observer designs," *Systems and Control Letters*, vol. 39, pp. 183–191, 2000.

[51] J. Chen, A. Behal, and D. M. Dawson, "Adaptive output feedback control for a class of mimo nonlinears systems," in *Proc. 2006 Amer. Contr. Conf.*, (Minneapolis, MN), pp. 5300–5305, 2006.

[52] S. H. Said and F. M'Sahli, "Output feedback nonlinear gpc using high gain observer," in *Proc. 2007 Int. Symp. on Comp. Intel. and Intel. Inf.*, (Agadir, Morocco), pp. 125–129, 2007.

[53] H. J. Sussmann and P. V. Kokotovic, "The peaking phenomenon and the global stabilization of nonlinear systems," *IEEE Trans. on Automatic Control*, vol. 36, pp. 424–440, 1991.

[54] A. Levant, "High-order sliding modes, differentiation and output-feedback control," *Int. J. Control*, vol. 76, no. 9, pp. 924–941, 2003.

[55] W. Chen and M. Saif, "Output feedback controller design for a class of mimo nonlinear systems using high-order sliding-mode differentiators with application to a laboratory 3-d crane," *IEEE Trans. on Industrial Electronics*, vol. 55, no. 11, pp. 3985–3997, 2008.

[56] J. X. Xu, Q. W. Jia, and T. H. Lee, "On the design of a nonlinear adaptive variable structure derivative estimator," *IEEE Trans. on Automatic Control*, vol. 45, no. 5, pp. 1028–1033, 2000.

[57] C.-C. Cheng and M.-W. Chang, "Design of derivative estimator using adaptive sliding mode," in *Proc. 2006 IEEE Amer. Contr. Conf.*, (Minneapolis, MN), pp. 2611–2615, 2006.

[58] J. Chen, A. Behal, and D. M. Dawson, "Robust feedback control for a class of uncertain mimo nonlinear systems," *IEEE Trans. on Autom. Contr.*, vol. 53, no. 2, pp. 591–596, 2008.

[59] C. Cao and N. Hovakimyan, "$\mathcal{L}_1$ adaptive output feedback controller for systems of unknown dimension," *IEEE Trans. on Autom. Contr.*, vol. 53, no. 3, pp. 815–821, 2008.

[60] S. J. Yoo, J. B. Park, and Y. H. Choi, "Adaptive output feedback control of flexible-joint robots using neural networks: Dynamic surface design approach," *IEEE Trans. on Neural Networks*, vol. 19, no. 10, pp. 1712–1726, 2008.

[61] D. Swaroop, J.-K. Hedrick, P.-P. Yip, and J.-C. Gerdes, "Dynamic surface control for a class of nonlinear systems," *IEEE Trans. Autom. Contr.*, vol. 45, pp. 1893–1899, 2000.

[62] N. Hovakimyan, F. Nardy, A. Calise, and K. Nakwan, "Adaptive output feedback control of uncertain nonlinear systems using single-hidden-layer neural networks," *IEEE Trans. on Neural Networks*, vol. 13, pp. 1420–1431, 2002.

[63] A. Mokhtari, A. Benallegue, and B. Daachi, "Robust feedback lineariztion and GH_∞ controller for a quadrotor unmanned aerial vehicle," in *Proc. 2005 IEEE/RSJ Int. Conf. Intelligent Robots and Systems*, pp. 1198–1203, 2005.

[64] A. T. Kutay, A. Calise, and N. Hovakimyan, "Experimental results on adaptive output feedback control using a laboratory model helicopter," *IEEE Trans. on Control Systems Technology*, vol. 13, pp. 196–202, 2005.

[65] Y. Morel and A. Leonessa, "Model reference adaptive tracking control of non-minimum phase marine vehicles," in *Proc. 2005 ASME Int. Mech. Eng. Congress and Exposition*, (Orlando, FL), 2005.

[66] E. Fredriksen and K. Y. Pettersen, "Global κ-exponential way-point manoeuvering of ships," in *Proc. 43rd IEEE Conf. Dec. Contr.*, (Paradise Island, Bahamas), pp. 5360–5367, 2004.

[67] Y. U. Cao, A. S. Fukunaga, and A. B. Kahng, "Cooperative mobile robotics: Antecedents and directions," *Autonomous Robots*, vol. 4, pp. 7–23, March 1997.

[68] T. Balch and L. E. Parker, eds., *Robot Teams: from Diversity to Polymorphism*. Natick, MA: A. K. Peters, Ltd., 2002.

[69] L. Panait and S. Luke, "A pheromone-based utility model for collaborative foraging," in *The International Conference on Autonomous Agents and Multiagent Sytems*, "July" 2004.

[70] K. L. Doty and R. E. V. Aken, "Swarm robot materials handling paradigm for a manufacturing workcell," in *IEEE International Conference on Robotics and Automation*, pp. 778–782, 1993.

[71] N. Hovakimyan, E. Lavretsky, B.-J. Yang, and A. Calise, "Coordinated decentralized adaptive output feedback for control of interconnected systems," *IEEE Transactions on Neural Networks*, vol. 16, no. 1, 2005.

[72] N. Hovakimyan, E. Lavretsky, A. Calise, and R. Sattigeri, "Decentralized adaptive output feedback control via input/output inversion," *CDC*, pp. 1699–1704, Maui, HI, 2003.

[73] K. Narendra and N. Oleng, "Decentralized adaptive control," *IEEE Trans. Autom. Contr.*, vol. 47, no. 2, pp. 390–395, 2002.

[74] A. Leonessa, W. M. Haddad, T. Hayakawa, and Y. Morel, "Adaptive dynamic control of nonlinear systems with actuator amplitude and rate saturation constraints," in *Proc. 2007 ASME Int. Mech. Eng. Congress and Exposition*, (Seattle, WA), 2007.

[75] W. M. Haddad and T. Hayakawa, "Direct adaptive control for nonlinear uncertain systems with exogenous disturbances," *Int. J. Adapt. Control and Signal Process.*, vol. 16, pp. 151–172, 2002.

[76] T. Hayakawa, W. M. Haddad, and A. Leonessa, "A Lyapunov-based adaptive control framework for discrete-time nonlinear systems with exogenous disturbances," *Int. J. Contr.*, vol. 77, pp. 250–263, 2004.

[77] A. Isidori, *Nonlinear Control Systems*. New York, NY: Springer-Verlag, 1995.

[78] C. T. Chen, *Linear System Theory and Design*. New York, NY: Holt, Rinehart, and Winston, 1984.

[79] N. P. Bhatia and G. P. Szegö, *Stability Theory of Dynamical Systems*. Springer-Verlag, 1970.

[80] A. Leonessa, W. M. Haddad, and V. Chellaboina, *Hierarchical Nonlinear Switching Control Design with Applications to Propulsion Systems*. Springer-Verlag, 2000.

[81] S. L. Waslander, G. M. Hoffmann, J. S. Jang, and C. J. Tomlin, "Multi-agent quadrotor testbed control design: Integral and sliding more vs. reinforcement learning," in *Proc. 2005 IEEE/RSJ Int. Conf. Intelligent Robots and Systems*, pp. 3712–3717, 2005.

[82] S. Bouadballah, A. Noth, and R. Siegwart, "PID vs LQ control techniques applied to an indoor micro quadrotor," in *Proc. 2004 IEEE/RSJ Int. Conf. Intelligent Robots and Systems*, pp. 2451–2456, 2004.

[83] S. Bouadballah and R. Siegwart, "Backstepping and sliding-mode techniques applied to an indoor micro quadrotor," in *Proc. 2005 IEEE Int. Conf. on Robotics and Automation*, pp. 2247–2252, 2005.

[84] E. Altug, J. P. Ostrowski, and R. Mahony, "Control of a quadrotor helicopter using visual feedback," in *Proc. 2002 IEEE Int. Conf. on Robotics and Automation*, pp. 72–77, 2002.

[85] E. Altug, J. P. Ostrowski, and C. J. Taylor, "Quadrotor control using dual camera visual feedback," in *Proc. 2003 IEEE Int. Conf. on Robotics and Automation*, pp. 4294–4299, 2003.

[86] T. L. Fossen, *Guidance and Control of Ocean Vehicles*. Chichester, England: John Wiley & Sons Ltd., 1999.

[87] R. C. Nelson, *Flight Stability and Automatic Control*. McGraw-Hill, 1997.

[88] J. LaSalle and S. Lefschets, *Stability by Liapunov's Direct Method with Applications*. Academic Press, 1961.

[89] I. Fantoni, R. Lozano, F. Mazenc, and K. Pettersen, "Stabilization of a nonlinear underactuated hovercraft," *International Journal of Robust and Nonlinear Control*, vol. 10, no. 8, pp. 645–654, 2000.

[90] K. Do, Z.-P. Jiang, and J. Pan, "Universal controllers for stabilization and tracking of underactuated ships," *Sys. Contr. Lett.*, vol. 47, pp. 299–317, 2002.

[91] K. Do, Z.-P. Jiang, and J. Pan, "Underactuated ship global tracking without measurement of velocities," in *Proc. 2003 IEEE Am. Contr. Conf.*, 2003.

[92] P. M. M. Encarnacão, "Nonlinear path following control systems for ocean vehicles," *PHD Thesis, Instituto Superior Technico*, 2002.

[93] T. I. Fossen, J. M. Godhavn, S. P. Berge, and K. P. Lindegaard, "Nonlinear control of underactuated ships with forward speed compensation," in *Proc. IFAC NOLCOS98*, vol. 1, (Enschede, Netherlands), pp. 121–126, 1998.

[94] J. M. Godhavn, "Nonlinear control of underactuated surface vessels," in *Proc. 35th IEEE Conf. Dec. Contr.*, vol. 1, (Kobe, Japan), pp. 975–980, 1996.

[95] G. Toussaint, T. Basar, and F. Bullo, "H^∞-optimal tracking control techniques for nonlinear underactuated systems," in *Proc. 39th IEEE Conf. Dec. Contr.*, vol. 3, (Sydney, Australia), pp. 2078–2083, 2000.

[96] G. Toussaint, T. Basar, and F. Bullo, "Tracking for nonlinear underactuated surface vessels with generalized forces," in *Proc. Int. Conf. Contr. App.*, (Anchorage, AK), pp. 355–360, 2000.

[97] Y. Fang, E. Zergeroglu, M. de Queiroz, and D. Dawson, "Global output feedback control of dynamically positioned surface vessels: an adaptive control approach," *Mechatronics*, vol. 14, no. 4, pp. 341–356, 2004.

[98] T. Hayakawa, W. M. Haddad, N. Hovakimyan, and V. Chellaboina, "Neural Network Adaptive Control for Nonlinear Nonnegative Dynamical Systems," in *Proc. American Control Conf.*, (Denver, CO), pp. 561–566, June 2003.

[99] P. Encarnação and A. Pascoal, "Combined trajectory tracking and path following: an application to the coordinated control of autonomous marine craft," in *Proc. 40th IEEE Conf. Dec. Contr.*, vol. 1, (Orlando, FL), pp. 964–969, 2001.

[100] F. Dougherty, T. Sherman, G. Woolweaver, and G. Lovell, "An autonomous underwater vehicle (auv) flight control system using sliding mode control," in *Proc. OCEANS'88 Conf.*, (Baltimore, MD), pp. 1265–1270, 1988.

[101] O. E. Fjellstad and T. I. Fossen, "Position and attitude tracking of auv's: a quaternion feedback approach," *IEEE Journal of Oceanic Eng.*, vol. 19, pp. 512–518, 1994.

[102] D. Lainiotis, D. Menon, K. Plataniotis, and C. Charalampous, "Adaptive filter applications to autonomous underwater vehicle," in *Proc. OCEANS'93 Conf.*, vol. 2, (Victoria, Canada), pp. 295–300, 1993.

[103] A. Aguiar and A. Pascoal, "Regulation of a nonholonomic autonomous underwater vehicle with parametric modeling uncertainty using lyapunov functions," in *Proc. 40th IEEE Conf. Dec. Contr.*, (Orlando, FL), pp. 4178–4183, 2001.

[104] Y. Morel, "Design of an adaptive nonlinear controller for an autonomous underwater vehicle equipped with a vectored thruster," *Master Thesis, Florida Atlantic University*, 2002.

[105] H. K. Khalil, *Nonlinear Systems*. Upper Saddle River, NJ: Prentice-Hall, 1996.

[106] J. Slotine and W. Li, *Applied Nonlinear Control*. Englewood Cliffs, New Jersey: Prentice Hall, 1991.

[107] M. Breivik and T. I. Fossen, "A unified control concept for autonomous underwater vehicles," *Proc. Amer. Contr. Conf.*, pp. 4920–4926, Minneapolis, MN, June 2006.

[108] N. Hovakimyan, E. Lavretsky, and C. Cao, "Adaptive dynamic inversion via time-scale separation," in *Proc. 45nd IEEE Conf. Dec. Contr.*, (San Diego, CA), 2006.

[109] J. B. Pomet and L. Praly, "Adaptive nonlinear regulation: estimation from the lyapunov equation," *IEEE Trans. Autom. Contr.*, vol. 37, pp. 729–740, 1992.

[110] D. Bošković and M. Krstić, "Global attitude/position regulation for underwater vehicles," in *Proc. IEEE Int. Conf. Contr. Appl.*, vol. 2, (Kohala Coast, HI), pp. 1768–1773, 1999.

[111] A. M. Kovalev, "Criteria for the observability of nonlinear dynamic systems in multidiensional measurements," *Prikladnaya Mekhanika*, vol. 13, no. 12, pp. 95–101, 1977.

[112] R. Hermann and A. J. Krener, "Nonlinear controllability and observability," *IEEE Trans. on Automatic Control*, vol. AC-22, no. 5, pp. 728–740, 1977.

[113] S. G. Krantz and H. R. Parks, *The Implicit Function Theorem: History, Theory, and Applications*. Boston, MA: Birkhäuser, 2008.

[114] W. M. Haddad and V. Chellaboina, *Nonlinear Dynamical Systems and Control*. Princeton, NJ: Princeton, 2008.

[115] D. Liberzon, "Observer-based quantized output feedback control of nonlinear systems," in *Proc. 2007 Mediterranean Conf. on Contr. and Automation*, (Athens, Greece), 2007.

[116] L. Parker, "Current state of the art in distributed autonomous mobile robotics," 2000.

[117] E. Bonabeau, M. Dorigo, and G. Theraulaz, *Swarm Intelligence: From Natural to Artificial Systems*. New York, New York: Oxford University Press, 1999.

[118] M. J. Mataric, "Designing emergent behaviors: From local interactions to collective intelligence," in *Proceedings, From Animals to Animats, Second International Conference on Simulation of Adaptive Behavior*, pp. 432–441, MIT Press, 1992.

[119] A. Martinoli, *Swarm Intelligence in Autonomous Collective Robotics: From Tools to the Analysis and Synthesis of Distributed Control Strategies*. PhD thesis, Ecole Polytechnique Federale de Lausanne, 1999.

[120] D. J. Stilwell and B. E. Bishop, "Platoon of underwater vehicles: Communication feedback and decentralized control," *IEEE Control Systems Magazine*, vol. 20, no. 6, pp. 45–52, 2000.

[121] P. R. Chandler and M. Patcher, "Hierarchical control for autonomous teams," in *AIAA Guidance, Navigation, and Control Conference and Exhibit*, (Montreal, Canada), pp. 632–642, MIT Press, 2001.

[122] H. Yamaguchi, "A cooperative hunting behavior by mobile robot troops," *Int. J. Rob. Res.*, vol. 18, no. 9, pp. 931–940, 1999.

[123] K. Ozaki, H. Asama, and I. Endo, "Distributed and cooperative object pushing by multiple mobile robot based on communication," *Advanced Robotics*, vol. 11, no. 5, pp. 501–517, 1997.

[124] X. Yun, "Line and circle formation of distributed physical mobile robots," *J. Robot. Syst.*, vol. 14, no. 2, pp. 63–81, 1997.

[125] S. H. Young, P. P. Budulas, and P. J. Emmerman, "Mother ship and physical agents collaboration," *Unmanned Ground Vehicle Technology*, 1999.

[126] P. P. Budulas, S. H. Young, and P. Emmerman, "Robot mother ship design," in *Unmanned Ground Vehicle Technology II*, 2000.

[127] P. P. Budulas, S. H. Young, and P. Emmerman, "Battlefield agent collaboration," in *Unmanned Ground Vehicle Technology III*, 2001.

[128] A. Das, R. Fierro, V. Kumar, J. Ostrowski, J. Spletzer, and C. Taylor, "A framework for vision based formation control," in *IEEE Transactions on Robotics and Automation*, 2001.

[129] A. Das, R. Fierro, V. Kumar, J. Ostrowski, J. Spletzer, and C. Taylor, "A vision-based formation control framework," in *IEEE Transactions on Robotics and Automation*, 2002.

[130] D. Stipanovic, G. Inalhan, R. Teo, and C. Tomlin, "Decentralized overlapping control of a formation of unmanned aerial vehicles," *Automatica*, vol. 40, pp. 1285–1296, August 2003.

[131] W. B. Dunbar, R. Olfati-Saber, and R. M. Murray, "Nonlinear and cooperative control of multiple hovercraft with input constraints," in *European Control Conference*, 2003.

[132] H. Yamaguchi, *A Distributed Motion Coordination Strategy for Multiple Nonholonomic Mobile Robots in Cooperative Hunting Operations*. 2003.

[133] R. Wei and R. W. Beard, "Trajectory tracking for unmanned air vehicles with velocity and heading rate constraints," *IEEE Transactions on Control Systems Technology*, vol. 12, no. 5, pp. 706–716, 2004.

[134] H. J. Kim, D. H. Shim, and S. Sastry, "Flying robots: Modeling, control and decision making," in *Proc. IEEE Int. Conf. on Robotic and Automation*, vol. 1, (Washington, DC), pp. 66–71, 2002.

[135] L. Weng and D. Y. Song, "Path planning and path tracking control of unmanned ground vehicles (ugvs)," in *Proc. 37th Southeastern Symposium on System Theory*, pp. 262–266, 2005.

[136] I. Le Goff, "Design, implementation and testing of a bio-inspired propulsion system for autonomous underwater vehicles," *Master Thesis, Florida Atlantic University*, 2003.